Chapter 4: Reactor
Table of Contents

Section	Title	Page
4.1	SUMMARY DESCRIPTION	4.1-1
4.1	References	4.1-5
4.2	MECHANICAL DESIGN	4.2-1
4.2.1	Fuel	4.2-2
4.2.1.1	Design Bases	4.2-2
4.2.1.2	Design Description	4.2-5
4.2.1.3	Design Evaluation	4.2-13
4.2.1.4	Tests and Inspections	4.2-22
4.2.2	Reactor Vessel Internals	4.2-28
4.2.2.1	Design Bases	4.2-28
4.2.2.2	Description and Drawings	4.2-29
4.2.2.3	Design-Loading Conditions	4.2-33
4.2.2.4	Design-Loading Categories	4.2-34
4.2.2.5	Design Criteria Bases	4.2-35
4.2.3	Reactivity Control System	4.2-35
4.2.3.1	Design Bases	4.2-35
4.2.3.2	Design Description	4.2-38
4.2.3.3	Design Evaluation	4.2-48
4.2.3.4	Tests, Verification, and Inspections	4.2-56
4.2.3.5	Instrumentation Applications	4.2-58
4.2	References	4.2-60
4.3	NUCLEAR DESIGN	4.3-1
4.3.1	Design Bases	4.3-1
4.3.1.1	Fuel Burnup	4.3-2
4.3.1.2	Negative Reactivity Feedback (Reactivity Coefficient)	4.3-2
4.3.1.3	Control of Power Distribution	4.3-3
4.3.1.4	Maximum Controlled Reactivity Insertion Rate	4.3-4
4.3.1.5	Shutdown Margins	4.3-4
4.3.1.6	Stability	4.3-5
4.3.1.7	Anticipated Transients without Trip	4.3-6

Chapter 4: Reactor
Table of Contents (continued)

Section	Title	Page
4.3.2	Description	4.3-6
4.3.2.1	Nuclear Design Description	4.3-6
4.3.2.2	Power Distribution	4.3-8
4.3.2.3	Reactivity Coefficients	4.3-21
4.3.2.4	Control Requirements	4.3-25
4.3.2.5	Control	4.3-27
4.3.2.6	Control Rod Patterns and Reactivity Worth	4.3-29
4.3.2.7	Criticality of Fuel Assemblies	4.3-31
4.3.2.8	Stability	4.3-32
4.3.2.9	Vessel Irradiation	4.3-36
4.3.3	Analytical Methods (PDQ Two-Zone/NOMAD)	4.3-37
4.3.3.1	Fuel Temperature (Doppler) Calculations	4.3-37
4.3.3.2	Macroscopic Group Constants	4.3-38
4.3.3.3	Spatial Few-Group Diffusion Calculations	4.3-40
4.3.4	Analytical Methods (CMS)	4.3-42
4.3.4.1	Fuel Temperature (Doppler) Calculations	4.3-43
4.3.4.2	Macroscopic Group Constants	4.3-43
4.3.4.3	Spatial Few-Group Nodal Calculations	4.3-45
4.3	References	4.3-47
4.4	THERMAL AND HYDRAULIC DESIGN	4.4-1
4.4.1	Design Basis	4.4-1
4.4.1.1	Departure from Nucleate Boiling Design Basis	4.4-1
4.4.1.2	Fuel Temperature Design Basis	4.4-2
4.4.1.3	Core Flow Design Basis	4.4-3
4.4.1.4	Hydrodynamic Stability Design Basis	4.4-3
4.4.1.5	Other Considerations	4.4-3
4.4.1.6	Use of Reconstituted Fuel	4.4-4

Chapter 4: Reactor
Table of Contents (continued)

Section	Title	Page
4.4.2	Description	4.4-4
4.4.2.1	Summary Comparison	4.4-4
4.4.2.2	Fuel and Cladding Temperatures	4.4-5
4.4.2.3	Critical Heat Flux Ratio or Departure from Nucleate Boiling Ratio and Mixing Technology	4.4-9
4.4.2.4	Flux Tilt Considerations	4.4-19
4.4.2.5	Void Fraction Distribution	4.4-19
4.4.2.6	Core Coolant Flow Distribution	4.4-20
4.4.2.7	Core Pressure Drops and Hydraulic Loads	4.4-20
4.4.2.8	Correlation and Physical Data	4.4-22
4.4.2.9	Thermal Effects of Operational Transients	4.4-24
4.4.2.10	Uncertainties in Estimates	4.4-25
4.4.2.11	Plant Configuration Data	4.4-27
4.4.3	Evaluation	4.4-28
4.4.3.1	Core Hydraulics	4.4-28
4.4.3.2	Influence of Power Distribution	4.4-30
4.4.3.3	Core Thermal Response	4.4-31
4.4.3.4	Analytical Techniques	4.4-32
4.4.3.5	Hydrodynamic and Flow Power Coupled Instability	4.4-36
4.4.3.6	Temperature Transient Effects Analysis	4.4-38
4.4.3.7	Potentially Damaging Temperature Effects During Transients	4.4-39
4.4.3.8	Energy Release During Fuel Element Burnout	4.4-39
4.4.3.9	Energy Release or Rupture of Waterlogged Fuel Elements	4.4-40
4.4.3.10	Fuel Rod Behavior Effects From Coolant Flow Blockage	4.4-40
4.4.4	Testing and Verification	4.4-41
4.4.4.1	Tests Before Initial Criticality	4.4-41
4.4.4.2	Initial Power and Plant Operation	4.4-42
4.4.4.3	Component and Fuel Inspections	4.4-42
4.4.5	Instrumentation Application	4.4-42
4.4.5.1	Incore Instrumentation	4.4-42
4.4.5.2	Overtemperature and Overpower Delta T Instrumentation	4.4-43
4.4.5.3	Instrumentation to Limit Maximum Power Output	4.4-43
4.4	References	4.4-44

Chapter 4: Reactor
Table of Contents (continued)

Section	Title	Page
4.5	ADVANCED MARK-BW FUEL	4.5-1
4.5.1	Summary Description	4.5-1
4.5.2	Mechanical Design	4.5-1
4.5.2.1	Fuel	4.5-1
4.5.3	Nuclear Design	4.5-15
4.5.3.1	Design Basis	4.5-15
4.5.3.2	Description	4.5-15
4.5.3.3	Analytical Methods (PDQ Two-Zoned/NOMAD)	4.5-19
4.5.3.4	Analytical Methods (CMS)	4.5-20
4.5.4	Thermal and Hydraulic Design	4.5-20
4.5.4.1	Design Bases	4.5-20
4.5.4.2	Description of Thermal and Hydraulic Design of the Reactor Core	4.5-24
4.5.4.3	Evaluation	4.5-33
4.5.4.4	Testing and Verification	4.5-37
4.5.4.5	Instrumentation Application	4.5-38
4.5	References	4.5-38

Chapter 4: Reactor
List of Tables

Table	Title	Page
Table 4.1-1	Reactor Design Comparison Table at Time of Power Uprating	4.1-6
Table 4.1-2	Analytic Techniques in Core Design	4.1-10
Table 4.1-3	Design Loading Conditions for Reactor Core Components	4.1-12
Table 4.2-1	Maximum Deflections Allowed for Reactor Internal Support Structures	4.2-62
Table 4.2-2	Comparison of 17 x 17 Lopar Assembly and 17 x 17 NAIF Assembly Nominal Design Parameters	4.2-63
Table 4.3-1	Reactor Core Description (First Cycle)	4.3-50
Table 4.3-2	Nuclear Design Parameters (First Cycle)	4.3-52
Table 4.3-3	Reactivity Requirement for Rod Cluster Control Assemblies	4.3-53
Table 4.3-4	Axial Stability Index, PWR Core With A 12-ft Height	4.3-54
Table 4.3-5	Typical First Core Neutron Flux Levels (N/cm^2-sec) at Full Power	4.3-54
Table 4.3-6	Summary of PDQ Two-Zone/NOMAD Nuclear Reliability Factors (NRF)	4.3-55
Table 4.3-7	NOMAD ECP Results	4.3-55
Table 4.3-8	NOMAD Startup Physics Testing Results	4.3-56
Table 4.3-9	NOMAD FQ and FZ Results	4.3-57
Table 4.3-10	Summary of CMS Nuclear Reliability Factors (NRF)	4.3-58
Table 4.4-1	Reactor Design Comparison Table (Original Design)	4.4-51
Table 4.4-2	Reactor Design Comparison Table (Current Operating Conditions)	4.4-53
Table 4.4-3	Thermal-Hydraulic Design Parameters for One of Three Coolant Loops Out of Service	4.4-55
Table 4.4-4	Void Fractions at Nominal Reactor Conditions With Design Hot-channel Factors	4.4-56
Table 4.4-5	Comparison of THINC-IV and THINC-I Predictions With Data from Representative Westinghouse Two- and Three-Loop Reactors	4.4-57
Table 4.5-1	Advanced Mark-BW Fuel Assembly Nominal Design Parameters	4.5-41
Table 4.5-2	Reactor Core Description	4.5-42
Table 4.5-3	Thermal-Hydraulic Analysis Design Parameters	4.5-43

Chapter 4: Reactor
List of Figures

Figure	Title	Page
Figure 4.1-1	Reactor Vessel Schematic	4.1-13
Figure 4.2-1	Fuel Assembly Cross Section 17 x 17	4.2-65
Figure 4.2-2	LOPAR Fuel Assembly Outline 17 x 17	4.2-66
Figure 4.2-3	17 x 17 NAIF Fuel Assembly	4.2-67
Figure 4.2-4	Comparison of 17 x 17 NAIF Fuel Assembly With and Without Protective Grid	4.2-68
Figure 4.2-5	Bottom Nozzle/Protective Grid/Fuel Rod Interface	4.2-69
Figure 4.2-6	LOPAR Fuel Rod Schematic	4.2-70
Figure 4.2-7	17 x 17 NAIF Fuel Rod Schematic	4.2-71
Figure 4.2-8	Typical Clad and Pellet Dimensions as a Function of Exposure (Based on Initial North Anna Core)	4.2-72
Figure 4.2-9	Representative Rod Internal Pressure and Linear Power Density as a Function of Time for the Lead Burnup Rod in the Initial North Anna Core	4.2-73
Figure 4.2-10	Removable Rod Compared to Standard Rod, Initial Core Fuel	4.2-74
Figure 4.2-11	Initial Core Removable Fuel Rod Assembly, Details of Upper End of Assembly	4.2-75
Figure 4.2-12	Location of Removal Rods Within an Assembly (First Core)	4.2-76
Figure 4.2-13	Lower Core Support Assembly (Core Barrel Assembly)	4.2-77
Figure 4.2-14	Upper Core Support Assembly	4.2-78
Figure 4.2-15	Plane View of Upper Core Support Structure	4.2-79
Figure 4.2-16	Rod Cluster Control and Drive Rod Assembly With Interfacing Components	4.2-80
Figure 4.2-17	Rod Cluster Control Assembly Outline	4.2-81
Figure 4.2-18	Absorber Rod	4.2-82
Figure 4.2-19	Burnable Poison Assembly	4.2-83
Figure 4.2-20	Current Burnable ABSORBER Rod Cross-Section	4.2-84
Figure 4.2-21	Primary Source Assembly	4.2-85
Figure 4.2-22	17 x 17 Secondary Source Assembly	4.2-86
Figure 4.2-23	Thimble Plug Assembly	4.2-87
Figure 4.2-24	Control Rod Drive Mechanism	4.2-88
Figure 4.2-25	Control Rod Drive Mechanism Schematic	4.2-89
Figure 4.2-26	Control Rod Drive Mechanism Nominal Latch Clearance at Minimum and Maximum Temperature	4.2-90
Figure 4.2-27	Control Rod Drive Mechanism Latch Clearance Thermal Effect	4.2-91
Figure 4.3-1	Fuel Loading Arrangement	4.3-59
Figure 4.3-2	Production and Consumption of Higher Isotopes	4.3-60
Figure 4.3-3	Boron Concentration versus First Cycle Burnup With and Without Burnable Poison Rods	4.3-61
Figure 4.3-4	Sample Burnable Poison Rod Arrangement Within an Assembly	4.3-62

Chapter 4: Reactor
List of Figures (continued)

Figure	Title	Page
Figure 4.3-5	Burnable Poison Loading Pattern Unit No. 1 (First Cycle)	4.3-63
Figure 4.3-6	Burnable Poison Loading Pattern Unit No. 2 (First Cycle)	4.3-64
Figure 4.3-7	Normalized Power Density Distribution Near Beginning of Life, Unrodded Core, Hot Full Power, No Xenon	4.3-65
Figure 4.3-8	Normalized Power Density Distribution Near Beginning of Life, Unrodded Core, Hot Full Power, Equilibrium Xenon	4.3-66
Figure 4.3-9	Normalized Power Density Distribution Near Beginning of Life, Group D 30%, Hot Full Power, Equilibrium Xenon	4.3-67
Figure 4.3-10	Normalized Power Density Distribution Near Middle of Life, Unrodded Core, Hot Full Power, Equilibrium Xenon	4.3-68
Figure 4.3-11	Normalized Power Density Distribution Near End of Life, Unrodded Core, Hot Full Power, Equilibrium Xenon	4.3-69
Figure 4.3-12	Rodwise Power Distribution in a Typical Assembly (Assembly G-9) Near Beginning of life, Hot Full Power, Equilibrium Xenon, Unrodded Core	4.3-70
Figure 4.3-13	Rodwise Power Distribution in a Typical Assembly (Assembly G-9) Near End of life, Hot Full Power, Equilibrium Xenon, Unrodded Core	4.3-71
Figure 4.3-14	Typical Axial Power Shapes Occurring at Start of Life	4.3-72
Figure 4.3-15	Typical Axial Power Shapes Occurring at Middle of Life	4.3-73
Figure 4.3-16	Typical Axial Power Shapes Occurring at End of Life	4.3-74
Figure 4.3-17	Comparison of Assembly Axial Power Distribution With Core Average Axial Distribution, Bank Slightly Inserted Part Length at Mid-Plane	4.3-75
Figure 4.3-18	Flow Chart for Determining the Densification Spike Factor	4.3-76
Figure 4.3-19	Predicted Power Spike Due to Single Nonflattened Gap in the Adjacent Fuel	4.3-77
Figure 4.3-20	Power Spike Factor as a Function of Axial Position	4.3-78
Figure 4.3-21	Maximum F_Q x Power versus Axial Height During Normal Operation	4.3-79
Figure 4.3-22	Peak Power During Control Rod Malfunction Overpower Transients	4.3-80
Figure 4.3-23	Typical Peak Power During Boration/Dilution Overpower Transients	4.3-81
Figure 4.3-24	Comparison Between Calculated and Measured Relative Fuel Assembly Power Distribution	4.3-82
Figure 4.3-25	Comparison of Calculated and Measured Axial Shape	4.3-83
Figure 4.3-26	Measured Values of F_Q for Full Power Rod Configurations	4.3-84
Figure 4.3-27	Doppler Temperature Coefficient at BOL and EOL Cycle 1	4.3-85
Figure 4.3-28	Doppler - Only Power Coefficient - BOL, EOL Cycle 1	4.3-86
Figure 4.3-29	Doppler - Only Power Defect- BOL, EOL Cycle 1	4.3-87
Figure 4.3-30	Moderator Temperature Coefficient - BOL, Cycle 1, No Rods	4.3-88
Figure 4.3-31	Moderator Temperature Coefficient - EOL, Cycle 1	4.3-89

Chapter 4: Reactor
List of Figures (continued)

Figure	Title	Page
Figure 4.3-32	Moderator Temperature Coefficient as a Function of Boron Concentration - BOL Cycle 1, No Rods	4.3-90
Figure 4.3-33	Hot Full Power Temperature Coefficient During Cycle 1 for the Critical Boron Concentration	4.3-91
Figure 4.3-34	Total Power Coefficient - BOL, EOL, Cycle 1	4.3-92
Figure 4.3-35	Total Power Defect- BOL, EOL Cycle 1	4.3-93
Figure 4.3-36	Rod Cluster Control Assembly Pattern	4.3-94
Figure 4.3-37	Accidental Simultaneous Withdrawal of Two Control Banks, EOL, HZP Banks A and B Moving in the Same Plane, PL at 140 Steps	4.3-95
Figure 4.3-38	Axial Offset Versus Time PWR Core with a 12-ft. Height and 121 Assemblies	4.3-96
Figure 4.3-39	X-Y Xenon Test Thermocouple Response Quadrant Tilt Difference Versus Time	4.3-97
Figure 4.4-1	Fuel Average and Surface Temperatures Versus Linear Power: Typical Peak Values During Fuel Rod Lifetime	4.4-58
Figure 4.4-2	Fuel Centerline Temperature Versus Linear Power: Typical Peak Values During Fuel Rod Lifetime	4.4-59
Figure 4.4-3	Thermal Conductivity of UO_2 (Data Corrected to 95% Theoretical Density)	4.4-60
Figure 4.4-4	Axial Variation of Average Clad Temperature for Rod Operating at 5.43 kW/ft	4.4-61
Figure 4.4-5	Comparison of All “R” Grid Data for Typical Cell	4.4-62
Figure 4.4-6	Comparison of All “R” Grid Data for Thimble Cells	4.4-63
Figure 4.4-7	Comparison of 17 x 17 DNB Data with Grid Spacing of 26 inches	4.4-64
Figure 4.4-8	Comparison of Measured to Predicted CHF with Grid Spacing of 22 Inches	4.4-65
Figure 4.4-9	Measured Versus Predicted Critical Heat Flux - WRB-I Correlation	4.4-66
Figure 4.4-10	TDC versus Reynolds Number for 26-in. Grid Spacing	4.4-67
Figure 4.4-11	Normalized Radial Flow and Enthalpy Distribution at 4-ft Elevation (Representative)	4.4-68
Figure 4.4-12	Normalized Radial Flow and Enthalpy Distribution at 8-ft Elevation (Representative)	4.4-69
Figure 4.4-13	Normalized Radial Flow and Enthalpy Distribution at 12-ft Elevation - Core Exit (Representative)	4.4-70
Figure 4.4-14	Thermodynamic Quality, $X = H - H_{sat}/ H_g - H_{sat}$ Void Fraction Versus Thermodynamic Quality $H - H_{sat}/h_g - H_{sat}$	4.4-71
Figure 4.4-15	PWR Natural Circulation Test	4.4-72
Figure 4.4-16	Comparison of a Representative W Two-Loop Reactor Incore Thermocouple Measurements With THINC-IV Predictions	4.4-73

Chapter 4: Reactor
List of Figures (continued)

Figure	Title	Page
Figure 4.4-17	Comparison of a Representative W Three-Loop Reactor Incore Thermocouple Measurements with THINC-IV Predictions	4.4-74
Figure 4.4-18	Hanford Subchannel Temperature Data Comparison with THINC-IV	4.4-75
Figure 4.4-19	Hanford Subcritical Temperature Data Comparison with THINC-IV	4.4-76
Figure 4.4-20	Distribution of Incore Instrumentation - Unit 1	4.4-77
Figure 4.4-21	Distribution of Incore Instrumentation - Unit 2	4.4-78
Figure 4.5-1	Advanced mark-BW Fuel Assembly Outline	4.5-45
Figure 4.5-2	Advanced mark-BW Fuel Rod Assembly	4.5-46

Intentionally Blank

Chapter 4
REACTOR

The North Anna reactors described in this report are designed to operate at the licensed core power rating of 2893 MWt with sufficient margins to allow for transient operation and instrument error without causing damage to the core and without exceeding the safety valve settings in the coolant system. This corresponds to a nuclear steam supply system rating of 2905 MWt. The 12-MWt difference is the net contribution of heat to the reactor coolant system from the reactor coolant pumps. The calculated capacity of the plant is 2910 MWt, and plant equipment has been designed and purchased for this capacity. The portions of the safety analysis dependent on heat removal capacity of the plant and engineered safety systems have assumed a power rating of 2905 MWt.

The uprated core design parameters presented in this chapter are those associated with a core power of either 2893 or 2898 MWt. The analyses in support of the uprated license application were performed for a core power level of 2898 MWt. The core rated thermal power for which the license amendment was applied (Reference 89 of Section 4.4) is 2893 MWt, equivalent to 2905 MWt for the total plant (including reactor coolant pump heat). The 2905 MWt value, the maximum calculated turbine capacity at the design steam generator outlet pressure of 850 psia, was established as a desired limit for uprated operation.

This chapter describes the design of the reactors and presents an evaluation of the design. The evaluation demonstrates the capability of the reactors to perform their intended functions without releasing more than minimal amounts of fission products to the coolant. In addition, this chapter provides supporting information for the safety analyses discussed in Chapter 15.

Note: As required by the Renewed Operating Licenses for North Anna Units 1 and 2, issued March 20, 2003, various systems, structures, and components discussed within this chapter are subject to aging management. The programs and activities necessary to manage the aging of these systems, structures, and components are discussed in Chapter 18.

Intentionally Blank

4.1 SUMMARY DESCRIPTION

This chapter describes 1) the mechanical components of the reactor and reactor core including the fuel rods and fuel assemblies, reactor internals, and the control rod drive mechanisms, 2) the nuclear design, and 3) the thermal-hydraulic design. A schematic of the reactor vessel is presented in Figure 4.1-1.

The reactor core is comprised of an array of fuel assemblies that are similar in mechanical design and fuel enrichment. The North Anna Unit 1 and 2 cores may consist of any combination of 17 x 17 low-parasitic (LOPAR), 17 x 17 North Anna Improved Fuel (NAIF), or Advanced Mark-BW fuel assemblies. The LOPAR and NAIF designs are described in Section 4.2 and the Advanced Mark-BW design is described in Section 4.5. Small numbers of demonstration or lead fuel assemblies which differ from the fuel described in Chapter 4 may sometimes be used in the Unit 1 or Unit 2 cores. These assemblies are substantially the same as the fuel described in Chapter 4, but may incorporate some dimensional, material, or mechanical differences. Changes to fuel assembly design features are demonstrated to satisfy applicable NRC staff-approved codes and methods. Otherwise NRC approval is obtained prior to the use of the assemblies. The design differences of such assemblies are described in detail in the supporting documentation for the NRC-approved exemption, license condition, or license amendment. The effects of operation with demonstration or lead assemblies will be assessed for each reload core in which they are irradiated.

The core is cooled and moderated by light water at a pressure of 2250 psia in the reactor coolant system. The moderator coolant contains boron as a neutron poison. The concentration of boron in the coolant is varied as required to control relatively slow reactivity changes including the effects of fuel burnup. Additional boron, in the form of burnable poison rods, can be employed to establish the desired initial reactivity and control the power distribution.

Two hundred and sixty-four fuel rods are mechanically joined in a square array to form a fuel assembly. The fuel rods are supported at intervals along their length by grid assemblies that maintain the lateral spacing between the rods throughout the design life of the assembly. The grid assembly consists of an “egg-crate” arrangement of interlocked straps. The straps contain spring fingers and dimples for fuel rod support. Straps for mixing vane grids used in the high heat flux region of the assembly also contain coolant mixing vanes. The fuel rods consist of slightly enriched uranium dioxide ceramic cylindrical pellets contained in slightly cold-worked Zircaloy-4 or ZIRLO tubing that is plugged and seal-welded at the ends to encapsulate the fuel. All fuel rods are pressurized with helium during fabrication to reduce stresses and strains to increase fatigue life. Reconstituted fuel assemblies (see Section 4.2.1.2) may also be used.

The center position in the assembly is reserved for the incore instrumentation, while the 24 additional positions in the array are equipped with guide thimbles joined to the grids and the top and bottom nozzles. Depending upon the position of the assembly in the core, the guide thimbles

may be used as core locations for rod cluster control assemblies, neutron source assemblies, or burnable poison rods. The remaining guide thimbles may be fitted with plugging devices to limit bypass flow. The use of plugging devices is optional.

The bottom nozzle is a boxlike structure that serves as a bottom structural element of the fuel assembly and directs the coolant flow distribution to the assembly.

The top nozzle assembly functions as the upper structural element of the fuel assembly in addition to providing a partial protective housing for the rod cluster control assembly or other components.

The rod cluster control assemblies each consist of a group of individual absorber rods fastened at the top end to a common hub or spider assembly.

The control rod drive mechanisms for the rod cluster control assemblies are of the magnetic latch type. The latches are controlled by three magnetic coils. They are so designed that upon a loss of power to the coils, the rod cluster control assembly is released and falls by gravity to shut down the reactor.

Also present is one part-length control rod drive mechanism housing on Unit 1 and one on Unit 2, used as part of the reactor vent system. All part-length control rods have been removed. The part-length control rod drive mechanisms not used for the reactor vent system have been removed from both units and the CRD nozzle housings capped.

Use of part-length control rods was considered undesirable because of the possibility of generating an adverse core power shape. The modification eliminated the potential for an inadvertent part-length rod insertion. Furthermore, implementation of the change eliminated the radiological exposure associated with part-length rod uncoupling requirements during refueling.

The components of the reactor internals are divided into three parts, consisting of the lower core support structure (including the entire core barrel and neutron shield pad assembly), the upper core support structure, and the incore instrumentation support structure. The reactor internals support the core, maintain fuel alignment, limit fuel assembly movement, maintain alignment between fuel assemblies and control rod drive mechanisms, direct coolant flow past the fuel elements and to the pressure vessel head, provide gamma and neutron shielding, and provide guides for the incore instrumentation.

The nuclear design analysis and evaluation establish physical locations for control rods and burnable poisons and physical parameters such as fuel enrichments and boron concentration in the coolant so that the reactor core has inherent characteristics which, together with corrective actions of the reactor control, protection, and emergency cooling systems, provide adequate reactivity control even if the highest reactivity worth rod cluster control assembly is stuck in the fully withdrawn position.

The thermal-hydraulic design analyses and evaluation establish coolant flow parameters that ensure adequate heat transfer between the fuel cladding and the reactor coolant. The thermal design takes into account local variations in dimensions, power generation, flow distribution, and mixing. The mixing vanes incorporated in the fuel assembly spacer grid design induce additional flow mixing between the various flow channels within a fuel assembly as well as between adjacent assemblies.

Instrumentation is provided in and out of the core to monitor the nuclear, thermal-hydraulic, and mechanical performance of the reactor and to provide inputs to automatic control functions.

The reactor core design, together with corrective actions of the reactor control, protection, and emergency cooling systems, can meet the reactor performance and safety criteria specified in Section 4.2.

Table 4.1-1 presents a comparison of the principal nuclear, thermal-hydraulic, and mechanical design parameters for the North Anna 17 x 17 LOPAR fuel assemblies for uprated and non-uprated cores. The purpose of Table 4.1-1 is to provide reactor design parameters and data applicable at the time of the original plant licensing and at the time of core uprating. This table will not be routinely updated unless there is a significant nuclear, thermal-hydraulic, or mechanical design change.

The effects of fuel densification were evaluated with the methods described in References 1, 7, and 8.

The analysis techniques employed in the core design are tabulated in Table 4.1-2. The loading conditions considered in general for the core internals and components are tabulated in Table 4.1-3. Specific or limiting loads considered for design purposes of the various components are listed as follows: fuel assemblies in Section 4.2.1.1.2; reactor internals in Section 4.2.2.3 and Table 5.2-4; neutron absorber rods, burnable poison rods, neutron source rods, and thimble plug assemblies in Section 4.2.3.1.3; and control rod mechanisms in Section 4.2.3.1.4. The dynamic analyses, input forcing functions, and response loadings are presented in Section 3.9.

Beginning with North Anna Unit 1, Cycle 8 and North Anna Unit 2, Cycle 7, the North Anna Improved Fuel (NAIF) assemblies were introduced, in mixed fuel cores with the standard low-parasitic (LOPAR) fuel assemblies (Reference 3).

The NAIF fuel assembly, which incorporates several features of the modified fuel assembly design known as VANTAGE 5 Hybrid (VANTAGE 5H), has been designed to be compatible with the LOPAR fuel assembly, reactor internals interfaces, the fuel handling equipment, and refueling equipment. The NAIF design dimensions are essentially equivalent to the LOPAR fuel design from an exterior assembly envelope and reactor internals interface standpoint.

The significant different mechanical features of the NAIF design relative to the LOPAR fuel design included Zircaloy Intermediate Grids, Reconstitutable Top Nozzle (RTN), Reconstitutable Debris Filter Bottom Nozzle (DFBN), and Extended Burnup Capability. Beginning with the feed for North Anna Unit 2 Cycle 10 (Batch 12) and North Anna Unit 1 Cycle 11 (Batch 13), the fuel assemblies have included additional debris resistance features. These features include: addition of a protective bottom Inconel grid, located directly above the nozzle; positioning the fuel rods immediately above the bottom nozzle; and use of longer bottom end plugs on the fuel rods to ensure a solid Zircaloy interface between the protective grid and the fuel rods.

Beginning with North Anna 1 Cycle 11 and North Anna 2 Cycle 11, the fuel rods, guide thimble tubes, instrumentation tubes, and mixing vane mid-grids were fabricated from ZIRLO. This material change was made to improve the corrosion resistance of the fuel assemblies, and also increase the dimensional stability upon irradiation. This material change is discussed in Section 4.2.

Beginning with Cycle 17 for Unit 2 and Cycle 18 for Unit 1, the Advanced Mark-BW fuel product was introduced in mixed cores with the LOPAR and NAIF assemblies. The Advanced Mark-BW fuel assembly incorporates several advanced features, and has been designed to be compatible with the LOPAR and NAIF assemblies, reactor internals interfaces, the fuel handling equipment, and refueling equipment. The Advanced Mark-BW dimensions are essentially equivalent to the existing LOPAR and NAIF designs from an exterior assembly envelope and reactor internals interface standpoint (Reference 9). Reconstituted Advanced Mark-BW fuel assemblies (see Section 4.5.2.1.2) may be included among the fuel assemblies used for reloading the core.

Beginning with Cycle 19 for Unit 2 and Cycle 20 for Unit 1, North Anna cores will be fully loaded (157 assemblies) with Advanced Mark-BW fuel. Westinghouse LOPAR and NAIF fuel will not be used. Transient and core thermal-hydraulic analysis of Westinghouse fuel has been discontinued starting with Cycle 19 for Unit 2 and Cycle 20 for Unit 1. If any Westinghouse fuel assemblies are used in the future, a review of the plant safety analyses is required. For example, the ECCS containment backpressure analysis for Westinghouse fuel in Section 6.3.3.12 has not been updated for the AECL containment sump strainer that is being installed during refueling outages leading into Cycle 19 for Unit 2 and Cycle 20 for Unit 1.

4.1 REFERENCES

1. J. M. Hellman, editor, *Fuel Densification Experimental Results and Model for Reactor Application*, WCAP-8218-P-A (Proprietary), 1975, and WCAP-8219-A (Non proprietary), 1975.
2. F. W. Sliz & K. L. Basehore, *Vepco Reactor Core Thermal-Hydraulic Analysis Using the COBRA III C/MIT Computer Code*, VEP-FRD-33-A, October 1983.
3. N. P. Wolfhope, *Reload Transition Safety Report for North Anna 1 and 2*, Technical Report NE-756, Rev. 0, November 1989.
4. Davidson, S. L. (Ed.) *Westinghouse Reference Core Report-VANTAGE 5H Fuel Assembly*, Addendum 2-A to WCAP-10444-P-A, February 1989.
5. T. A. Brookmire (Ed.), *Reload Transition Safety Report for Implementation of PERFORMANCE+ Debris Resistance Features at North Anna Units 1 and 2*, Technical Report NE-949, Rev. 0, August 1993.
6. Letter from W. L. Stewart (Virginia Electric and Power Company) to U.S. Nuclear Regulatory Commission, *North Anna Power Station Units 1 and 2, Proposed Technical Specifications Changes, Implementation of ZIRLO Cladding,* Serial Number 93-614, October 4, 1993.
7. J. V. Miller, *Improved Analytical Models Used in Westinghouse Fuel Rod Design Computations,* WCAP-8720 (Proprietary), October 1976.
8. R. A. Weiner et al., *Improved Fuel Performance Models for Westinghouse Fuel Rod Design and Safety Evaluations,* WCAP-10851-P-A, August 1988.
9. Letter from Leslie N. Hartz (Virginia Electric and Power Company) to USNRC, *Virginia Electric and Power Company, North Anna Power Station Units 1 and 2, Proposed Technical Specifications Changes and Exemption Request, Use of Framatome ANP Advanced Mark-BW Fuel,* Serial Number 02-167, March 28, 2002.
10. Letter from USNRC to D. A. Christian, *North Anna Power Station, Units 1 and 2, Issuance of Exemption from the Requirements of 10 CFR 50.44, 10 CFR 50.46, and 10 CFR Part 50, Appendix K, to Allow the Use of the M5 Alloy for Fuel Cladding Material (TAC Nos. MB4700 and MB4701),* September 23, 2003.
11. Letter from USNRC to D. A. Christian, *North Anna Power Station, Unit 2 - Issuance of Amendment Re: Use of Framatome ANP Advanced Mark-BW Fuel (TAC No. MB4715),* April 1, 2004.
12. Letter from USNRC to D. A. Christian, *North Anna Power Station, Unit 1 - Issuance of Amendments Re: Use of Framatome ANP Advanced Mark-BW Fuel (TAC No. MB4174),* August 20, 2004.

Table 4.1-1
REACTOR DESIGN COMPARISON TABLE AT TIME OF POWER UPRATING

Thermal and Hydraulic Design Parameters	Uprating Design Parameters 17 x 17 LOPAR Fuel Assembly	FSAR Design Parameters 17 x 17 LOPAR Fuel Assembly
Reactor core heat output	2898[a] MWt	2775 MWt
Reactor core heat output	9888×10^6 Btu/hr	9471×10^6 Btu/hr
Heat generated in fuel	97.4%	97.4%
System pressure, nominal	2250 psia	2250 psia
System pressure, minimum, steady-state	2250 psia	2220 psia
Minimum DNBR for design transients	Typical cell 1.59	1.30
Coolant flow	Thimble cell 1.57	
Total thermal flow rate	108.2×10^{6}[(b)] lb/hr	105.2×10^6 lb/hr
Effective flow rate for heat transfer	105.0×10^6 lb/hr	100.5×10^6 lb/hr
Effective flow area for heat transfer	41.5 ft^2	41.5 ft^2
Average velocity along fuel rods	15.93 ft/sec	15.10 ft/sec
Average mass velocity	2.53×10^6 lb/hr-ft^2	2.42×10^6 lb/hr-ft^2
Coolant temperature		
Nominal inlet	553.5°F	546.8°F
Average rise in vessel	66.6°F	67.0°F
Average rise in core	68.4°F	69.8°F
Average in core	590.4°F	583.4°F
Average in vessel	586.8°F	580.3°F

a. These parameters are for a core rated thermal power of 2898 MWt, which bounds the current licensed maximum core power of 2893 MWt.

b. Value used in DNB analyses (ITDP Transients)

Table 4.1-1 (continued)
REACTOR DESIGN COMPARISON TABLE AT TIME OF POWER UPRATING

Thermal and Hydraulic Design Parameters	Uprating Design Parameters 17 x 17 LOPAR Fuel Assembly	FSAR Design Parameters 17 x 17 LOPAR Fuel Assembly
Heat transfer		
Active heat transfer, surface area	48,600 ft^2	48,600 ft^2
Average heat flux	198,218 Btu/hr-ft^2	189,800 Btu/hr-ft^2
Maximum heat flux for normal operation	426,170[c] Btu/hr-ft^2	440,500[d] Btu/hr-ft^2
Average thermal output	5.69 kW/ft	5.445 kW/ft
Maximum thermal output for normal operation	12.2[c] kW/ft	12.6[c] kW/ft
Peak linear power for determination of protection setpoints	21.1 kW/ft	18 kW/ft
Heat flux hot-channel factor, F_Q	2.15	2.32
Fuel central temperature,°F		
Peak at 100% power	3150	3250
Peak at maximum thermal output for maximum overpower trip point	4500	4150
Fuel assemblies		
Design	RCC canless	RCC canless
Number of fuel assemblies	157	157
UO_2 rods per assembly	264	264
Rod pitch	0.496 in.	0.496 in.
Overall dimensions	8.426 in. x 8.426 in.	8.426 in. x 8.426 in.
Fuel weight (as UO_2)	181,205 lb	181,205 lb
Zircaloy weight	41,450 lb	41,450 lb

c. These parameter values are associated with an F_Q value of 2.15.

d. These parameter values are associated with an F_Q value of 2.32.

Table 4.1-1 (continued)
REACTOR DESIGN COMPARISON TABLE AT TIME OF POWER UPRATING

Thermal and Hydraulic Design Parameters	Uprating Design Parameters 17 x 17 LOPAR Fuel Assembly	FSAR Design Parameters 17 x 17 LOPAR Fuel Assembly
Fuel assemblies (continued)		
Number of grids per assembly	8 - type R	8 - type R
Loading technique	3 region, nonuniform	3 region, nonuniform
Fuel rods		
Number	41,448	41,448
Outside diameter	0.374 in.	0.374 in.
Diametral gap	0.0065 in.	0.0065 in.
Clad thickness	0.0225 in.	0.0225 in.
Clad material	Zircaloy-4	Zircaloy-4
Fuel pellets		
Material	UO_2 Sintered	UO_2 Sintered
Density (% of theoretical)	95	95
Diameter	0.3225 in.	0.3225 in.
Length	0.530 in.	0.530 in.
Rod cluster control assembles		
Neutron absorber	Ag-In-Cd	Ag-In-Cd
Cladding material	SS 304, cold-worked	SS 304, cold-worked
Clad thickness	0.0185 in.	0.0185 in.
Number of clusters, full-length	48	48
Number of absorber rods per cluster	24	24

Table 4.1-1 (continued)
REACTOR DESIGN COMPARISON TABLE AT TIME OF POWER UPRATING

Thermal and Hydraulic Design Parameters	Uprating Design Parameters 17 x 17 LOPAR Fuel Assembly	FSAR Design Parameters 17 x 17 LOPAR Fuel Assembly
Core structure		
Core barrel, i.d./o.d.	133.86 in./137.939 in.	133.875 in./137.939 in.
Thermal shield, i.d.	142.625 in.	142.625 in.
Thermal shield, o.d.	147.999 in.	147.999 in.
Structure characteristics		
Core diameter (equivalent)	119.7 in.	119.7 in.
Core average active fuel height	143.7 in.	143.7 in.
Reflector thickness and composition		
Top - water plus steel	≈10 in.	≈10 in.
Bottom - water plus steel	≈10 in.	≈10 in.
Side - water plus steel	≈15 in.	≈15 in.
H_2O/U, cold molecular ratio (lattice)	3.43 volume 2.41 molecular	3.43 volume 2.41 molecular
Feed enrichment, wt%		
Region 1	N/A	2.10
Region 2	N/A	2.60
Region 3	N/A	3.10
U1 cycle 6/U2 cycle 5 Batch	3.6/3.8	N/A

Table 4.1-2
ANALYTIC TECHNIQUES IN CORE DESIGN

Analysis	Technique	Computer Code	Section Referenced
Mechanical design of core internals			
Loads, deflections, and stress analysis	Static and dynamic modeling	Blowdown code, FORCE, finite element structural analysis code, and others	3.7.3.3.2 3.9.1.2 3.9.3
Fuel rod design			
Fuel performance characteristics (temperature, internal pressure, clad stress, etc.)	Semiempirical thermal model of fuel rod with consideration of fuel density changes, heat transfer, fission gas release, etc.	Westinghouse fuel rod design model	4.2.1.3.1 4.3.3.1 4.4.2.2 4.4.3.4.2
		TACO3	4.5.2.1 4.5.4.1.2 4.5.4.2.2 4.5.4.3.4.2
Nuclear design			
Cross sections and group constants	Microscopic data	ENDF/B ENDF/B-4	4.3.3.2 4.3.4.2
	Macroscopic constants for homogenized core regions	CELL2 CASMO-4	4.3.3.2 4.3.4.2
	Multi-group Monte Carlo calculations for control rods	KENO	4.3.3.2
X-Y power distributions, fuel depletion, critical boron concentrations, x-y xenon distributions, reactivity coefficients	3-D, 2-group diffusion theory 3-D, 2-group Nodal theory	3D PDQ SIMULATE	4.3.3.3 4.3.4.3
Axial power distributions, control rod worths, and axial xenon distribution	1-D, 2-group diffusion theory 3-D, 2-group Nodal theory	NOMAD SIMULATE	4.3.3.3 4.3.4.3

Table 4.1-2 (continued)
ANALYTIC TECHNIQUES IN CORE DESIGN

Analysis	Technique	Computer Code	Section Referenced
Fuel rod power	Semiempirical thermal model of fuel rod with consideration of fuel density changes, heat transfer, fission gas release, etc.	ESCORE	4.3.3.1
Effective resonance temperature	Resonance weighting function	XSDRNPM/NITAWL	4.3.3.1
Thermal-hydraulic design			
Steady-state	Subchannel analysis of local fluid conditions in rod bundles, including inertial and crossflow resistance terms.	THINC-IV COBRA III C/MIT (Ref. 2) LYNXT VIPRE-D	4.4.3.4.1 4.5.4.2.3 4.5.4.3.4.1.3
Transient DNB analysis	Subchannel analysis of local fluid conditions in rod bundles during transients, including inertial and cross flow resistance terms.	COBRA III C/MIT (Ref. 2) LYNXT VIPRE-D	4.4.3.4.1 4.5.4.2.3 4.5.4.3.4.1.3

Table 4.1-3
DESIGN LOADING CONDITIONS FOR REACTOR CORE COMPONENTS

Fuel assembly weight

Fuel assembly spring forces

Internals weight

Control rod scram (equivalent static load)

Differential pressure

Spring preloads

Coolant flow forces (static)

Temperature gradients

Differences in thermal expansion

- Due to temperature differences
- Due to expansion of different materials

Interference between components

Vibration (mechanically or hydraulically induced)

One or more loops out of service

All operational transients listed in Table 5.2-4

Pump overspeed

Seismic loads (operational-basis earthquake and safe shutdown earthquake)

Blowdown forces (due to cold- and hot-leg break)

Figure 4.1-1
REACTOR VESSEL SCHEMATIC

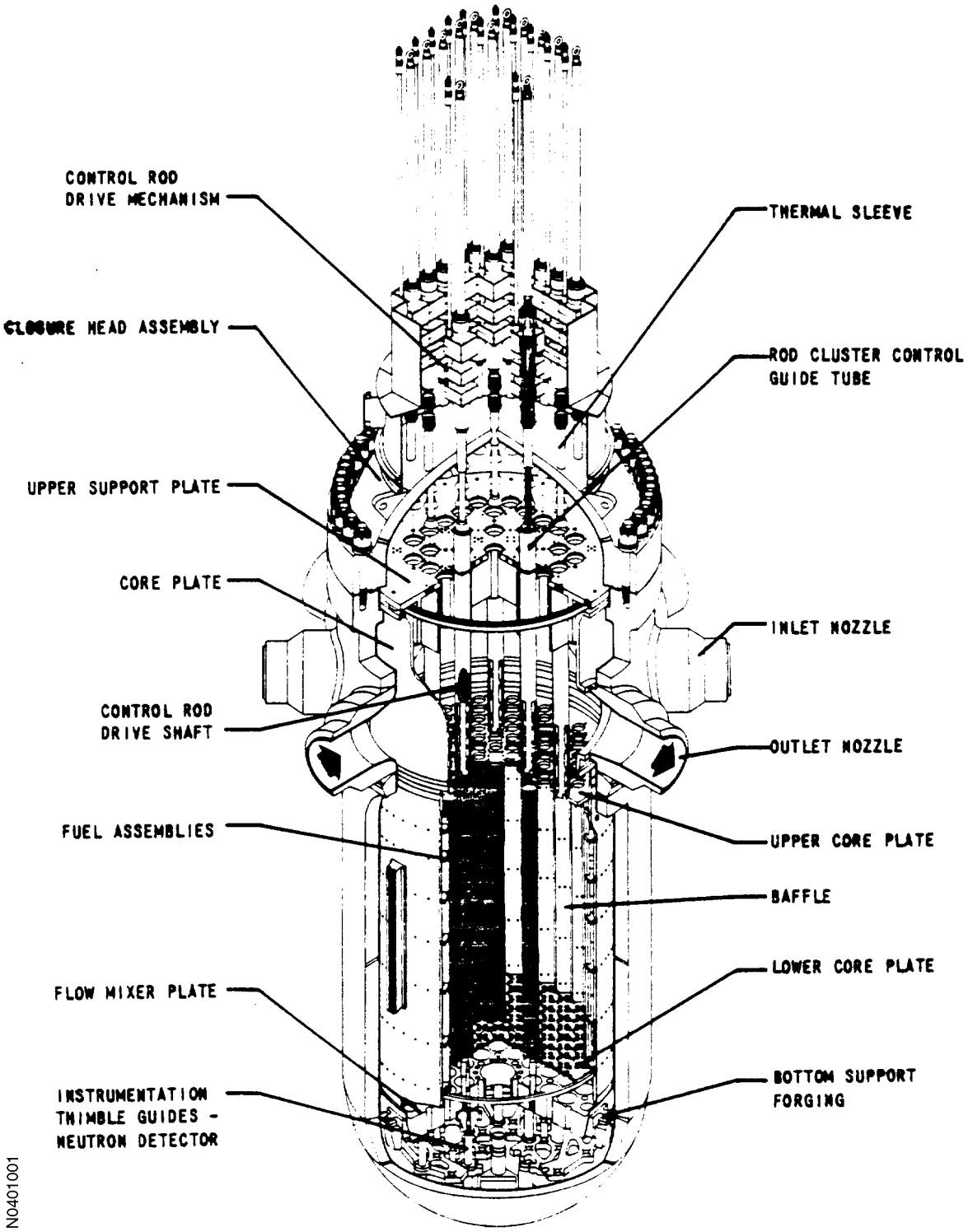

Intentionally Blank

4.2 MECHANICAL DESIGN

The plant conditions for design are divided into four categories in accordance with their anticipated frequency of occurrence and risk to the public: Condition I - Normal Operation, Condition II - Incidents of Moderate Frequency, Condition III - Infrequent Incidents, and Condition IV - Limiting Faults.

The reactor is designed so that its components meet the following performance and safety criteria:

1. The mechanical design of the reactor core components and their physical arrangement, together with corrective actions of the reactor control, protection, and emergency cooling systems (when applicable), ensure the following:

   a. Fuel damage is not expected during Condition I and Condition II events.[1] It is not possible, however, to preclude a very small number of rod failures. These are within the capability of the plant cleanup system and are consistent with the plant design bases.

   b. The reactor can be brought to a safe state following a Condition III event with only a small fraction of fuel rods damaged,[1] although sufficient fuel damage might occur to preclude resumption of operation without considerable outage time.

   c. The reactor can be brought to a safe stage and the core can be kept subcritical with acceptable heat transfer geometry following transients arising from Condition IV events.

2. The fuel assemblies are designed to accommodate expected conditions for handling during assembly, inspection, and refueling operations, and shipping loads.

3. The fuel assemblies are designed to accept control rod insertions in order to provide the required reactivity control for power operations and reactivity shutdown conditions.

4. All fuel assemblies have provisions for the insertion of incore instrumentation necessary for plant operation.

5. The reactor internals in conjunction with the fuel assemblies direct reactor coolant through the core to achieve acceptable flow distribution and to restrict bypass flow so that the heat transfer performance requirements can be met for all modes of operation. In addition, the internals provide core support and distribute coolant flow to the pressure vessel head so that the temperature differences between the vessel flange and head do not result in leakage from the flange during the Condition I and Condition II modes of operation. Required inservice inspection can be carried out, as the internals are removable and provide access to the inside of the pressure vessel.

---

1. Fuel damage as used here is defined as penetration of the fission product barrier (i.e., the fuel rod clad).

4.2.1 Fuel

4.2.1.1 Design Bases

The fuel rod and fuel assembly design bases are established to satisfy the general performance and safety criteria presented in Section 4.2 and specific criteria noted below. The same design bases apply to both the 17 x 17 Low parasitic (LOPAR) and North Anna Improved Fuel (NAIF) fuel rods and assemblies.

4.2.1.1.1 Fuel Rods

The integrity of the fuel rods is ensured by designing to prevent excessive fuel temperatures, excessive internal rod gas pressures due to fission gas releases, and excessive cladding stresses and strains. This is achieved by designing the fuel rods so that the following conservative design bases are satisfied during Condition I and Condition II events over the fuel lifetime:

1. Fuel Pellet Temperatures - The center temperature of the hottest pellet is to be below the melting temperature of the UO_2 (melting point of 5080°F (Reference 1) unirradiated and reducing by 58°F per 10,000 MWd/MTU). While a limited amount of center melting can be physically tolerated, the design conservatively precludes center melting. A calculated centerline fuel temperature of 4700°F has been selected as an overpower limit to ensure no fuel melting. This provides sufficient margin for uncertainties, as described in Sections 4.4.1.2 and 4.4.2.10.1.

2. Internal Gas Pressure - The internal pressure of the lead rod in the reactor is limited to a value below that which could cause the diametral gap to increase due to outward creep during steady-state operation and that could cause extensive departure from nucleate boiling (DNB) propagation to occur.

3. Clad Stress - The effective clad stresses are less than those that would cause general yield of the clad. While the clad has some capability for accommodating plastic strain, the yield strength has been accepted as a conservative design basis.

4. Clad Tensile Strain - The total plastic tensile creep strain is less than 1% from the unirradiated condition. The elastic tensile strain during a transient is less than 1% from the pre-transient value. These limits are consistent with proven practice.

5. Strain Fatigue - The cumulative strain fatigue cycles are less than the design strain fatigue life. This basis is consistent with proven practice.

The effective clad stress is less than that which would cause general yield of the clad. While the clad has some capability for accommodating plastic strain, the yield strength has been accepted as a conservative design basis limit. A volume average effective stress is calculated that considers interference due to uniform cylindrical pellet-clad contact and pressure differences. The pellet-clad contact is caused by pellet thermal expansion, pellet swelling, and uniform clad creep. The von Mises criterion is used to evaluate if the yield strength has been exceeded. The von Mises criterion states than an isotopic material under multiaxial stress will begin to yield plastically

when the effective stress becomes equal to the material yield stress in simple tension as determined by a uniaxial tensile test. Prior to comparison with the yield stress, the calculated volume average effective stress is increased by an allowance that accounts for local stress concentrations in the cladding. The yield strength correlation for irradiated cladding is used for comparison with the calculated stress. This is appropriate since the changes to cladding properties occur at low exposures, whereas the fuel/clad interaction conditions that lead to minimum margin to the design-basis stress limit occur at much higher exposures.

Parameters such as pellet size and density, clad-pellet diametral gap, gas plenum size, and helium prepressure may vary between fuel batches. The detailed fuel rod design ensures that all criteria will be satisfied for the values of these parameters used for a given fuel batch and the planned operating conditions of the fuel. The design also considers effects such as fuel density changes, fission gas release, clad creep, and other physical properties that vary with burnup.

Fuel irradiation testing and surveillance operational experience is used by Westinghouse to verify the adequacy of the fuel, and to improve fuel rod design and manufacturing processes. The results are discussed in Reference 2.

4.2.1.1.2 Fuel Assembly Structure

Structural integrity of the LOPAR AND NAIF fuel assemblies is ensured by setting limits on stresses and deformations due to various loads and by determining that the assemblies do not interfere with the functioning of other components. The following types of loads are considered:

1. Nonoperational loads such as those due to shipping and handling.
2. Normal and abnormal loads that are defined for Conditions I and II.
3. Abnormal loads that are defined for Conditions III and IV.

These criteria are applied to the design and evaluation of the top and bottom nozzles, the guide thimbles, the grids, and the thimble joints.

The design bases for evaluating the structural integrity of the fuel assemblies are the following:

1. Nonoperational - For fuel manufactured prior to 1984, the design bases was 6g's with dimensional stability for both axial and lateral loading. For fuel manufactured after 1984 the design bases was changed to 4g axial loading with dimensional stability and 6g lateral loading.
2. Normal Operation (Condition I) and Incidents of Moderate Frequency (Condition II).

   For normal operating (Condition I) and upset conditions (Condition II), the fuel assembly component structural design criteria are classified into two material categories, namely, austenitic steels and Zirconium-based alloys (e.g., Zircaloy or ZIRLO). The stress categories and strength theory presented in the ASME Boiler and Pressure Vessel Code, Section III, are

used as a general guide. The maximum shear theory (Tresca criterion) for combined stresses is used to determine the stress intensities for the austenitic steel components. The stress intensity is defined as the numerically largest difference between the various principal stresses in a three-dimensional field. The allowable stress intensity value for austenitic steels, such as nickel-chromium-iron alloys, is given by the lowest of the following:

a. One-third of the specified minimum tensile strength or two-thirds of the specified minimum yield strength at room temperature.

b. One-third of the tensile strength or 90% of the yield strength at temperature, but not to exceed two-thirds of the specified minimum yield strength at room temperature.

The stress intensity limits for the austenitic steel components are given below:

Categories	Limit
General primary membrane stress intensity	Sm
Local primary membrane stress intensity	1.5 Sm
Primary membrane plus bending stress intensity	1.5 Sm
Total primary plus secondary stress intensity	3.0 Sm

The Zirconium-based alloy structural components, which consist of guide thimble and fuel tubes on all fuel assemblies, and also the inner six grids on the NAIF fuel assemblies, are in turn subdivided into two categories because of material differences and functional requirements. The fuel tube design criteria are covered separately in Section 4.2.1.3.1. For the guide thimble design, the stress intensities and the stress intensity limit are calculated using the same methods as for the austenitic steel structural components, and account for component thinning due to corrosion (Reference 27). For conservative purposes the unirradiated properties of these alloys are used.

With respect to fuel assembly guide thimble tube wear, a safety analysis performed by Westinghouse shows adequate safety margins even in the extreme case of worn-through guide thimble tubes (Reference 3). A surveillance program confirming the results of the Westinghouse guide tube wear model was submitted to the Nuclear Regulatory Commission (Reference 4). The Commission concluded that the submittal adequately confirmed the acceptability of the Westinghouse 17 x 17 fuel assembly relative to its propensity for guide thimble tube wear (Reference 5).

3. Abnormal loads during Conditions III or IV - worst cases represented by combined seismic and blowdown loads.

   a. Deflections of components cannot interfere with the reactor shutdown or emergency cooling of the fuel rods.

b. The fuel assembly structural component stresses under faulted conditions are evaluated using primarily the methods outlined in Appendix F of the ASME Boiler and Pressure Vessel Code, Section III. Since the current analytical methods use elastic analysis, the stress allowables are defined as the smaller value of 2.4 Sm or 0.70 Su for primary membrane, and 3.6 Sm or 1.05 Su for primary membrane plus primary bending. For the austenitic steel fuel assembly components, the stress intensity is defined in accordance with the rules described in the previous section for normal operating conditions. For the Zirconium-based alloy components, the stress limits are set at two-thirds of the material yield strength, Su, at reactor operating temperature. This results in stress intensity limits for these components being the smaller of 1.6 Sy or 0.70 Su for primary membrane and 2.4 Sy or 1.05 Su for primary membrane plus bending. For conservative purposes, the unirradiated properties of the Zirconium-based alloys are used to define the stress limits, and the evaluation accounts for thinning of the structural components due to corrosion (Reference 27).

The grid component strength values are based on experimental tests. The grid component strength values used to assess the assembly structural behavior during a transient are based on the lower 95% confidence level on the true mean from the distribution of grid strength data at temperature.

4.2.1.2 **Design Description**

The fuel assembly and fuel rod design data for the first cycle core (LOPAR assemblies) are given in Table 4.3-1. The comparison of 17 x 17 LOPAR and NAIF fuel assembly and fuel rod design data are illustrated in Table 4.2-2.

Two hundred and sixty-four fuel rods, 24 guide thimble tubes, and one instrumentation thimble tube are arranged within a supporting structure to form a fuel assembly. The instrumentation thimble is located in the center position and provides a channel for insertion of an incore neutron detector if the fuel assembly is located in an instrumented core position. The guide thimbles provide channels that allow for the insertion of a component such as a rod cluster control assembly, a neutron source assembly, a burnable poison assembly, or a plugging device, depending on the position of the particular fuel assembly in the core. The use of plugging devices and neutron source assemblies is optional. Figure 4.2-1 shows a cross section of the fuel assembly array, and Figure 4.2-2 shows a LOPAR fuel assembly full-length view. The fuel rods are loaded into the fuel assembly structure so that there is clearance between the top end of the fuel rods and the top nozzle. In some fuel assemblies there may also be clearance between the bottoms of the fuel rods and the bottom nozzle; however, fuel assemblies with protective grids for additional debris resistance require that the bottom of the fuel rods be located directly above the bottom nozzle at beginning of life. Sufficient total clearance is maintained between the nozzles to accommodate fuel rod growth.

The NAIF assembly design is shown in Figure 4.2-3. The NAIF assembly incorporates several features of the VANTAGE 5 Hybrid (VANTAGE 5H) fuel assembly design which is

described/evaluated in Reference 7. These features (changes to the LOPAR assembly) include six Zircaloy intermediate grids, a reconstitutable top nozzle (RTN) and an extended burnup capability. Another NAIF assembly feature is the use of a reconstitutable debris filter bottom nozzle (DFBN). Changes from the standard bottom nozzle design include a reduced nozzle height and a new pattern of smaller flow holes to minimize passage of debris particles that could cause fretting damage to fuel rod cladding. Starting with North Anna 2 Batch 12 (first use in Cycle 10) and North Anna 1 Batch 13 (first use in Cycle 11), the fuel assemblies also incorporate an additional protective bottom Inconel grid, located directly above the bottom nozzle. The straps of the protective grid (P-grid) subdivide the flow holes in the debris filter bottom nozzle, to further reduce the amount and size of debris that can enter the fuel assembly.

The NAIF assembly has been designed to be compatible with the LOPAR fuel assembly, reactor internals interfaces, the fuel handling equipment, and refueling equipment. The 17 x 17 NAIF design is intended to replace and be compatible with fuel cores containing fuel of the 17 x 17 LOPAR design. The NAIF assembly overall length has been increased slightly to accommodate fuel rod growth at extended burnups. The NAIF design dimensions are otherwise essentially equivalent to the LOPAR fuel design from an exterior assembly envelope and reactor internals interface standpoint.

Beginning with Batch 13 at both units, the North Anna fuel assemblies include fuel rod cladding, guide thimbles, instrumentation tubes and mixing vane grids fabricated from ZIRLO (Reference 8). This advanced Zirconium alloy is being incorporated to improve the corrosion resistance of the fuel. ZIRLO is also dimensionally more stable than Zircaloy under irradiation. Minor changes to some as-built dimensions (e.g., fuel rod length) were made to reflect the different behavior of the ZIRLO alloy. The as-built fuel assembly length has also been decreased slightly (to approximately that of the LOPAR assembly design) to allow for assembly growth to higher burnups. The fuel assembly envelope dimensions remain unchanged.

Additional small dimensional changes were made to the fuel for North Anna 1 Batch 19. The fuel assembly length was increased to match that of the Zircaloy-4 NAIF design (159.975 inches), and the fuel rod length was increased by a comparable amount, as indicated in Table 4.2-2, to take advantage of the low growth rate of ZIRLO.

Reconstituted fuel assemblies, which contain small numbers of non-fueled solid rods of stainless steel or Zirconium-based alloy in place of fuel rods, may also be used in North Anna reload cores. Assemblies which have low burnup and have been determined to contain failed rods may be reconstituted to allow for the continued utilization of the energy remaining in the fuel assembly. The non-fueled rods (also called dummy rods or filler rods) are manufactured from solid Zirconium-based alloy (e.g., Zircaloy or ZIRLO) or solid stainless steel. The dummy rods generally have the same nominal cold dimensions as fuel-bearing rods; however, in some cases, the dummy rods might be slightly oversized in diameter to compensate for grid spring relaxation and any grid top degradation that may occur during the removal of the rods. Dummy rods may

also have tapered ends to facilitate insertion of the rod and prevent grid damage. NRC approval of the use of reconstituted fuel assemblies at North Anna is given in Reference 24.

Each fuel assembly is installed vertically in the reactor vessel and stands upright on the lower core plate, which is fitted with alignment pins to locate and orient the assembly. After all fuel assemblies are set in place, the upper support structure is installed. Alignment pins, built into the upper core plate, engage and locate the upper ends of the fuel assemblies. The upper core plate then bears downward against the fuel assembly top nozzle via the hold-down springs to hold the fuel assemblies in place.

4.2.1.2.1 Fuel Rods

The 17 x 17 LOPAR and NAIF fuel rods consist of uranium dioxide ceramic pellets contained in slightly cold-worked Zircaloy-4 or ZIRLO tubing that is plugged and seal-welded at the ends to encapsulate the fuel. Schematics of the LOPAR and NAIF fuel rod are shown in Figures 4.2-6 and 4.2-7. The fuel pellets are right circular cylinders consisting of enriched uranium dioxide powder that has been compacted by cold pressing and then sintered to the required density. The ends of each pellet are dished slightly to allow greater axial expansion at the center of the pellets.

The NAIF fuel rod is of the same basic design as the 17 x 17 LOPAR fuel rod, except for use of a tapered bottom end plug on the NAIF fuel rod. As on later batches of LOPAR fuel, the NAIF fuel rod uses a bottom end plug with an internal grip feature to facilitate rod loading during fabrication. However, the end plug on the NAIF design is longer, to provide an improved lead-in for use with the removable top nozzle reconstitution feature. The NAIF fuel uses a chamfered fuel pellet design that was also used in later batches of LOPAR fuel. This pellet design helps improve manufacturability while maintaining or improving performance (e.g., improved pellet chip resistance during manufacturing and handling). The pellet length has also been reduced from the original design used in most LOPAR fuel (see Table 4.2-2).

Both the NAIF and LOPAR fuel rod designs retain the same nominal pellet stack height, clad wall thickness and rod and fuel pellet diameters. However, the NAIF fuel design uses an increased rod length, due to an increased gas plenum (for extended burnups), as well as the previously described longer bottom end plug.

Fuel rods used in assemblies with protective grids have a slightly longer bottom end plug than the original NAIF fuel rods. This ensures that the bottom end plug extends into the protective grids. Debris which passes through the bottom nozzle and is trapped by the protective grid will therefore act against the solid end plug and not the cladding. The top end plugs of these fuel rods are of an external grip design, to facilitate positioning of the rods during fuel assembly fabrication. The external grip top end plug is also slightly longer than the top end plug in the LOPAR and original NAIF fuel rod designs. The fuel rod and pellet stack lengths were not changed when these changes were made to the end plugs for use with the protective grids. This

resulted in a small decrease in the plenum volume in these fuel rods relative to the original NAIF design.

For North Anna 1 Batch 19, the fuel rod length was increased slightly, as indicated in Table 4.2-2, to take advantage of the low growth rate of ZIRLO. The external grip feature was also removed from the fuel rod top end plug, slightly decreasing its length. These changes resulted in a minor increase in the fuel rod plenum volume, providing a small benefit for rod internal pressure analyses.

Fuel rods with ZIRLO cladding are slightly longer than fuel rods with Zircaloy cladding. The length change was made to offset the effect of the lower irradiation induced growth rate of ZIRLO on the fuel rod plenum volume at high burnups. There is no change to the pellet stack height.

To avoid overstressing of the cladding or seal welds, void volume and clearances are provided within the rods to accommodate fission gases released from the fuel, differential thermal expansion between the cladding and the fuel, and fuel density changes during burnup. Shifting of the fuel within the cladding during handling or shipping before core loading is prevented by a stainless steel helical spring that bears on top of the fuel pellet stack. Some recent fuel rod designs have used modified spring designs, in which the spring volume has been adjusted to provide additional volume in the fuel rod plenum. These modified spring designs continue to exert sufficient force to preclude axial movement of the fuel stack during handling and shipping prior to irradiation. All fuel rods are internally pressurized during fabrication. The presence of helium backfill gas minimizes compressive clad stresses and clad creep due to differential pressure across the cladding at operating conditions. The initial fuel rod pressurization level specified for a batch of fuel is dependent on the planned fuel burnup as well as other fuel design parameters and fuel characteristics (particularly densification potential). The fuel rods are designed so that:

1. The internal gas pressure of the lead rod in the reactor will be limited to a value below that which could cause the diametral gap to increase due to outward creep during steady-state operation and which could cause extensive DNB propagation to occur.
2. Clad flattening will not occur during the core life of the fuel.

4.2.1.2.2 Fuel Assembly Structure

The LOPAR and NAIF fuel assembly structures consist of a bottom nozzle, top nozzle, guide thimbles, and grids, as shown in Figures 4.2-2 and 4.2-3. Figure 4.2-4 schematically illustrates the changes to the NAIF fuel assembly design when the protective grid is added for improved debris resistance.

Bottom Nozzle

The LOPAR and NAIF fuel assembly bottom nozzle is a boxlike structure that serves as a bottom structural element of the fuel assembly and directs the coolant flow distribution to the

assembly. The square nozzle is fabricated from stainless steel and consists of a perforated plate and four angle legs with bearing plates as shown in Figures 4.2-2, 4.2-3, and 4.2-5. The legs form a plenum for the inlet coolant flow to the fuel assembly. The plate itself acts to prevent a downward ejection of the fuel rods from the fuel assembly. The bottom nozzle is fastened to the fuel assembly guide tubes by screws that penetrate through the nozzle and mate with an inside fitting in each guide tube. Each screw is retained in position by either a lock wire welded across the screw or a locking cup that is expanded into detents (lobes) on the bottom nozzle.

Beginning with North Anna 2 Batch 9 and North Anna 1 Batch 10, the North Anna fuel, including all the NAIF assemblies, has used a debris filter bottom nozzle (DFBN) design to help reduce the possibility of fuel rod damage due to debris-induced fretting. The stainless steel DFBN is similar to the conventional bottom nozzle design used previously for LOPAR fuel assemblies. However, the DFBN design incorporates a modified flow hole size and pattern, as described below, a decreased nozzle height and thinner top plate to accommodate the high burnup fuel rods. Skirts have been added to the bottom periphery of the plate between the legs to strengthen the plate and legs; one batch of fuel with DFBNs was delivered to each North Anna unit before this feature was added. The DFBN retains the design reconstitution feature which facilitates easy removal of the nozzle from the fuel assembly.

The relatively large flow holes in a conventional bottom nozzle are replaced with a new pattern of smaller flow holes in the DFBN. The holes are sized to minimize passage of debris particles large enough to cause damage. The holes were also sized to provide sufficient flow area, comparable pressure drops, and continued structural integrity of the nozzle. Tests to measure pressure drop and demonstrate structural integrity were performed to verify that the DFBN is totally compatible with fuel with the original bottom nozzle design.

Coolant flow through the fuel assembly is directed from the plenum in the bottom nozzle upward through the penetrations in the plate to the channels between the fuel rods. The penetrations in the plate are positioned between the rows of the fuel rods.

Axial loads (hold-down) imposed on the fuel assembly and the weight of the fuel assembly are transmitted through the bottom nozzle to the lower core plate. Indexing and positioning of the fuel assembly is controlled by alignment holes in two diagonally opposite bearing plates that mate with locating pins in the lower core plate. Any lateral loads on the fuel assembly are transmitted to the lower core plate through the locating pins.

Top Nozzle

The top nozzle assembly functions as the upper structural element of the fuel assembly in addition to providing a partial protective housing for the rod cluster control assembly or other components. It consists of an adapter plate, enclosure, top plate, and pads. The completed top nozzle has hold-down springs mounted on the top plate of the nozzle, as shown in Figures 4.2-2 and 4.2-3. The fuel assembly hold-down springs are made of Inconel 718, and the bolts that attach

the springs to the top nozzle are made of Inconel 718 or Inconel 600. The remainder of the top nozzle is made of stainless steel.

The reconstitutable top nozzle (RTN) design for the NAIF assembly differs from the conventional design used in the LOPAR assembly in two ways: (1) a groove is provided in each thimble thru-hole in the nozzle plate to facilitate attachment and removal, and (2) the nozzle plate thickness is reduced to provide additional axial space for fuel rod growth. Additional details of this design feature, the design bases and evaluation of the reconstitutable top nozzle are given in Section 2.3.2 in Reference 10.

The square adapter plate is provided with round and oblong penetrations to permit the flow of coolant upward through the top nozzle. Other round holes are provided in the top nozzle adapter plate to allow the top nozzle to be joined to the thimble tubes. The structural connection between the top nozzle and the guide thimbles may be accomplished with either a welded or a mechanical joint. The ligaments in the plate cover the tops of the fuel rods and prevent their upward ejection from the fuel assembly. The enclosure is a box-like structure, which sets the distance between the adapter plate and the top plate. The top plate has a large square hole in the center to permit access for the control rods and the control rod spiders. Hold-down springs are mounted on the top plate. The springs are fastened in place at two diagonally opposite corners of the top nozzle by spring screws that pass through a cover (also called the spring clamp) and the springs, and are threaded through the top plate of the top nozzle. On the other two corners, integral pads are positioned that contain alignment holes for locating the upper end of the fuel assembly.

Guide and Instrumentation Thimbles

The guide thimbles are structural members that also provide channels for the insertion of components such as rod cluster control assemblies, burnable poison rods, or, if needed, neutron source assemblies. Each one is fabricated from Zircaloy-4 or ZIRLO tubing having two different diameters. The larger diameter at the top provides a relatively large annular area to permit rapid insertion of the control rods during a reactor trip, as well as to accommodate the flow of coolant during normal operation. Four holes are provided in the thimble tube above the dashpot to reduce the rod drop time. The lower portion of the guide thimbles has a reduced diameter to produce a dashpot action near the end of the control rod travel during normal operation and to accommodate the outflow of water from the dashpot during a reactor trip. The dashpot is closed at the bottom by means of an end plug that is provided with a small flow port to avoid fluid stagnation in the dashpot volume during normal operation. The top end of the guide thimble is fastened to either a tubular sleeve (non-reconstitutable top nozzles) or reconstitutable top nozzle insert by expansion swages. The sleeve or insert fits into the top nozzle adapter plate, where it is welded (sleeve) or mechanically locked into place. The guide thimble is attached to the bottom nozzle by a screw that extends through the bottom nozzle into the end plug at the bottom of the guide thimble dashpot. This screw is retained in position during operation by either a weld or by an expanded-locking cap/screw.

The central instrumentation thimble of each fuel assembly is not attached to either the top or bottom nozzles, but the thimble is constrained by its seating in counterbores of each nozzle. Unlike the guide thimbles, the instrumentation thimble's internal diameter does not vary. A hole through the bottom nozzle, centered on the counterbore used to position the instrumentation thimble, allows incore neutron detectors to pass through the bottom nozzle into the center thimble.

With the exception of a reduction in the guide thimble diameter and increased length above the dashpot, the NAIF guide thimbles are identical to those in the 17 x 17 LOPAR design. A reduction in the guide thimble outside and inside diameters is required due to the use of thicker grid straps with the Zirconium-based alloy. The NAIF guide thimble ID provides adequate clearance for the control rods. The reduced NAIF thimble tube ID also provides sufficient diametral clearance for burnable absorber rods and source rods. The thimble plugs that have been used at North Anna were designed for use with LOPAR assemblies, and are not compatible with the smaller guide thimbles on the NAIF assemblies. Use of thimble plugs is now optional at North Anna. The reduced guide thimble diameter, compared to that of the LOPAR design, results in an increased control rod drop time (to the dashpot) from 2.2 seconds for the LOPAR assembly to 2.7 seconds for the NAIF assembly for use in accident analyses.

The NAIF instrumentation tube diameter has also been decreased relative to the 17 x 17 LOPAR assembly instrumentation tube. This decrease still allows sufficient diametral clearance for the flux thimble to traverse the tube without binding.

The grid sleeve for the top Inconel grid, the top nozzle insert, and thimble tube of the NAIF design are joined together using bulge joint mechanical attachments similar to that used in the 17 x 17 LOPAR design. This bulge joint connection was mechanically tested and found to meet all applicable design criteria.

The intermediate Zircaloy and ZIRLO grids of the NAIF assembly design are also connected to the grid sleeves and guide thimbles by means of mechanical bulge connections, similar to those used for the Inconel grids in the LOPAR assemblies. Mechanical testing of this bulge joint connection showed that it meets all applicable design criteria.

Grid Assemblies

The fuel rods, as shown in Figure 4.2-2 and 4.2-3, are supported laterally at intervals along their length by grid assemblies that maintain the lateral spacing between the rods throughout the design life of the assembly. Each fuel rod is afforded lateral support at six contact points within each structural grid by a combination of support dimples and springs. The grid assembly consists of individual slotted straps interlocked in an "egg-crate" arrangement. The points of intersection between the straps are either brazed or welded to join the straps permanently. Grid features such as springs, support dimples, and mixing vanes are incorporated into the grid straps. To attach the grids to the thimble tubes, tubular sleeves are placed in the grid locations where the thimble tubes are located. These sleeves are either brazed or welded to the grids, and are then attached to the thimble tubes by expansion swages.

For the LOPAR assemblies, the grid material is Inconel 718, chosen because of its corrosion resistance and high-strength properties. The magnitude of the grid restraining force on the fuel rod is set high enough to minimize possible fretting, without overstressing the cladding at the points of contact between the grids and fuel rods. The grid assemblies also allow axial thermal expansion of the fuel rods without imposing restraint sufficient to develop buckling or distortion of the fuel rods.

Two types of structural grid assemblies are used in each LOPAR or NAIF fuel assembly. One type, with mixing vanes projecting from the edges of the straps into the coolant steam, is used in the high-heat-flux region of the fuel assemblies to promote mixing of the coolant. The other type, located at the ends of the assembly, does not contain mixing vanes on the internal straps. The outside straps on all grids contain mixing vanes which, in addition to their mixing function, aid in guiding the grids and fuel assemblies past projecting surfaces during handling or during the loading and unloading of the core.

During 1989, the current snag-resistant grid design was introduced. The outer straps on these grids were modified to better prevent fuel assembly interactions from grid strap interference during core loading and unloading. This was accomplished by changing the grid strap corner geometry, and the addition of guide tabs on the lower edge of the outer grid strap.

The NAIF assemblies utilize VANTAGE 5H intermediate grids made of Zircaloy or ZIRLO. The top and bottom (non-mixing vane) grids are the conventional Inconel grid design. The VANTAGE 5H intermediate grid (Reference 7) is based on the OFA Zircaloy grid design and operation experience. The grid strap thickness, type of strap welding, basic mixing vane design and pattern, method of thimble tube attachment, type of fuel rod support (6 point), and envelope are identical to the OFA Zircaloy grid. The OFA grid has had many years of operating experience (Reference 8). Relative to the OFA grid, the VANTAGE 5H grid includes features that minimize hydraulic resistance while maintaining required structural capability. This original evaluation of the VANTAGE 5H grid performance was based on the extensive design and irradiation experience with previous grid designs, as well as, full grid testing completed with the VANTAGE 5H grid design.

Starting with North Anna 2 Batch 12 (first used in Cycle 10) and North Anna 1 Batch 13 (fresh feed to Cycle 11), the orientation of the mixing vane grids (i.e., the Zircaloy-4 or ZIRLO grids in the NAIF fuel design) was slightly modified (Reference 23). The odd numbered mixing vane grids with reference to the bottom (bottom Inconel structural grid is Grid #1), the first Zircaloy-4 or ZIRLO mixing vane grid from the bottom is Grid #2, etc.) are rotated 90 degrees in the clockwise direction. On an 8 grid assembly, this means that Grids #3, 5, and 7 are rotated as described above. The purpose for the rotation is to minimize the susceptibility of the fuel assembly to flow induced vibration.

There are no physical or material changes to the grids or their axial positions, so this change does not impact the pressure drops, DNB performance, or other thermal-hydraulic performance of the fuel assembly.

Also starting with North Anna 2 Batch 12 and North Anna 1 Batch 13, the fuel assemblies incorporate an additional protective bottom Inconel grid (P-grid), located directly above the bottom nozzle (Reference 23). The straps of the P-grid subdivide the flow holes in the debris filter bottom nozzle, to further reduce the amount and size of debris that can enter the fuel assembly. The P-grid inner grid straps contain paired horizontal dimples that provide coplanar four-point contact within each grid cell. (To accommodate the coplanar dimples, alternating cells have the dimples at alternating elevations.) The P-grid is designed to have its dimples on the full diameter of the solid bottom end plug throughout the design life of the fuel assembly.

The protective grid is fabricated from Inconel-718, with the inner straps the same thickness as the Inconel end (structural) grids, and outer straps which are slightly thicker than those of the end grids. The straps are laser welded at the intersects and to the outer grid strap, similar to the Zirconium-based alloy grids. The top of the P-grid outer grid strap retains the anti-snag features used in the top and bottom Inconel grids. The bottom portion of the outer grid strap is bent inward toward the top perimeter chamfer on the bottom nozzle to minimize potential for hang-up. In addition, the protective grid also has a smaller envelope relative to the bottom non-mixing vane grid and the DFBN. The axial position of the protective grid is fixed by spot-welding the P-grid to four of the twenty-four grid inserts normally used to fix the position of the bottom non-mixing vane grid. To avoid an excessively stiff composite structure, these four inserts are not spot welded to the bottom grid in fuel assemblies with the P-grid (i.e., the bottom grid is attached to the remaining 20 inserts in these assemblies). The interface between the P-grid, the bottom nozzle, and the fuel rod is illustrated in Figure 4.2-5.

Hydraulic tests showed that positioning the fuel rods on the bottom nozzle effectively offsets the impact of incorporating the protective grids into the fuel assemblies. The magnitude of the effect on the pressure drop loss coefficients was negligible, so there is no change to the DNB performance of the fuel.

4.2.1.3 **Design Evaluation**

4.2.1.3.1 Fuel Rods

The fuel rods are designed to ensure that the design bases are satisfied for Condition I and Condition II events. This ensures that the fuel performance and safety criteria are satisfied.

Materials - Fuel Cladding

The desired fuel rod cladding is a material that has a superior combination of neutron economy (low absorption cross section), high strength (to resist deformation due to differential pressures and mechanical interaction between fuel and clad), high corrosion resistance (to coolant, fuel, and fission products), and high reliability. Zircaloy-4 and ZIRLO have this desired

combination of cladding properties. As shown in Reference 2, there is considerable pressurized-water reactor (PWR) operating experience on the capability of both Zircaloy and ZIRLO as a cladding material. Primary clad hydriding has not been a significant cause of clad failures since current controls on moisture levels in the fuel were instituted (Reference 2).

Materials - Fuel Pellets

Sintered, high-density uranium dioxide fuel reacts only slightly with the cladding at core operating temperatures and pressures. In the event of cladding defects, the high resistance of uranium dioxide to attack by water protects against fuel deterioration although limited fuel erosion can occur.

As has been shown by operating experience and extensive experimental work, the thermal design parameters conservatively account for changes in the thermal performance of the fuel elements due to pellet fracture that may occur during power operation. The consequences of defects in the cladding are greatly reduced by the ability of uranium dioxide to retain fission products including those which are gaseous or highly volatile.

Observations from several operating Westinghouse PWRs have shown that fuel pellets can densify under irradiation to a density higher than the manufactured values (References 6 & 9). Fuel densification and subsequent incomplete settling of the fuel pellets may result in local and distributed gaps in the fuel rods.

An extensive analytical and experimental effort was conducted by Westinghouse to characterize the fuel-densification phenomenon (Reference 9). Improvements in pellet manufacturing have minimized the effects of this phenomenon (Reference 25).

The effects of fuel densification have been taken into account in the nuclear and thermal-hydraulic designs of the reactor described in Sections 4.3 and 4.4, respectively.

Metallographic examination of irradiated commercial fuel rods has shown occurrences of fuel/clad chemical interaction. Reaction layers of less than 1 mil in thickness have been observed between fuel and clad at limited points around the circumference. Westinghouse metallographic data indicate that this interface layer remains very thin even at high burnup. Thus, there is no indication of propagation of the layer and eventual clad penetration.

Stress corrosion cracking is another postulated phenomenon related to fuel/clad chemical interaction. Out-of-reactor tests have shown that in the presence of high clad tensile stresses, large concentrations of iodine can chemically attack Zirconium-based alloy tubing and can lead to eventual clad cracking. Westinghouse has no evidence that this mechanism is operative in commercial fuel.

Materials - Strength Considerations

An important factor in fuel element duty is the mechanical interaction of fuel and cladding. This fuel-cladding interaction produces cyclic stresses and strains in the cladding, and these in turn consume cladding fatigue life. The reduction of fuel-cladding interaction is therefore a goal of design. The use of prepressurized fuel rods in Westinghouse PWRs helps to achieve this goal, and also enhances the cyclic operational capability of the fuel rod.

Initially, the gap between the fuel and cladding is sufficient to prevent hard contact between the two. However, during power operation a gradual compressive creep of the cladding onto the fuel pellet occurs due to the external pressure exerted on the rod by the coolant. Cladding compressive creep eventually results in hard fuel-cladding contact. During this period of fuel-cladding contact, changes in power level could result in significant changes in cladding stresses and strains. By using prepressurized fuel rods to partially offset the effect of the coolant external pressure, the rate of cladding-creep toward the surface of the fuel is reduced. Fuel rod prepressurization delays the time at which substantial fuel-cladding interaction and hard contact occur and hence significantly reduces the number and extent of cyclic stresses and strains experienced by the cladding both before and after fuel-cladding contact. These factors result in an increase in the fatigue life margin of the cladding and lead to reactor cladding reliability. Although gaps do not typically occur in the fuel stack with current generation fuel (Reference 25), if gaps should form in the fuel stacks, clad flattening will be prevented by the rod prepressurization so that the flattening time will be greater than the fuel core life (Reference 11).

Steady-State Performance Evaluation

In the calculation of the steady-state performance of a nuclear fuel rod, the following interacting factors must be considered:

1. Cladding creep and elastic deflection.
2. Pellet density changes, thermal expansion, gas release, and thermal properties as a function of temperature and fuel burnup.
3. Internal pressure as a function of fission gas release, rod geometry, and temperature distribution.

These effects are evaluated using an overall fuel rod design model (References 8, 12, 13, & 26). With these interacting factors considered, the model determines the fuel rod performance characteristics for a given rod geometry, power history, and axial power shape. In particular, internal gas pressure, fuel and cladding temperatures, and cladding deflections are calculated. The fuel rod is divided lengthwise into several sections and radially into a number of annular zones. Fuel-density changes, cladding stresses, strains, and deformations, and fission gas releases are calculated separately for each axial segment. The effects are integrated to obtain the internal rod pressure.

Pressurization of the fuel rod helps delay fuel/clad mechanical interaction. Fuel rod pressurization also precludes flattened rod formation when significant fuel densification occurs, although this phenomenon is not a problem in current generation fuel (Reference 25). The initial pressure, which may vary between batches of fuel, is selected to ensure that the internal pressure of the lead rod in the reactor will remain below a value that could cause the diametral gap to increase due to outward creep during steady-state operation and that could cause extensive DNB propagation to occur (Reference 14).

A two component fission gas release model is used, with one component giving the gas release from the high fuel temperature regions of the high power rods and the second component giving the major contribution to the gas release from the normal power rods and the cooler outer regions of the high power rods. The high temperature gas release model is based on concepts drawn from mechanistic models of gas release, while the low temperature model is an empirical correlation. The total fractional gas release is obtained by adding the high and low temperature contributions (Reference 13). The gas release is calculated for each axial zone of the fuel rod, and summed to obtain the total fission gas release that is used to calculate the rod internal pressure.

The code shows good agreement in fit for a variety of published and proprietary data on fission gas release, fuel temperatures, and clad creep (References 13 & 26).

Included in this spectrum are variations in power, time, fuel density, and geometry. The inpile fuel temperature measurement comparisons used are identified in Reference 12.

An example of the variation in fuel clad inner diameter and fuel pellet outer diameter as a function of exposure, based on a fuel rod for the initial North Anna core, is presented in Figure 4.2-8. The cycle to cycle changes in the pellet outer diameter represent the effects of power changes as the fuel is moved into different positions as a result of refueling. The gap size at any time is merely the difference between clad inner diameter and pellet outer diameter. Total clad-pellet surface contact typically occurs before the end of cycle 2. The dimensions shown in Figure 4.2-8 were based on the fuel rod operating history shown in the lower portion of Figure 4.2-9. Figure 4.2-9 illustrates the variation in fuel rod internal gas pressure versus irradiation time for a high burnup rod in the initial North Anna core. The linear power versus time used to determine these pressures is also illustrated. In addition, it identifies the range of internal gas pressure that would typically be predicted for the other fuel rods in the same region of initial core fuel. A “best estimate” fission gas release model was used in determining the internal gas pressures as a function of irradiation time. The fuel rod has been designed to provide sufficient void volume to ensure that the maximum internal pressure of the gas in the fuel rod will not exceed the pressure that could cause the fuel-clad diametrical gap to increase due to outward clad creep during steady-state operation. Conservative calculations of the rod internal pressure are performed each reload cycle to confirm that this pressure criterion will be satisfied for all the fuel in the core for the cycle specific operating conditions.

The clad stresses at a constant local fuel rod power are low. Stresses are created by the pressure differential between the coolant pressure and the rod internal pressure. These will typically be compressive stresses, but tensile stresses will be created if the rod internal pressure exceeds the external pressure. Because of the prepressurization with helium, the volume average effective stresses remain substantially below the clad stress design limit. Stresses due to the temperature gradient are not included in this average effective stress because thermal stresses are, in general, negative at the clad inner diameter and positive at the clad outer diameter and their contribution to the clad volume average stress is small. Furthermore, the thermal stress decreases with time during steady-state operation due to stress relaxation. The stress due to pressure differential is typically highest in fuel with low beginning of life internal gas pressure (the minimum power rod in the initial core, or fresh fuel in reload cores), and the thermal stress is highest in the maximum power rod (due to steep temperature gradient).

Tensile stresses could be created once the clad has come in contact with the pellet. These stresses are induced by the fuel pellet swelling during irradiation. As illustrated in Figure 4.2-8 for an initial core rod, there is very limited clad pushout after pellet-clad contact. For current reload fuel, the end of life cladding diameter will be slightly greater than shown in Figure 4.2-8 because of the higher burnups typically attained by reload fuel. Fuel swelling can result in small clad strains (less than 1%) for expected discharge burnups, but the associated clad stresses are very low because of clad creep (thermal and irradiation-induced creep). Furthermore, the 1% strain criterion is extremely conservative for fuel-swelling driven clad strain because the strain rate associated with solid fission products swelling is very slow (approximately 5×10^{-7} hr-1). Inpile experiments have shown that Zirconium alloy tubing exhibits “super-plasticity” at slow strain rates during neutron irradiation (Reference 16). Uniform clad strains of more than 10% have been achieved under these conditions with no sign of plastic instability.

Transient Evaluation Method

During power changes, the fuel pellet outer diameter changes due to thermal expansion. Power escalations or spikes early in life do not lead to hard clad-pellet interaction since the pellet merely expands into the gap. Power increases that occur after considerable gap closure will result in hard clad-pellet interaction. The extent of the interaction determines the clad stress level.

Pellet thermal expansion due to power increases is considered the only mechanism by which significant stresses and strains can be imposed on the clad. Power increases in commercial fuel rods can result from fuel repositioning during refueling outages (e.g., movement of a fuel assembly from near the periphery in its first operating cycle to a more interior location in its second operating cycle), reactor power escalation following extended reduced-power operation, and control rod movement. In the fuel rod mechanical design model, limiting rods for the clad stress criterion are depleted using best-estimate power histories from core physics calculations. During the depletion, the amount of diametral gap closure is evaluated based upon the fuel densification and swelling models, as well as the clad-creep model. At various times during the depletion, the power is increased locally on the rod to the burnup-dependent attainable power

density as determined by core physics calculations. The radial, tangential, and axial clad stresses resulting from the power increase are combined into a volume average effective clad stress.

The volume-averaged von Mises effective stress is used to determine whether the clad stress design basis is exceeded. The yield stress correlation is that for irradiated cladding since the fuel/clad interaction occurs at sufficiently high burnup that the cladding will have experienced irradiation hardening. Furthermore, the effective stress is increased by an allowance, which accounts for stress concentrations in the clad adjacent to radial cracks in the pellet, prior to the comparison with the yield stress. This allowance was evaluated using a two-dimensional (r, θ) finite element model.

Slow transient power increases can result in large clad strains without exceeding the clad yield stress because of clad creep and stress relaxation. Therefore, in addition to the yield stress criterion, a criterion on allowable clad positive strain is necessary. Based upon high strain rate burst and tensile test data on irradiated tubing, 1% strain was determined to be the lower limit on irradiated clad ductility, and thus adopted as a design criterion.

In addition to the mechanical design models and design criteria, Westinghouse relies on performance data accumulated through transient power test programs in experimental and commercial reactors, and through normal operation in commercial reactors.

It is recognized that a possible limitation to the satisfactory behavior of the fuel rods in a reactor that is subjected to daily load follow is the failure of the cladding by low cycle strain fatigue. (Cycle specific fatigue usage calculations are also performed for plants that do not load-follow.) During their normal residence time in reactor, the fuel rods may be subjected to approximately 1000 cycles with typical changes in power level from 50 to 100% of their steady-state values.

The assessment of the fatigue life of the fuel rod cladding is subjected to considerable uncertainty due to the difficulty of evaluating the strain range that results from the cyclic interaction of the fuel pellets and claddings. This difficulty arises, for example, from such highly unpredictable phenomena as pellet cracking, fragmentation, and relocation. Nevertheless, since early 1968, Westinghouse has been investigating this particular phenomenon both analytically and experimentally. Strain-fatigue tests on irradiated and nonirradiated hydrided Zircaloy-4 claddings were performed that permitted a definition of a conservative fatigue life limit and recommendation of methodology to treat the strain fatigue evaluation of the Westinghouse reference fuel rod designs.

However, Westinghouse is convinced that the final proof of the adequacy of a given fuel rod design to meet the load-follow requirements can only come from inpile experiments performed on actual reactors. The Westinghouse fuel experience in load-follow operation dates back to early 1970 with the load-follow operation of the Saxton reactor. Successful load-follow operation has been performed on reactor A (over 400 load-follow cycles) and reactor B (over 500 load-follow

cycles). In both cases, there was no significant coolant activity increase that could be associated with the load-follow mode of operation.

The following paragraphs present briefly the Westinghouse analytical approach to strain fatigue.

A comprehensive review of the available strain fatigue models was conducted by Westinghouse as early as 1968.

This included the Langer-O'Donnell model (Reference 18), the Yao-Munse model, and the Manson-Halford model. Upon completion of this review and using the results of the Westinghouse experimental programs discussed below, it was concluded that the approach defined by Langer-O'Donnell would be retained and the empirical factors of their correlation modified in order to conservatively bound the results of the Westinghouse testing program.

The Langer-O'Donnell empirical correlation has the following form:

$$S_a = \frac{E}{4\sqrt{N_f}} \ln \frac{100}{100 - RA} + S_e \qquad (4.2\text{-}1)$$

where:

$S_a = \frac{1}{2} E \Delta\varepsilon_t$ = pseudo-stress amplitude that causes failure in N_f cycles, lb/in.^{2}

$\Delta\varepsilon_t$ = total strain range, in./in.

E = Young's Modulus, lb/in^2

N_f = number of cycles to failure

RA = reduction in area at fracture in uniaxial tensile test,%

S_e = endurance limit, lb/in^2

Both RA and S_e are empirical constants that depend on the type of material, the temperature, and the irradiation. The Westinghouse testing program was subdivided in the following subprograms:

1. A rotating bend fatigue experiment on unirradiated Zircaloy-4 specimens at room temperature and at 725°F. Both hydrided and nonhydrided Zircaloy-4 cladding were tested.
2. A biaxial fatigue experiment in a gas autoclave on unirradiated Zircaloy-4 cladding, both hydrided and nonhydrided.
3. A fatigue test program on irradiated cladding from the Carolinas Virginia Tube Reactor (CVTR) and Yankee Core V conducted at Battelle Memorial Institute.

The results of these test programs provided information on different cladding conditions, including the effects of irradiation, of hydrogen level, and of temperature.

The Westinghouse design equations followed the concept for the fatigue design criterion according to Section III of the ASME Code.

1. The calculated pseudo-stress amplitude (S_a) has to be multiplied by a factor of two in order to obtain the allowable number of cycles (N_f).
2. The allowable cycles for a given S_a is 5% of N_f, or a safety factor of 20 on the allowable number of cycles.

The lesser of the two allowable numbers of cycles is selected. The cumulative fatigue life fraction is then computed as follows:

$$\sum_{1}^{k} \frac{n_k}{N_{fk}} \leq 1 \qquad (4.2\text{-}2)$$

where:

n_k = number of diurnal cycles of mode k

The potential effects of operation with waterlogged fuel are discussed in Section 4.4.3.6. Waterlogging is not considered to be a concern during operational transients.

4.2.1.3.2 Fuel Assembly Structure

Stresses and Deflections

The potential sources of high stresses in the assembly are avoided by the design. For example, stresses in the fuel rod due to thermal expansion and irradiation growth are limited by the relative motion of the rod as it slips over the grid spring and dimple surfaces. Sufficient distance is provided between the fuel assembly top and bottom nozzles to accommodate irradiation growth of the fuel rod cladding during the design lifetime of the fuel. As another example, stresses due to hold-down springs in opposition to the hydraulic lift force are limited by the deflection characteristic of the springs. Stresses in the fuel assembly caused by tripping of the rod cluster control assembly have little influence because of the small number of events during the life of an assembly. Welded mechanical joints in the fuel assembly structure are considered in the structural analysis of the assembly. Appropriate material properties are specified for all structural joints (both welded and mechanical) to ensure that the design bases are met.

Assembly components and prototype fuel assemblies made from production parts are subjected to structural tests to verify that the design bases requirements are met.

The fuel assembly is designed to withstand shipping loads of at least 4g axial and 6g lateral. Instrumentation is provided for the shipping container to detect fuel assembly accelerations that would result from loads in excess of the criteria. Exceeding the limits requires the reinspection of the fuel assembly for damage. Tests on various fuel assembly components such as the grid assembly, sleeves, inserts, and structure joints have been performed to ensure that the shipping design limits do not result in the impairment of fuel assembly function.

Seismic analysis of the LOPAR fuel assembly is presented in Reference 19. The structural integrity of the NAIF fuel assembly under seismic loads is addressed in Reference 7.

Dimensional Stability

Prior to irradiation in commercial reactors, a prototype LOPAR fuel assembly was subjected to column loads in excess of those expected in normal service and faulted conditions (Section 1.5). Full assembly testing also confirmed the mechanical hydraulic stability of the NAIF assembly design.

The coolant flow channels are established and maintained by the structure composed of grids and guide thimbles. The lateral spacing between fuel rods is provided and controlled by the support dimples of adjacent grid cells. For Inconel grids, contact of the fuel rods on the dimples is ensured by the force provided by the grid springs. Lateral motion of the fuel rods is opposed by the spring force and the internal moments generated between the spring and the support dimples. For the zirconium alloy mid-grids of the NAIF design, which experience greater material relaxation than the Inconel grids, the grids are designed to provide sufficient fuel rod support to limit fuel rod vibration and maintain cladding wear within acceptable limits. Testing of Inconel grids is discussed in Section 1.5, and testing of the zirconium-alloy mid-grids for the NAIF design is addressed in Reference 7.

No interference with control rod insertion into thimble tubes will occur during a postulated loss-of-coolant accident (LOCA) due to fuel rod swelling, thermal expansion, or bowing. In the early phase of the transient following the coolant break, the high axial loads that potentially could be generated by the difference in thermal expansion between fuel clad and thimbles are relieved by the slippage of the fuel rods through the grids. The relatively low drag force restraint on the fuel rods will only induce minor thermal bowing not sufficient to close the fuel rod-to-thimble tube gap. This rod-to-grid slip mechanism occurs simultaneously with control rod drop. Subsequent to the control rod insertion, the transient temperature increase of the fuel rod clad can result in swelling sufficient to contact the thimbles.

Vibration and Wear

The effect of flow-induced vibration on the fuel assembly and individual fuel rods is minimal. The cyclic stress range associated with deflections of such small magnitude is insignificant and has no effect on the structural integrity of the fuel rods.

The conclusion that the effect of flow-induced vibrations on the LOPAR fuel assembly and fuel rod is minimal is based on test results and analysis, documented in Reference 20, that take into consideration the conditions normally encountered in reactor operation. The high cross flows that produced the fuel rod failures in the Jose Cabrera plant were the result of a baffle leakage problem that was anomalous and is not normally included as part of the test programs.

To alleviate the problem in Jose Cabrera, a baffle repair operation was instituted during the 1972 refueling. The success of the repair was confirmed by the absence of failed rods at the baffle locations as verified by inspection during the 1973 refueling.

The reaction on the grid support due to vibration motions is also small. For Inconel grids, the reaction is less than the spring preload. Firm contact is maintained between these grids and the fuel rods, so no significant wear of the cladding or grid supports is expected during the life of the fuel assembly. For zirconium alloy grids that experience greater material relaxation with irradiation, the magnitude of the grid restraining force on the fuel rod is designed to minimize possible fretting due to vibration motion.

Clad fretting and fuel rod vibration were experimentally investigated for the LOPAR design, as discussed in Section 1.5.

Pressure drop results from comparative fuel assembly flow testing, performed prior to the introduction of the NAIF fuel at North Anna, indicated that the NAIF and the LOPAR 17 x 17 fuel assemblies are hydraulically equivalent (Reference 7). Full assembly testing also confirmed the hydraulic stability of the NAIF design prior to its introduction at North Anna (Reference 7). The same testing indicated that the expected fuel rod contact wear with the spacer grids would be within the allowable design limits. Additionally, starting with North Anna 2 Batch 12 (fresh feed to Cycle 10) and North Anna 1 Batch 13 (fresh feed to Cycle 11), every other mixing vane (Zircaloy-4 or ZIRLO) grid has been rotated 90 degrees to minimize the susceptibility of the fuel assembly to flow induced vibration. There were no associated physical or material changes to the grids or their axial positions, and the change did not impact the thermal-hydraulic performance of the North Anna fuel.

4.2.1.3.3 Operational Experience

A discussion of fuel operating experience is given in Reference 2.

4.2.1.4 **Tests and Inspections**

4.2.1.4.1 Quality Assurance Program

The Quality Assurance Program of the Westinghouse Nuclear Fuel Division, as summarized in Reference 21, has been developed to serve the division in planning and monitoring its activities for the design and manufacture of nuclear fuel assemblies and associated components.

The program provides for control over all activities affecting product quality, commencing with design and development and continuing through procurement, materials handling, fabrication, testing and inspection, storage, and transportation. The program also provides for the indoctrination and training of personnel and for the auditing of activities affecting product quality through a formal auditing program.

4.2.1.4.2 Manufacturing

Quality control philosophy is generally based on the following inspections being performed to a 95% confidence that at least 95% of the product meets specification, unless otherwise noted.

1. Component Parts

   The characteristics inspected depend upon the component parts and include dimensional, visual, check audits of test reports, material certification, and nondestructive testing such as x-ray and ultrasonic testing.

   All materials used in the manufacture of fuel assemblies and core components are accepted and released by Quality Control.

2. Pellets

   Inspection is performed to 95% confidence level for the dimensional characteristics such as diameter, density, length and squareness of ends. Additional visual inspections are performed for cracks, chips, and surface conditions according to established standards.

   Density is determined in terms of weight per unit length. Chemical analyses are performed on each blend of pellets.

3. Rod Inspection

   Fuel rod, control rodlet, burnable poison, and source rod inspection consists of the following nondestructive examination techniques and methods as applicable:

   a. Leak Testing

   Each rod is leak tested using a calibrated mass spectrometer, with helium being the detectable gas.

   b. Enclosure Welds

   Rod welds are inspected by ultrasonic test or, alternatively, x-ray in accordance with a qualified technique and vendor specification meeting the requirements of applicable ASTM standards. Beginning with Cycle 18 at both units, the feed fuel and burnable poison rods are fabricated with a new end plug welding process, and the vendor no longer performs ultrasonic testing or x-ray on these components.

   c. Dimensional

   All rods are dimensionally inspected prior to final release. The requirements include such items as length, camber, and visual appearance.

   d. Plenum Dimensions

   All rods are inspected by gamma scanning or other approved methods to ensure proper plenum dimensions.

e. Pellet-to-Pellet Gaps

All rods are inspected by gamma scanning or other approved methods to ensure that no significant gaps exist between pellets.

f. Enrichment

All fuel rods are active gamma scanned to verify enrichment control prior to acceptance for assembly loading.

g. Traceability

Traceability of rods and associated rod components is established by Quality Control.

4. Assemblies

Each fuel, control rod, burnable poison and source rod assembly is inspected for compliance with drawing and/or specification requirements.

5. Other Inspections

The following inspections are performed as part of the routine inspection operation:

a. Measurements, other than those specified above, that are critical to thermal and hydraulic analyses are obtained to enable the evaluation of manufacturing variations to a 95% confidence level.

b. Tool and gauge inspection and control includes standardization to primary and/or secondary working standards. Tool inspection is performed at prescribed intervals on all serialized tools. Complete records are kept of the calibration and condition of tools.

c. Audits are performed of inspection activities and records to ensure that prescribed methods are followed and that all records are correct, complete, and properly maintained.

d. Surveillance inspections where appropriate, and audits of outside contractors, are performed to ensure conformance with all final specific requirements.

6. Process Control

To prevent the possibility of mixing enrichments during fuel manufacture and assembly, strict enrichment segregation and other process controls are exercised. The UO_2 powder is kept in sealed containers. The contents are fully identified by preselected color coding. Isotopic content is confirmed by analysis.

Powder withdrawal from storage can only be made by authorized groups who direct the powder to the correct pellet production line. All pellet production lines are physically separated from each other and pellets of only a single enrichment are produced in a given production line or a segregated part of the line.

Finished pellets are placed on trays identified to maintain traceability, and are transferred to segregated storage racks within the confines of the pelleting area. Samples from each pellet lot are tested for isotopic content, impurity levels, and physical characteristics before acceptance by Quality Control. Physical barriers prevent mixing of pellets of different nominal densities and enrichments in this storage area. Unused powder and substandard pellets are returned to storage.

Loading of pellets into the cladding is performed in isolated production lines, and again only one enrichment is loaded on a line at a time.

A barcode is laser etched on each fuel tube that provides traceability information. The end plugs are inserted and inert welded to seal the tube. The fuel tube remains coded and traceability identified. The barcode provides a reference of the fuel pellets contained in the fuel rods.

At the time of installation into an assembly, a matrix is generated to establish each rod position within a given assembly. After the fuel rods are installed an inspector verifies that all fuel rods in an assembly carry the correct identification character describing the fuel enrichment and density for the core region being fabricated. The top nozzle is inscribed with a permanent identification number providing traceability to the fuel contained in the assembly.

Removable traceability stickers are provided for burnable absorber source rods and control rods during the manufacturing process. These stickers are removed during final assembly of the core component.

4.2.1.4.3 New Fuel and Insert Component Inspection

Detailed written procedures are used by the station staff and nuclear fuel quality assurance personnel for the preshipment and postshipment inspection of all new fuel and associated insert components such as control rods, thimble plugs, burnable poison rod assemblies, and primary/secondary source insert components. The procedures are specific and have been field-tested. Quality assurance personnel audit the data or information compiled as a result of the use of these procedures. A master fuel-handling procedure specifies the sequence in which handling and inspection takes places.

Specifically, the procedures for inspection of new fuel assemblies and associated insert components require the following:

1. Surveying the new-fuel shipping containers for radiation and contamination levels.
2. External inspection of new-fuel shipping containers for visible signs of damage, including integrity of seals.
3. Checking the condition of new-fuel shipping container accelerometers for indications of improper handling.

4. Observing the physical condition of the inside of new-fuel shipping containers, including hardware used to secure fuel assemblies and associated insert components.
5. Verifying fuel assembly and insert component (if any) serial numbers.
6. Visual inspection of new fuel assembly and insert component (for foreign material, manufacturing defects, and physical damage).
7. Performing drag test measurements on the new fuel assembly and RCCA inserts. For other inserts check to see if they are seated. If not, drag test these inserts (e.g., burnable poison assemblies). Fuel assembly drag testing is either performed by the vendor prior to shipment, or during postshipment inspections.
8. Checking the radiation and contamination level of the new fuel assembly.

Surveillance of fuel and reactor performance is routinely conducted on Westinghouse reactors. Power distribution is monitored using the ex-core fixed and incore movable detectors. Coolant activity and chemistry are followed, which permits early detection of any fuel clad defects.

Visual fuel inspection is routinely conducted during refueling to detect such problems as grid strap damage, fuel rod bow, and fuel assembly bow or twist. Additional fuel inspections are dependent on the results of the operational monitoring and the visual inspections. The fuel handling system is described in Section 9.1.4.

The first available Westinghouse 17 x 17 irradiated fuel assemblies and rods (of the North Anna design) underwent an extended surveillance program following each cycle of operation. Onsite examinations included fuel rod integrity, fuel rod and fuel assembly dimensions and alignment, and surface deposits. Both non-destructive and destructive examinations were also conducted at a hot cell on removable rods from some of the first 17 x 17 fuel assemblies to be irradiated. Hot cell examinations were performed on twelve fuel rods taken from one of these assemblies. Onsite fuel examinations used hardware that had previously been employed at such reactors as Saxton, Ginna, San Onofre, and Cabrera. The inspection of reactor internals is discussed in Section 3.9.1.2.4.

The following information is HISTORICAL and is not intended or expected to be updated for the life of the plant.

4.2.1.4.4 Removable Fuel Rod Assembly

One surveillance fuel assembly, containing 88 removable fuel rods, was included in region 3 of the initial North Anna core loading. This was to facilitate interim and end-of-life fuel evaluation as a function of exposure, if such an evaluation is performed. The rods can be removed, nondestructively examined, and reinserted at the end of intermediate fuel cycles. At end of life, the rods can be removed easily and subjected to a destructive examination.

The following information is HISTORICAL and is not intended or expected to be updated for the life of the plant.

The overall dimensions, rod pitch, number of rods, and materials are the same as for other region 3 assemblies. These fuel rods will be fabricated in parallel with the regular region 3 rods, using selected region 3 clad and pellets, assembled and released to the same manufacturing tolerance limits. Mechanically, the special assemblies differ only slightly from other region 3 assemblies. These differences are as follows:

1. The end plugs on the removable rods are designed to facilitate removal and reinsertion.
2. The upper nozzle adapter plate on the assembly is modified to allow access to the removable rods.
3. The baseplate on the thimble plug assembly is modified to provide axial restraint of the fuel rods normally provided by the upper nozzle adapter plate for standard assemblies. The distances between the top of the rods and the restraining plates, for both types of rods in the removable rod assembly, are identical to those of the standard assembly.

Figure 4.2-10 compares the mechanical design of a removable fuel rod to that of a standard rod; Figure 4.2-11 shows the removable rod fuel assembly, the modified upper nozzle adapter plate, and thimble plug assembly, to compare with a standard assembly shown in Figure 4.2-2. The location of the removable rods within the fuel assembly is shown in Figure 4.2-12.

Previous experience with removable rods has been attained at Saxton, Yankee, San Onofre, Zorita, Zion Unit 1, Point Beach Unit 1, H. B. Robinson Unit 2, and Surry Unit 1 reactors. Over 300 fuel rods were removed and reinserted into assemblies during the Saxton reconstitution without evidence of failure. Leak-detection tests were performed on the assemblies after all rods were reinserted, and no leakage was detected. An equally large number of rods have been successfully removed, examined, and reinserted into more than 12 3 x 3 subassemblies at Saxton. In addition, 28 full-length rods were removed, examined, and reinserted into Yankee Core V special assemblies. Similar handling of removable rods was successfully completed during San Onofre and Zorita refuelings. All such fuel handlings have been done routinely and without difficulty.

The following information is HISTORICAL and is not intended or expected to be updated for the life of the plant.

The same fuel rod design limits indicated in Section 4.2.1 for standard fuel rods and assemblies are maintained for these removable rods. Over the active fuel length, the removable rod cladding and pellet dimensions and enrichment are identical to other rods in the same fuel region. Therefore, there is no reduction in margin to departure from nucleate boiling (DNB) or other thermal limits. Their inclusion in the initial North Anna core loading introduces no additional safety considerations and in no way changes the safeguard analyses and related engineering information presented in previously submitted material in support of the license application.

4.2.2 Reactor Vessel Internals

4.2.2.1 Design Bases

The design bases for the mechanical design of the reactor vessel internals components are as follows:

1. The reactor internals in conjunction with the fuel assemblies shall direct reactor coolant through the core to achieve acceptable flow distribution and to restrict bypass flow so that the heat transfer performance requirements are met for all modes of operation. In addition, required cooling for the pressure vessel head is provided so that the temperature differences between the vessel flange and head do not result in leakage from the flange during reactor operation.
2. In addition to neutron shielding provided by the reactor coolant, a separate thermal shield is provided to limit the exposure of the pressure vessel in order to maintain the required ductility of the material for all modes of operation.
3. The reactor vessel internals include provisions for installation of incore instrumentation useful for the plant operation, and vessel material test specimens required for a pressure vessel irradiation surveillance program.
4. The core internals are designed to withstand mechanical loads arising from the operating-basis earthquake, the design-basis earthquake, and pipe ruptures, and to meet the requirement of item 5 below.
5. The reactor shall have mechanical provisions that are sufficient to adequately support the core and internals and to ensure that the core is intact, with acceptable heat transfer geometry following transients arising from abnormal operating conditions.
6. Following the design-basis accident, the plant shall be capable of being shut down and cooled in an orderly fashion so that the fuel cladding temperature is kept within specified limits. This implies that the deformation of certain critical reactor internals must be kept sufficiently small to allow core cooling.

The functional limitations for the core structures during the design-basis accident are shown in Table 4.2-1. To ensure no column loading of rod cluster control guide tubes, the upper core plate deflection is limited so as not to exceed the value shown in Table 4.2-1.

Details of the dynamic analyses, input forcing functions, and response loadings are presented in Section 3.9.

4.2.2.2 **Description and Drawings**

The components of the reactor internals consist of the lower core support structure (including the entire core barrel and thermal shield), the upper core support structure, and the incore instrumentation support structure. The reactor internals support the core, maintain fuel alignment, limit fuel assembly movement, maintain alignment between fuel assemblies and control rod drive mechanisms, direct coolant flow past the fuel elements, direct coolant flow to the pressure vessel head, provide gamma and neutron shielding, and provide guides for the incore instrumentation. The coolant flows from the vessel inlet nozzles down the annulus between the core barrel and the vessel wall and then into a plenum at the bottom of the vessel. It then reverses and flows up through the core support and through the lower core plate. The lower core plate is sized to provide the desired inlet flow distribution to the core. After passing through the core, the coolant enters the region of the upper support structure and then flows radially to the core barrel outlet nozzles and directly through the vessel outlet nozzles. A small portion of the coolant flows between the baffle plates and the core barrel to provide additional cooling of the barrel. Similarly, a small amount of the entering flow is directed into the vessel head plenum and exits through the vessel outlet nozzles.

The North Anna Unit 1 reactor internals have been modified to change the flow path of the reactor coolant from downflow between the core barrel and baffle plates to an upflow direction. This was accomplished by plugging the core barrel flow holes and creating new flow holes in the top former plate. The Unit 2 Reactor Internals were not modified.

All the major material for the reactor internals is type 304 stainless steel. Parts not fabricated from type 304 stainless steel include bolts and dowel pins, which are fabricated from type 316 stainless steel. The radial support clevis insert and bolts are fabricated from Inconel. The only stainless steel materials used in the reactor core support structures that have yield strengths greater than 90,000 lb are the 403 series used for hold-down springs. The use of these materials is compatible with the reactor coolant and is acceptable based on the 1971 ASME Boiler and Pressure Vessel Code, Case Number 1337.

All reactor internals are removable from the vessel for the purpose of their inspection as well as the inspection of the vessel internal surface.

Lower Core Support Structure

The major containment and support member of the reactor internals is the lower core support structure, shown in Figure 4.2-13. This support structure assembly consists of the core

barrel, the core baffle, the lower core plate and support columns, the thermal shield, and the core support that is welded to the core barrel. All the major material for this structure is type 304 stainless steel. The lower core support structure is supported at its upper flange from a ledge in the reactor vessel and its lower end is restrained from transverse motion by a radial support system attached to the vessel wall. Within the core barrel are an axial baffle and a lower core plate, both of which are attached to the core barrel wall and form the enclosure periphery of the core. The lower core support structure and core barrel provide passageways and direct the coolant flow. The lower core plate is positioned at the bottom level of the core below the baffle plates and provides support and orientation for the fuel assemblies.

The lower core plate is a member through which the necessary flow distribution holes for each fuel assembly are machined. Fuel assembly locating pins (two for each assembly) are also inserted into this plate. Columns are placed between the lower core plate and the core support of the core barrel to provide stiffness and to transmit the core load to the core support. Adequate coolant distribution is obtained through the use of the lower core plate and core support.

The one-piece thermal shield is fixed to the core barrel at the top with rigid bolted connections. The bottom of the thermal shield is connected to the core barrel by means of axial flexures. This bottom support allows for differential axial growth of the shield/core barrel but restricts radial or horizontal movement of the bottom of the shield. Rectangular specimen guides in which material samples can be inserted and irradiated during reactor operation are welded to the thermal shield and extended to the top of the thermal shield. These samples are held in the rectangular specimen guides by a preloaded spring device at the top and bottom.

Vertically downward loads from weight, fuel assembly preload, control rod dynamic loading, hydraulic loads, and earthquake acceleration are carried by the lower core plate into the lower core plate support flange on the core barrel shell and through the lower support columns to the core support and thence through the core barrel shell to the core barrel flange supported by the vessel flange. Transverse loads from earthquake acceleration, coolant cross flow, and vibration are carried by the core barrel shell and distributed between the lower radial support to the vessel wall, and to the vessel flange. Transverse loads of the fuel assemblies are transmitted to the core barrel shell by direct connection of the lower core plate to the barrel wall and by upper core plate alignment pins that are welded into the core barrel.

The radial support system of the core barrel is accomplished by “key” and “keyway” joints to the reactor vessel wall. At six equally spaced points around the circumference, an Inconel clevis block is welded to the vessel inner diameter. An Inconel insert block is bolted to each of these clevis blocks, and has a keyway geometry. Opposite each of these is a key that is welded to the lower core support. At assembly, as the internals are lowered into the vessel, the keys engage the keyways in the axial direction. With this design, the internals are provided with a support at the further extremity, and may be viewed as a beam fixed at the top and simply supported at the bottom.

Radial and axial expansions of the core barrel are accommodated, but transverse movement of the core barrel is restricted by this design. With this system, cyclic stresses in the internal structures are within the ASME Code Section III limits. In the event of an abnormal downward vertical displacement of the internals following a hypothetical failure, energy-absorbing devices limit the displacement of the core after contacting the vessel bottom head. The load is then transferred through the energy-absorbing devices of the lower internals to the vessel.

The energy absorbers are mounted on a baseplate that is contoured on its bottom surface to the reactor vessel bottom internal geometry. Their number and design are determined so as to limit the stresses imposed on all components except the energy absorber to less than yield (ASME Code, Section III, 1968 Code Winter Addenda). Assuming a downward vertical displacement, the potential energy of the system is absorbed mostly by the strain energy of the energy-absorbing devices.

Upper Core Support Assembly

The upper core support assembly, shown in Figures 4.2-14 and 4.2-15, consists of the upper support assembly and the upper core plate between which are contained support columns and guide tube assemblies. The support columns establish the spacing between the upper support assembly and the upper core plate and are fastened at top and bottom to these plates. The support columns transmit the mechanical loadings between the upper support and upper core plate.

The guide tube assemblies shield and guide the control rod drive rods and control rods. They are fastened to the upper support and are guided by pins in the upper core plate for proper orientation and support. Additional guidance for the control rod drive rods is provided by the upper guide which is attached to the upper support.

The upper core support assembly, which is removed as a unit during refueling operation, is positioned in its proper orientation with respect to the lower support structure by slots in the upper core plate that engage flat-sided upper core plate alignment pins that are welded into the core barrel. At an elevation in the core barrel where the upper core plate is positioned, the flat-sided pins are located at angular positions of 90 degrees from each other. As the upper support structure is lowered into the lower internals, the slots in the plate engage the flat-sided pins in the axial direction. Lateral displacement of the plate and of the upper support assembly is restricted by this design. Fuel assembly locating pins protrude from the bottom of the upper core plate and engage the fuel assemblies as the upper assembly is lowered into place. Proper alignment of the lower core support structure, the upper core support assembly, the fuel assemblies, and control rods is thereby ensured by this system of locating pins and guidance arrangement. The upper core support assembly is restrained from any axial movements by a large circumferential spring that rests between the upper barrel flange and the upper core support assembly. The spring is compressed when the reactor vessel head is installed on the pressure vessel.

Vertical loads from weight, earthquake acceleration, hydraulic loads, and fuel assembly preload are transmitted through the upper core plate via the support columns to the upper support

assembly and then into the reactor vessel head. Transverse loads from coolant cross flow, earthquake acceleration, and possible vibrations are distributed by the support columns to the upper support and upper core plate. The upper support plate is particularly stiff to minimize deflection.

Incore Instrumentation Support Structures

The incore instrumentation support structures consist of an upper system to convey and support thermocouples penetrating the vessel through the head and a lower system to convey and support flux thimbles penetrating the vessel through the bottom. (Figure 7.7-13 shows the basic flux-mapping system.)

The upper system uses the reactor vessel head penetrations. Instrumentation port columns are slip-connected to in-line columns that are in turn fastened to the upper support plate. These port columns protrude through the head penetrations. The thermocouples are carried through these port columns and the upper support plate at positions above their readout locations. The thermocouple conduits are supported from the columns of the upper core support system. The thermocouple conduits are type 304 stainless steel tubes.

In addition to the upper incore instrumentation, there are reactor vessel bottom port columns that carry the retractable, cold-worked stainless steel flux thimbles that are pushed upward into the reactor core. Conduits extend from the bottom of the reactor vessel down through the concrete shield area and up to a thimble seal line. The minimum bend radii are about 144 in. and the trailing ends of the thimbles (at the seal line) are extracted approximately 15 feet during refueling of the reactor in order to avoid interference within the core. The thimbles are closed at the leading ends and serve as the pressure barrier between the reactor pressurized water and the containment atmosphere.

Mechanical seals between the retractable thimbles and the conduits are provided at the seal line. During normal operation, the retractable thimbles are stationary and move only during refueling or for maintenance, at which time a space of approximately 15 feet above the seal line is cleared for the retraction operation.

The incore instrumentation support structure is designed for adequate support of instrumentation during reactor operation and is rugged enough to resist damage or distortion under the conditions imposed by handling during the refueling sequence. These are the only conditions that affect the incore instrumentation support structure. Reactor vessel surveillance specimen capsules are covered in Section 5.4.3.6. That section covers all the necessary details with regard to irradiation surveillance, including a cross section of the reactor showing the capsule identity and location.

4.2.2.3 **Design-Loading Conditions**

The design-loading conditions that provide the basis for the design of the reactor internals are the following:

1. Fuel assembly weight.
2. Fuel assembly spring forces.
3. Internals weight.
4. Control rod scram (equivalent static load).
5. Differential pressure.
6. Spring preloads.
7. Coolant flow forces (static).
8. Temperature gradients.
9. Differences in thermal expansion
   a. Due to temperature differences.
   b. Due to expansion of different materials.
10. Interference between components.
11. Vibration (mechanically or hydraulically induced).
12. One or more loops out of service.
13. All operational transients listed in Table 5.2-4.
14. Pump overspeed.
15. Seismic loads (operating-basis earthquake and design-basis earthquake).
16. Blowdown forces (due to cold- and hot-leg break).

Combined seismic and blowdown forces are included in the stress analysis as a design-loading condition by assuming the maximum amplitude of each force to act concurrently.

The main objectives of the design analysis are to satisfy allowable stress limits, to ensure an adequate design margin, and to establish deformation limits that are concerned primarily with the functioning of the components. The stress limits are established not only to ensure that peak stresses will not reach unacceptable values, but also to limit the amplitude of the oscillatory stress component in consideration of fatigue characteristics of the materials. Both low- and high-cycle fatigue stresses are considered when the allowable amplitude of oscillation is established. Dynamic analyses on the reactor internals are provided in Section 3.9.

As part of the evaluation of design-loading conditions, extensive testing and inspections are performed from the initial selection of raw materials up to and including component installation and plant operation. Among these tests and inspections are those performed during component fabrication, plant construction, start-up and checkout, and during plant operation.

4.2.2.4 **Design-Loading Categories**

The combination of design loadings fits into either the normal, upset, or faulted conditions as defined in the ASME Code, Section III, 1968, Winter Addenda.

Loads and deflections imposed on components from shock and vibration are determined analytically and experimentally in both scaled modes and operating reactors. The cyclic stresses due to these dynamic loads and deflections are combined with the stresses imposed by loads from component weights, hydraulic forces, and thermal gradients for the determination of the total stresses of the internals.

The reactor internals are designed to withstand stresses originating from various operating conditions as summarized in Table 5.2-4.

The scope of the stress analysis problem is very large and requires many different techniques and methods, both static and dynamic. The analysis performed depends on the mode of operation under consideration.

Allowable Deflections

For normal operating conditions, downward vertical deflection of the lower core support plate is negligible.

For the LOCA plus the design-basis earthquake condition, the deflection criteria of critical internal structures are the limiting values given in Table 4.2-1. The corresponding no-loss-of-function limits are included in Table 4.2-1 for comparison purposes with the allowed criteria.

The criteria for the core-drop accident are based upon analyses that have been performed to determine the total downward displacement of the internal structures following a hypothesized core drop resulting from loss of the normal core barrel supports. The initial clearance between the secondary core support structures and the reactor vessel lower head in the hot condition is approximately 0.5 inch. An additional displacement of approximately 0.75 inch would occur due to the strain of the energy-absorbing devices of the secondary core support; thus the total drop distance is about 1.25 inches, which is insufficient to permit the tips of the rod cluster control assembly to come out of the guide thimble in the fuel assemblies.

Specifically, the secondary core support is a device that will never be used, except during a hypothetical failure of the core support (core barrel, barrel flange, etc.). There are four supports in each reactor. This device limits the fall of the core and absorbs the energy of the fall that would

otherwise be imparted to the vessel. The energy of the fall is calculated assuming a complete and instantaneous failure of the primary core support and is absorbed during the plastic deformation of the controlled volume of stainless steel, loaded in tension. The maximum deformation of this austenitic stainless piece is limited to approximately 15%, after which a positive step is provided to ensure support.

For additional information on design-loading categories, see Section 3.9.

4.2.2.5 Design Criteria Bases

The bases for the design stress and deflection criteria are identified below.

Allowable Stress

For normal operating conditions, Section III (1971) of the ASME Nuclear Power Plant Components Code is used as a basis for evaluating acceptability of calculated stresses. Both static and alternating stress intensities are considered. Under code case 1618, bolt material type 316 stainless steel is now covered in ASME Code, Section III, and is so treated. It should be noted that the allowable stresses in Section III are based on unirradiated material properties. In view of the fact that irradiation increases the strength of the 304 stainless steel used for the internals, although decreasing its elongation, it is considered that use of the allowable stresses in Section III is appropriate and conservative for irradiated internal structures.

The allowable stress limits during the design-basis accident used for the core support structures are based on the January 1971 draft of the ASME Code for Core Support Structures, Subsection NG, and the Criteria for Faulted Conditions.

4.2.3 Reactivity Control System

4.2.3.1 Design Bases

Bases for temperature, stress on structural members, and material compatibility are imposed on the design of the reactivity control components.

4.2.3.1.1 Design Stresses

The reactivity control system is designed to withstand stresses originating from various operating conditions as summarized in Table 5.2-4.

Allowable Stresses

For normal operating conditions, ASME Code Section III is used. All components are analyzed as Class I components under Article NB-3000, with the exception of burnable poison assemblies, which meet the stress allowables of Subsection NG-3000.

Dynamic Analysis

The determination of the total stresses on the reactivity control system includes the cyclic stresses due to dynamic loads and deflections, as well as the stresses imposed by loads from component weights, hydraulic forces, and thermal gradients.

4.2.3.1.2 Material Compatibility

Materials are selected for compatibility in a pressurized-water reactor (PWR) environment, for adequate mechanical properties at room and operating temperatures, for resistance to adverse property changes in a radioactive environment, and for compatibility with interfacing components.

4.2.3.1.3 Reactivity Control Components

Reactivity control components used at North Anna include rod cluster control assemblies, burnable poison assemblies, optional neutron source assemblies, and optional thimble plug assemblies. Although the thimble plug assembly does not directly contribute to the reactivity control of the reactor, it is presented as a reactivity control system component in this document because it may be used to restrict bypass flow through those thimbles not occupied by absorber, source, or burnable poison rods. The design bases for each of the mentioned components are described below.

Absorber Rods

The design requirements for the North Anna control rods included the following:

1. The external pressure equal to the reactor coolant system operating pressure.
2. The wear allowance equivalent to at least 750 reactor trips.
3. Bending of the rod due to a misalignment in the guide tube.
4. Forces imposed on the rods during rod drop.
5. Loads caused by accelerations imposed by the control rod drive mechanism.
6. Radiation exposure.

The materials used in the control rods are selected based on their corrosion resistance, susceptibility to stress corrosion cracking, wear characteristics, embrittlement properties, and compatibility with interfacing components on the operating environment. Stainless steel components, such as the high purity type 304 stainless steel used for the control rod clad, must meet the requirements of Regulatory Guide 1.44.

The absorber material temperature is not expected to exceed its melting temperature (1470°F for Ag-In-Cd absorber material Reference 22) except under LOCA conditions.

Based on a conservative LOCA peak clad temperature, an evaluation of absorber rod temperature was made that indicates no melting of the poison material will occur adjacent to the fuel clad hot spot following a LOCA. Although the rod is not expected to melt, it should be noted that if the Ag-In-Cd were assumed to melt at the hot spot, the stainless steel cladding would maintain the integrity of the rod and the melting would be a small local effect.

Burnable Poison Rods

The current burnable poison rod cladding is designed to maintain stresses within the limits based on Subsection NG-3000 (Core Support Structures) of the ASME Code, Section III, for Conditions I and II. The ASME Code is used as a general guide in classifying stresses into various categories, and combining these stresses to determine stress intensities. For abnormal loads during Conditions III and IV, Code type stresses are not considered limiting. Failures of the burnable poison rods during these conditions must not interfere with reactor shutdown or emergency cooling of the fuel rods.

The burnable poison absorber material is nonstructural. The structural elements of the burnable poison rod are designed to maintain the absorber geometry even if the absorber material is fractured.

Neutron Source Rods

If used in the core (optional), the neutron source rods are designed to withstand the following:

1. An external pressure equal to the reactor coolant system operating pressure.
2. An internal pressure equal to the pressure generated by released gases over the source rod life.

Thimble Plug Assembly

If used in the core (optional), the thimble plug assemblies satisfy the following criteria:

1. They accommodate the differential thermal expansion between the fuel assembly and the core internals.
2. They maintain positive contact with the fuel assembly and the core internals.
3. They are inserted into or withdrawn from the fuel assembly by a force not to exceed 65 lb.

4.2.3.1.4 Control Rod Drive Mechanisms

The mechanisms are Class I components designed to meet the stress requirements for normal operating conditions of ASME Code Section III (see Table 5.2-1 for codes applicable to specific components). Both static and alternating stress intensities are considered. The stresses originating from the required design transients are included in the analysis.

A dynamic seismic analysis is required on the control rod drive mechanism when a seismic disturbance has been postulated to confirm the ability of the mechanism to meet ASME Code Section III (1968 Edition through Winter 1968 Addenda) allowable stresses and to confirm its ability to trip when subjected to the seismic disturbance.

The control rod drive mechanism design used for the 17 x 17 fuel assembly control rod is identical to the 15 x 15 control rod drive mechanism. The seismic analysis and response of the 17 x 17 control rod drive mechanism are identical to those of the 15 x 15 mechanisms.

Control Rod Drive Mechanism Operational Requirements

The basic operational requirements for the control rod drive mechanisms are as follows:

1. 5/8-in. step.
2. 150-in. travel.
3. 360-lb maximum load.
4. Step in or out at 45 in./min (72 steps/min).
5. Power interruption shall initiate release of drive rod assembly.
6. Trip delay of less than 150 millisecond. Free fall of drive rod assembly shall begin less than 150 millisecond after power interruption no matter what holding or stepping action is being executed with any load and coolant temperatures of 100°F to 550°F.
7. 60-year design life with normal refurbishment.
8. 28,000 complete travel excursions, which is 13 x 10^6 steps with normal refurbishment.

4.2.3.2 Design Description

Reactivity control is provided by neutron-absorbing rods and a soluble chemical neutron absorber (boric acid). The boric acid concentration is varied to control long-term reactivity changes such as the following:

1. Fuel depletion and fission product buildup.
2. Cold to hot, zero-power reactivity change.
3. Reactivity change produced by intermediate-term fission products such as xenon and samarium.
4. Burnable poison depletion.

Chemical and volume control is covered in Section 9.3.4.

The rod cluster control assemblies provide reactivity control for the following:

1. Shutdown.

2. Reactivity changes due to coolant temperature changes in the power range.
3. Reactivity changes associated with the power coefficient of reactivity.
4. Reactivity changes due to void formation.

The first fuel cycle contains more excess reactivity than subsequent cycles due to the loading of all fresh (unburned) fuel. If soluble boron were the sole means of control, the moderator temperature coefficient would be positive. Excess reactivity in the core is controlled by the soluble boron and burnable poison assemblies. As the boron concentration is increased, the moderator temperature coefficient becomes less negative due to the reduction in boron associated with the reduction in water density. The use of a soluble boron alone could result in a positive moderator temperature coefficient at beginning of life (BOL). Limits on the moderator temperature coefficient for design analyses require that the moderator temperature coefficient not be positive at hot full power conditions. Therefore, burnable poison assemblies are used to reduce the soluble boron concentration sufficiently to ensure that the moderator temperature coefficient is within the limits of the accident analysis.

The neutron source assemblies, if used, provide one means of monitoring the core during periods of low neutron activity. However, neutron source assemblies are not required on a reload basis, as minimum detector count rates for core loading, refueling, shutdown and approach to criticality can be met by the neutron production from isotopic decay in irradiated assemblies.

The most effective reactivity control components are the full-length rod cluster control assemblies and their corresponding drive rod assemblies, which are the only kinetic parts in the reactor. Figure 4.2-16 identifies the rod cluster control and drive rod assembly, in addition to the arrangement of these components in the reactor relative to the interfacing fuel assembly, guide tubes, and control rod drive mechanism. The reactivity control components are described in detail in Section 4.2.3.2.1.

The guidance system for the control rod cluster is provided by the guide tube as shown in Figure 4.2-16. The guide tube provides two regimes of guidance. First, in the lower section, a continuous guidance system provides support immediately above the core. This system protects the rod against excessive deformation and wear due to hydraulic loading. Second, the region above the continuous section provides support and guidance at uniformly spaced intervals.

The envelope of support, shown in Figure 4.2-16, is determined by the pattern of the control rod cluster shown in Figure 4.2-17. The guide tube ensures alignment and support of the control rods, spider body, and drive rod while maintaining trip times at or below required limits.

4.2.3.2.1 Reactivity Control Components

Rod Cluster Control Assembly

The rod cluster control assemblies are divided into two categories: control and shutdown. The control groups compensate for reactivity changes due to variations in operating conditions of

the reactor, that is, power and temperature variations. Two criteria were employed for the selection of the control group. First, the total reactivity worth had to be adequate to meet the nuclear requirements of the reactor. Second, in view of the fact that some of these rods could be partially inserted at power operation, the total power peaking factor had to be low enough to ensure that the power capability requirements were met. The control and shutdown groups provide an adequate shutdown margin, defined as the amount by which the core would be subcritical at hot shutdown if all rod cluster control assemblies are tripped, assuming that the highest-worth assembly remains fully withdrawn and assuming no changes in xenon or boron concentration.

A rod cluster control assembly comprises a group of individual neutron absorber rods fastened at the top end to a common spider assembly, as illustrated in Figure 4.2-17.

The absorber material used in the control rods is a silver-indium-cadmium alloy that is essentially “black” to thermal neutrons and has sufficient additional resonance absorption to significantly increase its worth. The alloy is in the form of extruded rods that are sealed in stainless steel tubes to prevent the rods from coming in direct contact with the coolant. Each absorber rod is sealed at the top and bottom with end plugs that are welded to the cladding. Figure 4.2-18 provides an illustration of an absorber rod. Sufficient diametral and end clearance is provided to accommodate relative thermal expansions.

The bottom plugs are made bullet-nosed to reduce the hydraulic drag during reactor trip to guide smoothly into the dashpot section of the fuel assembly guide thimbles. The upper plug is threaded for assembly to the spider and has a reduced end section to make the joint more flexible.

The spider assembly is in the form of a central hub with radial vanes containing cylindrical fingers from which the absorber rods are suspended. Handling detents and detents for connection to the drive rod assembly are machined into the upper end of the hub. A spring pack inside the spider body absorbs the impact energy at the end of a trip. The radial vanes are joined to the hub by tack welds and brazing; the fingers are joined to the vanes by furnace brazing. A bolt which holds the spring pack and its retainer is threaded into the hub, and welded to prevent loosening in service. All components of the spider assembly are made from 304 and 308 stainless steel except for the retainer, which is type 630 (17-4 PH) stainless steel, and the springs, which are Inconel alloy 718.

The absorber rods are fastened securely to the spider to ensure trouble-free service. The rods are first threaded into the spider fingers and then pinned to maintain joint-tightness, after which the pins are welded in place. The end plug below the pin position is designed with a reduced section to permit flexing of the rods to correct for small operating or assembly misalignments.

The overall length is such that when the assembly is withdrawn through its full travel, the tips of the absorber rods remain engaged in the guide thimbles so that alignment between rods and

thimbles is always maintained. Since the rods are long and slender, they are relatively free to conform to any small misalignments with the guide thimble.

Burnable Poison Assembly

Each burnable poison assembly consists of burnable poison rods attached to a hold-down assembly. The burnable poison assemblies are shown in Figure 4.2-19.

The current poison rods consist of $A1_2O_3$-B_4C pellets contained within Zircaloy-4 tubular cladding that is plugged and seal-welded at the ends to encapsulate the pellets. The void volume for the helium in the burnable poison rods is obtained through the use of spring spacers and, in some instances, solid or tubular spacers. Figure 4.2-20 shows a cross section of a poison rod for the current burnable poison assembly.

The rods are statically suspended and positioned in selected guide thimbles within specified fuel assemblies. The poison rods in each fuel assembly are grouped and attached together at the top end of the rods to a hold-down assembly by a flat, perforated retaining plate that fits within the fuel assembly top nozzle and rests on the adapter plate. The retaining plate (and the poison rods) is held down and restrained against vertical motion through a spring pack that is attached to the plate and is compressed by the upper core plate when the reactor upper internals assembly is lowered into the reactor. This arrangement ensures that the poison rods cannot be ejected from the core by flow forces. Each rod is permanently attached to the baseplate.

The clad in the current burnable poison rods is cold-worked Zircaloy-4 seamless tubing. The upper and lower end plugs, nuts, and tubular and solid spacers are fabricated from Zircaloy-4. The spring spacers are 302 or 304 stainless steel. The hold-down assembly is fabricated from stainless steel, except for the hold-down springs, which are wound from Inconel 718 wire. The $A1_2O_3$ - B_4C pellets provide sufficient boron content to meet the criteria discussed in Section 4.3.1.

Prior to North Anna 2 Cycle 8 and North Anna 1 Cycle 9, the North Anna burnable poison assemblies used a borosilicate glass absorber encapsulated in stainless steel cladding, with a holddown assembly similar to that on the current burnable poison assemblies. The original design burnable poison assemblies had up to 20 absorber rods each, with thimble plugs at guide thimble locations that did not have absorber rods. These original burnable poison assemblies are not dimensionally compatible with the smaller-diameter guide thimbles of the NAIF fuel assembly design. Although they could be reinserted into North Anna cores in LOPAR fuel assemblies, further use of burnable poison assemblies of the original design is not anticipated.

Neutron Source Assembly

If used in the core (optional), the purpose of the neutron source assembly would be to provide a base neutron level to ensure that the detectors are operational and responding to core multiplication neutrons. If it is determined there will be insufficient neutron activity during loading, refueling, shutdown, and approach to criticality, it may be necessary to place a neutron

source in the reactor to provide a positive neutron count of at least 2 counts per second on the source range detectors attributable to core neutrons. However, this can normally be accommodated by the neutron production from isotopic decay in irradiated fuel assemblies. The source range detectors are used primarily when the core is subcritical and during special subcritical modes of operation.

The production of neutrons from the source assembly or irradiated fuel also permits the detection of changes in the core multiplication factor during core loading, refueling, and approach to criticality. This can be done since the multiplication factor is related to an inverse function of the detector count rate. Therefore, a change in the multiplication factor can be detected during the addition of fuel assemblies while loading the core, during a change in control rod positions, and during changes in boron concentration.

The primary source rod contains a radioactive material which spontaneously emits neutrons for use during initial core loading and reactor start-up. After the primary source rod decays beyond the desired neutron flux level, neutrons are then supplied by the secondary source rod. The secondary source rod contains a stable material that must be activated by neutron bombardment during reactor operation. The activation results in the subsequent release of neutrons. This becomes a source of neutrons during refueling and the subsequent start-ups.

The North Anna initial reactor cores employed four source assemblies, two primary source assemblies and two secondary source assemblies. Each primary source assembly contained one primary source rod and between zero and 19 burnable poison rods. Each secondary source assembly contained a symmetrical grouping of four secondary source rods, and between zero and 16 burnable poison rods. Locations not filled with a source or burnable poison rod may contain a thimble plug. The source assemblies are shown in Figures 4.2-21 and 4.2-22.

Source assemblies, when used, are employed at diametrically opposite sides of the core. The assemblies are inserted into the rod cluster control guide thimbles in fuel assemblies at selected unrodded locations.

The source assemblies contain a hold-down assembly similar to that used on the burnable poison assembly.

The primary and secondary source rods both use 304 stainless steel tubular cladding. The secondary source rods contain approximately 500 grams of stacked Sb-Be pellets. The primary source rods contain capsules of Californium source material and alumina spacer rods to position the source material within the cladding. The rods in each assembly are permanently fastened at the top end to a hold-down assembly, similar to the arrangement used in the burnable poison assemblies.

The other structural members are constructed of type 304 stainless steel except for the springs. The springs exposed to the reactor coolant are wound from an age-hardened nickel-base

alloy for corrosion resistance and high strength. The springs, when contained within the rods where corrosion resistance is not necessary, are oil-tempered carbon steel.

No primary sources are currently placed in reload cycles. Secondary source assemblies may be optionally loaded in reload cores to charge them for possible future use. The shutdown count rate is provided primarily by the highly burned fuel assemblies placed on the periphery of the core.

Thimble Plug Assembly

Thimble plugs assemblies were used in some North Anna cores to limit bypass flow through the guide thimbles in the fuel assemblies that did not contain control rods, source rods or burnable poison rods. However, improvements in the core design process have permitted removal of the thimble plugs while maintaining core design margins. Use of the thimble plug assemblies is now optional for core design.

The thimble plug assemblies as shown in Figure 4.2-23 consist of a flat baseplate with short rods suspended from the bottom surface and a spring pack assembly. The 24 short rods, called thimble plugs, project into the upper ends of the guide thimbles to reduce the bypass flow area, although the use of thimble plugs on such inserts is now optional. Similar short rods may also be used on the source assemblies and burnable poison assemblies to plug the ends of all vacant fuel assembly guide thimbles. At installation in the core, the thimble plug assemblies interface with both the upper core plate and with the fuel assembly top nozzles by resting on the adapter plate. The spring pack is compressed by the upper core plate when the upper internals assembly is lowered into place. Each thimble plug is permanently attached to the baseplate.

All components in the thimble plug assembly, except for the springs, are constructed from type 304 stainless steel. The springs are wound from an age-hardened nickel-base alloy for corrosion resistance and high strength.

4.2.3.2.2 Control Rod Drive Mechanism

All parts exposed to reactor coolant are made of metals that resist the corrosive action of the water. Three types of metals are used exclusively: stainless steels, Inconel-X, and cobalt-based alloys. The only steels used other than austenitic stainless steels are martensitic stainless steels. (This is necessary for the desired magnetic properties.) These materials are not heat-treated under conditions that cause susceptibility to stress-corrosion cracking or accelerated corrosion in the Westinghouse PWR water chemistry. Wherever magnetic flux is carried by parts exposed to the main coolant, 400 series stainless steel is used. Cobalt-based alloys are used for the pins and latch tips. Inconel-X is used for the springs of both latch assemblies and 304 stainless steel is used for all pressure-containing parts. Hard chrome plating provides wear surfaces on the sliding parts and prevents galling between mating parts.

A position indicator assembly slides over the control rod drive mechanism rod travel housing. It detects the drive rod assembly position by means of 42 discrete coils that magnetically

sense the entry and presence of the rod drive line through its centerline over the normal length of the drive rod travel.

Control Rod Drive Mechanism (Model L106A)

Control rod drive mechanisms are located on the dome of the reactor vessel. They are coupled to rod control clusters that provide the required reactivity control of the core. The control rod drive mechanism is shown in Figure 4.2-24 and schematically in Figure 4.2-25.

The primary function of the control rod drive mechanism is to insert or withdraw rod control clusters within the core to control average core temperature and to shut down the reactor.

The control rod drive mechanism is a magnetically operated jack. A magnetic jack is an arrangement of three electromagnets that are energized in a controlled sequence by a power cycler to insert or withdraw rod control clusters in the reactor core in discrete steps.

The control rod drive mechanism consists of four separate subassemblies. They are the pressure vessel, coil stack assembly, the latch assembly, and the drive rod assembly.

1. The pressure vessel includes a latch housing and a rod travel housing that are connected by a threaded, seal-welded, maintenance joint that facilitates replacement of the latch assembly. The closure at the top of the rod travel housing is a threaded plug with a canopy seal weld for pressure integrity.

   The latch housing is the lower portion of the vessel and contains the latch assembly. The rod travel housing is the upper portion of the vessel and provides space for the drive rod during its upward movement as the control rods are withdrawn from the core.

2. The coil stack assembly includes the coil housing, an electrical conduit and connecter, and three operating coils: (1) the stationary gripper coil, (2) the movable gripper coil, and (3) the lift coil.

   The coil stack assembly is a separate unit that is installed on the drive mechanism by sliding it over the outside of the latch housing. It rests on the base of the latch housing without mechanical attachment.

   The energizing of the operating coils causes movement of the pole pieces and latches in the latch assembly.

3. The latch assembly includes the guide tube, stationary pole pieces, movable pole pieces, and two sets of latches: (1) the movable gripper latch, and (2) the stationary gripper latch.

   The latches engage grooves in the drive rod assembly. The movable gripper latches are moved up or down in 5/8-inch steps by the lift pole to raise or lower the drive rod. The stationary gripper latches hold the drive rod assembly while the movable gripper latches are repositioned for the next 5/8-inch step.

4. The drive rod assembly includes a flexible coupling, a drive rod, a disconnect button, a disconnect rod, and a locking button.

   The drive rod has 5/8-inch grooves that receive the latches during holding or moving of the drive rod. The flexible coupling is attached to the drive rod and produces the means for coupling to the rod control cluster assembly.

   The disconnect button, disconnect rod, and locking button provide positive locking of the coupling to the rod control cluster assembly and permits remote disconnection of the drive rod.

The control rod drive mechanism is a trip design. Tripping can occur during any part of the power cycler sequencing if power to the coils is interrupted.

The control rod drive mechanism is threaded and seal-welded on an adapter on top of the reactor vessel and is coupled to the rod control cluster assembly directly below.

The mechanism is capable of handling a 360-lb load, including the drive rod weight, at a rate of 45 in./min. Withdrawal of the rod control cluster is accomplished by magnetic forces, while insertion is by gravity.

The mechanism internals are designed to operate in 650°F reactor coolant. The pressure vessel is designed to contain reactor coolant at 650°F and 2500 psia. The three operating coils are designed to operate at a maximum temperature of 392°F with forced air cooling required to maintain that temperature.

The control rod drive mechanism, shown schematically in Figure 4.2-25, withdraws and inserts its control rod as electrical pulses are received by the operator coils. An ON or OFF sequence, repeated by silicon-controlled rectifiers in the power programmer, causes either withdrawal or insertion of the control rod. The position of the control rod is measured by 42 discrete coils mounted on the position indicator assembly surrounding the rod travel housing. Each coil magnetically senses the entry and presence of the top of the ferromagnetic drive rod assembly as it moves through the coil centerline.

During plant operation the stationary gripper coil of the drive mechanism holds the control rod withdrawn from the core in a static position until the movable gripper coil is energized.

Rod Cluster Control Assembly Withdrawal

The control rod is withdrawn by the repetition of the following sequence of events:

1. Movable Gripper Coil (B) - ON

   The latch-locking plunger raises and swings the movable gripper latches into the drive rod assembly groove. A 1/16-inch axial clearance exists between the latch teeth and the drive rod.

2. Stationary Gripper Coil (A) - OFF

   The force of gravity, acting on the drive rod assembly and attached control rod, causes the stationary gripper latches and plunger to move downward 1/16 inch until the load of the drive rod assembly and attached control rod is transferred to the movable gripper latches. The plunger continues to move downward and swings the stationary gripper latches out of the drive rod assembly groove.

3. Lift Coil (C) - ON

   The 5/8-inch gap between the movable gripper pole and the lift pole closes and the drive rod assembly raises one step length (5/8 inch).

4. Stationary Gripper Coil (A) - ON

   The plunger raises and closes the gap below the stationary gripper pole. The three links, pinned to the plunger, swing the stationary gripper latches into a drive rod groove. The latches contact the drive rod and lift it (and the attached control rod) 1/16 inch. The 1/16-inch vertical drive rod movement transfers the drive rod load from the movable gripper latches to the stationary gripper latches.

5. Movable Gripper Coil (B) - OFF

   The latch-locking plunger separates from the movable gripper pole under the force of a spring and gravity. Three links, pinned to the plunger, swing the three movable gripper latches out of the drive rod groove.

6. Lift Coil (C) - OFF

   The gap between the movable gripper pole and lift pole opens. The movable gripper latches drop 5/8 inch to a position adjacent to a drive rod groove.

7. Repeat Step 1

   The sequence described above (1 through 6) is termed as one step or one cycle. The control rod moves 5/8 inch for each step or cycle. The sequence is repeated at a rate of up to 72 steps/min and the drive rod assembly (which has a 5/8-inch groove pitch) is raised 72 grooves/min. The control rod is thus withdrawn at a rate up to 45 in./min.

Rod Cluster Control Assembly Insertion

The sequence for control rod insertion is similar to that for control rod withdrawal, except that the timing of lift coil (C) ON and OFF is changed to permit lowering the control rod.

1. Lift Coil (C) - ON

   The 5/8-inch gap between the movable gripper and lift pole closes. The movable gripper latches are raised to a position adjacent to a drive rod groove.

2. Movable Gripper Coil (B) - ON

   The latch-locking plunger raises and swings the movable gripper latches into a drive rod groove. A 1/16-inch axial clearance exists between the latch teeth and the drive rod assembly.

3. Stationary Gripper Coil (A) - OFF

   The force of gravity, acting upon the drive rod and attached control rod, causes the stationary gripper latches and plunger to move downward 1/16 inch until the load of the drive rod and attached control rod is transferred to the movable gripper latches. The plunger continues to move downward and swings the stationary gripper latches out of the drive rod groove.

4. Lift Coil (C) - OFF

   The force of gravity separates the movable gripper pole from the lift pole, and the drive rod and attached control rod drop down 5/8 inch.

5. Stationary Gripper (A) - ON

   The plunger raises and closes the gap below the stationary gripper pole. The three links, pinned to the plunger, swing the three stationary gripper latches into a drive rod groove. The latches contact the drive rod and lift it (and the attached control rod) 1/16 inch. The 1/16-inch vertical drive rod movement transfers the drive rod load from the movable gripper latches to the stationary gripper latches.

6. Movable Gripper Coil (B) - OFF

   The latch-locking plunger separates from the movable gripper pole under the force of a spring and gravity. Three links, pinned to the plunger, swing the three movable gripper latches out of the drive rod groove.

7. Repeat Step 1

   The sequence is repeated, as for control rod withdrawal, up to 72 times/min, which gives a control rod insertion rate of 45 in./min.

Holding and Tripping of the Control Rods

During most of the plant operating time, the control rod drive mechanisms hold the control rods withdrawn from the core in a static position. In the holding mode, only one coil, the stationary gripper coil (A), is energized on each mechanism. The drive rod assembly and attached control rod hang suspended from the three latches.

If power to the stationary gripper coil is cut off, the combined weight of the drive rod assembly and the rod cluster control assembly is sufficient to move latches out of the drive rod assembly groove. The control rod falls by gravity into the core. The trip occurs as the magnetic field, holding the stationary gripper plunger half against the stationary gripper pole, collapses and the stationary gripper plunger half is forced down by the weight acting upon the latches. After the

drive rod assembly is released by the mechanism, it falls freely until the control rods enter the buffer section of their thimble tubes.

Part-Length Control Rod Drive Mechanism

Part-length control rod drive mechanisms have been removed from all core locations except D08. The mechanism housing at location D08 is used for the reactor vessel head vent system. To maintain the pressure boundary function, adapter plugs were threaded on the part-length locations and then seal welded with a canopy weld. To maintain cooling airflow characteristics, dummy cans were attached to the adapter plugs to occupy the volume of the removed part-length control rod drive mechanisms.

4.2.3.3 Design Evaluation

4.2.3.3.1 Reactivity Control Components

The components are analyzed for loads corresponding to normal, upset, emergency, and faulted conditions. The analysis performed depends on the mode of operation under consideration.

The scope of the analysis requires many different techniques and methods, both static and dynamic.

Some of the loads that are considered on each component where applicable are as follows:

1. Control rod trip (equivalent static load).
2. Differential pressure.
3. Spring preloads.
4. Coolant flow forces (static).
5. Temperature gradients.
6. Differences in thermal expansion
   a. Due to temperature differences.
   b. Due to expansion of different materials.
7. Interference between components.
8. Vibration (mechanically or hydraulically induced).
9. All operational transients listed in Table 5.2-4.
10. Pump overspeed.
11. Seismic loads (operational-basis earthquake and design-basis earthquake).

The main objectives of the analysis are to satisfy allowable stress limits, to ensure an adequate design margin, and to establish deformation limits that are concerned primarily with the functioning of the components. The stress limits are established not only to ensure that peak stresses will not reach unacceptable values, but also to limit the amplitude of the oscillatory stress component in consideration of fatigue characteristics of the materials. Standard methods of strength of materials are used to establish the stresses and deflections of these components. The dynamic behavior of the reactivity control components has been studied using experimental test data (D-Loop, Section 1.5) and experience from operating reactors.

The design of reactivity component rods provides a sufficient cold void volume within the burnable poison and source rods to limit the internal pressures to a value that satisfies the criteria in Section 4.2.3.1. The void volume for the helium in the burnable poison rods is obtained through the use of spring spacers and, in some instances, solid or tubular spacers. Helium gas is not released by the neutron absorber rod material, thus the absorber rod only sustains an external pressure during operating conditions. The internal pressure of source rods continues to increase from ambient until end of life, at which time the internal pressure never exceeds that allowed by the criteria in Section 4.2.3.1. The stress analysis of reactivity component rods assumes 100% gas release to the rod void volume, considers the initial pressure within the rod, and assumes the pressure external to the component rod is zero.

Sufficient diametral and end clearances have been provided in the neutron absorber, burnable poison, and source rods to accommodate the relative thermal expansions between the enclosed material and the surrounding clad and end plugs. There is no bending or warping induced in the rods, although the clearance offered by the guide thimbles would permit a postulated warpage to occur without restraint on the rods. Bending, therefore, is not considered in the analysis of the rods. The radial and axial temperature profiles have been determined by considering gap conductance, thermal expansion, and neutron and/or gamma heating of the contained material as well as gamma heating of the clad. The maximum neutron absorber material temperature was found to be less than 850°F, which occurs axially at only the highest flux region. Rod, guide thimble, and dashpot flow analysis performed indicates that the flow is sufficient to prevent coolant boiling and maintain clad temperatures at which the clad material has adequate strength to resist coolant operating pressures and rod internal pressures.

Analysis performed on the rod cluster control spider indicates that the spider is structurally adequate to withstand the various operating loads, including the higher loads that occur during the drive mechanism stepping action and rod drop. Experimental verification of the spider structural capability was performed (Section 1.5).

Previous operating experience has shown that the materials of construction exhibit satisfactory resistance to adverse property changes in a radioactive environment.

At high fluences, the austenitic materials increase in strength with a corresponding decrease in ductility (as measured by tensile tests), but energy absorption (as measured by impact tests)

remains quite high. Corrosion of the materials exposed to the coolant is quite low and proper control of $C1^-$ and O_2 in the coolant will prevent the occurrence of stress corrosion. All of the austenitic stainless steel base materials used are processed and fabricated to preclude sensitization. Although the control rod spiders are fabricated by furnace brazing, the procedure used requires that the process be rapidly cooled so that the time-at-temperature is minimized. The time that is spent by the control rod spiders in the sensitization range, 800° to 1500°F, is not more than 0.2 hour, during fabrication to preclude sensitization. The 17-4 PH parts are all aged at the highest standard aging temperature of 1100°F to avoid stress corrosion problems exhibited by aging at lower temperatures.

An analysis of the rod cluster control assemblies shows that if the drive mechanism housing ruptures, the rod cluster control assembly will be ejected from the core by the pressure differential of the operating pressure and ambient pressure across the drive rod assembly. The ejection is also predicated on the failure of the drive mechanism to retain the drive rod/rod cluster control assembly position. It should be pointed out that a drive mechanism housing rupture will cause the ejection of only one rod cluster control assembly, with the other assemblies remaining in the core. Analysis also showed that a pressure drop in excess of 4000 psi must occur across a two-fingered vane to break the vane/spider body joint, causing ejection of two neutron absorber rods from the core. Since the greater pressure of the primary system coolant is only 2250 psi, a pressure drop in excess of 4000 psi could not be expected to occur. Thus, the ejection of the neutron absorber rods is not possible.

An ejection of a burnable poison or thimble plug (if used) assembly is conceivable based on the postulation that the hold-down bar fails and that the baseplate and burnable poison rods are severely deformed. In the unlikely event that failure of the hold-down bar occurs, the upward displacement of the burnable poison assembly only permits the baseplate to contact the upper core plate. Since this displacement is small, the major portion of the burnable absorber tubing remains positioned within the core. In the case of the thimble plug assembly, the thimble plugs will partially remain in the fuel assembly guide thimbles, thus maintaining a majority of the desired flow impedance. Further displacement or complete ejection would necessitate that the square baseplate and burnable poison rods be forced, and thus plastically deformed, to fit up through a smaller-diameter hole. It is expected that this condition requires a substantially higher force or pressure drop than that of the hold-down bar failure.

Experience with control rods, burnable poison rods, and source rods is discussed in Reference 2.

The mechanical design of the reactivity control components provides for the protection of the active elements to prevent the loss of control capability and functional failure of critical components. The components have been reviewed for potential and consequences of a functional failure of critical parts. The results of the review are summarized below.

Rod Cluster Control Assemblies

1. The basic absorbing material is sealed from contact with the primary coolant and the fuel assembly and guidance surfaces by a high-quality stainless steel clad. Potential loss of absorber mass or reduction in reactivity control material due to mechanical or chemical erosion or wear is therefore reliably prevented.

2. A breach of the cladding for any postulated reason does not result in serious consequences. The absorber material silver-indium-cadmium is relatively inert and would still remain remote from high-coolant-velocity regions. Rapid loss of material resulting in significant loss of reactivity control material would not occur.

3. The individually clad absorber rods are doubly secured to the retaining spider vane by a threaded joint and a welded lock pin. No failure of this joint has ever been experienced in functional testing or in years of actual service in operating plants such as San Onofre, Connecticut Yankee, Zorita, Beznau No. 1, and Robert Emmett Ginna.

   It should also be noted that in several instances of control rod jamming caused by foreign particles, the individual rods at the site of the jam have borne the full capacity of the control rod drive mechanism and higher impact loads to dislodge the jam without failure. The guide tube/guide thimble arrangement is such that large loads are required to buckle individual control rods. The conclusion to be drawn from this experience is that this joint is extremely insensitive to potential mechanical damage. A failure of the joint would result in the insertion of the individual rod into the core. This results in reduced reactivity, which is a fail-safe condition.

4. The spider finger braze joint by which the individual rods are fastened to the vanes has also experienced the service described above and been subjected to the same jam-freeing procedures, also without failure. A failure of this joint would also result in the insertion of the individual rod into the core.

5. The radial vanes are attached to the spider body, again by brazed joint. The joints are designed to a theoretical strength in excess of that of the components joined.

   It is a feature of the design that the guidance of the rod cluster control is accomplished by the inner fingers of these vanes. They are therefore the most susceptible to mechanical damage. Since these vanes carry two rods, failure of the vane-to-hub joint such as the isolated incidents at Connecticut Yankee does not prevent the free insertion of the rod pair (Reference 2). Neither does such a failure interfere with the continuous free operation of the drive line, also as experienced at Connecticut Yankee (Reference 2).

   Failure of the vane-to-hub joint of a single rod vane could potentially result in failure of the separated vane and rod to insert. This could occur only at withdrawal elevations where the spider is above the continuous guidance section of the guide tube (in the upper internals). A

rotation of the disconnected vane could cause it to hang on one of the guide cards in the intermediate guide tube. Such an occurrence would be evident from the failure of the rod cluster control to insert below a certain elevation but with free motion above this point.

This possibility is considered extremely remote because the single rod vanes are subjected to only vertical loads and very light lateral reactions from the rods. The lateral loads are light even during a seismic event because the guide tube/guide thimble arrangement allows very limited lateral motion. The consequences of such a failure are not considered critical since only one drive line of the reactivity control system would be involved. This condition is readily observed and can be cleared at shutdown.

6. The spider hub of single unit cylindrical construction is very rugged and of extremely low potential for damage. It is difficult to postulate any condition to cause failure. Should some unforeseen event cause fracture of the hub above the vanes, the lower portion with the vanes and rods attached would insert by gravity into the core causing reactivity decrease. The rod could then not be removed by the drive line, again a fail-safe condition. Fracture below the vanes cannot be postulated since all loads, including scram impact, are taken above the vane elevation.

7. The rod cluster control rods are provided a clear channel for insertion by the guide thimbles of the fuel assemblies. All fuel rod failures are protected against by providing this physical barrier between the fuel rod and the intended insertion channel. Distortion of the fuel rods by bending cannot apply sufficient force to damage or significantly distort the guide thimble. Fuel rod distortion by swelling, though precluded by design, would be terminated by fracture before contact with the guide thimble occurs. If such were not the case, it would be expected that a force reaction at the point of contact would cause a slight deflection of the guide thimble. The radius of curvature of the deflected shape of the guide thimbles would be sufficiently large to have a negligible influence on rod cluster control insertion.

Burnable Poison Assemblies

The burnable poison assemblies are static, temporary reactivity control elements. The axial position is ensured by the hold-down assembly that bears against the upper core plate. Their lateral position is maintained by the guide thimbles of the fuel assemblies. The individual rods are shouldered against the underside of the retainer plate and securely fastened at the top by a threaded nut which is then welded or crimped into place. The square dimension of the retainer plate is larger than the diameter of the flow holes through the core plate. Failure of the hold-down bar or spring pack therefore does not result in ejection of the burnable poison rods from the core.

The only incident that could potentially result in ejection of the burnable poison rods is a multiple fracture of the retainer plate. This is not considered credible because of the light loads borne by this component. During normal operation, the loads borne by the plate are approximately 5 lb/rod or a total of 100 lb distributed at the points of attachment. Even a multiple fracture of the retainer plate should result in jamming of the plate segments against the upper core

plate, again preventing ejection. Excessive reactivity increase due to burnable poison ejection is therefore prevented.

Burnable poison rods are placed in static assemblies and are not subjected to motion that might damage the rods. Further, the guide thimble tubes of the fuel assembly afford additional protection from damage.

Drive Rod Assemblies

All postulated failures of the drive rod assemblies either by fracture or uncoupling lead to the fail-safe conclusion. If the drive rod assembly fractures at any elevation, that portion remaining coupled falls with, and is guided by, the rod cluster control assembly. This will always result in a reactivity decrease.

4.2.3.3.2 Control Rod Drive Mechanism

Material Selection

All pressure-containing materials comply with Section III of the ASME Code, and with the exception of the needle vent valve, will be fabricated from austenitic (304) stainless steel or CF-8 stainless steel. The vent valve is a modified austenitic stainless steel cap screw.

Magnetic pole pieces are fabricated from 410 stainless steel. All nonmagnetic parts, except pins and springs, are fabricated from 304 stainless steel. Haynes 25 is used to fabricate link pins. Springs are made from Inconel-X. Latch arm tips are clad with Stellite-6 to provide improved wearability. Hard chrome plate and Stellite-6 are used selectively for bearing and wear surfaces.

At the start of the development program, a survey was made to determine whether a material better than 410 stainless steel was available for the magnetic pole pieces. Ideal material requirements are as follows:

1. High magnetic saturation value.
2. High permeability.
3. Low coercive force.
4. High resistivity.
5. High curie temperature.
6. Corrosion resistant.
7. High-impact strength.
8. Nonoriented.
9. High machinability.
10. Low susceptibility to radiation damage.

After a comprehensive material trade-off study was made, it was decided that the 410 stainless steel was satisfactory for this application.

The cast coil housings require a magnetic material. Both low-carbon cast steel and ductile iron have been successfully tested for this application. The choice, made on the basis of cost, indicates that ductile iron will be specified on the control rod drive mechanism. The finished housings are zinc-plated to provide corrosion resistance.

Coils are wound on bobbins of molded Dow Corning 302 material, with double glass-insulated copper wire. Coils are then vacuum-impregnated with silicon varnish. A wrapping of mica sheet is secured to the coil outer surface. The result is a well-insulated coil capable of sustained operation at 200°C.

The drive shaft assembly uses a 410 stainless steel drive rod. The coupling is machined from 403 stainless steel. Other parts are 304 stainless steel with the exception of the springs, which are Inconel-X, and the locking button, which is Haynes-25.

Radiation Damage

As required by the equipment specification, the control rod drive mechanisms are designed to meet a radiation requirement of 10 rads/hour. Materials have been selected to meet this requirement. The above radiation level, which amounts to 1.753×10^6 rads in 20 years, will not limit control rod drive mechanism life. Control rod drive mechanisms at Yankee Rowe, which have been in operation from 1960 through the licensing of North Anna, had not experienced problems due to radiation.

Positioning Requirements

The mechanism has a step length of 5/8 inch, which determines the positioning capabilities of the control rod drive mechanism. (Note: Positioning requirements are determined by reactor physics.)

Evaluation of Materials Adequacy

The ability of the pressure-housing components to perform throughout the design lifetime as defined in the equipment specification is confirmed by the stress analysis report required by the ASME Code, Section III. Internal components subjected to wear will withstand a minimum of 3 million steps without refurbishment, as confirmed by life tests.

Results of Dimensional and Tolerance Analysis

With respect to the control rod drive mechanism systems as a whole, critical clearances are present in the following areas:

1. Latch assembly - diametral clearances.
2. Latch arm - drive clearances.

3. Coil stack assembly - thermal clearances.
4. Coil fit in coil housing.

Clearances that are designed to provide reliable operation in the control rod drive mechanism in these four critical areas are defined below. These clearances have been proven by life tests and actual field performance at operating plants.

Latch Assembly - Thermal Clearances

The magnetic jack has several clearances where parts made of 410 stainless steel fit over parts made from 304 stainless steel. Differential thermal expansion is therefore important. Minimum clearance of these parts at 68°F is 0.011 inch. At the maximum design temperature of 650°F, minimum clearance is 0.0045 inch, and at the maximum expected operating temperature of 550°F it is 0.0057 inch.

Latch Arm - Drive Rod Clearances

The control rod drive mechanism incorporates a load transfer action. The movable or stationary gripper latch is not under load during engagement, as previously explained, due to load transfer action.

Figure 4.2-26 shows latch clearance variation with the drive rod as a result of minimum and maximum temperatures. Figure 4.2-27 shows clearance variations over the design temperature range.

Coil Stack Assembly - Thermal Clearances

The assembly clearance of the coil stack assembly over the latch housing was selected so that the assembly could be removed under all anticipated conditions of thermal expansion.

At 70°F, the inside diameter of the coil stack is 7.308/7.298 inches. The outside diameter of the latch housing is 7.260/7.270 inches.

Thermal expansion of the mechanism due to the operating temperature of the control rod drive mechanism results in the minimum inside diameter of the coil stack being 7.310 inches at 222°F and the maximum latch housing diameter being 7.302 inches at 532°F.

Under the extreme tolerance conditions listed above, it is necessary to allow time for a 70°F coil housing to heat during a replacement operation.

Four coil stack assemblies were removed from four hot control rod drive mechanisms mounted on 11.035-inch centers on a 550°F test loop, allowed to cool, and then replaced without incident as a test to prove the preceding.

Coil Fit in Coil Housing

Control rod drive mechanism and coil housing clearances are selected so that coil heatup results in a close to tight fit. This is done to facilitate thermal transfer and coil cooling in a hot control rod drive mechanism.

4.2.3.4 Tests, Verification, and Inspections

4.2.3.4.1 Reactivity Control Components

Tests and inspections are performed on each reactivity control component to verify the mechanical characteristics. In the case of the rod cluster control assembly, prototype testing has been conducted and both manufacturing test/inspections and functional testing at the plant are performed.

During the component manufacturing phase, the following requirements apply to the reactivity control components to ensure the proper functioning during reactor operation:

1. All materials are procured to specifications to attain the desired standard of quality.
2. Each spider is proof-tested by applying a 5000-lb load to the spider body, so that approximately 310 lb is applied to each vane. This proof load provides a bending moment at the spider body greater than the load caused by the acceleration imposed by the control rod drive mechanism.
3. All clad/end plug and/or seal welds in neutron absorber rods, burnable poison rods, and source rods are checked for integrity by visual inspection, ultrasonic test (or alternatively, x-ray), and helium leakage in accordance with qualified techniques and vendor specifications. Beginning with Cycle 18 at both units, the feed fuel and burnable poison rods are fabricated with a new end plug welding process, and the vendor no longer performs ultrasonic testing or x-ray on these components.
4. To ensure proper fitup with the fuel assembly, the rod cluster control, burnable poison, and source assemblies are installed in the fuel assembly without restriction or binding of the rod in the dry condition with a force not to exceed 15 lb. Also a straightness of 0.010 in./ft is required on the entire inserted length of each rod assembly.

   The rod cluster control assemblies are functionally tested following core loading but before criticality to demonstrate reliable operation of the assemblies. Each assembly is operated (and tripped) one time at no-flow/cold conditions and one time at full-flow/hot conditions. In addition, selected assemblies, amounting to about 15% to 20% of the total assemblies, are operated at no-flow/operating temperature conditions and full-flow/ambient conditions. Also, the slowest rod and the fastest rod are tripped 10 times at no-flow/ambient conditions and at full-flow/operating temperature conditions. Thus, each assembly is tested at least twice, or up to 14 times maximum to ensure that the assemblies are properly functioning.

4.2.3.4.2 Control Rod Drive Mechanisms

Quality assurance procedures during production of control rod drive mechanisms include material selection, process control, mechanism component tests during production, and hydrotests.

After all manufacturing procedures had been developed, several prototype control rod drive mechanisms and drive rod assemblies were life-tested with the entire drive line under environmental conditions of temperature, pressure, and flow. All acceptance tests were of duration equal to or greater than service required for the plant operation. All drive rod assemblies tested in this manner have shown minimal wear damage.

These tests include verification that the trip time achieved by the control rod drive mechanisms meets the design requirement of 2.2 seconds from start of rod cluster control assembly motion to dashpot entry. This trip time requirement was confirmed for each control rod drive mechanism before initial reactor operation. In addition, for current operation, a Technical Specification has been set to ensure that the safety analysis trip time requirement is met. The surveillance procedure limits for measured drop times are set below the Technical Specifications Surveillance Requirement 3.1.4.3 criterion. The surveillance procedure limits account for the drop time measurement uncertainty. Also, measured rod drop time data is trended to ensure that adverse trends in drop time performance are readily identified and evaluated.

It is expected that all control rod drive mechanisms will meet specified operating requirements for the duration of plant life with normal refurbishment. However, a Technical Specification pertaining to an inoperable rod cluster control assembly has been set.

If a rod cluster control assembly cannot be moved by its mechanism, adjustments in the boron concentration ensure that adequate shutdown margin would be achieved following a trip. Thus, inability to move one rod cluster control assembly can be tolerated, but would impose additional demands on the plant operator. Therefore, the number of inoperable rod cluster control assemblies has been limited to one.

In order to demonstrate continuous free movement of the rod cluster control assemblies and to ensure acceptable core power distributions during operation, partial-movement checks are performed on every rod cluster control assembly during reactor critical operation as required by the Technical Specifications. In addition, periodic drop tests of the rod cluster control assemblies are performed at each refueling shutdown to demonstrate continued ability to meet trip time requirements, to ensure core subcriticality after reactor trip, and to limit potential reactivity insertions from a hypothetical rod cluster control assembly ejection. During these tests, the acceptable drop time of each assembly is not greater than the acceptance limit at full flow and operating temperature from the beginning of motion to dashpot entry.

To confirm the mechanical adequacy of the fuel assembly and rod cluster control assembly, functional test programs have been conducted on a full-scale control rod. The prototype assembly

was tested under simulated conditions of reactor temperature, pressure, and flow for approximately 1000 hours. The prototype mechanism accumulated about 3 million steps and 6000 trips. At the end of the test, the control rod drive mechanism was still operating satisfactorily.

Actual experience on the Ginna, Mihama No. 1, Point Beach No. 1, and H. B. Robinson plants indicates excellent performance of control rod drive mechanisms.

All units are production tested before shipment to confirm ability of control rod drive mechanisms to meet design specification operational requirements.

4.2.3.5 **Instrumentation Applications**

Instrumentation for determining reactor coolant average temperature (T_{avg}) is provided to create demand signals for moving groups of rod cluster control assemblies to provide load following (determined as a function of turbine impulse pressure) during normal operation and to counteract operational transients. The hot- and cold-leg resistance temperature detectors in the reactor coolant loops are described in Section 7.2. The location of the resistance temperature detectors in each loop is shown on the flow diagrams in Chapter 5. The reactor control system that controls the reactor coolant average temperature by regulation of control rod bank position is described in Section 7.7.

Rod position indication instrumentation is provided to sense the actual position of each control rod so that the actual position of the individual rod may be displayed to the operator. Signals are also supplied by this system as input to the rod deviation comparator. The rod position indication system is described in Chapter 7.

The reactor makeup control system, whose functions are to permit adjustment of the reactor coolant boron concentration for reactivity control (as well as to maintain the desired operating fluid inventory in the volume control tank), consists of a group of instruments arranged to provide a manually preselected makeup composition that is borated or diluted as required to the charging pump suction header or the volume control tank. This system, as well as other systems including boron sampling provisions that are part of the chemical and volume control system, is described in Section 9.3.

When the reactor is critical, the normal indication of reactivity status in the core is the position of the control bank in relation to reactor power (as indicated by the reactor coolant system loop delta T) and coolant average temperature. These parameters are used to calculate insertion limits for the control banks to give warning to the operator of excessive rod insertion. Monitoring of the neutron flux for various phases of reactor power operation as well as of core loading, shutdown, start-up, and refueling is by means of the nuclear instrumentation system. The monitoring functions and readout and indication characteristics for the following means of

monitoring reactivity are included in the discussion of safety-related display instrumentation in Section 7.5.

1. Nuclear instrumentation system.
2. Temperature indicators.
   a. T_{avg} (measured).
   b. Delta T (measured).
   c. Median T_{avg}.
   d. T reference.
3. Demand position of rod cluster control assembly group.
4. Actual rod position indicator.

4.2 REFERENCES

1. J. A. Christensen, R. J. Allio, and A. Biancheria, *Melting Point of Irradiated UO_2*, WCAP-6065, 1965.
2. *Operational Experience With Westinghouse Cores*, WCAP-8183, (latest revision).
3. *Information on Fuel Assembly Guide Tube Thimble Wear (Westinghouse Proprietary)*, submitted as an attachment to letters 756A/090779 and 1162/121879, from C. M. Stallings, Vepco, to H. R. Denton, NRC, dated January 22, 1980.
4. Letter from R. H. Leasburg, Vepco, to H. R. Denton, NRC, *North Anna Power Station Unit 2, License Condition 2.C.(15).(a),* Serial Number 124, dated March 1, 1982, Enclosure: *Salem Unit 1, 17 x 17 Fuel Assembly Guide Thimble Tube Wear Examination Report*, January 1982.
5. Letter from R. A. Clark, NRC, to R. H. Leasburg, Vepco, Subject: License Condition 2.C.(15)(a), North Anna Power Station, Unit 2, dated April 21, 1982.
6. C. J. Kubit, editor, *Safety Related Research and Development for Westinghouse Pressurized Water Reactor - Program Summaries, Spring-Fall 1973*, WCAP-8204, 1973.
7. Davidson, S. L. (Ed.), et al., *VANTAGE 5H Fuel Assembly*, WCAP-10444-P-A, Addendum 2-A, February 1989.
8. S. L. Davidson and T. L. Ryan, V*ANTAGE+ Fuel Assembly Reference Core Report*, WCAP-12610-P-A (Proprietary), April 1995.
9. J. M. Hellman, editor, *Fuel Densification Experimental Results and Model for Reactor Operation*, WCAP-8219, 1973.
10. Davidson, S. L. (Ed.), et al., *VANTAGE 5 Fuel Assembly Reference Core Report*, WCAP-10444-P-A, September 1985.
11. R. A. George, Y. C. Lee, and G. H. Eng, *Revised Clad Flattening Model*, WCAP-8381, July 1974.
12. W. J. Leech, et al., *Revised PAD Code Thermal Safety Model,* WCAP-8720-A2 (Proprietary), October 1982.
13. R. A. Weiner, et al, *Improved Fuel Performance Models for Westinghouse Fuel Rod Design and Safety Evaluations*, WCAP-10851-P-A (Proprietary), August 1988.
14. D. H. Risher, *Safety Analysis of the Revised Fuel Rod Internal Pressure Design Basis*, WCAP-8963-P-A (Proprietary), August 1978.
15. J. Weisman, P. E. MacDonald, A. J. Miller, and H. M. Ferrari, *Fission Gas Release from UO_2 Fuel Rods with Time-Varying Power Histories*, *Transactions of the American Nuclear Society*, Vol. 1 (12), pp. 900-901, 1969.

16. B. Watkins and D. S. Wood, *The Significance of Irradiation-Induced Creep on Reactor Performance of a Zircaloy-2 Pressure Tube*, *Applications-Related Phenomena for Zirconium and Its Alloys*, ASTM STP 458, American Society for Testing and Materials, pp. 226-240, 1969.

17. C. M. Friedrich and W. H. Guilinger, *CYGRO-2, A Fortran IV Computer Program for Stress Analysis of the Growth of Cylindrical Fuel Elements with Fission Gas Bubbles*, WAPD-TM-547, 1966.

18. W. J. O'Donnell and B. F. Langer, *Fatigue Design Basis for Zircaloy Components*, *Nuclear Science and Engineering*, Vol. 20, pp. 1-12, 1964.

19. L. Gesinski, D. Chiang, and S. Nakazato, *Safety Analysis of the 17 x 17 Fuel Assembly for Combined Seismic and Loss-of-Coolant Accident*, WCAP-8288, 1973.

20. E. E. Demario and S. Nakazato, *Hydraulic Flow Test of the 17 x 17 Fuel Assembly*, WCAP-8279, 1974.

21. J. Moore, *Nuclear Fuel Division Quality Assurance Program Plan*, WCAP-7800, Revision 5A, 1979.

22. J. Cohen, *Development and Properties of Silver Base Alloys as Control Rod Materials for Pressurized Water Reactors*, WAPD-214, 1959.

23. T. A. Brookmire (Ed.), *Reload Transition Safety Report for Implementation of PERFORMANCE+ Debris Resistance Features at North Anna Units 1 and 2*, Technical Report NE-949, Rev. 0, August 1993.

24. Letter from L. B. Engle (U.S. NRC) to J.P. O'Hanlon (Virginia Electric and Power Company), *North Anna Units 1 and 2 - Issuance of Amendments Re: Fuel Assembly Reconstitution (TAC Nos. M88364 and M88365*), August 9, 1994.

25. S. L. Davidson et al., *Assessment of Clad Flattening and Densification Power Spike Factor Elimination in Westinghouse Nuclear Fuel,* WCAP-13589-A (Proprietary), March 1995.

26. J. P. Foster et al., *Westinghouse Improved Performance Analysis and Design Model (PAD 4.0),* WCAP-15063-P-A, Revision 1, with Errata, (Proprietary), July 2000.

27. *Addendum 1 to WCAP-12488-A, Revision to Design Criteria,* WCAP-12488-A, Addendum 1-A, Revision 1 (Proprietary), January 2002.

Table 4.2-1
MAXIMUM DEFLECTIONS ALLOWED
FOR REACTOR INTERNAL SUPPORT STRUCTURES

Component	Allowable Deflections (in.)	No-Loss-of Function Deflections (in.)
Upper barrel		
Radial inward	4.38	8.77
Radial outward	1.0	1.5
Rod Cluster Control		
Guide tubes	1.0	1.6
Upper package	0.1	0.150

Table 4.2-2
COMPARISON OF 17 X 17 LOPAR ASSEMBLY
AND 17 X 17 NAIF ASSEMBLY NOMINAL DESIGN PARAMETERS

Parameter	17 x 17 LOPAR Design[c]	17 x 17 NAIF Design
Fuel Assembly Length[a]	159.765 in.	159.975 in. (Zircaloy) 159.775 in. to 159.975 in. (ZIRLO)
Fuel Rod Length[a]	151.560 in.	152.200 in. (Zircaloy) 152.600 in. to 152.800 in. (ZIRLO)
Assembly Envelope	8.426 in.	8.426 in.
Compatible with Core Internals	Yes	Yes
Fuel Rod Pitch	0.496 in.	0.496 in.
Number of Fuel Rods/Assembly[e]	264	264
Number of Guide Thimbles/ Assembly	24	24
Number of Instrumentation Tube Assembly	1	1
Compatible w/Movable In-core Detector System	Yes	Yes
Fuel Tube Material	Zircaloy-4	Zircaloy-4 or ZIRLO
Fuel Rod Clad o.d.	0.374 in.	0.374 in.
Fuel Rod Clad Thickness	0.0225 in.	0.0225 in.
Fuel/Clad Gap	6.5 mil	6.5 mil
Fuel Pellet Diameter	0.3225 in.	0.3225 in.
Fuel Pellet Length[d]	0.530	0.387
Guide Thimble Material	Zircaloy-4	Zircaloy-4 or ZIRLO
Guide Thimble o.d., (above dashpot).[a]	0.482 in	0.474 in
Guide Thimble Wall Thickness	0.016 in	0.016 in
Structural Material - Six Inner Grids[a]	Inconel	Zircaloy-4 or ZIRLO
Structural Material - Two End Grids	Inconel	Inconel
Grid Inner Strap Thickness[a]	10.5 mil (Inconel Grid)	18 mil (Zirc Grid or ZIRLO Grid) 10.5 mil (Inconel, P-grid)
Grid Outer Strap Thickness	17.0 mil (Inconel Grid)	26 mil (Zirc Grid or ZIRLO Grid) 17.0 mil (Inconel) 20.5 mil (P-grid)

Table 4.2-2 (continued)
COMPARISON OF 17 X 17 LOPAR ASSEMBLY
AND 17 X 17 NAIF ASSEMBLY NOMINAL DESIGN PARAMETERS

Parameter	17 x 17 LOPAR Design[c]	17 x 17 NAIF Design
Grid Support for Fuel Rods	6 Points 2 Springs 4 Dimples[b]	6 Points (structural grids) 2 Springs 4 Dimples[b] 4 Points (P-grid), dimples
Grid Height, less vanes/inner straps, in.[a]	1.322 (mid Grids) 1.322 (end Grids)	1.500 (mid Grids) 1.522 (end Grids) 0.690 (P-grid)
Grid Fabrication Method	Brazed joining of interlocking stamped straps	Laser welded interlocking stamped straps (six inner mixing vane grids and P-grid); Brazed joining (Top & Bottom Grids)
Grid/Guide Thimble Attachment	Thimbles and sleeves bulged together and sleeves prebrazed into grid straps	Thimbles and sleeves bulged together and sleeves laser prewelded into grid straps
Top Nozzle[a]	Standard	Removable
Top Nozzle Holdown Springs	3-leaf	3-leaf
Compatible With Fuel Handling Equipment	Yes	Yes
Bottom Nozzle[a]	Reconstitutable	Reconstitutable Debris Filter[b]

a. NAIF design change compared to the LOPAR design. The increased ZIRLO fuel assembly and fuel rod lengths were introduced with North Anna 1 Batch 19 fuel.
b. Vantage 5H design did not have a debris filter.
c. Extended burnup, Reconstitutable Top Nozzle and Reconstitutable Debris Filter Bottom Nozzle Features Introduced on:
- Cycle 8, Unit 1
- Cycle 7, Unit 2
P-grids introduced on:
- Cycle 11, Unit 1
- Cycle 10, Unit 2
d. The shorter pellet design was implemented at North Anna in Unit 2 Region 8 fuel and Unit 1 Region 9 fuel.
e. Reconstituted fuel assemblies may contain some solid metal filler rods in place of fuel rods.

Figure 4.2-1
FUEL ASSEMBLY CROSS SECTION 17 X 17

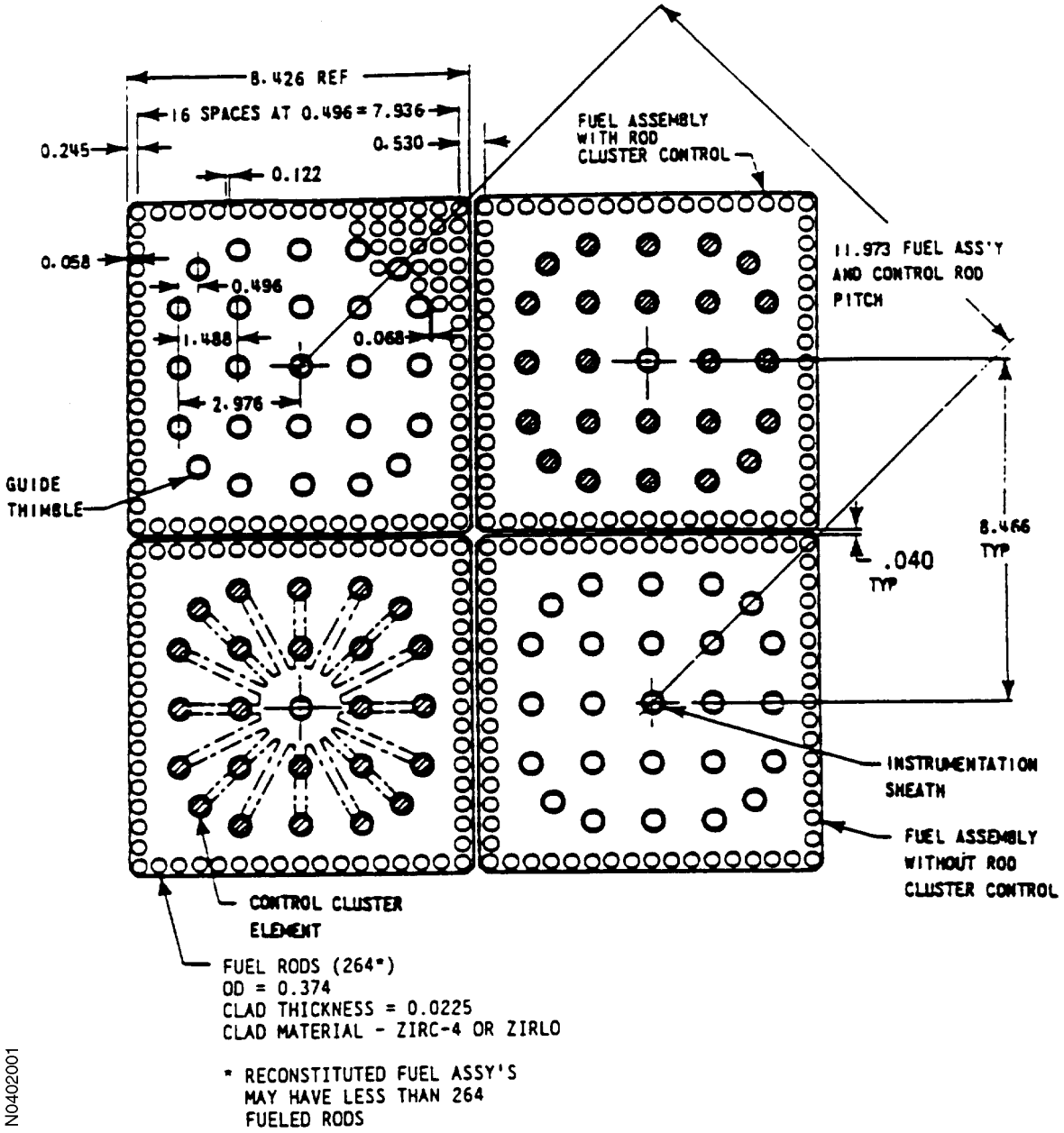

Figure 4.2-2
LOPAR FUEL ASSEMBLY OUTLINE 17 X 17

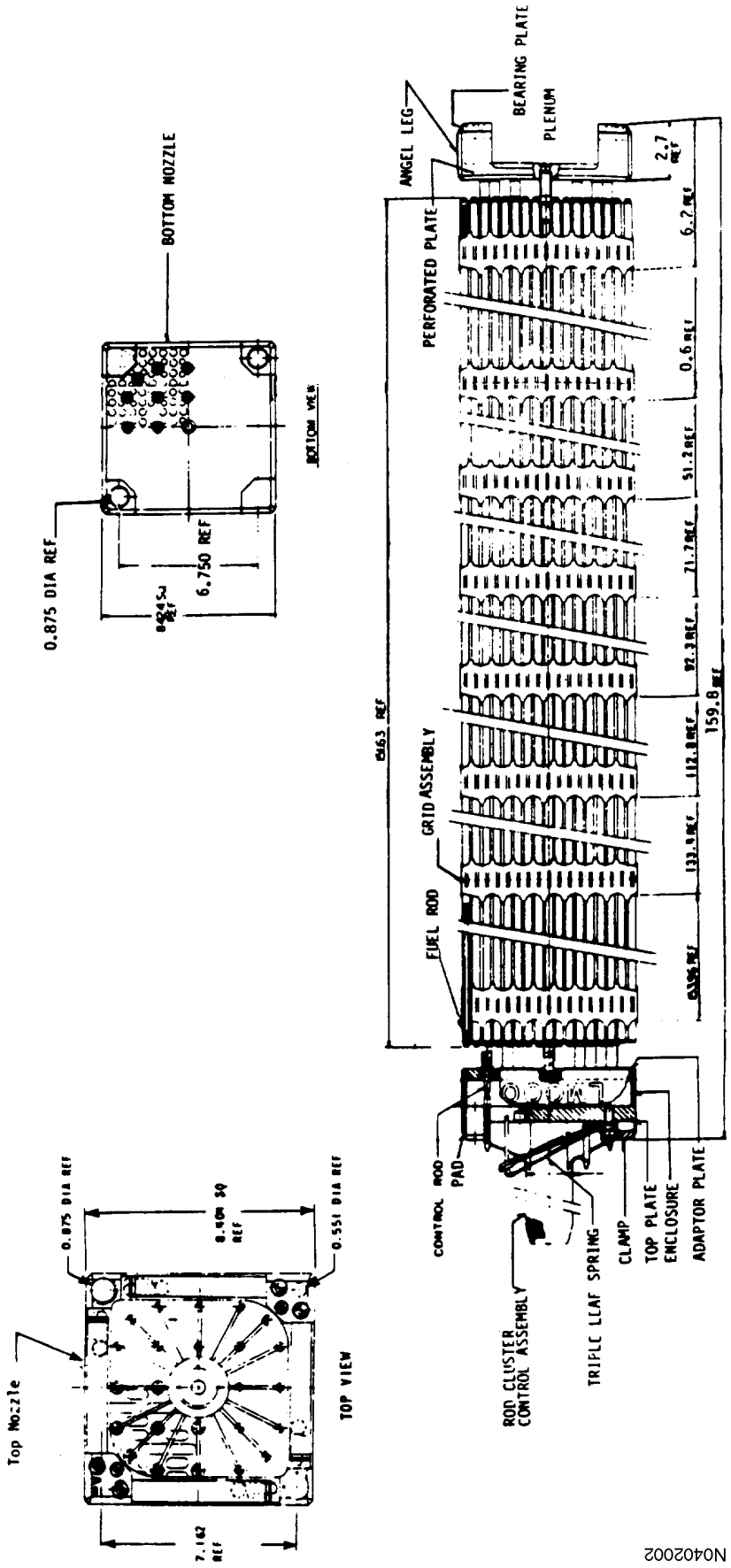

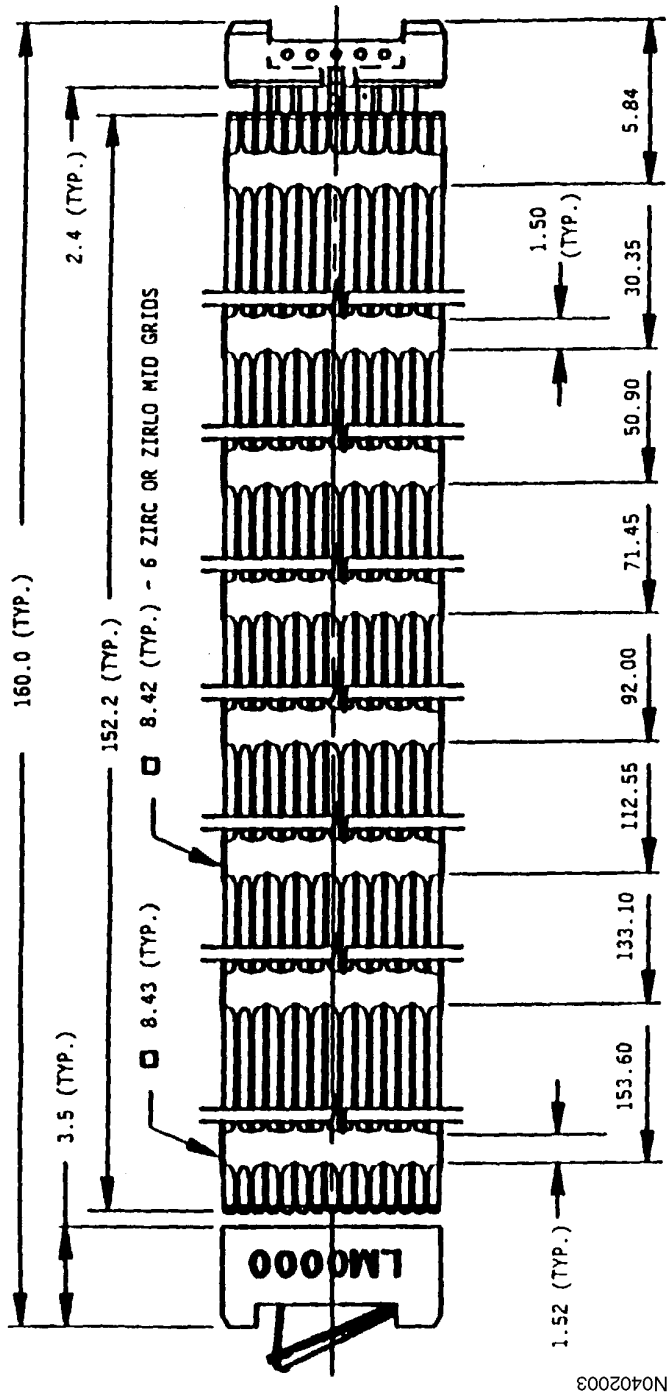

Figure 4.2-3
17 X 17 NAIF FUEL ASSEMBLY
All Dimensions Typical. Also see Table 4.2-2

Figure 4.2-4
COMPARISON OF 17 X 17 NAIF FUEL ASSEMBLY
WITH AND WITHOUT PROTECTIVE GRID

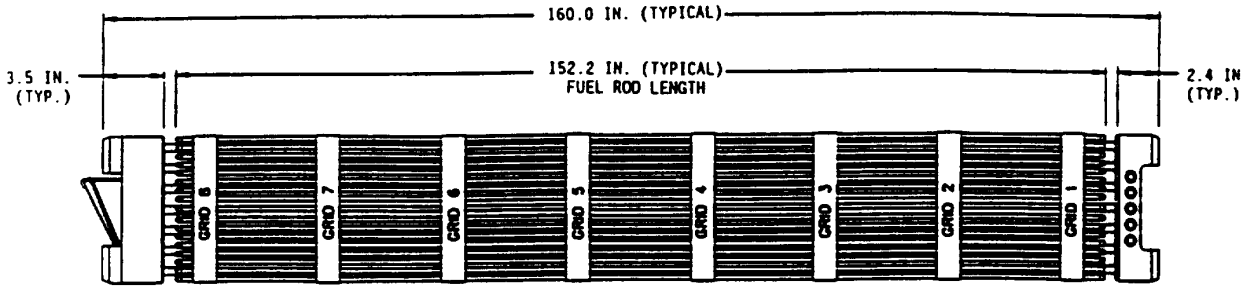

ORIGINAL 17 X 17 NAIF FUEL ASSEMBLY

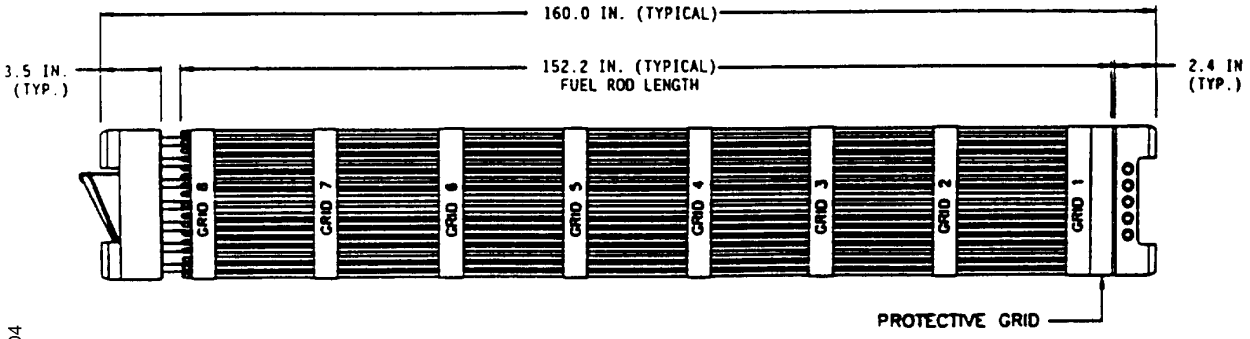

N0402004

17 X 17 NAIF FUEL ASSEMBLY WITH PROTECTIVE GRID

Figure 4.2-5
BOTTOM NOZZLE/PROTECTIVE GRID/FUEL ROD INTERFACE

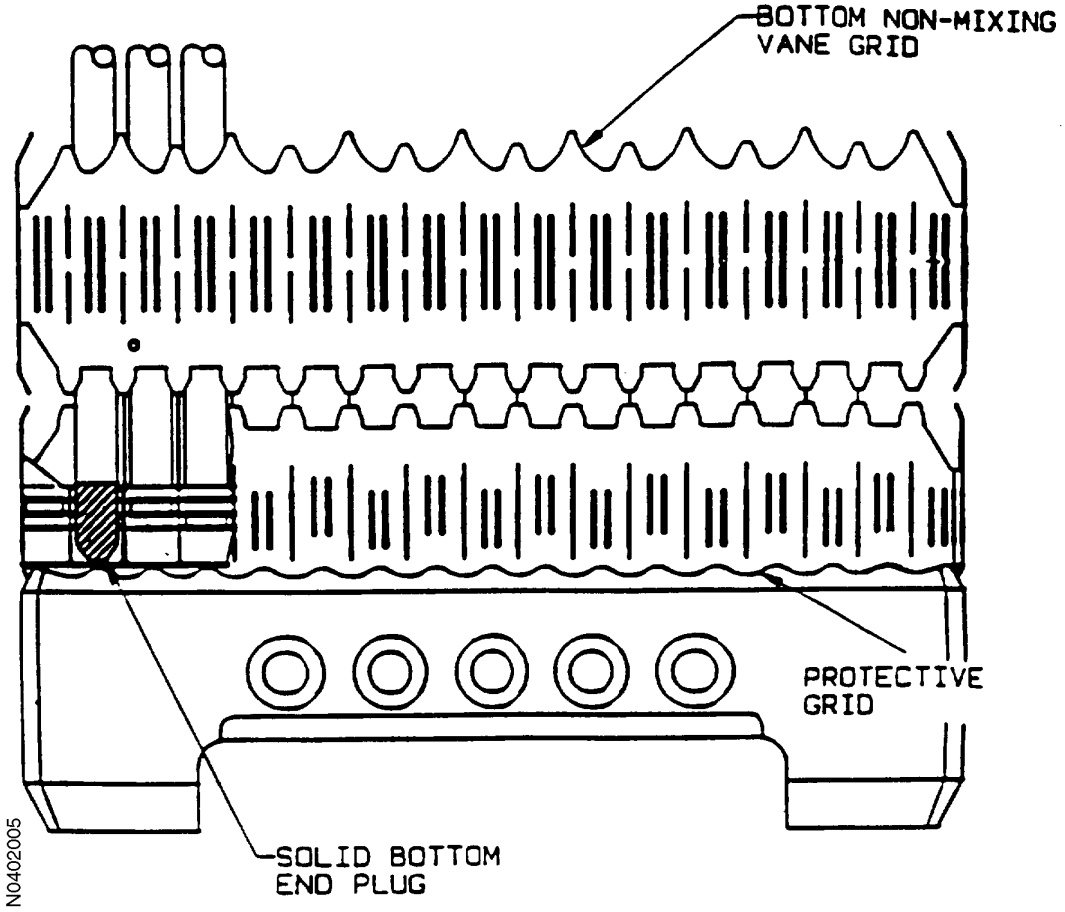

Figure 4.2-6
LOPAR FUEL ROD SCHEMATIC

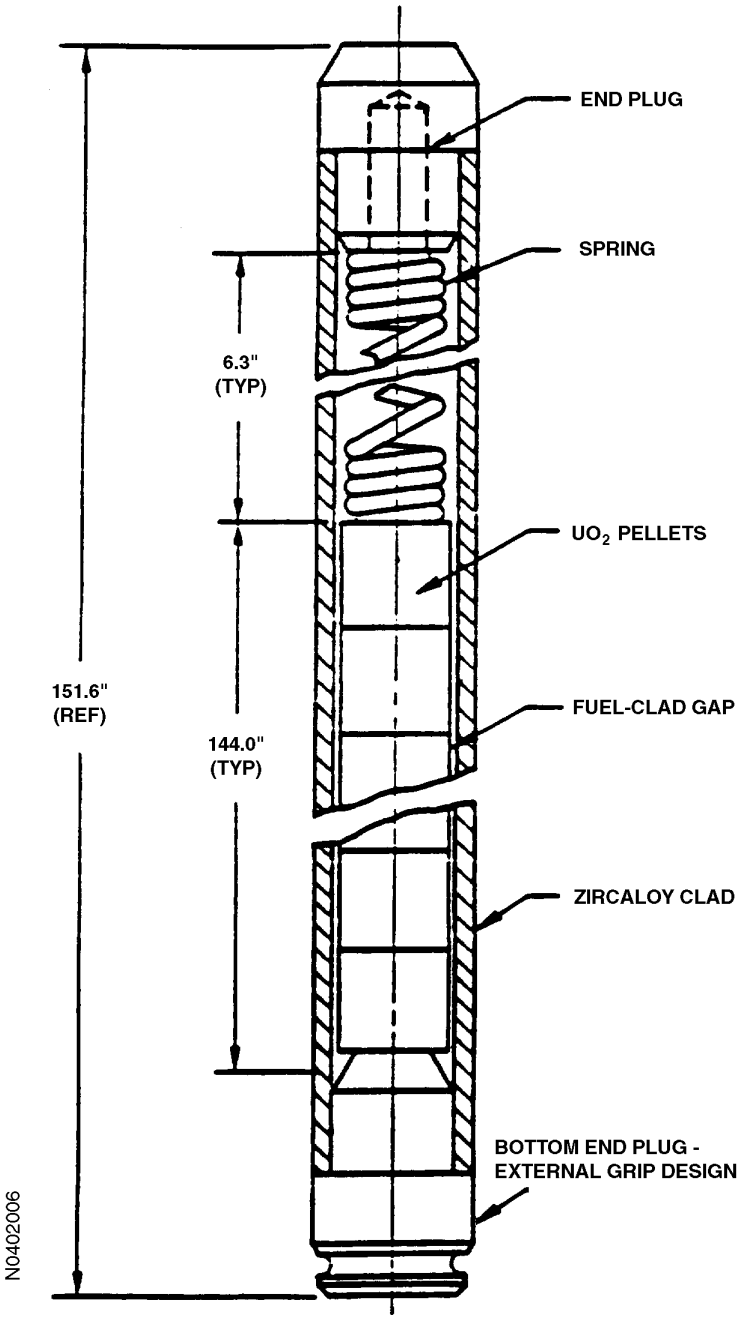

SPECIFIC DIMENSIONS DEPEND ON DESIGN VARIABLES SUCH AS PRE-PRESSURIZATION, POWER HISTORY, AND DISCHARGE BURNUP.

Figure 4.2-7
17 X 17 NAIF FUEL ROD SCHEMATIC

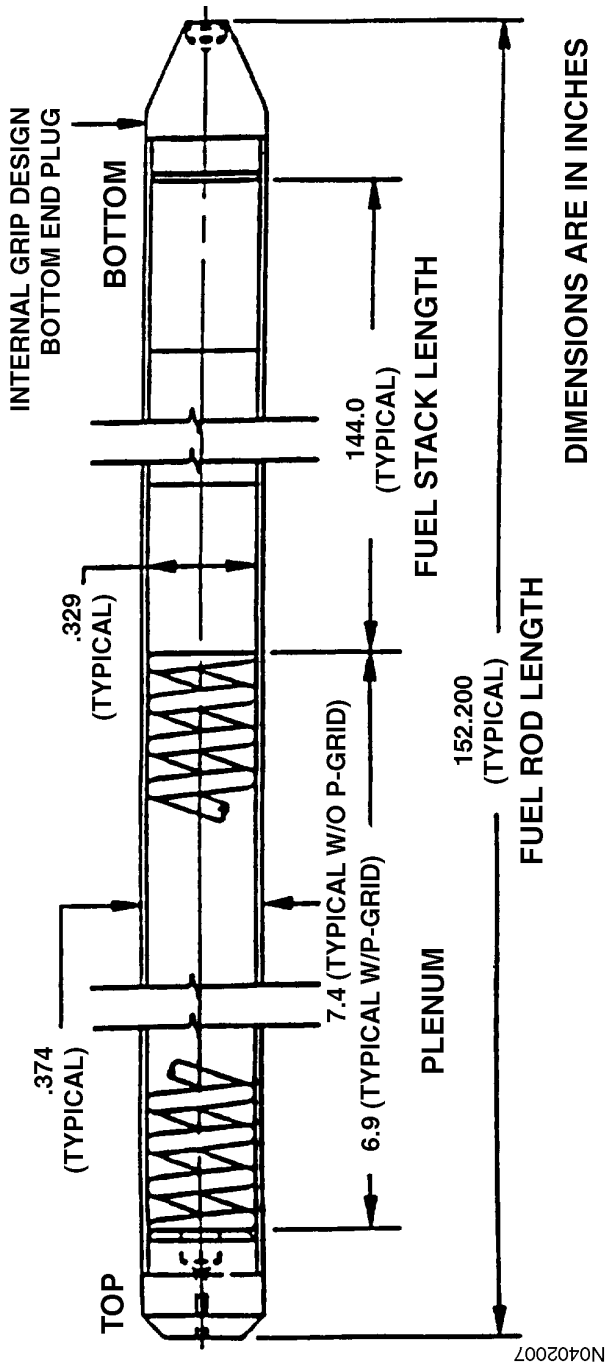

Figure 4.2-8
TYPICAL CLAD AND PELLET DIMENSIONS AS A FUNCTION OF EXPOSURE
(BASED ON INITIAL NORTH ANNA CORE)

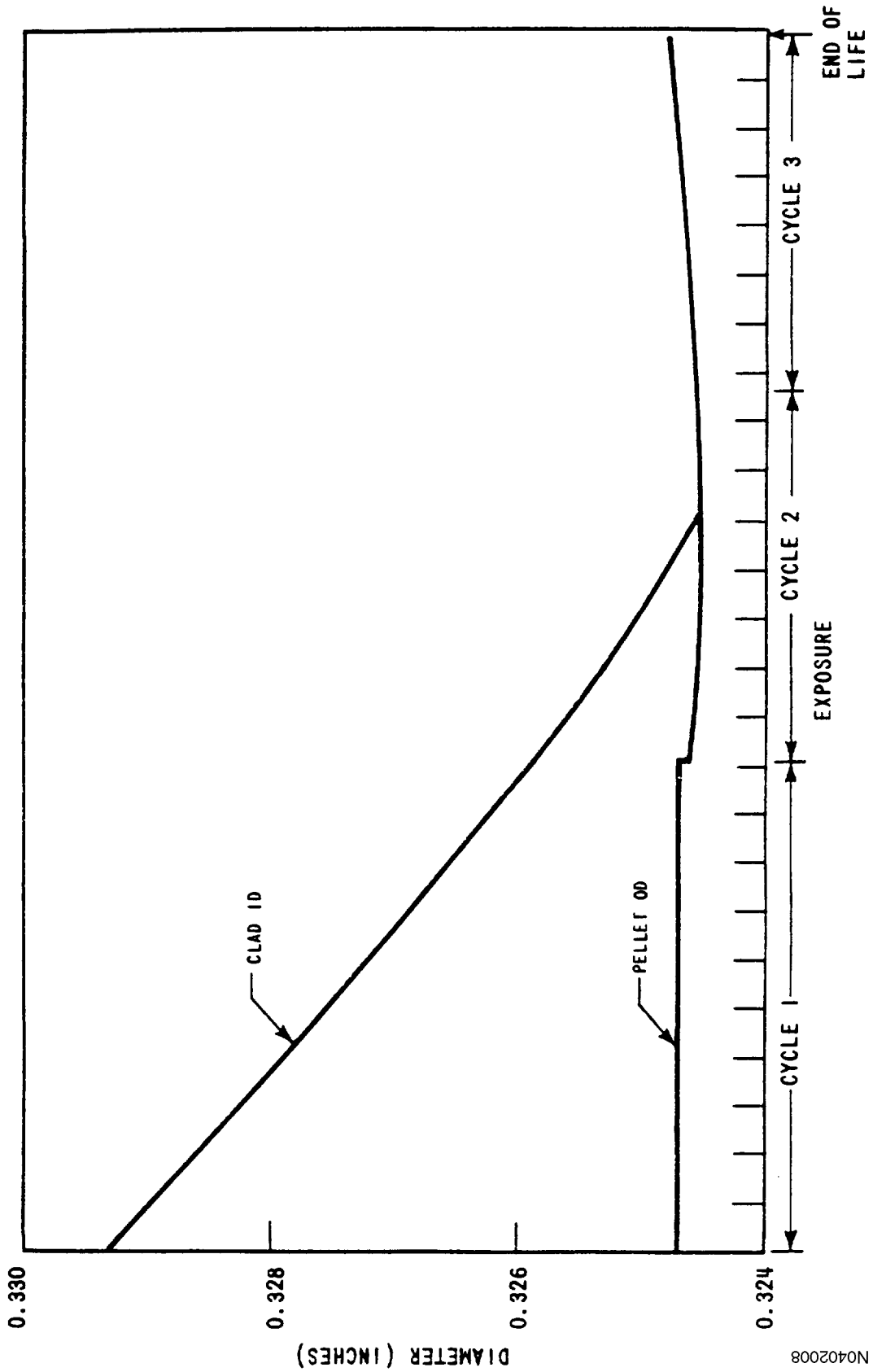

Figure 4.2-9
REPRESENTATIVE ROD INTERNAL PRESSURE AND LINEAR POWER DENSITY AS A FUNCTION OF TIME FOR THE LEAD BURNUP ROD IN THE INITIAL NORTH ANNA CORE

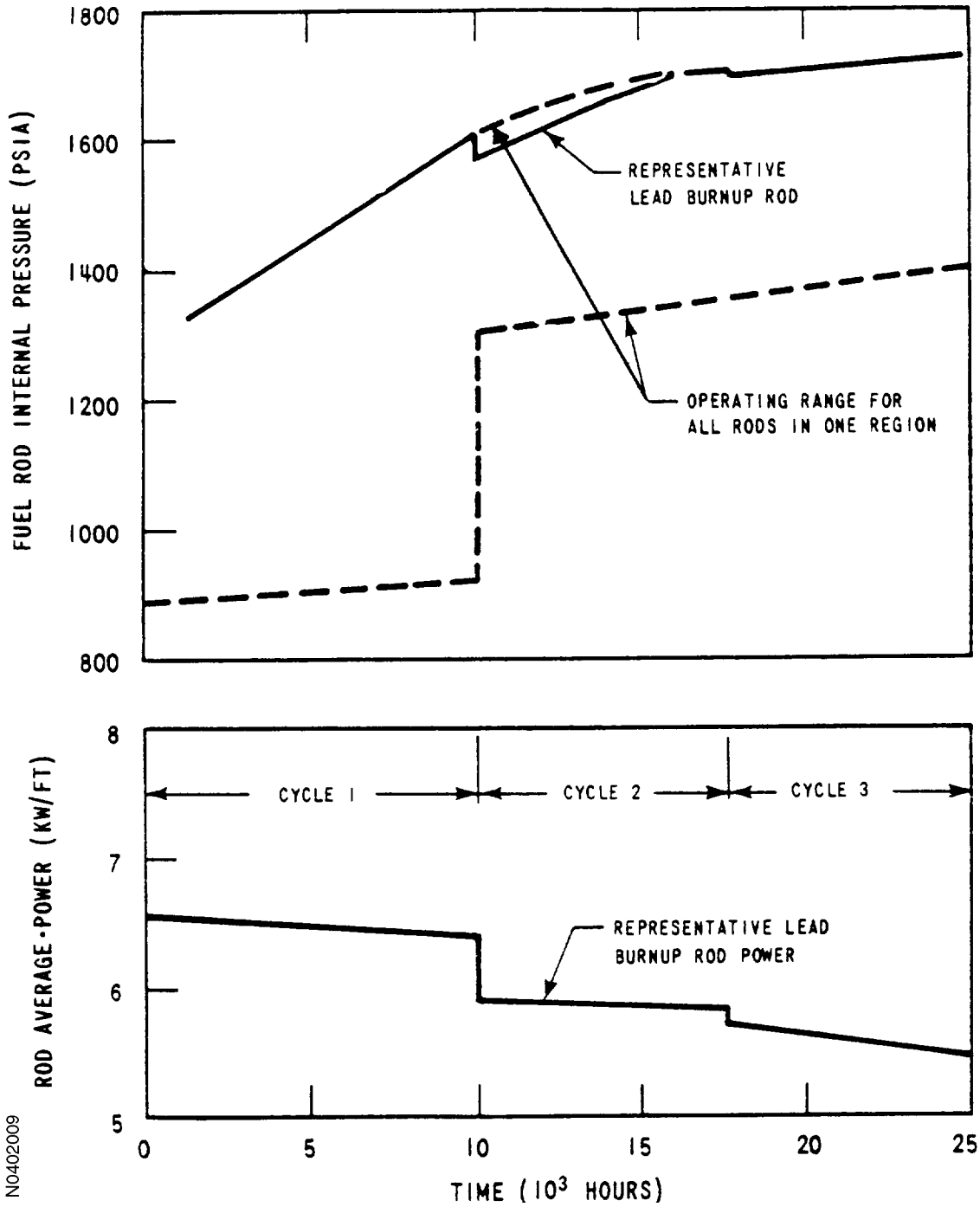

Figure 4.2-10
REMOVABLE ROD COMPARED TO STANDARD ROD, INITIAL CORE FUEL

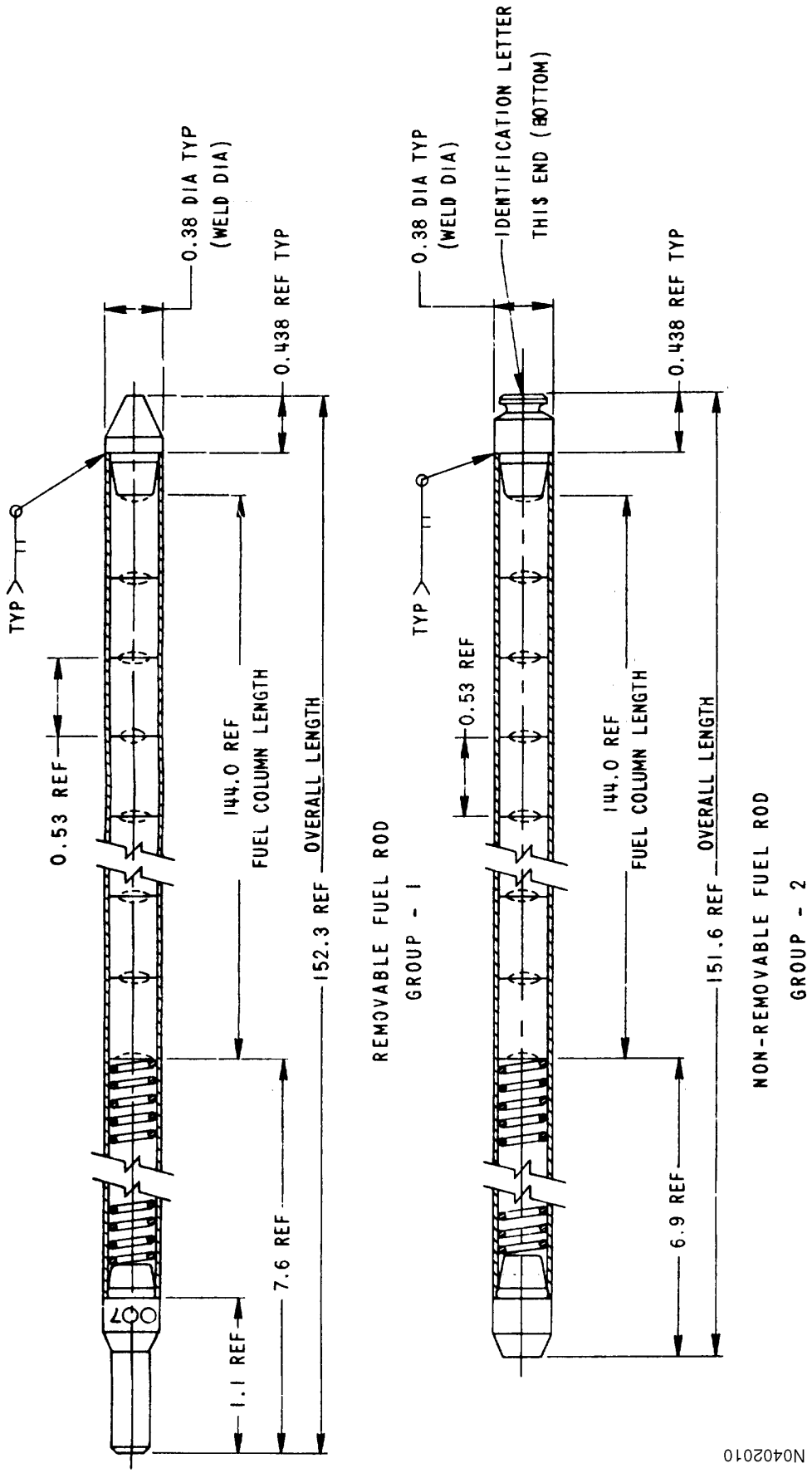

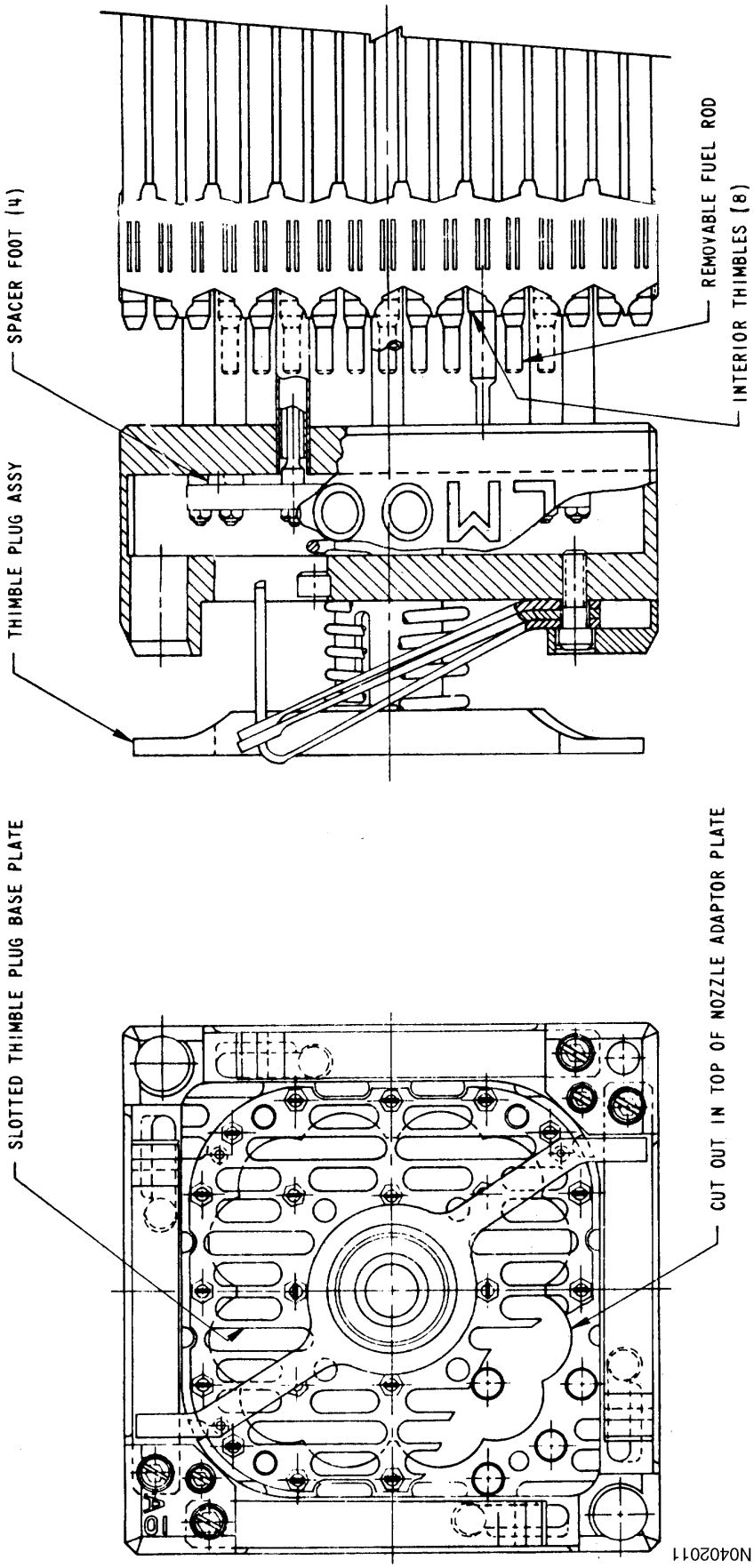

Figure 4.2-11
INITIAL CORE REMOVABLE FUEL ROD ASSEMBLY,
DETAILS OF UPPER END OF ASSEMBLY

Figure 4.2-12
LOCATION OF REMOVAL RODS WITHIN AN ASSEMBLY (FIRST CORE)

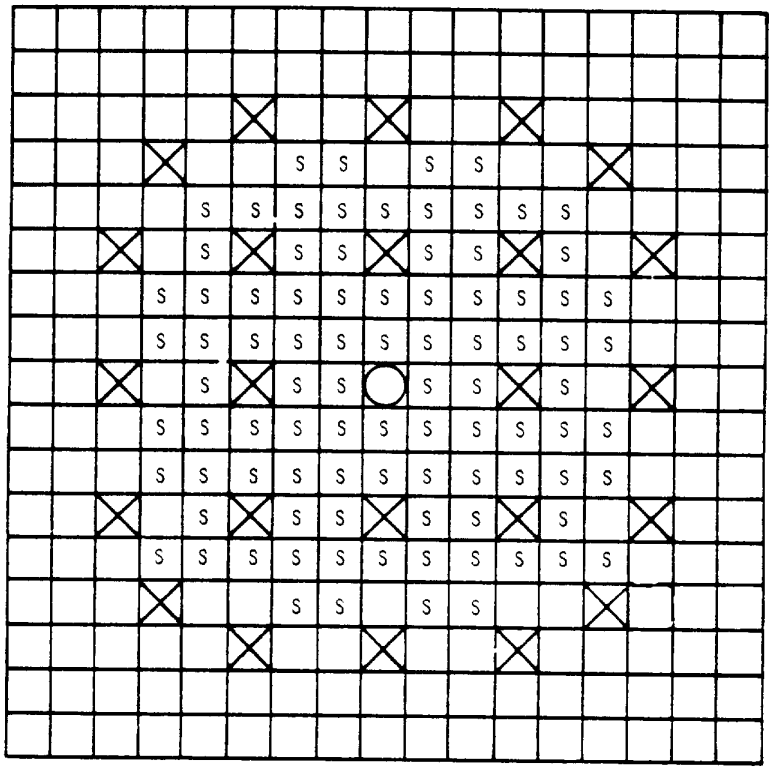

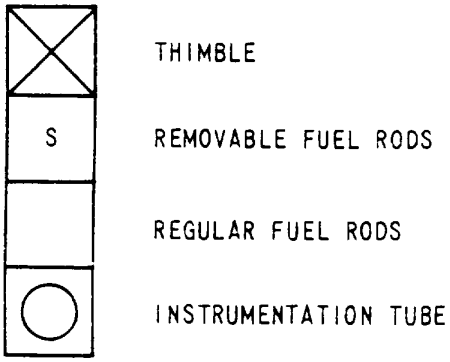

N0402012

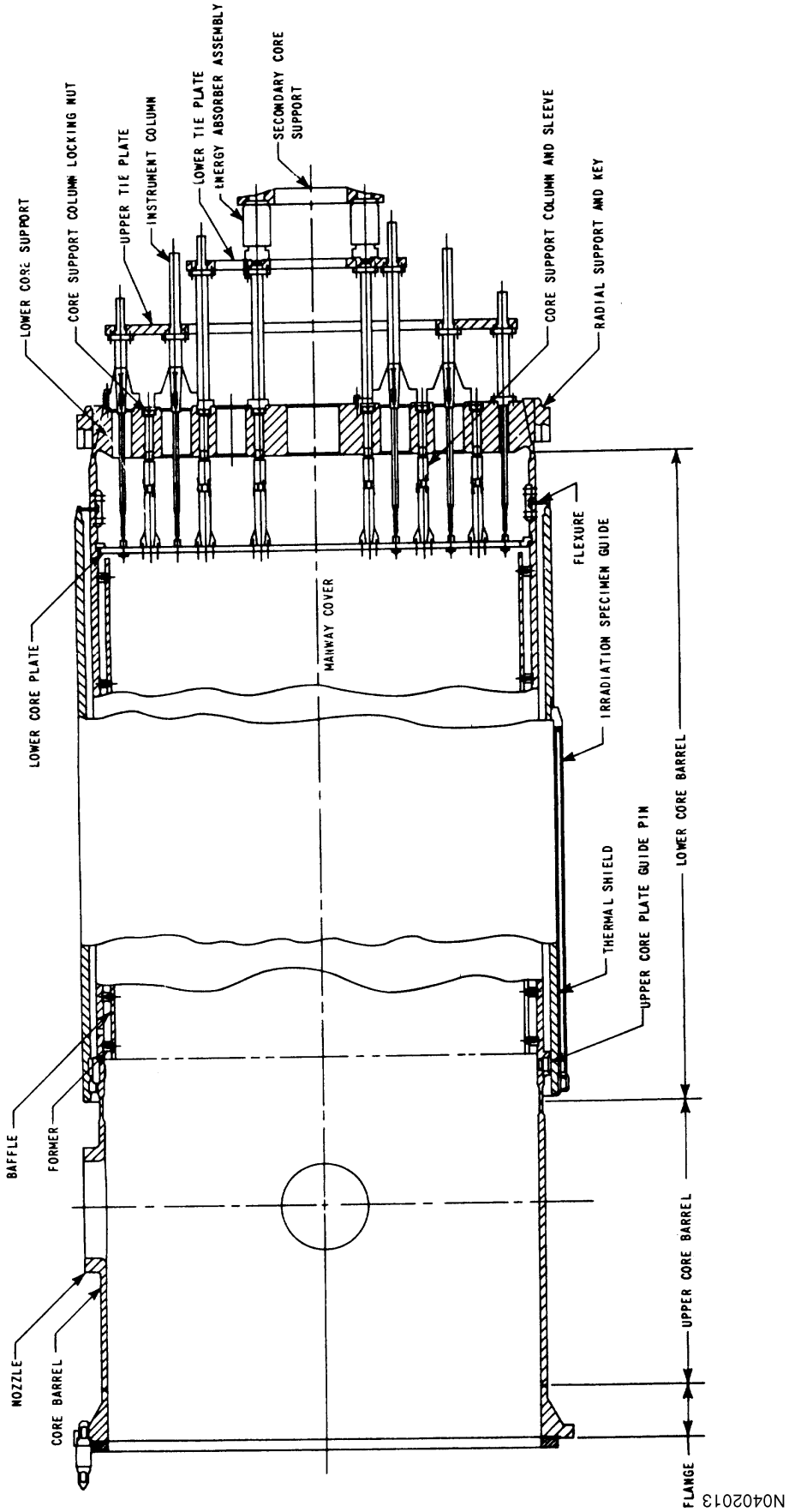

Figure 4.2-13
LOWER CORE SUPPORT ASSEMBLY (CORE BARREL ASSEMBLY)

Figure 4.2-14
UPPER CORE SUPPORT ASSEMBLY

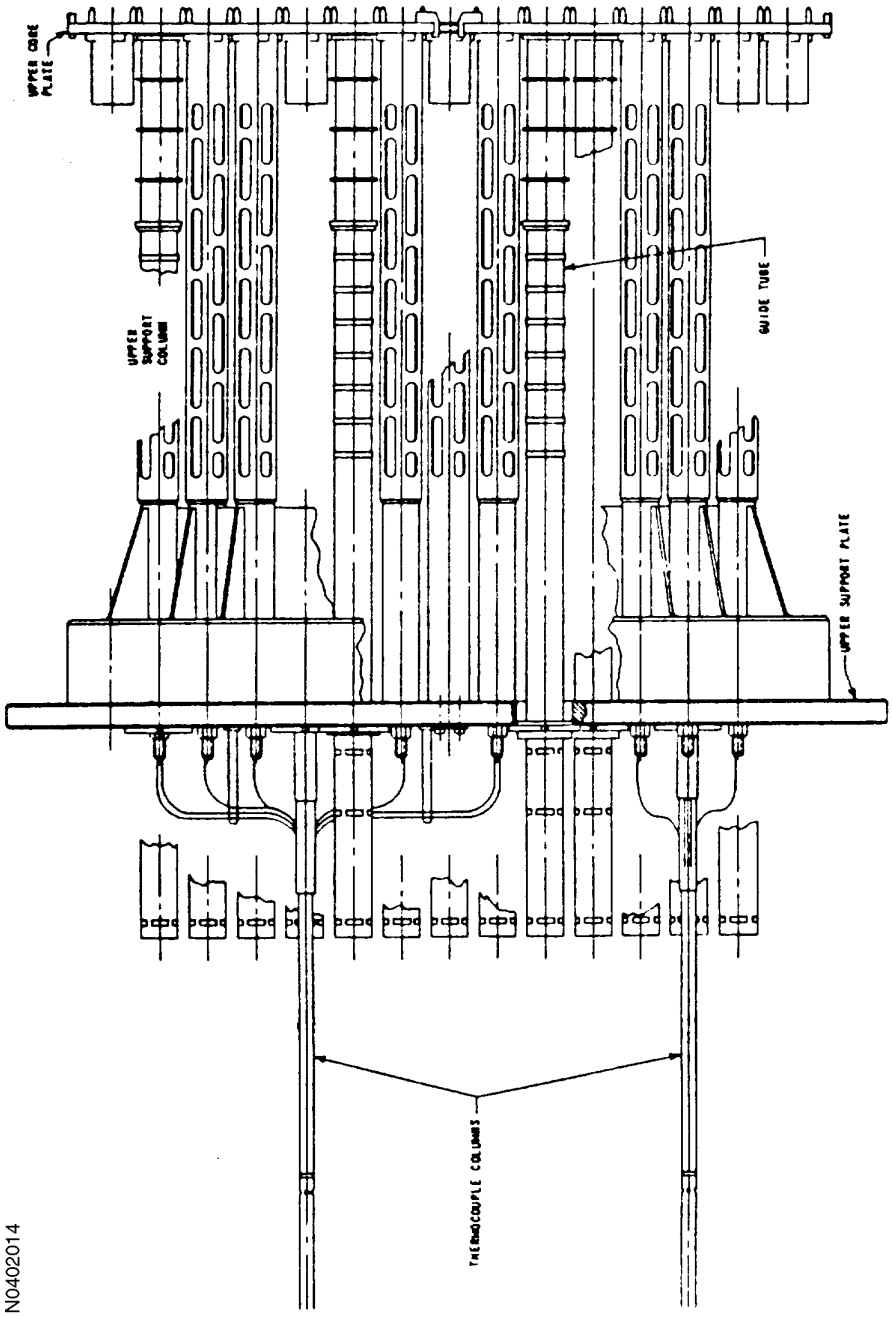

Figure 4.2-15
PLANE VIEW OF UPPER CORE SUPPORT STRUCTURE

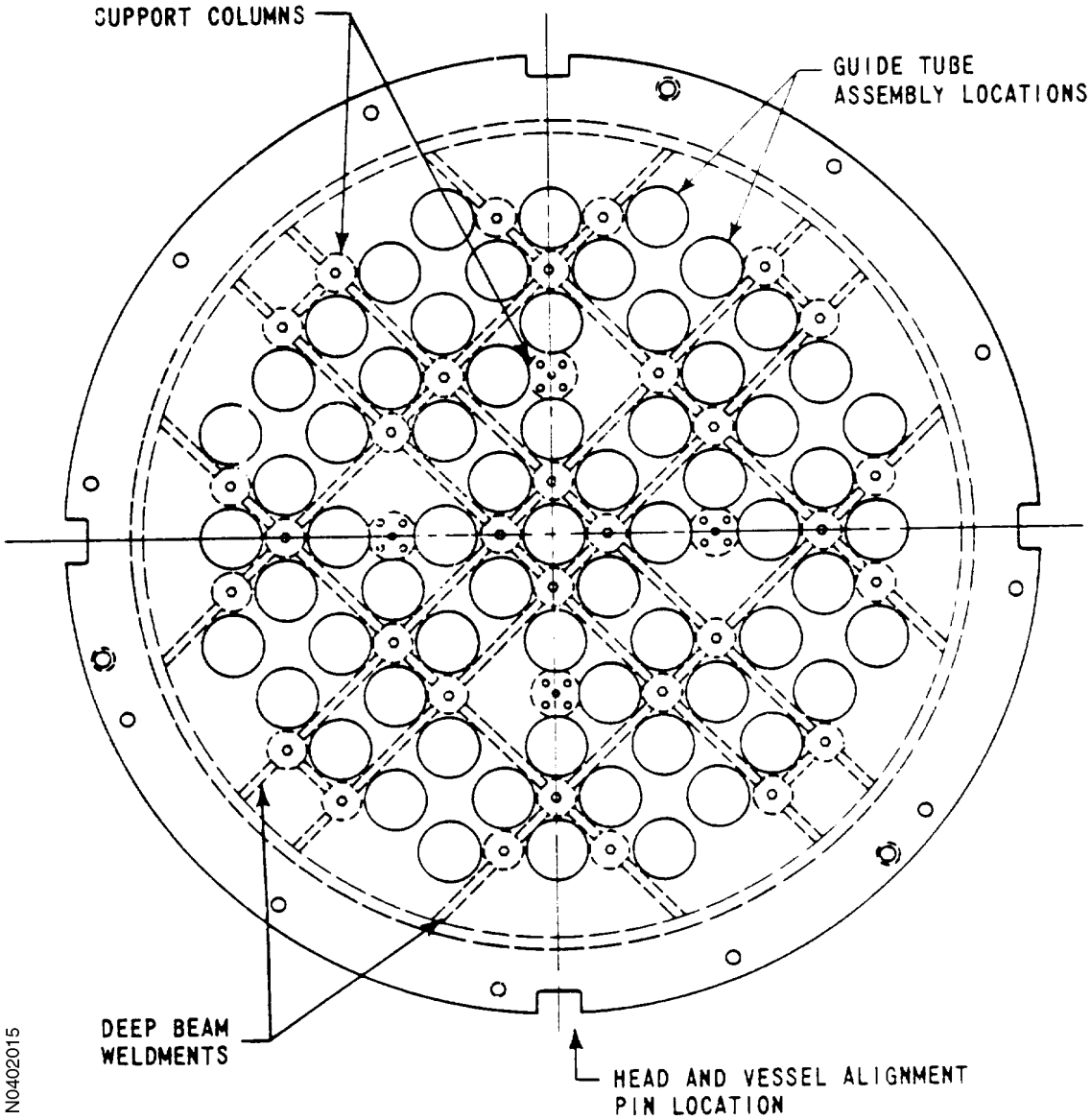

Figure 4.2-16
ROD CLUSTER CONTROL AND DRIVE ROD
ASSEMBLY WITH INTERFACING COMPONENTS

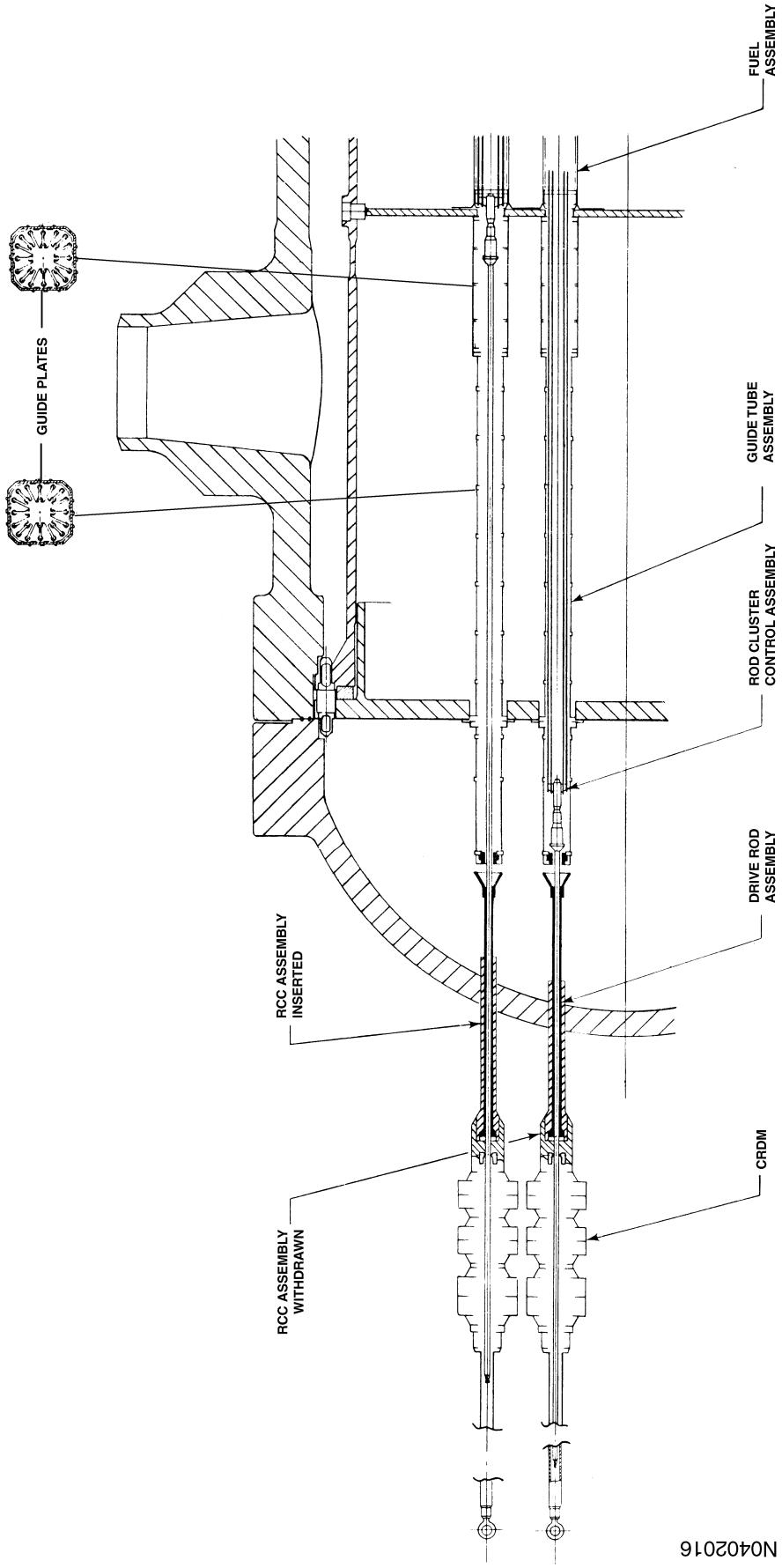

Figure 4.2-17
ROD CLUSTER CONTROL ASSEMBLY OUTLINE

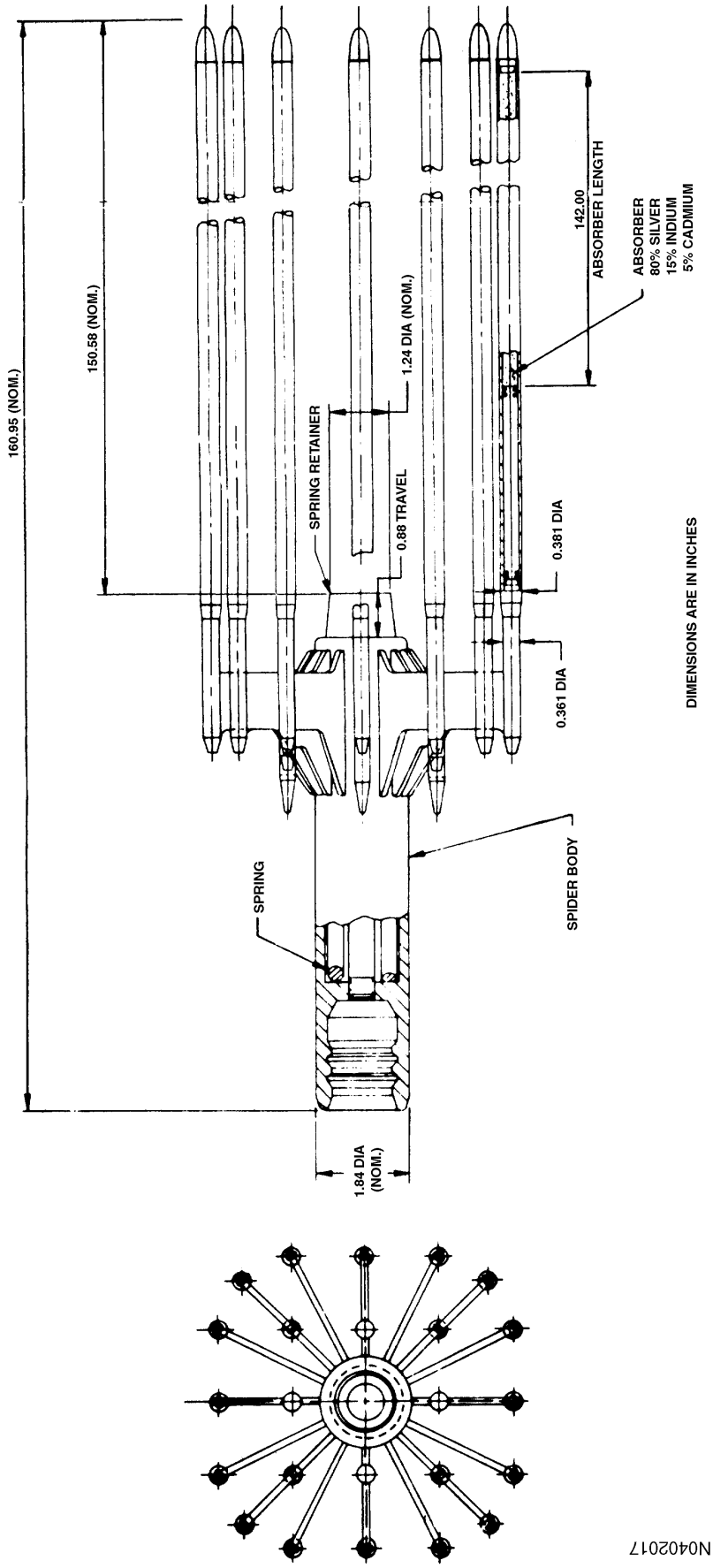

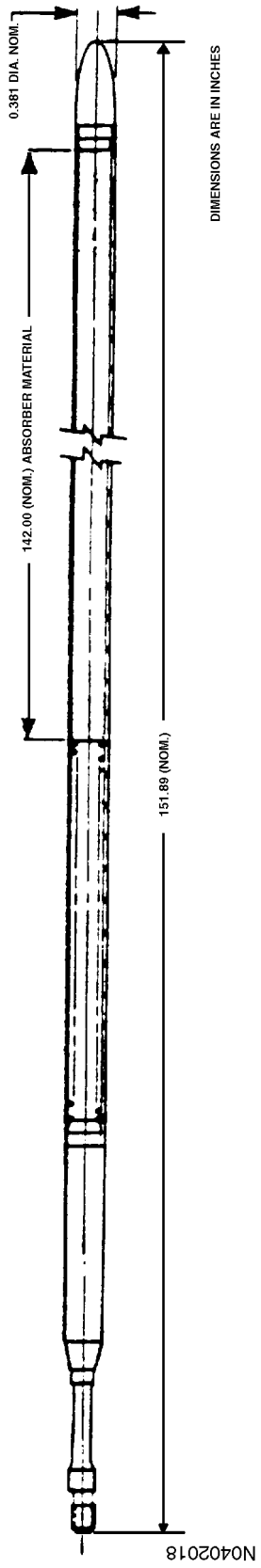

Figure 4.2-18
ABSORBER ROD

Figure 4.2-19
BURNABLE POISON ASSEMBLY

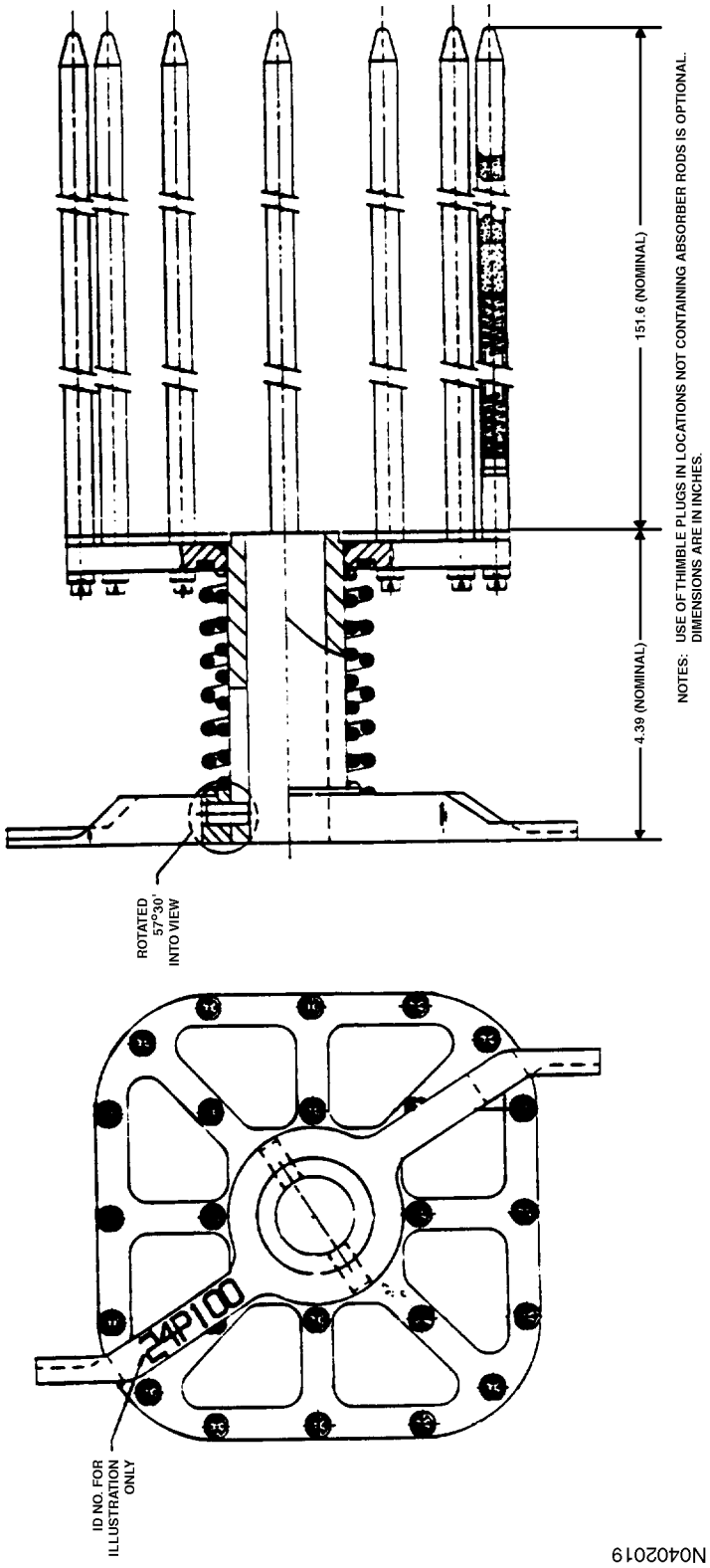

Figure 4.2-20
CURRENT BURNABLE ABSORBER ROD CROSS-SECTION

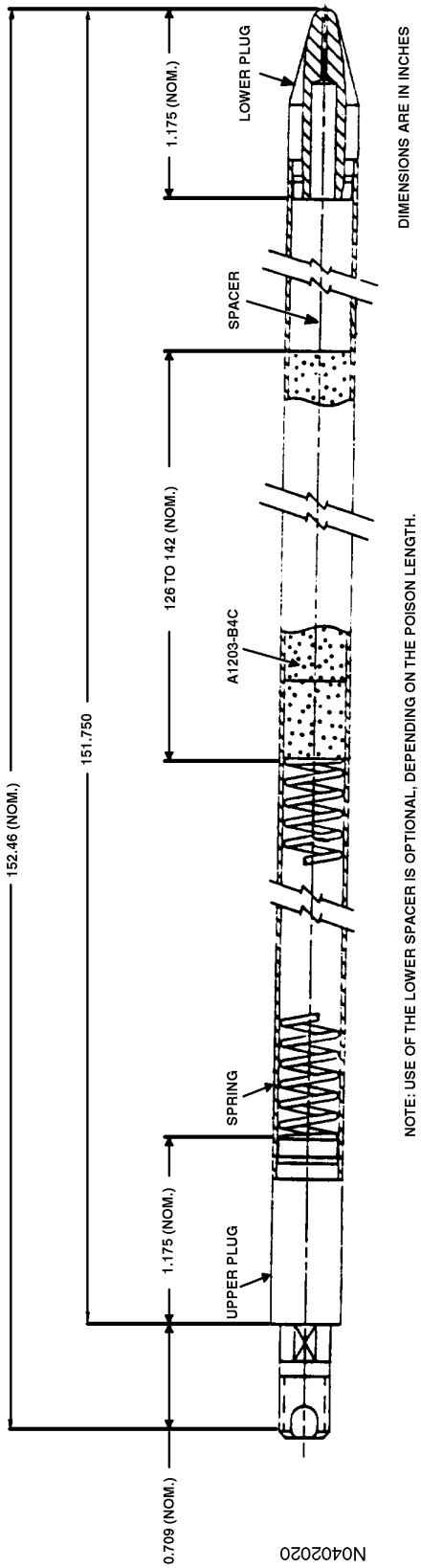

Figure 4.2-21
PRIMARY SOURCE ASSEMBLY

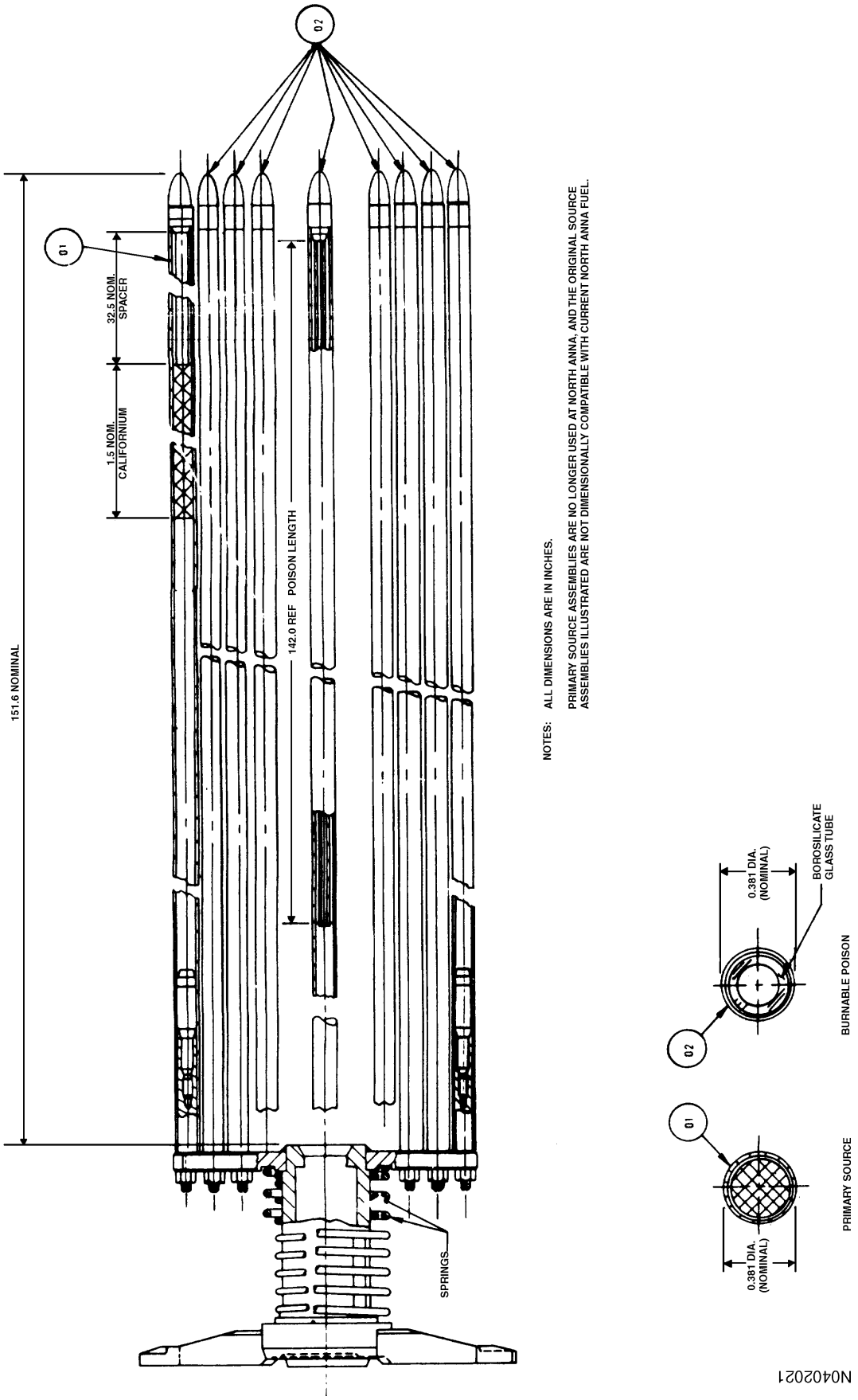

NOTES: ALL DIMENSIONS ARE IN INCHES.

PRIMARY SOURCE ASSEMBLIES ARE NO LONGER USED AT NORTH ANNA, AND THE ORIGINAL SOURCE ASSEMBLIES ILLUSTRATED ARE NOT DIMENSIONALLY COMPATIBLE WITH CURRENT NORTH ANNA FUEL.

Figure 4.2-22
17 X 17 SECONDARY SOURCE ASSEMBLY

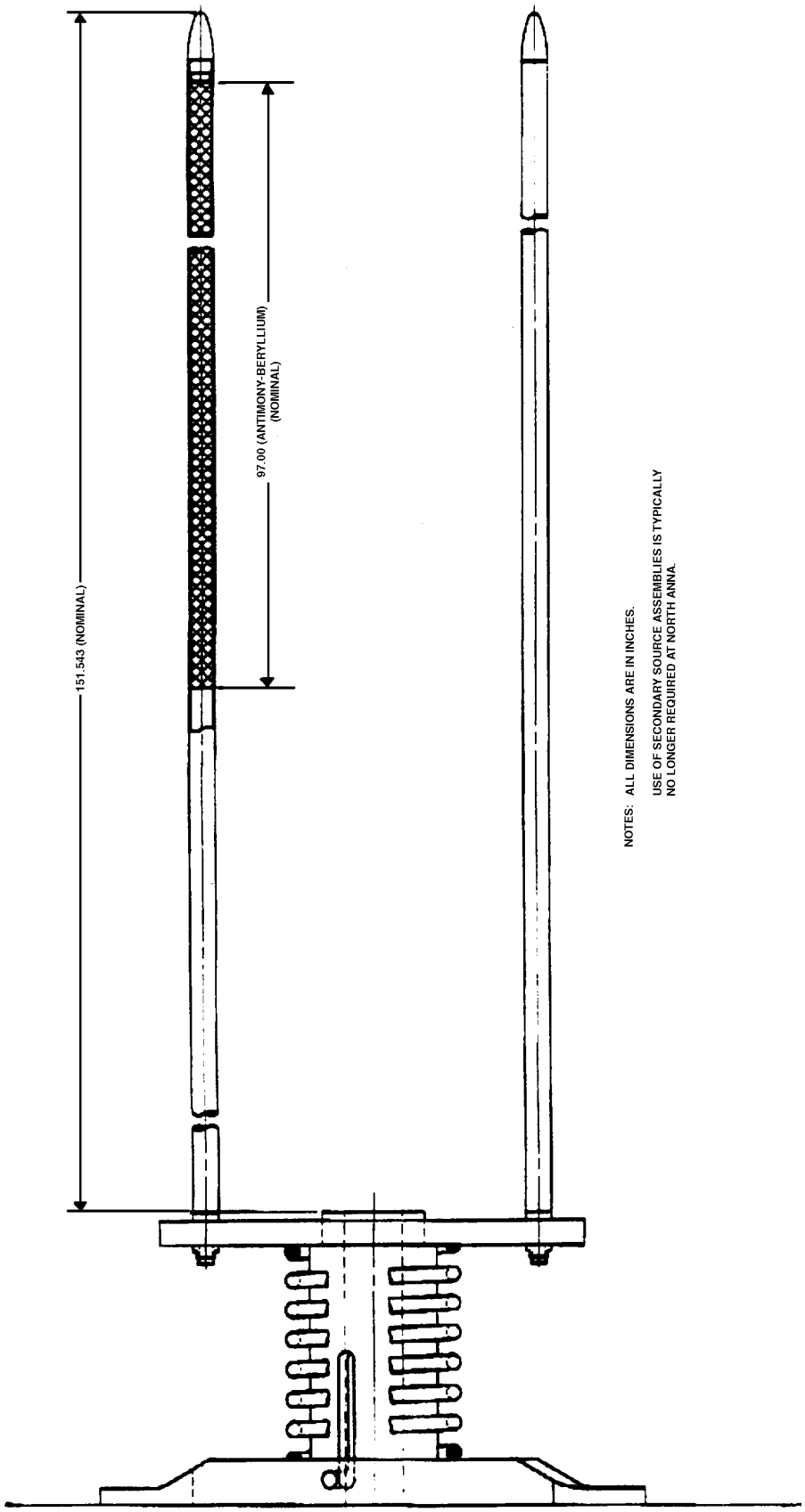

Figure 4.2-23
THIMBLE PLUG ASSEMBLY

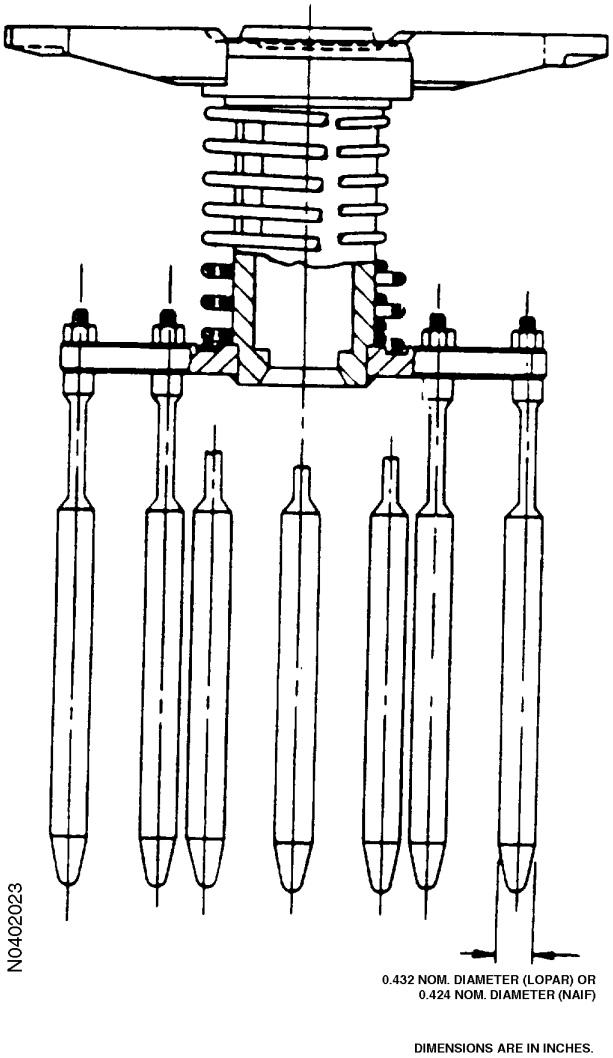

Figure 4.2-24
CONTROL ROD DRIVE MECHANISM

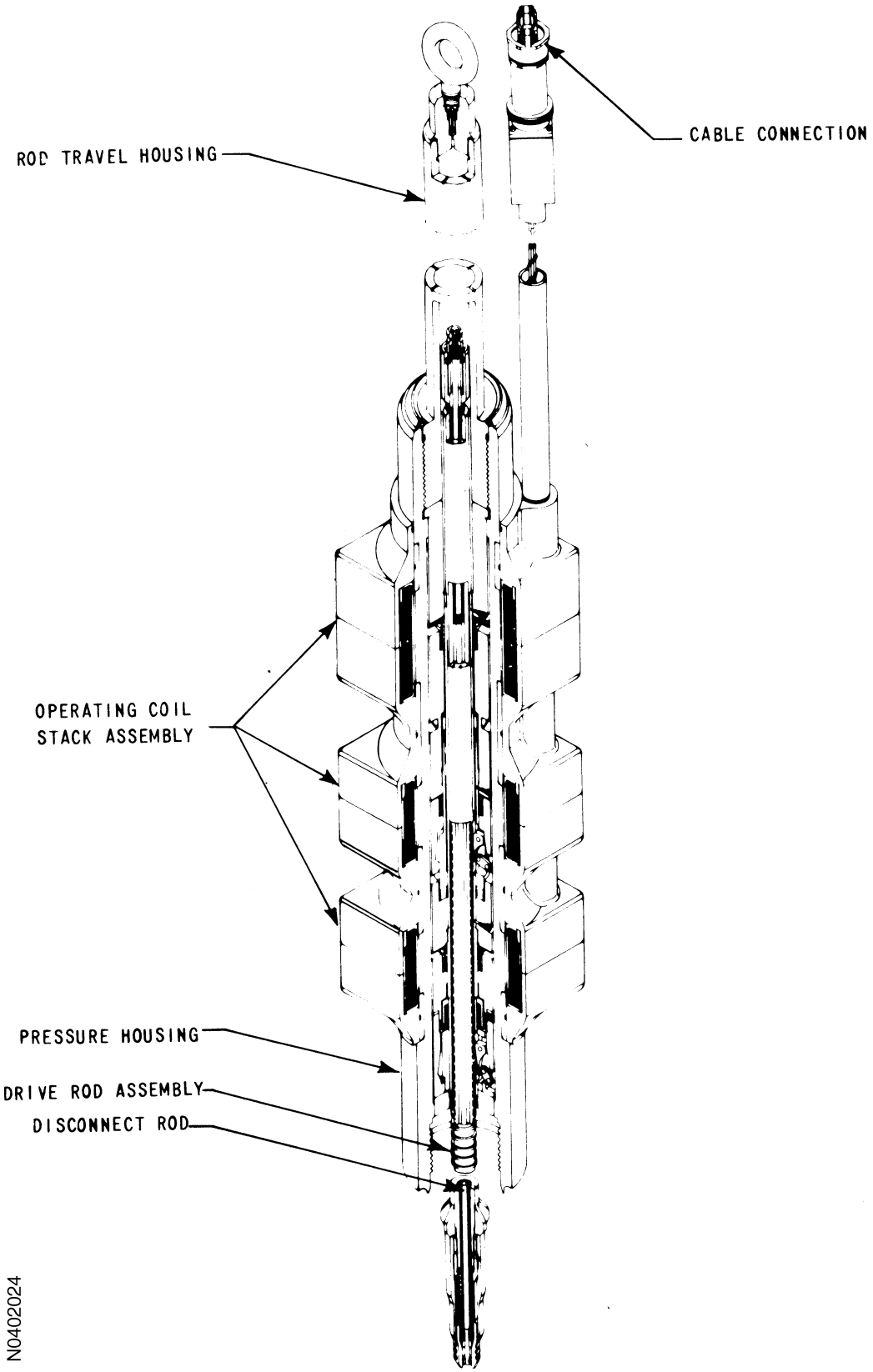

Figure 4.2-25
CONTROL ROD DRIVE MECHANISM SCHEMATIC

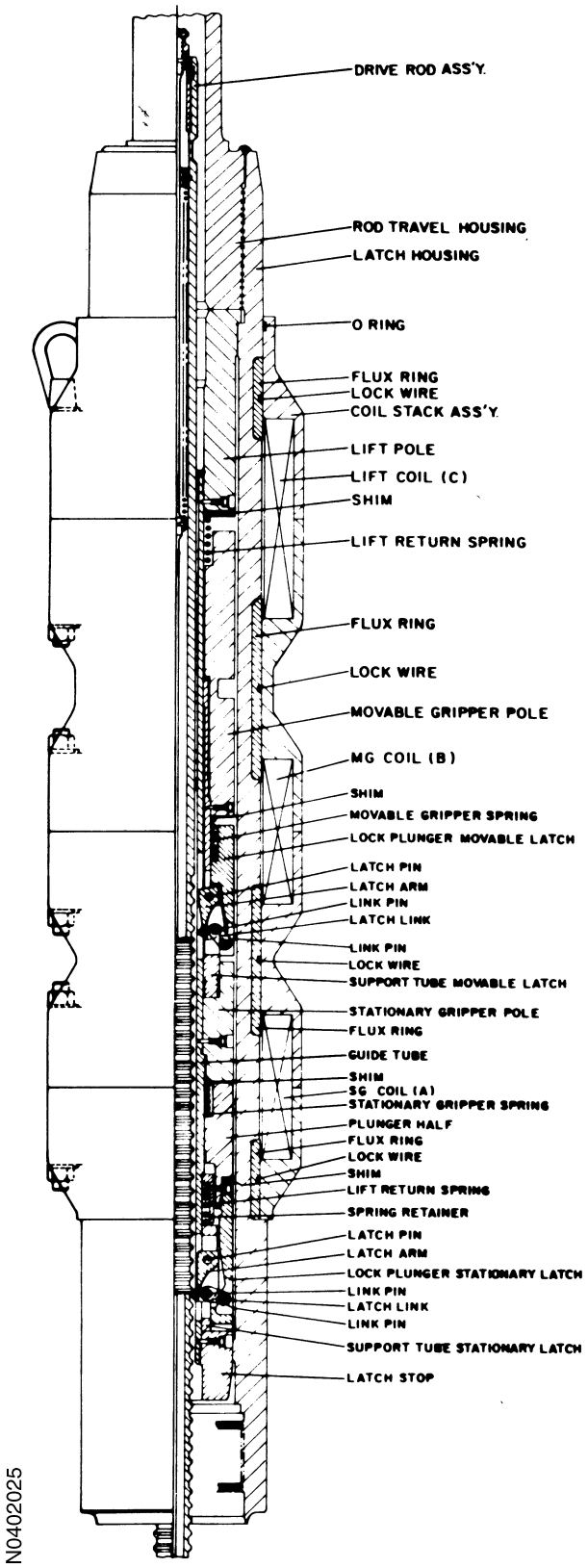

Figure 4.2-26
CONTROL ROD DRIVE MECHANISM
NOMINAL LATCH CLEARANCE AT MINIMUM AND MAXIMUM TEMPERATURE

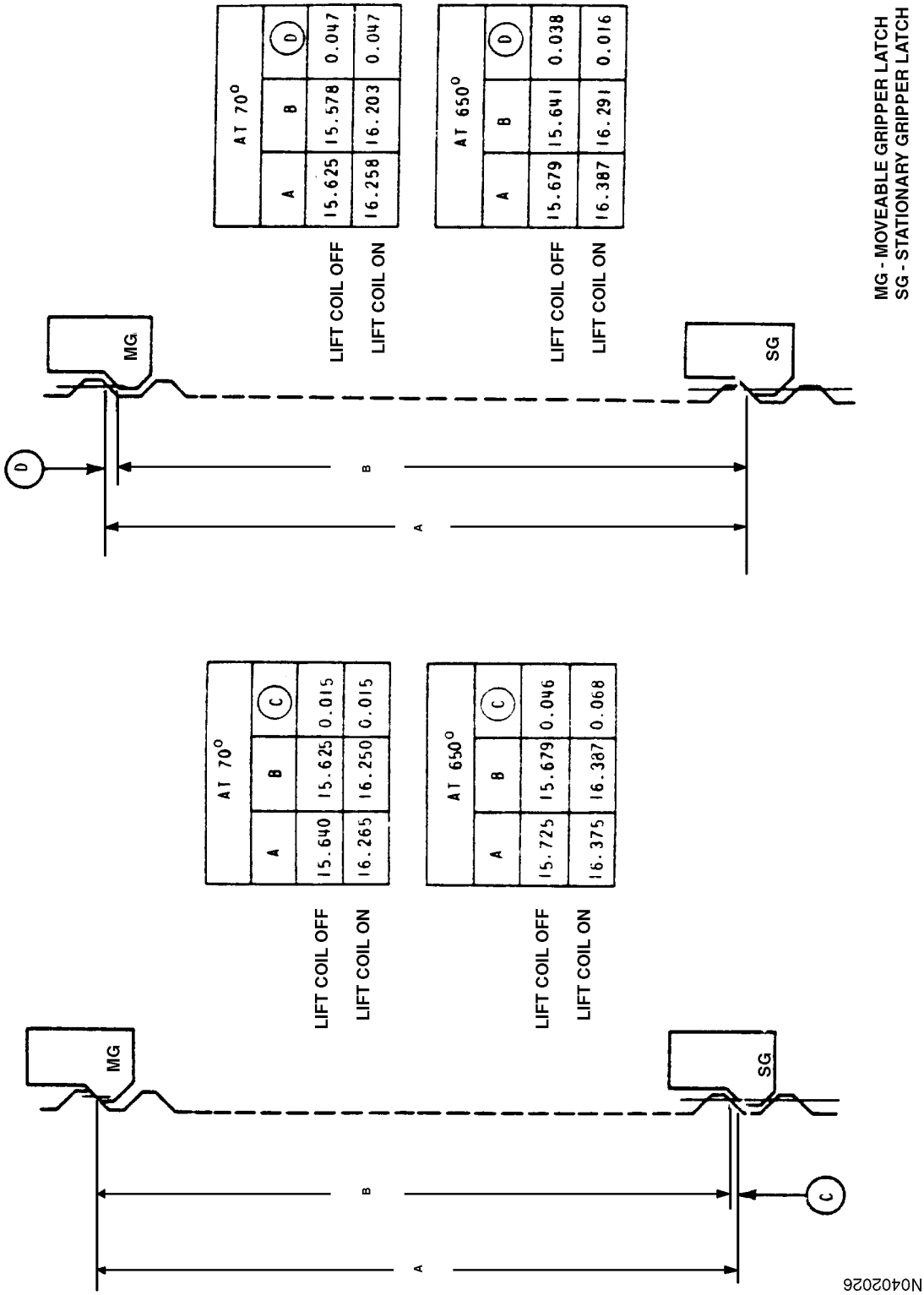

Figure 4.2-27
CONTROL ROD DRIVE MECHANISM LATCH CLEARANCE THERMAL EFFECT

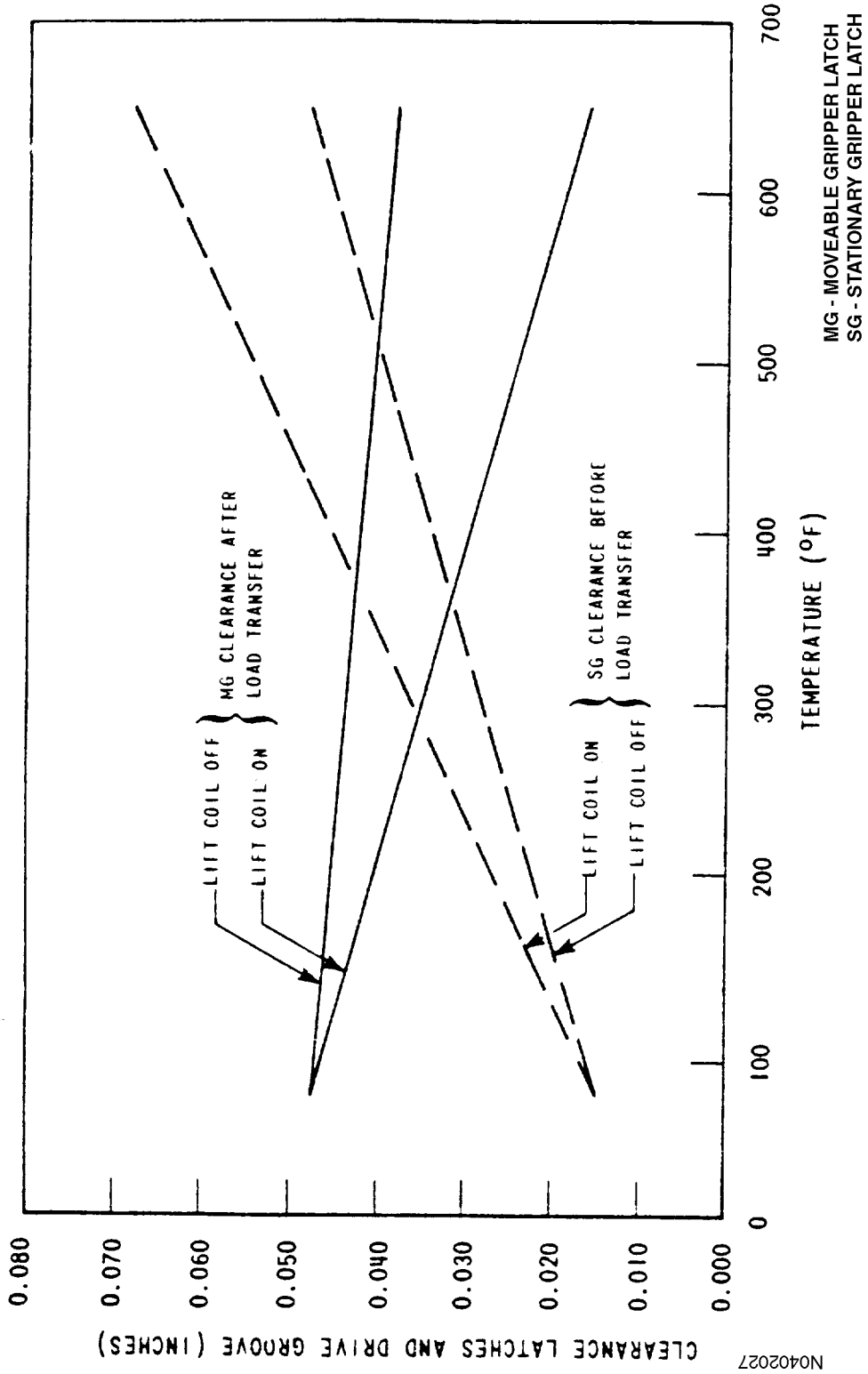

Intentionally Blank

4.3 NUCLEAR DESIGN

4.3.1 Design Bases

This section describes the design bases and functional requirements used in the nuclear design of the fuel and reactivity control system and relates these design bases to the U. S. Atomic Energy Commission (AEC) General Design Criteria (GDC) of July 1971. Where appropriate, supplemental criteria such as the Interim and/or Final Acceptance Criteria for emergency core cooling systems are addressed. Before discussing the nuclear design bases, it is appropriate to briefly review the four major categories ascribed to conditions of plant operation.

The full spectrum of plant conditions is divided into the following four categories, in accordance with the anticipated frequency of occurrence and risk to the public:

1. Condition I - normal operation.
2. Condition II - incidents of moderate frequency.
3. Condition III - infrequent faults.
4. Condition IV - limiting faults.

In general, the Condition I occurrences are accommodated with margin between any plant parameter and the value of that parameter that would require either automatic or manual protective action. Condition II incidents are accommodated with, at most, a shutdown of the reactor with the plant capable of returning to operation after corrective action. Fuel damage is not expected during Condition I and Condition II events.[1] It is not possible, however, to preclude a very small number of rod failures. These are within the capability of the plant cleanup system and are consistent with the plant design bases.

Condition III incidents shall not cause more than a small fraction of the fuel elements in the reactor to be damaged, although sufficient fuel element damage might occur to preclude immediate resumption of operation. The release of radioactive material due to Condition III incidents should not be sufficient to interrupt or restrict public use of these areas beyond the exclusion radius. Furthermore, a Condition III incident shall not by itself generate a Condition IV fault or result in a consequential loss of function of the reactor coolant system or reactor containment barriers.

Condition IV occurrences are faults that are not expected to occur but are defined as limiting faults that must be designed against. Condition IV faults shall not cause a release of radioactive material that results in an undue risk to public health and safety.

The core design power distribution limits related to fuel integrity are met for Condition I occurrences through conservative design and maintained by the action of the control system. The requirements for Condition II occurrences are met by providing an adequate protection system

1. Fuel damage as used here is defined as penetration of the fission product barrier (i.e., the fuel rod clad).

that monitors reactor parameters. The control and protection systems are described in Chapter 7 and the consequences of Conditions II, III, and IV occurrences are given in Chapter 15.

4.3.1.1 Fuel Burnup

Basis

The fuel rod design basis is described in Section 4.2. The nuclear design basis is to install sufficient reactivity in the fuel to maintain fuel assembly lead rod burnups within the NRC approved 60,000 MWd/MTU lead rod burnup limit (Reference 33). The above, along with the Section 4.3.1.3 design basis, satisfies GDC 10.

Discussion

Fuel burnup is a measure of fuel depletion that represents the integrated energy output of the fuel (MWd/MTU) and is a convenient means for quantifying fuel exposure.

The core design lifetime and design discharge burnup is achieved by determining the number of assemblies and initial enrichment required for each fuel region and developing reload core designs that meet all safety-related criteria. These designs are evaluated using the methodology described in Reference 1.

Initial excess reactivity installed in the fuel, although not a design basis, must be sufficient to maintain core criticality at full-power operating conditions throughout cycle life with equilibrium xenon, samarium, and other fission products present. The end of full-power cycle life is defined to occur when the chemical shim concentration is essentially zero, no control rods are inserted, and the RCS temperature remains at the nominal full-power value (i.e., essentially no T_{avg}/T_{ref} deviation). Operation beyond the full-power design cycle life in a coastdown mode is normally evaluated during the reload cycle design and may be employed to reach the scheduled cycle shutdown date.

A limitation on initial installed excess reactivity is not required other than as is quantified in terms of other design bases such as core negative reactivity feedback and shutdown margin, discussed below.

4.3.1.2 Negative Reactivity Feedback (Reactivity Coefficient)

Basis

The fuel temperature coefficient will be negative and the moderator temperature coefficient of reactivity will be nonpositive for full-power operating conditions, thereby providing negative reactivity feedback characteristics. The design basis meets GDC 11.

Discussion

When compensation for a rapid increase in reactivity is considered, there are two major effects. These are the resonance absorption effects (Doppler) associated with changing fuel

temperature, and the spectrum effect resulting from changing moderator density. These basic physics characteristics are often identified by reactivity coefficients. The use of slightly enriched uranium ensures that the Doppler coefficient of reactivity is negative. This coefficient provides the most rapid reactivity compensation. The core is also designed to have an overall negative moderator temperature coefficient of reactivity so that average coolant temperature or void content provides another, slower compensatory effect. Full-power operation is permitted only in a range of overall negative moderator temperature coefficient. The negative moderator temperature coefficient can be achieved through the use of fixed burnable poison and/or control rods by limiting the reactivity held down by soluble boron.

Burnable poison content (quantity and distribution) is not stated as a design basis other than as it relates to the accomplishment of a nonpositive moderator temperature coefficient at full-power operation conditions discussed above.

4.3.1.3 Control of Power Distribution

Basis

The nuclear design basis is that, with at least a 95% confidence level:

1. The fuel will not be operated at power greater than allowed by Technical Specifications under normal operating conditions including an allowance of 2% for calorimetric error and not including power spike factor due to densification. For the current value of the heat flux hot-channel factor (F_Q) see the Core Operating Limits Report (COLR).
2. Under abnormal conditions including the maximum overpower condition, the fuel peak power will not cause melting as defined in Section 4.4.1.2.
3. The fuel will not operate with a power distribution that violates the departure from nucleate boiling (DNB) design basis (i.e., the DNB ratio (DNBR) shall not be less than the design DNBR value, as discussed in Section 4.4.1) under Condition I and II events including the maximum overpower condition.
4. Fuel management will be such as to produce rod powers and burnups consistent with the assumptions in the fuel rod mechanical integrity analysis of Section 4.2.

The above basis meets GDC 10.

Discussion

The calculation of extreme power shapes that affect fuel design limits is performed with proven methods that were benchmarked against measurements from operating reactors. The conditions under which limiting power shapes are assumed to occur are chosen conservatively with regard to any permissible operating state.

Even though there is good agreement between peak power calculations and measurements, a nuclear uncertainty margin is applied to calculated peak local power. Such a margin is provided both for the analysis of normal operating states and for anticipated transients.

4.3.1.4 Maximum Controlled Reactivity Insertion Rate

Basis

The maximum reactivity insertion rate due to withdrawal of rod cluster control assemblies or by boron dilution is limited. This limit, expressed as a maximum reactivity change rate is set such that peak heat generation rate and DNBR do not exceed the maximum allowable at overpower conditions. This satisfies GDC 25.

The maximum reactivity worth of control rods and the maximum rates of reactivity insertion employing control rods are limited so as to preclude rupture of the coolant pressure boundary or disruption of the core internals to a degree that would impair core cooling capacity due to a rod withdrawal or ejection accident (Chapter 15).

Following any Condition IV event (rod ejection, steam-line break, etc.) the reactor can be brought to the shutdown condition and the core will maintain acceptable heat transfer geometry. This satisfies GDC 28.

Discussion

Reactivity addition associated with an accidental withdrawal of a control bank (or banks) is limited by the maximum rod speed (or travel rate) and by the worth of the bank(s). For this reactor, the maximum control rod speed is 45 in./min and the maximum rate of reactivity change considering two control banks moving is less than that which would exceed the maximum allowable peak heat generation rate and DNBR at overpower conditions.

4.3.1.5 Shutdown Margins

Basis

Minimum shutdown margin as specified in the COLR is required at any power operating condition, in the hot standby shutdown condition, and in the cold-shutdown condition.

In all analyses involving reactor trip, the single, highest-worth rod cluster control assembly is postulated to remain untripped in its full-out position (stuck-rod criterion). This satisfies GDC 26.

Discussion

Two independent reactivity control systems are provided, namely control rods and soluble boron in the coolant. The control rod system can compensate for the reactivity effects of the fuel and water temperature changes accompanying power level changes over the range from full-load to no-load. In addition, the control rod system provides the minimum shutdown margin under

Condition I events and is capable of making the core subcritical rapidly enough to prevent exceeding acceptable fuel damage limits assuming that the highest-worth control rod is stuck out upon trip.

The boron system can compensate for all xenon burnout reactivity changes and will maintain the reactor in the cold shutdown condition. Thus, backup and emergency shutdown provisions are provided by a mechanical and a chemical shim control system that satisfies GDC 26.

Basis

When fuel assemblies are in the pressure vessel and the vessel head is not in place, k_{eff} will be maintained at or below 0.95 with control rods and soluble boron. Further, the fuel will be maintained sufficiently subcritical that removal of all rod cluster control assemblies will not result in criticality.

A k_{eff} not to equal or exceed 0.95 will be maintained in the spent fuel storage racks and transfer equipment when flooded with borated water. K_{eff} in the spent fuel storage racks will not equal or exceed 1.0 when this area is flooded with pure water. In the normally dry new fuel storage racks, a k_{eff} not to equal or exceed 0.98 will be maintained assuming optimum moderation. No criterion is given for the refueling operation; however, a 5% margin, which is consistent with spent-fuel storage and transfer and 3% below the new-fuel storage, is adequate for the controlled and continuously monitored operations involved.

The boron concentrations required to meet the refueling shutdown criteria and the criticality limits in the spent fuel pool are specified in the Technical Specifications. Verification that the refueling shutdown criteria is met, including uncertainties, occurs on a cycle by cycle basis using standard Virginia Power design methods. Verification of the spent fuel pool criticality limits was achieved for maximum allowed fuel enrichment using industry standard techniques including Monte Carlo codes. The subcriticality of the core is continuously monitored as described in Technical Specifications.

4.3.1.6 Stability

Basis

The core will be inherently stable to power oscillations of the fundamental mode. This satisfies GDC 12.

Discussion

Oscillations of the total power output of the core, from whatever cause, are readily detected by the loop temperature sensors and by the nuclear instrumentation. The core is protected by these systems, and a reactor trip would occur if power increased unacceptably, preserving the design margins to fuel design limits. The stability of the turbine/steam generator/core systems and the reactor control system is such that total core power oscillations are not normally possible. The

redundancy of the protection circuits ensures an extremely low probability of exceeding design power levels.

Basis

Spatial power oscillations within the core, with a constant core power output, can be reliably and readily detected and suppressed should they occur.

Discussion

The core is designed so that diametral and azimuthal oscillations due to spatial xenon effects are self-damping and no operator action or control action is required to suppress them. The stability to diametral oscillations is so great that this excitation is highly improbable. Convergent azimuthal oscillations can be excited by prohibited motion of individual control rods. Such oscillations are readily observable and alarmed, using the ex-core long ion chambers. Indications are also continuously available from incore thermocouples and loop temperature measurements. Movable incore detectors can be activated to provide more detailed information. In all presently proposed cores, these horizontal plane oscillations are self-damping by virtue of reactivity feedback effects designed into the core.

However, axial xenon spatial power oscillations may occur late in core life. The control bank and ex-core detectors are provided for control and monitoring of axial power distributions. Assurance that fuel design limits are not exceeded is provided by reactor overpower delta T and overtemperature delta T trip functions that use the measured axial power imbalance as an input.

4.3.1.7 Anticipated Transients without Trip

An anticipated transient without scram (ATWS) mitigation system actuation circuitry (AMSAC) is installed per 10 CFR 50.62 to mitigate failure of the existing reactor trip system (RTS) by initiating a turbine trip and actuating auxiliary feedwater flow. The RTS is a part of the reactor protection system that includes the 7300 process instrumentation and control system (7300 System), and solid state protection system (SSPS). The AMSAC must be independent of the RTS and be diverse from sensor output to final actuation device.

4.3.2 Description

4.3.2.1 Nuclear Design Description

The reactor core consists of a specified number of fuel rods that are held in bundles by spacer grids and top and bottom fittings. The fuel rods are constructed of Zircaloy or ZIRLO cylindrical tubes containing UO_2 fuel pellets. The bundles, known as fuel assemblies, are arranged in a pattern that approximates a right circular cylinder.

Each fuel assembly contains a 17 x 17 rod array composed of 264 fuel rods, 24 rod cluster control (RCC) thimbles, and an incore instrumentation thimble. Figure 4.2-1 shows a cross-sectional view of a 17 x 17 fuel assembly and the locations of the guide thimbles used for

insertion of control rods or other insert components. Further details of the fuel assembly are given in Section 4.2.1. Reconstituted fuel assemblies (See Section 4.2.1.2) may be included among the fuel assemblies used for reloading the core.

The fuel rods within a given assembly have the same uranium enrichment in both the radial and axial planes. Fuel assemblies of three different enrichments were used in the initial core loading to establish a favorable radial power distribution. Figure 4.3-1 shows the fuel-loading pattern used in the first core. Two regions consisting of the two lower enrichments were interspersed so as to form a checkerboard pattern in the central portion of the core. The third region was arranged around the periphery of the core and contained the highest enrichment. The reference reloading pattern for Cycle 3 and subsequent cycles involves the placement of new fuel generally in the core interior with burnable poison and depleted fuel in a checkerboard pattern in the interior and in most of the peripheral locations. The core will normally operate approximately 18 months between refuelings, accumulating approximately 20,000 MWd/MTU per cycle. The enrichments for the first core are shown in Table 4.3-1.

The core average enrichment is determined by the amount of fissionable material required to provide the desired core lifetime and energy requirements. Typically the region average discharge burnup is between approximately 45,000 and 55,000 MWd/MTU. The physics of the burnout process is such that the operation of the reactor depletes the amount of fuel available due to the absorption of neutrons by the U-235 atoms and their subsequent fission. The rate of U-235 depletion is directly proportional to the power level at which the reactor is operated. In addition, the fission process results in the formation of fission products, some of which readily absorb neutrons. These effects, depletion and the buildup of fission products, are partially offset by the buildup of plutonium, shown in Figure 4.3-2 for the 17 x 17 fuel assembly, which occurs due to the nonfission absorption of neutrons in U-238. Therefore, at the beginning of any cycle a reactivity reserve equal to the depletion of the fissionable fuel and the buildup of fission product poisons over the specified cycle life must be “built” into the reactor. This excess reactivity is controlled by removable neutron-absorbing material in the form of boron dissolved in the primary coolant and burnable poison rods.

The concentration of boric acid in the primary coolant is varied to provide control and to compensate for long-term reactivity requirements. The concentration of the soluble neutron absorber is varied to compensate for reactivity changes due to fuel burnup, fission product poisoning including xenon and samarium, burnable poison depletion, and the cold-to-operating moderator temperature change. Using its normal makeup path, the chemical and volume control system is capable of inserting negative reactivity at a rate of approximately 20 pcm/min when the reactor coolant boron concentration is 1000 ppm and approximately 23 pcm/min when the reactor coolant boron concentration is 100 ppm. If the emergency boration path is used, the chemical and volume control system is capable of inserting negative reactivity at a rate of approximately 43 pcm/min when the reactor coolant boron concentration is 1000 ppm and approximately 50 pcm/min when the reactor coolant boron concentration is 100 ppm. The peak burnout rate for xenon is 25 pcm/min. (Section 9.3.4.3.1 discusses the capability of the CVCS to counteract xenon

decay.) Rapid transient reactivity requirements and safe-shutdown requirements are met with control rods.

As the boron concentration is increased, the moderator temperature coefficient becomes less negative. The use of a soluble poison alone could result in a positive moderator coefficient at beginning of life (BOL). Therefore, burnable poison rods may be used to reduce the soluble boron concentration sufficiently to ensure that the moderator temperature coefficient is negative for power operating conditions. During operation, the poison content in these rods is depleted, thus adding positive reactivity to offset some of the negative reactivity from fuel depletion and fission product buildup. The depletion rate of the burnable poison rods is not critical since chemical shim is always available and flexible enough to cover any possible deviations in the expected burnable poison depletion rate. Figure 4.3-3 is a graph of a typical core depletion with and without burnable poison rods. Note that even at end-of-life conditions some residual poison remains in the burnable poison rods, resulting in a net decrease in the first cycle lifetime.

In addition to reactivity control, the burnable poison rods are strategically located to provide a favorable radial power distribution. Figure 4.3-4 shows the burnable poison distribution within a fuel assembly for several burnable poison patterns used in a 17 x 17 array. The burnable poison loading pattern used in the first core is shown in Figures 4.3-5 and 4.3-6.

Tables 4.3-1 through 4.3-3 contain a summary of the reactor core design parameters for the first fuel cycle, including reactivity coefficients, delayed neutron fraction, and neutron lifetimes. Sufficient information is included to permit an independent calculation of the nuclear performance characteristics of the core.

4.3.2.2 **Power Distribution**

The accuracy of power distribution calculations has been confirmed through approximately 1000 flux maps during some 20 years of operation under conditions very similar to those expected for North Anna Units 1 and 2. Details of this confirmation are given in Reference 4 and in Section 4.3.2.2.6.

4.3.2.2.1 Definitions

Power distributions are quantified in terms of hot-channel factors (Reference 4). These factors are a measure of the peak pellet power within the reactor core and the total energy produced in a coolant channel and are expressed in terms of quantities related to the nuclear or thermal design as described below.

Power density is the thermal power produced per unit volume of the core (kW/liter).

Linear power density is the thermal power produced per unit length of active fuel (kW/ft). Since fuel assembly geometry is standardized, this is the unit of power density most commonly used. For all practical purposes, it differs from kW/liter by a constant factor that includes geometry and the fraction of the total thermal power that is generated in the fuel rod.

Average linear power density is the total thermal power produced in the fuel rods divided by the total active fuel length of all rods in the core.

Local heat flux is the heat flux at the surface of the cladding (Btu-ft^{-2}-hr^{-1}). For nominal rod parameters, this differs from linear power density by a constant factor.

Rod power or *rod integral power* is the length integrated linear power density in one rod (kW).

Average rod power is the total thermal power produced in the fuel rods divided by the number of fuel rods (assuming all rods have equal length).

The hot-channel factors used in the discussion of power distributions in this section are defined below.

F_Q, *heat flux hot-channel factor*, is defined as the maximum local heat flux on the surface of a fuel rod divided by the average fuel rod heat flux, allowing for manufacturing tolerances on fuel pellets and rods.

F_Q^N, *nuclear heat flux hot-channel factor*, is defined as the maximum local fuel rod linear power density divided by the average fuel rod linear power density, assuming nominal fuel pellet and rod parameters.

F_Q^E, *engineering heat flux hot-channel factor*, is the allowance on heat flux required for manufacturing tolerances. The engineering factor allows for local variations in enrichment, pellet density and diameter, surface area of the fuel rod, and eccentricity of the gap between pellet and clad. Combined statistically, the net effect is a factor of 1.03 to be applied to fuel rod surface heat flux.

$F_{\Delta H}^N$, *nuclear enthalpy rise hot-channel factor*, is defined as the ratio of the integral of linear power along the rod with the highest integrated power to the average rod power.

Manufacturing tolerances, hot-channel power distribution, and surrounding channel power distributions are treated explicitly in the calculation of DNBR described in Section 4.4.

It is convenient for the purposes of discussion to define subfactors of F_Q; however, design limits are set in terms of the total peaking factor.

F_Q = total peaking factor (or heat flux hot-channel factor)

$$= \frac{\text{maximum kW/ft}}{\text{average kW/ft}}$$

without densification effects

$$F_Q = F_Q^N \times F_Q^E \tag{4.3-1}$$

$$= F_{XY}^N \times F_Z^N \times F_U^N \times F_Q^E \tag{4.3-2}$$

where:

F_Q^N and F_Q^E are defined above

F_U^N = factor for conservatism, assumed to be 1.05

F_{XY}^N = ratio of peak power density to average power density in the horizontal plane of peak local power

F_Z^N = ratio of the power per unit core height in the horizontal plane of peak local power to the average value of power per unit core height. If the plane of peak local power coincides with the plane of maximum power per unit core height, then F_Z^N is the core average axial peaking factor.

To include the allowances made for densification effects, which are height-dependent, the following quantities are defined:

S(Z) = allowance made for densification effects at height Z in the core (see Section 4.3.2.2.5)

P(Z) = ratio of the power per unit core height in the horizontal plane at height Z to the average value of power per unit core height

Then:

F_Q = total peaking factor = $\frac{\text{maximum kW/ft}}{\text{average kW/ft}}$

including densification allowance

$$F_Q = \max F_{XY}^N(Z) \times P(Z) \times S(Z) \times F_U^N \times F_Q^E \qquad (4.3\text{-}3)$$

4.3.2.2.2 Radial Power Distribution

The power shape in horizontal sections of the core at full power is a function of the fuel and burnable poison loading patterns, and the presence or absence of a single bank of control rods. Thus, at any time in the cycle any horizontal section of the core can be characterized as (a) unrodded, or (b) with group D control rods. These two situations combined with burnup effects determine the radial power shapes that can exist in the core at full power. The effect on radial power shapes of power level, xenon, samarium, and moderator density effects are also considered but these are quite small. The effect of nonuniform flow distribution is negligible. While radial power distributions in various planes of the core are often illustrated, the core radial enthalpy rise distribution as determined by the integral of power up each channel is of greater interest. Figures 4.3-7 through 4.3-11 show representative radial power distributions for

one-eighth of the core for representative operating conditions. These conditions are (a) hot full power at beginning of life, unrodded, no xenon; (b) hot full power at beginning of life, unrodded, equilibrium xenon; (c) hot full power at beginning of life, bank D in, equilibrium xenon; (d) hot full power at middle of life, unrodded, equilibrium xenon; and (e) hot full power at end of life, unrodded, equilibrium xenon.

Since the position of the hot channel varies from time to time, a single reference radial design power distribution is selected for DNB calculations. This reference power distribution is chosen conservatively to concentrate power in one area of the core, minimizing the benefits of flow redistribution. Assembly powers are normalized to core average power.

4.3.2.2.3 Assembly Power Distributions

For the purpose of illustration, assembly power distributions from the beginning-of-life and end-of-life conditions corresponding to Figures 4.3-8 and 4.3-11, respectively, are given for the same assembly in Figures 4.3-12 and 4.3-13, respectively.

Since the detailed power distribution surrounding the hot channel varies from time to time, a conservatively flat assembly power distribution is assumed in the DNB analysis, described in Section 4.4, with the rod of maximum integrated power artificially raised to the design value of $F^N_{\Delta H}$. Assembly power distributions are evaluated on a reload design basis to demonstrate that all specified design limits are met.

4.3.2.2.4 Axial Power Distributions

The shape of the power profile in the axial or vertical direction is largely under the control of the operator through the automatic motion of control rods responding to manual operation of the chemical and volume control system. Nuclear effects that cause variations in the axial power shape include moderator density, Doppler effect on resonance absorption, spatial xenon, and burnup. Automatically controlled variations in total power output and full-length rod motion are also important in determining the axial power shape at any time. Signals are available to the operator from the ex-core ion chambers, which are long ion chambers outside the reactor vessel running parallel to the axis of the core. Separate signals are taken from the top and bottom halves of the chambers. The difference between top and bottom signals from each of four pairs of detectors is displayed on the control panel and called the flux difference, delta I. Calculations of core average peaking factor for many plants and measurements from operating plants under many operating situations are associated with either delta I or axial offset in such a way that an upper bound can be placed on the peaking factor. For these correlations, axial offset is defined as:

$$\text{axial offset} = \frac{\phi_t - \phi_b}{\phi_t + \phi_b} \qquad (4.3\text{-}4)$$

where:

ϕ_t = top detector reading

ϕ_b = bottom detector reading

Representative axial power shapes from Reference 5 for beginning-of-life, middle-of-life, and end-of-life conditions are shown in Figures 4.3-14 through 4.3-16. These figures cover a wide range of axial offset including values not permitted at full power.

The radial power distribution shown in Figure 4.3-9 involving the partial insertion of control rods represents a synthesis of power shapes from the rodded and unrodded planes. The applicability of the separability assumption upon which this procedure is based is ensured through extensive three-dimensional calculations of possible rodded conditions. As an example, Figure 4.3-17 compares the axial power distribution for several assemblies at different distances from inserted control rods with the core average axial distribution. The only significant difference from the average occurs in the low-power peripheral assemblies, thus confirming the validity of the separability assumption.

4.3.2.2.5 Local Power Peaking

Fuel densification, which has been observed to occur under irradiation in several operating reactors, causes the fuel pellets to shrink both axially and radially. The pellet shrinkage combined with random hang-up of fuel pellets may result in gaps in the fuel column when the pellets below the hung-up pellet settle in the fuel rod. When present, such gaps vary in length and location in the fuel rod. Because of decreased neutron absorption in the vicinity of the gap, power peaking occurs in the adjacent fuel rods resulting in an increased power peaking factor. A quantitative measure of this local power peaking is given by the power spike factor S(Z) where Z is the axial location in the core.

The method used to compute the generic power spike factor is described in Reference 6 and is summarized in Figure 4.3-18. The information flow outlined in Figure 4.3-18 is as follows:

1. The probability that an axial gap of a certain size will occur at a given location in the core was determined from fuel performance data.
2. The magnitude of the power spike caused by a single axial gap of a certain size was determined from nuclear calculations as shown in Figure 4.3-19.
3. For each axial interval to be analyzed, axial gap occurrence probabilities and the single-event power spikes were entered into the DRAW computer code. The code produced a curve of power spike versus probability of exceeding power spike for each elevation in the core. The power census for a core was then statistically combined with the power spike probability curve to obtain a power spike penalty for the core such that less than one rod will exceed F_Q^N at a 95% confidence level.

The power spike factor due to densification is assumed to be a local perturbation applicable to overpower transients. Thus, densification affects F_Q but not $F_{\Delta H}$. It should be noted that

significant axial gaps do not occur in current generation fuel, and a densification power spike factor of 1.0 is now appropriate (Reference 37).

Results reported in a Westinghouse topical report concerning the spike penalty in LOCA analysis (Reference 7) show that the power spike penalty should not be included in the LOCA envelope.

4.3.2.2.6 Limiting Power Distributions

According to the American Nuclear Society (ANS) classification of plant conditions (Chapter 15), Condition I occurrences are those that are expected frequently or regularly in the course of power operation, maintenance, or maneuvering of the plant. As such, Condition I occurrences are accommodated with margin between any plant parameter and the value of that parameter that would require either automatic or manual protective action. Inasmuch as Condition I occurrences occur frequently or regularly, they must be considered from the point of view of affecting the consequences of fault conditions (Conditions II, III, and IV). In this regard, the analysis of each fault condition described is generally based on a conservative set of initial conditions corresponding to the most adverse set of conditions that can occur during Condition I operation.

The list of steady-state and shutdown conditions, permissible deviations, and operational transients is given in Section 15.1. Implicit in the definition of normal operation is proper and timely action by the reactor operator. That is, the operator follows recommended operating procedures for maintaining appropriate power distributions and takes any necessary remedial actions when alerted to do so by the plant instrumentation. Thus, as stated above, the worst or limiting power distribution that can occur during normal operation is to be considered as the starting point for an analysis of ANS Condition II, III, and IV events.

Improper procedure actions or errors by the operator are assumed in the design as occurrences of moderate frequency (ANS Condition II). Some of the consequences that might result are listed in Section 15.2. The limiting power shapes that result from Condition II events are those power shapes that deviate from the normal operating condition due to boration/dilution malfunctions (or operator error), control rod bank malfunctions, and excessive heat removal malfunctions. Power shapes that fall in this category are used for the determination of the reactor protection system setpoints so as to maintain margin to overpower or DNB limits.

The means for maintaining power distributions within the required hot-channel factor limits are described in the Technical Specifications. Detailed information on the design constraints on local power density in a Westinghouse PWR, on the defined operating procedures, and on the measures taken to preclude exceeding design limits using the Westinghouse Constant Axial Offset Control Methodology, is presented in the Westinghouse topical reports and power distribution control and load-following procedures (Reference 8). Since Cycle 5 for Unit 2 and Cycle 7 for Unit 1, the North Anna Power Station has been using the Relaxed Power Distribution Control (RPDC) methodology for maintaining power distributions within the required bounds set by the

peaking factors limits. The following paragraphs summarize these methodologies and describe the calculations used to establish the upper bound on peaking factors.

The calculations used to establish the upper bound on peaking factors, F_Q and $F_{\Delta H}$, include all of the nuclear effects that influence the radial and/or axial power distributions throughout core life for various modes of operation, including load follow, reduced power operation, and axial xenon transients.

Radial power distributions are calculated for the full-power condition. Fuel and moderator temperature feedback effects are included. The steady-state nuclear design calculations are done for normal flow with the same mass flow in each channel and flow redistribution effects neglected. The effect of flow redistribution is calculated explicitly where it is important in the DNB analysis of accidents. The effect of xenon on radial power distribution is small (compare Figures 4.3-7 and 4.3-8), but is included as part of the normal design process. Radial power distributions are relatively fixed and easily bounded with upper limits.

The core average axial profile, however, can experience significant changes that can occur rapidly as a result of rod motion and load changes and more slowly due to xenon distribution. For the study of points of closest approach to axial power distribution limits, several thousand cases are examined. Since the properties of the nuclear design dictate what axial shapes can occur, boundaries on the limits of interest can be set in terms of the parameters that are readily observed on the plant. Specifically, the nuclear design parameters that are significant to the axial power distribution analysis are as follows:

1. Core power level.
2. Core height.
3. Coolant temperature and flow.
4. Coolant temperature program as a function of reactor power.
5. Fuel cycle lifetimes.
6. Rod bank worths.
7. Rod bank overlaps.

Normal operation of the plant assumes compliance with the following conditions.

1. Control rods in a single bank move together with no individual rod insertion differing by more than 12 steps (indicated), according to Technical Specifications, from the bank demand position.
2. Control banks are sequenced with overlapping banks.
3. The control bank insertion limits are not violated.

4. Axial power distribution procedures, which are given in terms of flux difference control and control bank position, are observed.

The axial power distribution procedures referred to above are part of the required operating procedures that are followed in normal operation. For CAOC operations, they require control of the axial offset (flux difference divided by fractional power) at all power levels within a permissible operating band of a target value corresponding to the equilibrium full power value. In the first cycle, the target value changes from about -10% to 0% linearly through the life of the cycle. This minimizes xenon transient effects on the axial power distribution, since the procedures essentially keep the xenon distribution in phase with the power distribution.

Calculations are performed for normal operation of the reactor including load-following maneuvers. Beginning, middle, and end of cycle conditions are included in the calculations. Different histories of operation are assumed before calculating the effect of load-follow transients on the axial power distribution. These different histories assume base-loaded operation and extensive load following. The calculated points are synthesized from axial calculations combined with radial factors appropriate for rodded and unrodded planes. The calculated values have been increased by a factor of 1.05 for conservatism and a factor of 1.03 for the engineering factor F_Q^E.

The envelope drawn over the calculated ([$F_Q \times$ power] maximum) points in Figure 4.3-21 represents an upper bound envelope on local power density versus elevation in the core. It should be emphasized that this envelope is a conservative representation of the bounding values of local power density.

Expected values are considerably smaller and, in fact, less conservative bounding values may be justified with additional analysis or surveillance requirements. For example, Figure 4.3-21 bounds both beginning-of-life and end-of-life conditions but without consideration of radial power distribution flattening with burnup; that is, both beginning-of-life and end-of-life points presume the same radial peaking factor. The inclusion of the burnup flattening effect would reduce the local power densities corresponding to end-of-life conditions that may be limiting at the higher core elevations.

Finally, as previously discussed, this upper bound envelope is based on procedures of load follow that require the operator to operate within an allowed deviation from a target equilibrium value of axial flux difference. These procedures are detailed in the Technical Specifications and are predicated only upon ex-core surveillance supplemented by the normal monthly full core map requirement and by computer-based alarms on deviation.

Allowing for fuel-densification effects, the average power density at 2893 MWt is 5.68 kW/ft. The conservative upper bound value of normalized local power density during normal operation is based on Figure 4.3-21. For the current value of the heat flux hot-channel factor, see the COLR.

To determine reactor protection system setpoints, with respect to power distributions, three categories of events are considered: rod control equipment malfunctions, operator errors of commission, and operator errors of omission.

The first category comprises uncontrolled rod withdrawal (with rods moving in the normal bank sequence). Also included are motions of the banks below their insertion limits, which could be caused, for example, by uncontrolled dilution or primary coolant cooldown. Power distributions were calculated throughout these occurrences assuming short-term corrective action; that is, no transient xenon effects were considered to result from the malfunction. The event was assumed to occur from typical normal operating situations that did include normal xenon transients. It was further assumed in determining the power distributions that total power level would be limited by reactor trip to below 118%. Since the study is to determine protection limits with respect to power and axial offset, no credit was taken for trip setpoint reduction due to flux difference. The results are given in Figure 4.3-22 in units of kW/ft. The peak power density that can occur in such events, assuming reactor trip at or below 118%, is thus limited to 21.1 kW/ft including uncertainties and densification effects.

The second category, also appearing in Figure 4.3-22, assumes that the operator mispositions the rod bank in violation of the insertion limits and creates short-term conditions not included in normal operating conditions. The third category assumes that the operator fails to take action to correct a flux difference violation. The results shown on Figure 4.3-23 are F_Q multiplied by 102% power including an allowance for calorimetric error. The figure shows that, provided the assumed error in operation does not continue for a period that is long compared to the xenon time constant, the maximum local power does not exceed 20.0 kW/ft including the above factors. The Technical Specifications restrict delta I at 102% power such that the peak linear power density is less than 21.1 kW/ft. These events are considered Condition II events.

It should be noted that a reactor overpower accident is not assumed to occur coincident with an independent operator error.

Analyses of possible operating power shapes for the reactor described herein show that the appropriate hot-channel factors F_Q and $F^N_{\Delta H}$ for peak local power density and for DNB analysis at full power are the values given in Table 4.3-2 and addressed in the Technical Specifications. F_Q can be increased with decreasing power as shown in the Technical Specifications. Increasing $F^N_{\Delta H}$ with decreasing power is permitted by the DNB protection setpoints and allows radial power shape changes with rod insertion to the insertion limits as described in Section 4.4.3.2. It has been determined that provided the above conditions 1 through 4 are observed, the Technical Specification limits are met.

When a situation is possible in normal operation that could result in local power densities in excess of those assumed as the precondition for a subsequent hypothetical accident, but which would not itself cause fuel failure, administrative controls and alarms are provided for returning

the core to a safe condition. These alarms are described in detail in Chapter 7 and in the Technical Specifications.

The CAOC method described above relied on the use of part length control rods for much of its flexibility in controlling the axial power distribution especially at low power. When the part length rods were removed, full length control rods now had to be used for controlling the axial power distributions. This placed excessive requirements on the boron control system as the reactivity change associated with the movement of the rods to control the axial flux difference had to be compensated for through boration or dilution. This becomes especially hard to manage near end of cycle when the boron concentration has been reduced to low levels.

This operational restriction on delta-I imposed by CAOC has been eased by the implementation of a variable delta-I band control strategy, Relaxed Power Distribution Control (RPDC) (Reference 34), that takes credit for available full power delta-I margin while also providing for an increasing delta-I band with decreasing power. The widened delta-I band is formed by maintaining an approximately constant analysis margin to the Design Bases Limits at all power levels. This is in contrast to CAOC operation which has large amounts of margin available at reduced power. For North Anna, which has LOCA-limited total peaking factors, this variable delta-I band is selected such that the margin to the LOCA FQ*P*K(z) limit remains approximately constant for all power levels.

The benefits of this variable band delta-I control strategy over CAOC operation are as follows:

1. The ability to return to power after a trip, particularly at end-of-cycle, is enhanced;
2. Control rod motion necessary to compensate for the previous CAOC delta-I band restrictions is now reduced to only that motion needed to maintain operation within a much wider band;
3. The reactor coolant system boration/dilution requirements are decreased, due, in part, to the reduced control rod motion;
4. The plant has enhanced operational flexibility.

The objective of an RPDC analysis is to determine acceptable delta-I band limits that guarantee that margin to all the applicable design bases criteria is maintained and, at the same time, provide enhanced delta-I operating margin over CAOC. Because the RPDC delta-I band is an analysis output quantity rather than a fixed input limit as in CAOC, axial shapes which adequately bound the potential delta-I range must be generated. These axial shapes include the effect of all potential combinations of the key parameters such as burnup, control rod position, xenon distribution, and power level. The method for generating these shapes (outlined in Reference 34) involves the creation of axial xenon distributions by creating a divergent xenon-power oscillation in the 1D NOMAD or 3D SIMULATE Code (Reference 34) which produces xenon distributions more severe than any experienced during normal operation including load follow maneuvers. These xenon distributions combined with power levels from

50% to 100% power and control rod insertions governed by the rod insertion limits are used to produce the axial power distributions for the RPDC normal operation analysis.

After the axial power shapes have been created, two separate allowable delta-I limits for normal operation are established: one based on LOCA F_Q considerations and the other one based on a Loss of Flow (the limiting DNB transient) thermal/hydraulic evaluation.

When using the standard 1D/3D synthesis, the LOCA delta-I limit is established by combining the axial power shapes with $F_{xy}(z)$ data using a standard F_Q synthesis (Reference 34):

$$F_Q(z) = F_{xy}(z) \times P(z) \times Xe(z) \times F_{NU} \times F_Q^E \times F_{GR} \quad (4.3\text{-}5a)$$

where the following are non-dimensional parameters:

$F_{xy}(z)$ = F_{xy} distribution dependent upon burnup, core height, rod position and power level

$P(z)$ = Axial power shape function

$Xe(z)$ = Radial xenon redistribution factor

F_{NU} = Nuclear uncertainty factor

F_Q^E = Engineering heat-flux hot-channel factor

F_{GR} = Grid correction factor

The axially varying radial xenon factor, $Xe(z)$, compensates for increases to $F_Q(z)$ resulting from redistribution of the xenon in the radial plane due to rod movement. The radial xenon redistribution effect cannot be explicitly represented in a 1D code and is therefore applied in the synthesis as an uncertainty factor.

When using the 3D Model, the LOCA delta-I limit is established by using the determined $F_q(z)$ directly (Reference 34):

$$F_Q(z) = F_q(z) \times F_{NU} \times F_Q^E \quad (4.3\text{-}5b)$$

Where the following are non-dimensional parameters:

$F_q(z)$ = Fq distribution calculated directly, dependent upon burnup, core height and rod position and power level (Includes xenon redistribution and grid effects)

F_{NU} = Nuclear uncertainty factor

F_Q^E = Engineering heat-flux hot-channel factor

When using either the standard 1D/3D synthesis or the 3D Model, the $F_Q \times$ Power for each shape is compared to the LOCA $F_Q \times$ Power $\times$ K(z) limit at each power level to determine which axial shapes approach the LOCA limit, thereby establishing a preliminary allowable delta-I versus power band. This comparison replaces the traditional CAOC FAC analysis and ensures that the margin to the LOCA $F_Q \times$ Power $\times$ K(z) envelope is maintained during the cycle as long as reactor operation remains within the delta-I limits.

The Loss of Flow Accident (LOFA) represents the most limiting DNB transient not terminated by the Overtemperature Delta-T trip. In order to ensure the applicability of the current LOFA analysis, the entire set of axial power distributions formed by the RPDC normal operation analysis are evaluated against the 1.55 cosine design axial power distribution for the Loss of Flow Accident analysis. The thermal/hydraulic evaluation methods used in this LOFA evaluation are similar to those of the present CAOC techniques. As a result of this LOFA comparison, a second set of delta-I versus power limits is formed. These delta-I limits delineate the allowable operating band which will ensure that the margin to the DNB design base for LOFA is maintained.

The results of the LOFA delta-I limit generation are then combined with the LOCA delta-I limits to produce a set of limits which ensure the preconditions for both accidents are met.

As in the CAOC analysis, Condition II or abnormal operation events which may be the result of system malfunctions or operator errors and create reactor conditions that fall outside the bounds of normal operation established by the LOCA and LOFA precondition analyses, must be analyzed under RPDC. The RPDC analysis examines the most limiting Condition II events (control rod withdrawal, excessive heat removal, and erroneous boration/dilution) to confirm the Overtemperature Delta-T (OTDT) setpoints have been conservatively calculated and that margin to the fuel design limits is maintained.

The OTDT trip function and setpoints provide DNB protection for Condition II accidents. Part of this function, the f(delta-I) term, responds to changes in the indicated delta-I created by skewed axial power distributions. The axial power distributions formed by the RPDC simulations of the above Condition II accidents, are evaluated to confirm that the assumptions used to form the f(delta-I) term and the rest of the OTDT trip function remain valid. If the RPDC power distributions for any subsequent reload should be more limiting than those previously used to establish the OTDT trip setpoints, the OTDT setpoints are reformulated using the appropriate RPDC power distribution parameters.

4.3.2.2.7 Experimental Verification of Power Distribution Analysis

This subject is discussed in depth in Reference 4. A summary of this report is given here.

In a measurement of peak local power density, F_Q, with the movable detector system described in Sections 7.7.1 and 4.4.5, the following uncertainties have to be considered:

1. Reproducibility of the measured signal.

2. Errors in the calculated relationship between detector current and local flux.
3. Errors in the calculated relationship between detector flux and peak rod power some distance from the measurement thimble.

The appropriate allowance for category 1 above has been quantified by repetitive measurements made with several intercalibrated detectors by using the common thimble features of the incore detector system. This system allows more than one detector to access any thimble. Errors in category 2 above are quantified to the extent possible, by using the fluxes measured at one thimble location to predict fluxes at another location that is also measured. Local power distribution predictions were verified in critical experiments on arrays of rods with simulated guide thimbles, control rods, burnable poisons, etc. These critical experiments provided quantification of errors of types 2 and 3 above.

Reference 4 describes critical experiments performed at the Westinghouse Reactor Evaluation Center and measurements taken on two Westinghouse plants with incore systems of the same type as used in the plant described herein.

The report concludes that the uncertainty associated with the peak nuclear heat flux factor, FQ, is 4.58% at the 95% confidence level with only 5% of the measurements greater than the inferred value. This is the equivalent of a 2σ limit on a normal distribution and is the uncertainty to be associated with a full core flux map with movable detectors reduced with a reasonable set of input data incorporating the influence of burnup on the radial power distribution. The uncertainty is usually rounded up to 5%.

In comparing measured power distributions (or detector currents) against the calculations for the same situation, it is not possible to subtract out the detector reproducibility. Thus, a comparison between measured and predicted power distributions has to include some measurement error. Such a comparison is given in Figure 4.3-24 for one of the maps used in Reference 4. Since the first publication of the report, hundreds of maps have been taken on these and other reactors. The results confirm the adequacy of the 5% uncertainty allowance on F_Q.

A similar analysis for the uncertainty in $F_{\Delta H}$ (rod integral power) measurements results in an allowance of 3.65% at the equivalent of a 2σ confidence level.

An 8% uncertainty factor is allowed in the nuclear design basis; that is, the predicted rod integrals at full power must not exceed the design $F_{\Delta H}$ less 8%. This 8% consists of 4% calculational uncertainty and 4% measurement uncertainty. For statistical DNBR analysis, the 4% calculational uncertainty is added to the predicted value since the 4% measurement uncertainty is included in the statistical DNBR design limit. For non-statistical DNB analysis, the full 8% uncertainty is added to the predicted value.

A measurement in the second cycle of a 121-assembly 12-foot core is compared with a simplified one-dimensional core average axial calculation in Figure 4.3-25. This calculation does not give explicit representation to the fuel grids.

The accumulated data on power distributions in actual operation is basically of the following three types:

1. Much of the data is obtained in steady-state operation at constant power in the normal operating configuration.
2. Data with unusual values of axial offset were obtained as part of the ex-core detector calibration exercise.
3. Special tests have been performed in load-follow and other transient xenon conditions that have yielded useful information on power distributions.

These data are presented in detail in Reference 9. Figure 4.3-26 contains a summary of measured values of F_Q as a function of axial offset for five plants from that report.

4.3.2.2.8 Testing

A very extensive series of physics tests is performed on first cores. These tests and the criteria for satisfactory results are described in detail in Chapter 14. Since not all limiting situations can be created at beginning of life, the main purpose of the tests is to provide a check on the calculation methods used in the predictions for the conditions of the test. Tests are performed at the beginning of each reload cycle to verify that the physics models used to predict the core's behavior (power distributions, reactivity parameters, and kinetics parameters) are accurate and reflect the actual reload core characteristics.

4.3.2.2.9 Monitoring Instrumentation

The adequacy of instrument numbers, spatial deployment, required correlations between readings and peaking factors, calibration, and errors are described in References 3, 4, and 9. The relevant conclusions are summarized in Sections 4.3.2.2.7 and 4.4.5.

Provided the limitations given in Section 4.3.2.2.6 on rod insertion and flux difference are observed, the ex-core detector system provides adequate monitoring of power distributions.

Further details of specific limits on the observed rod positions and flux difference are given in the Technical Specifications together with a discussion of their bases.

Limits for alarms, reactor trip, etc., are given in the Technical Specifications. Descriptions of the systems provided are given in Sections 7.7 and 7.2.

4.3.2.3 **Reactivity Coefficients**

The kinetic characteristics of the reactor core determine the response of the core to changing plant conditions or to operator adjustments made during normal operation, as well as the core response during abnormal or accidental transients. These kinetic characteristics are quantified in reactivity coefficients. The reactivity coefficients reflect the changes in the neutron multiplication due to varying plant conditions such as power, moderator, or fuel temperatures, or

less significantly due to a change in pressure or void conditions. Since reactivity coefficients change during the life of the core, ranges of coefficients are employed in the transient analysis to determine the response of the plant throughout life. The results of such simulations and the reactivity coefficients used are presented in Chapter 15. The analytical methods and calculational models used in calculating the reactivity coefficients are given in Section 4.3.3. These models have been confirmed through extensive testing of more than 30 cores similar to those in the North Anna plant; results of these tests are discussed in Section 4.3.3. Quantitative information for calculated reactivity coefficients, including fuel-Doppler coefficient, moderator coefficients (density, temperature, pressure, void), and power coefficient is given in the following sections.

4.3.2.3.1 Fuel Temperature (Doppler) Coefficient

The fuel temperature (Doppler) coefficient is defined as the change in reactivity per degree change in effective fuel temperature and is primarily a measure of the Doppler broadening of U-238 and Pu-240 resonance absorption peaks. Doppler broadening of other isotopes such as U-236, Np-237, etc., are also considered, but their contributions to the Doppler effect are small. An increase in fuel temperature increases the effective resonance absorption cross sections of the fuel and produces a corresponding reduction in reactivity.

The fuel temperature coefficient is calculated by performing two-group multi-dimensional diffusion or nodal calculations using the PDQ or SIMULATE code. Moderator temperature is held constant and the power level is varied. Spatial variation of fuel temperature is taken into account by calculating the effective fuel temperature as a function of power density as discussed in Section 4.3.3.1.

The Doppler temperature coefficient is shown in Figure 4.3-27 as a function of the effective fuel temperature (at beginning-of-life and end-of-life conditions). The effective fuel temperature is lower than the volume averaged fuel temperature since the neutron flux distribution is nonuniform through the pellet and gives preferential weight to the surface temperature. The Doppler-only contribution to the power coefficient, defined later, is shown in Figure 4.3-28 as a function of relative core power. The integral of the differential curve in Figure 4.3-28 is the Doppler contribution to the power defect and is shown in Figure 4.3-29 as a function of relative power. The Doppler coefficient becomes more negative as a function of life as the Pu-240 content increases, thus increasing the Pu-240 resonance absorption, but becomes less negative as the fuel temperature changes with burnup. The upper and lower limits of Doppler coefficient used in accident analyses are given in Chapter 15.

4.3.2.3.2 Moderator Coefficients

The moderator coefficient is a measure of the change in reactivity due to a change in specific coolant parameters such as density, temperature, pressure, or void. The coefficients so obtained are moderator density, temperature, pressure, and void.

Moderator Density and Temperature Coefficients

The moderator temperature (density) coefficient is defined as the change in reactivity per degree change in the moderator temperature. Generally, the effect of the changes in moderator density as well as the temperature are considered together. A decrease in moderator density means less moderation and results in a negative moderator coefficient. An increase in coolant temperature, keeping the density constant, leads to a hardened neutron spectrum and results in an increase in resonance absorption in U-238, Pu-240, and other isotopes. The hardened spectrum also causes a decrease in the fission-to-capture ratio in U-235 and Pu-239. Both of these effects make the moderator coefficient more negative. Since water density changes more rapidly with temperature as temperature increases, the moderator temperature (density) coefficient becomes more negative with increasing temperature.

The soluble boron used in the reactor as a means of reactivity control also has an effect on the moderator density coefficient since the soluble boron poison density as well as the water density is decreased when the coolant temperature rises. A decrease in the soluble poison concentration introduces a positive component in the moderator density coefficient.

Thus, if the concentration of the soluble poison is large enough, the net value of the moderator temperature coefficient may be positive. With the burnable poison rods present, however, the initial hot boron concentration is sufficiently low that the moderator temperature coefficient is negative at operating temperatures. The effect of control rods is to make the moderator coefficient more negative by reducing the required soluble boron concentration and by increasing the “leakage” of the core.

With burnup, the moderator coefficient becomes more negative primarily as a result of boric acid dilution but also to a significant extent from the effects of the buildup of plutonium and fission products.

The moderator coefficient is calculated for the various plant conditions discussed above by performing two-group multi-dimensional diffusion or nodal calculations, varying the moderator temperature (and density) by about ±5°F for each of the mean temperatures. The moderator coefficient is shown as a function of core temperature and boron concentration for the unrodded and rodded cores in Figures 4.3-30 through 4.3-32. The temperature range covered is from 68°F (cold) to about 600°F. The contribution due to Doppler coefficient (because of change in moderator temperature) has been subtracted from these results. Figure 4.3-33 shows the hot, full-power moderator temperature coefficient plotted as a function of first-cycle lifetime for the just-critical boron concentration condition based on the design boron letdown condition.

The moderator coefficients presented here are calculated on a core-wise basis, since they are used to describe the core behavior in normal and accident situations when the moderator temperature changes can be considered to affect the whole core.

Moderator Pressure Coefficient

The moderator pressure coefficient relates the change in moderator density, resulting from a reactor coolant pressure change, to the corresponding effect on neutron production. This coefficient is of much less significance in comparison with the moderator temperature coefficient. A change of 50 psi in pressure has approximately the same effect on reactivity as a half-degree change in moderator temperature. This coefficient can be determined from the moderator temperature coefficient by relating change in pressure to the corresponding change in density. Historical calculations show that the moderator pressure coefficient is negative over a portion of the moderator temperature range at beginning of life (-0.004 pcm/psi, beginning of life), but is always positive at operating conditions and becomes more positive during life (+0.3 pcm/psi, end of life).

Moderator Void Coefficient

The moderator void coefficient relates the change in neutron multiplication to the presence of voids in the moderator. In a PWR, this coefficient is not very significant because of the low void content in the coolant. The core void content is less than one-half of 1% and is due to local or statistical boiling. Historical calculations show the void coefficient varies from 50 pcm/% void at beginning of life at low temperatures to -250 pcm/% void at end of life and at operating temperatures. The negative void coefficient at operating temperatures becomes more negative with fuel burnup.

4.3.2.3.3 Power Coefficient

The combined effect of moderator temperature and fuel temperature change as the core power level changes is called the total power coefficient and is expressed in terms of reactivity change per percent power change. The power coefficient at beginning-of-life and end-of-life conditions is given in Figure 4.3-34. It becomes more negative with burnup, reflecting the combined effect of moderator and fuel temperature coefficients with burnup. The power defect (integral reactivity effect) at beginning of life and end of life is given in Figure 4.3-35.

4.3.2.3.4 Comparison of Calculated and Experimental Reactivity Coefficients

Section 4.3.3 describes the comparison of calculated and experimental reactivity parameters in detail.

Experimental evaluation of the calculated parameters was done during the physics start-up tests described in Chapter 14.

4.3.2.3.5 Reactivity Coefficients Used in Transient Analysis

Table 4.3-2 gives the representative ranges for the reactivity coefficients used in transient analysis. The exact values of the coefficient used in the analysis depend on whether the transient of interest is examined at the beginning of life or end of life, whether the most negative or the most positive (least negative) coefficients are appropriate, and whether spatial nonuniformity must

be considered. Conservative values of coefficients, considering various aspects of analysis, are used in the transient analysis. This is completely described in Chapter 15.

The values listed in Table 4.3-2 and illustrated in Figures 4.3-27 through 4.3-35 apply to the core described in Table 4.3-1. The coefficients appropriate for use in subsequent cycles depend on the core operating history, the number and enrichment of fresh fuel assemblies, the loading pattern of burned and fresh fuels, the number and location of any burnable poison rods, etc. The need for a reevaluation of any accident in a subsequent cycle is contingent upon whether or not the coefficients for that cycle fall within the identified range used in the analysis presented in Chapter 15. Control rod requirements are given in Table 4.3-3 for the core described and for a hypothetical equilibrium cycle, since these are markedly different. These latter numbers are provided for information only.

4.3.2.4 **Control Requirements**

To ensure the shutdown margin stated in the Technical Specifications under conditions where a cooldown to ambient temperature is required, concentrated soluble boron is added to the coolant. Boron concentrations for several core conditions are listed in Table 4.3-2. For all core conditions including refueling, the boron concentration is well below the solubility limit. The rod cluster control assemblies are employed to bring the reactor to the hot-shutdown condition. The minimum required shutdown margin is given in the COLR.

The ability to accomplish the shutdown for hot conditions is demonstrated in Table 4.3-3 for the first cycle and for a typical reload cycle by comparing the difference between the rod cluster control assembly reactivity available with an allowance for the worst stuck rod with that required for control and protection purposes. The shutdown margin includes an allowance of 10% for analytic uncertainties (see Section 4.3.2.4.9). The largest reactivity control requirement appears at end of life when the moderator temperature coefficient reaches its peak negative value as reflected in the larger power defect.

The control rods are required to provide sufficient reactivity to account for the power defect from full power to zero power and to provide the required shutdown margin. The reactivity addition resulting from power reduction consists of contributions from Doppler, variable average moderator temperature, flux redistribution, and reduction in void content as discussed below.

4.3.2.4.1 Doppler Effect

The Doppler effect arises from the broadening of U-238 and Pu-240 resonance peaks with an increase in effective pellet temperature. This effect is most noticeable over the range of zero power to full power due to the large pellet temperature increase with power generation.

4.3.2.4.2 Variable Average Moderator Temperature

When the core is shut down to the hot, zero-power condition, the average moderator temperature changes from the equilibrium full-load value determined by the steam generator and

turbine characteristics (steam pressure, heat transfer, tube fouling, etc.) to the equilibrium no-load value, which is based on the steam generator shell-side design pressure. The design change in temperature is conservatively increased by 6.5°F to account for the control deadband and measurement errors.

Because the moderator coefficient is negative, there is reactivity addition with power reduction. The moderator coefficient becomes more negative as the fuel depletes because the boron concentration is reduced. This effect is the major contributor to the increased requirement at end of life.

4.3.2.4.3 Redistribution

During full-power operation, the coolant density decreases with core height, and this, together with the partial insertion of control rods, results in less fuel depletion near the top of the core. Under steady-state conditions, the relative power distribution will be slightly asymmetric toward the bottom of the core. On the other hand, at hot, zero-power conditions, the coolant density is uniform up the core, and there is no flattening due to Doppler. The result will be a flux distribution, which at zero power can be skewed toward the top of the core. The reactivity insertion due to the skewed distribution is calculated with an allowance for the most adverse effects of xenon distribution.

4.3.2.4.4 Void Content

A small void content in the core is due to nucleate boiling at full power. The void collapse coincident with power reduction makes a small reactivity contribution.

4.3.2.4.5 Rod Insertion Allowance

At full power, the control bank is operated within a prescribed band of travel to compensate for small, periodic changes in boron concentration, changes in temperature, and very small changes in the xenon concentration not compensated for by a change in boron concentration. When the control bank reaches either limit of this band, a change in boron concentration is required to compensate for additional reactivity changes. Since the insertion limit is set by a rod travel limit, a conservatively high calculation of the inserted worth is made that exceeds the normally inserted reactivity.

4.3.2.4.6 Burnup

Excess reactivity of approximately 10% $\Delta\rho$ to 25% $\Delta\rho$ (hot) is installed at the beginning of each cycle to provide sufficient reactivity to compensate for fuel depletion and fission products throughout the cycle. This reactivity is controlled by the addition of soluble boron to the coolant and by burnable poison. The soluble boron concentration for several core configurations, the unit boron worth, and burnable poison worth are given in Tables 4.3-1 and 4.3-2 for a first cycle core. Since the excess reactivity for burnup is controlled by soluble boron and/or burnable poison, it is not included in control rod requirements.

4.3.2.4.7 Xenon and Samarium Poisoning

Changes in xenon and samarium concentrations in the core occur at a sufficiently slow rate, even following rapid power level changes, that the resulting reactivity change is controlled by changing the soluble boron concentration.

4.3.2.4.8 pH Effects

Changes in reactivity due to a change in coolant pH, if any, are sufficiently small in magnitude and occur slowly enough to be controlled by the boron system. Further details are available in Reference 11.

4.3.2.4.9 Experimental Confirmation

Following a normal shutdown, the total core reactivity change during cooldown with a stuck rod has been measured on a 121-assembly, 10-foot-high core and a 121-assembly, 12-foot-high core. In each case, the core was allowed to cool down until it reached criticality, simulating the steam-line-break accident. For the 10-foot core, the total reactivity change associated with the cooldown was overpredicted by about 0.3% $\Delta\rho$ with respect to the measured result. This represents an error of about 5% in the total reactivity change and is about half the uncertainty allowance for this quantity. For the 12-foot core, the difference between the measured and predicted reactivity change was an even smaller 0.2% $\Delta\rho$. These measurements and others demonstrate the ability of the methods described in Section 4.3.3 to accurately predict the total shutdown reactivity of the core. Section 4.3.3 provides details about the control rod model and other factors important to reactivity for the current core design model.

4.3.2.5 **Control**

Core reactivity is controlled by means of a chemical poison dissolved in the coolant, rod cluster control assemblies, and burnable poison rods as described below.

4.3.2.5.1 Chemical Poison

Boron in solution as boric acid is used to control relatively slow reactivity changes associated with the following:

1. The moderator temperature defect in going from cold shutdown at ambient temperature to the hot operating temperature at zero power.
2. The transient xenon and samarium poisoning, such as that following power changes or changes in rod cluster control position.
3. The excess reactivity required to compensate for the effects of fissile inventory depletion and buildup of long-life fission products.
4. The burnable poison depletion.

The boron concentrations for various core conditions are presented in Table 4.3-2 for the first cycle.

4.3.2.5.2 Rod Cluster Control Assemblies

The number of rod cluster control assemblies is shown in Table 4.3-1. The rod cluster control assemblies are used for shutdown and control purposes to offset fast reactivity changes associated with the following:

1. The required shutdown margin in the hot, zero-power, stuck-rods condition.
2. The reactivity compensation as a result of an increase in power above hot zero power (power defect including Doppler and moderator reactivity changes).
3. Unprogrammed fluctuations in boron concentration, coolant temperature, or xenon concentration (with rods not exceeding the allowable rod insertion limits).
4. Reactivity ramp rates resulting from load changes.

The allowed control bank reactivity insertion is limited at full power to maintain shutdown capability. As the power level is reduced, control rod reactivity requirements are also reduced and more rod insertion is allowed. The control bank position is monitored and the operator is notified by an alarm if the limit is approached. The determination of the insertion limit uses conservative xenon distributions. In addition, the rod cluster control assembly withdrawal pattern determined from this analysis is used in determining power distribution factors and in determining the maximum worth of an inserted rod cluster control assembly ejection accident. For further discussion, refer to the Technical Specifications on rod insertion limits.

Power distribution, rod ejection, and rod misalignment analyses are based on the arrangement of the shutdown and control groups of the rod cluster control assemblies shown in Figure 4.3-36. All shutdown rod cluster control assemblies are withdrawn before the withdrawal of the control banks is initiated. In going from zero to 100% power, control banks A, B, C, and D are withdrawn sequentially. The limits of rod positions and further discussion of the basis for rod insertion limits are provided in the COLR and Technical Specifications.

4.3.2.5.3 Thimble Plug Assemblies

The use of part-length rod cluster control assemblies is not permitted by the Technical Specifications. The part-length rod cluster control assemblies were never installed at Unit 2. Although the part-length rod cluster control assemblies were installed at Unit 1, they were never used during operation, and were removed after Cycle 1. Thimble plug assemblies, described in Section 4.2.3.2.1 may be placed in the fuel assemblies in place of the part length control rods. Thimble plug assemblies may also be placed in the guide thimbles of fuel assemblies that do not contain other fuel inserts. When thimble plug assemblies are used, the lowest portion of the assembly is several inches away from the top of the fuel. Therefore, operation with thimble plugs does not invalidate any of the physics parameters.

4.3.2.5.4 Burnable Poison Rods

Burnable poison rods provide partial control of the excess reactivity. In doing so, these rods prevent the moderator temperature coefficient from being positive at normal operating conditions. They perform this function by reducing the requirement for soluble poison in the moderator at the beginning of the fuel cycle, as described previously. The burnable poison rod pattern in the first-cycle core together with the number of rods per assembly is shown in Figures 4.3-5 and 4.3-6, while the arrangements within an assembly are displayed in Figure 4.3-4. The reactivity worth of these rods is shown in Table 4.3-1. The boron in the rods is depleted with burnup but at a sufficiently slow rate so that the resulting critical concentration of soluble boron concentration is such that the moderator temperature coefficient remains negative at all times for power operating conditions.

4.3.2.5.5 Peak Xenon Start-up

Compensation for the peak xenon buildup is accomplished using the boron control system. Start-up from the peak xenon condition is accomplished with a combination of rod motion and boron dilution. The boron dilution may be made at any time, including during the shutdown period, provided the shutdown margin is maintained.

4.3.2.5.6 Load-Follow Control and Xenon Control

During load-follow maneuvers, power changes are accomplished using control rod motion and dilution or boration by the boron system as required. Control rod motion is limited by the control rod insertion limits as provided in the COLR and discussed in Section 4.3.2.5.2.

Reactivity changes due to the changing xenon concentration can be controlled by rod motion and/or changes in the soluble boron concentration.

4.3.2.5.7 Burnup

The control of the excess reactivity for burnup is accomplished using soluble boron and/or burnable poison. The boron concentration must be limited during operating conditions to ensure that the moderator temperature coefficient is negative. Sufficient burnable poison is installed at the beginning of a cycle to give the desired cycle lifetime without exceeding the boron concentration limits. The practical minimum boron concentration is 10 ppm.

4.3.2.6 **Control Rod Patterns and Reactivity Worth**

The rod cluster control assemblies are designated by function as the control groups and the shutdown groups. The terms “group” and “bank” are used synonymously throughout this report to describe a particular grouping of control assemblies. The rod cluster assembly pattern is displayed as Figure 4.3-36 and is not expected to change during the life of the plant. The control banks are labeled A, B, C, and D and the shutdown banks are labeled SA and SB. Each bank, although operated and controlled as a unit, is comprised of two subgroups. The axial position of the rod

cluster control assemblies may be controlled manually or automatically. These rod cluster control assemblies are all dropped into the core following the actuation of reactor trip signals.

Two criteria were employed for the selection of the control groups. First, the total reactivity worth had to be adequate to meet the requirements specified in Table 4.3-3. Second, in view of the fact that these rods could be partially inserted at power operation, the total power peaking factor had to be low enough to ensure that the power capability requirements were met. Analyses indicate that the first requirement could be met either by a single group or by two or more banks whose total worth was equal to at least the required amount. The axial power shape would be more peaked following the movement of a single group of rods worth 3% to 4% $\Delta\rho$; therefore, four banks (described as A, B, C, and D in Figure 4.3-36), each worth approximately 1% $\Delta\rho$, were selected.

The position of control banks for criticality under any reactor condition is determined by the concentration of boron in the coolant. On an approach to criticality, boron is adjusted to ensure that criticality will be achieved with control rods above the insertion limit set by shutdown and other considerations (see the Technical Specifications). Early in the cycle there may also be a withdrawal limit at low power to maintain a negative moderator temperature coefficient. Usual practice is to adjust boron to ensure that the rod position lies within the so-called maneuvering band, that is, such that an escalation from zero power to full power does not require further adjustment of boron concentration.

Ejected-rod worths are given in Section 15.4.6 for several different conditions. Experimental confirmation of these worths can be found by reference to start-up test reports such as Reference 12.

Allowable deviations due to misaligned control rods are discussed in the Technical Specifications.

A representative calculation for two banks of control rods withdrawn simultaneously (rod-withdrawal accident) is given in Figure 4.3-37.

The calculation of control rod reactivity worth versus time following reactor trip involves both control rod velocity and differential reactivity worth. The rod position versus time of travel after rod release assumed is given in Table 15.1-8. For nuclear design purposes, the reactivity worth versus rod position is calculated by a series of steady-state calculations at various control rod positions assuming all rods out of the core as the initial position in order to minimize the initial reactivity insertion rate. Also, to be conservative, the rod of highest worth is assumed stuck out of the core and the flux distribution (and thus reactivity importance) is assumed to be skewed to the bottom of the core. The result of these calculations is shown in Table 15.1-7.

The shutdown groups provide additional negative reactivity to ensure an adequate shutdown margin. Shutdown margin is defined as the amount by which the core would be subcritical at hot shutdown if all rod cluster control assemblies are tripped, but assuming that the highest-worth

assembly remains fully withdrawn and no changes in xenon or boron take place. The loss of control rod worth due to the material irradiation is negligible since only bank D may be in the core under normal operating conditions.

The values given in Table 4.3-3 show that the available reactivity in withdrawn rod cluster control assemblies provides the design bases minimum shutdown margin allowing for the highest-worth cluster to be at its fully withdrawn position. An allowance for uncertainty in the calculated worth of N-1 rods is made before the determination of the shutdown margin.

4.3.2.7 **Criticality of Fuel Assemblies**

The criticality of fuel assemblies outside of the reactor is precluded by adequate design of fuel transfer and fuel storage facilities and by administrative control procedures. This section identifies those criteria important to criticality safety analyses.

ANSI Standard N18.2 specifies a k_{eff} not to exceed 0.95 in spent-fuel storage racks and transfer equipment flooded with pure water.

For the new fuel storage, k_{eff} will not exceed 0.98 with fuel of the highest anticipated enrichment in place and assuming optimum moderation (e.g., aqueous foam). The normally dry new fuel storage racks are designed to ensure k_{eff} will not exceed 0.95 when fully loaded and flooded with unborated water. No criterion is given for the refueling operation; however, the margin resulting from the above referenced limits provided for the storage of the fuel is adequate for the controlled and continuously monitored operations involved.

In the analysis for the storage facilities, fuel of the highest licensed enrichment must be considered, and no credit may be taken for control rods or other removable neutron poisons. Assemblies cannot be closer together than the design separation provided by the storage facility except in special cases such as in fuel-shipping containers, where analyses are carried out to establish the acceptability of the design. The mechanical integrity of the fuel assembly is assumed.

The criticality analysis of the new fuel storage racks is based on Monte Carlo code calculations (Reference 13) for Westinghouse 17 x 17 fuel. Both normal and postulated abnormal variations in storage rack conditions were considered. The results of the analysis demonstrate that k_{eff} will remain below 0.95 for any potential aqueous moderator density for fresh fuel enrichments of 4.6 weight percent U-235 or less. The results of a detailed parametric study of k_{eff} versus water density for 4.6 weight percent initial enrichment fuel showed a peak k_{eff} of 0.936 (including calculational uncertainties) at an optimum moderator density of about 0.065 gm/cc. Another peak of slightly lower k_{eff} was found at a moderator density of 1.0 gm/cc.

The criticality analysis of the spent fuel storage racks was based on KENO-V Monte Carlo calculations. The fuel was considered to be axially infinite. The effect of axial burnup distributions (3D) versus the uniform average burnup (2D) was calculated and accounted for in the burnup credit requirements. Westinghouse 17 x 17 fuel was assumed. The Westinghouse

Owners Group (WOG) methodology (Reference 39) for criticality analysis was used. The WOG approach makes use of dual criticality limits. The first limit is that the effective multiplication factor (k_{eff}) of the spent fuel storage area is < 1.0 with no soluble boron. The second limit is $k_{eff} < 0.95$ with credit for soluble boron. The worst case k_{eff} without soluble boron, including uncertainties, was 0.99923. The worst case k_{eff} with soluble boron, including uncertainties, was 0.94908. A spent fuel pit boron concentration of 900 ppm will keep k_{eff} below this worst case number under all conditions including postulated accidents. The specified minimum boron concentration of 2500 ppm assures that the concentration will remain above this level. In addition, the boron concentration of 2500 ppm is consistent with the boron dilution evaluation that demonstrates that any credible dilution event could be terminated prior to reaching the boron concentration for $k_{eff} \geq 0.95$.

The analyses discussed above demonstrate that the design criteria are met for fuel enrichments of up to 4.6 weight percent U-235. The design criteria are met in the spent fuel storage racks by a combination of rack design, soluble boron and restrictions on the placement of fuel assemblies. Details regarding the criticality calculations, including incorporation of uncertainties, are found in References 13, 35, and 40.

4.3.2.8 **Stability**

4.3.2.8.1 Introduction

The stability of the PWR cores against xenon-induced spatial oscillations and the control of such transients are discussed extensively in References 3, 14, 15, and 16. A summary of these reports is given in the following discussion, and the design bases are given in Section 4.3.1.6.

In a large reactor core, xenon-induced oscillations can take place with no corresponding change in the total power of the core. The oscillation may be caused by a power shift in the core that occurs rapidly by comparison with the xenon-iodine time constants. Such a power shift occurs in the axial direction when a plant load change is made by control rod motion and results in a change in the moderator density and fuel temperature distributions. Such a power shift could occur in the diametral plane of the core as a result of abnormal control action.

Due to the negative power coefficient of reactivity, PWR cores are inherently stable to oscillations in total power. Protection against total power instabilities is provided by the control and protection system as described in Section 7.7. Hence, the discussion on the core stability will be limited here to xenon-induced spatial oscillations.

4.3.2.8.2 Stability Index

Power distributions, either in the axial direction or in the X-Y plane, can undergo oscillations due to perturbations introduced in the equilibrium distributions without changing the total core power. The xenon-induced oscillations are essentially limited to the first flux overtones in the current PWRs, and the stability of the core against xenon-induced oscillations can be determined in terms of the eigenvalues of the first flux overtones.

Writing, either in the axial direction or in the X-Y plane, the eigenvalue ζ of the first flux harmonic as:

$$\zeta = b + ic \tag{4.3-6}$$

then b is defined as the stability index and $T = 2\pi/c$ as the oscillation period of the first harmonic. The time-dependence of the first harmonic $\delta\phi$ in the power distribution can now be represented as:

$$\delta\phi(t) = Ae^{\zeta t} = ae^{bt} \cos ct \tag{4.3-7}$$

where A and a are constants. The stability index can also be obtained approximately by:

$$b = \frac{1}{T} \ln \frac{A_{n+1}}{A_n} \tag{4.3-8}$$

where A_n, A_{n+1} are the successive peak amplitudes of the oscillation and T is the time period between the successive peaks.

4.3.2.8.3 Prediction of the Core Stability

The stability of the core described herein (i.e., with 17 x 17 fuel assemblies) against xenon-induced spatial oscillations is expected to be equal to or better than that of earlier designs. The prediction is based on a comparison of the parameters that are significant in determining the stability of the core against the xenon-induced oscillations, namely (a) the overall core size is unchanged and spatial power distributions will be similar, (b) the moderator temperature coefficient is expected to be similar or slightly more negative, and (c) the Doppler coefficient of reactivity is expected to be equal or slightly more negative at full power.

An analysis of both the axial and X-Y xenon transient tests, discussed in Section 4.3.2.8.5, shows that the calculational model is adequate for the prediction of core stability.

4.3.2.8.4 Stability Measurements

Axial Measurements

Two axial xenon transient tests conducted in a PWR with a core height of 12 feet. and 121 fuel assemblies is reported in Reference 17, and will be briefly discussed here. The tests were performed at approximately 10% and 50% of cycle life.

Both a free-running oscillation test and a controlled test were performed during the first test. The second test at midcycle consisted of a free-running oscillation test only. In each of the free-running oscillation tests, a perturbation was introduced to the equilibrium power distribution through an impulse motion of the control bank D and the subsequent oscillation was monitored to measure the stability index and the oscillation period. In the controlled test conducted early in the cycle, the part-length rods were used to follow the oscillations to maintain an axial offset within

the prescribed limits. The axial offset power was obtained from the ex-core ion chamber readings (which had been calibrated against the incore flux maps) as a function of time for both free-running tests as shown in Figure 4.3-38.

The total core power was maintained constant during these spatial xenon tests, and the stability index and the oscillation period were obtained from a least-square fit of the axial offset data in the form of Equation 4.3-7. The axial offset of power is the quantity that properly represents the axial stability in the sense that it essentially eliminates any contribution from order harmonics including the fundamental mode. The conclusions of the tests are as follows:

1. The core was stable against induced axial xenon transients both at the core-averaged burnups of 1550 MWd/MTU and 7700 MWd/MTU. The measured stability indices are -0.041 hr^{-1} for the first test (curve 1 of Figure 4.3-38) and -0.014 hr^{-1} for the second test (curve 2 of Figure 4.3-38). The corresponding oscillation periods are 32.4 hours and 27.2 hours, respectively.
2. The reactor core becomes less stable as fuel burnup progresses and the axial stability index was essentially zero at 12,000 MWd/T.

Measurements in the X-Y Plane

Two X-Y xenon oscillation tests were performed at a PWR plant with a core height of 12 feet. and 157 fuel assemblies. This plant had the highest power output of any Westinghouse PWR then in operation (1972). The first test was conducted at a core average burnup of 1540 MWd/MTU and the second at a core average burnup of 12,900 MWd/MTU. Both of the X-Y xenon tests show that the core was stable in the X-Y plane at both burnups. The second test shows that the core became more stable as the fuel burnup increased and all Westinghouse PWRs with 121 and 157 assemblies are expected to be stable throughout their burnup cycles.

In each of the two X-Y tests, a perturbation was introduced to the equilibrium power distribution through an impulse motion of one RCC unit located along the diagonal axis. Following the perturbation, the uncontrolled oscillation was monitored using the movable detector and thermocouple system and the ex-core power range detectors. The quadrant tilt difference is the quantity that properly represents the diametral oscillation in the X-Y plane of the reactor core in that the differences of the quadrant average powers over two symmetrically opposite quadrants essentially eliminate the contribution to the oscillation from the azimuthal mode. The quadrant tilt difference (QTD) data were fitted in the form of Equation 4.3-7 through a least-square method. A stability index of -0.076 hr^{-1} with a period of 29.6 hours was obtained from the thermocouple data shown in Figure 4.3-39.

It was observed in the second X-Y xenon test that the PWR core with 157 fuel assemblies had become more stable due to an increased fuel depletion and the stability index was not determined.

4.3.2.8.5 Comparison of Calculations with Measurements

The analysis of the axial xenon transient tests was performed in an axial slab geometry using a flux synthesis technique. The direct simulation of the axial offset data was carried out using the PANDA code (Reference 18). The analysis of the X-Y xenon transient tests was performed in an X-Y geometry using a modified TURTLE code (Reference 10). Both the PANDA and TURTLE codes solve the two-group time-dependent neutron diffusion equation with time-dependent xenon and iodine concentrations. The fuel temperature and moderator density feedback is limited to a steady-state model. All the X-Y calculations were performed in an average enthalpy plane.

The basic nuclear cross sections used in this study were generated from a unit cell depletion program that has evolved from the codes LEOPARD (Reference 19) and CINDER (Reference 20). The detailed experimental data during the tests, including the reactor power level, enthalpy rise, and the impulse motion of the control rod assembly as well as the plant follow burnup data, were closely simulated in the study.

The results of the stability calculation for the axial tests are compared with the experimental data in Table 4.3-4. The calculations show conservative results for both of the axial tests with a margin of approximately 0.01 $hour^{-1}$ in the stability index.

An analytical simulation of the first X-Y xenon oscillation test showed a calculated stability index of -0.081 $hour^{-1}$, in good agreement with the measured value of -0.076 $hour^{-1}$. As indicated earlier, the second X-Y xenon test showed that the core had become more stable compared to the first test and no evaluation of the stability index was attempted. This increase in the core stability in the X-Y plane due to increased fuel burnup is due mainly to the increased magnitude of the negative moderator temperature coefficient.

Previous studies of the physics of xenon oscillations, including three-dimensional analysis, are reported in the series of topical reports, References 14, 15, and 16. A more detailed description of the experimental results and an analysis of the axial and X-Y xenon transient tests are presented in Reference 17 and Section 1 of Reference 21.

4.3.2.8.6 Stability Control and Protection

The ex-core detector system is used to provide indications of xenon-induced spatial oscillations. The readings from the ex-core detectors are available to the operator and also form part of the protection system.

Axial Power Distribution

For the maintenance of proper axial power distributions, the operator is instructed to maintain an axial offset within a prescribed operating band, based on the ex-core detector readings. Should the axial offset be permitted to move far enough outside this band, the protection limit would be reached and the power would be automatically cut back.

Twelve-foot PWR cores become less stable to axial xenon oscillations as fuel burnup progresses. However, free xenon oscillations are not allowed to occur except for special tests. The control rod banks present in all modern Westinghouse PWRs are sufficient to dampen and control any axial xenon oscillations present. Should the axial offset be inadvertently permitted to move far enough outside the control band due to an axial xenon oscillation, or any other reason, the protection limit on axial offset would be reached and the power would be automatically cut back.

Radial Power Distribution

The core described herein is calculated to be stable against X-Y xenon-induced oscillations at all times in life.

The X-Y stability of large PWRs was to be further verified as part of the start-up physics test program at a PWR core with 193 fuel assemblies. The measured X-Y stability of the PWR core with 157 assemblies and the good agreement between the calculated and measured stability indexes for this core, as discussed in Sections 4.3.2.8.4 and 4.3.2.8.5, make it very unlikely that a sustained X-Y oscillation can occur in a core with 193 assemblies. As discussed in Section 4.3.2.8.2, the X-Y stability of the new model core (i.e., with 17 x 17 fuel assemblies) is expected to be equal to or better than the earlier PWR cores. However, in the unlikely event that X-Y oscillations occur, backup actions are possible and would be implemented, if necessary, to increase the natural stability of the core until tests demonstrate a suitable stability. This is based on the fact that several actions could be taken to make the moderator temperature coefficient more negative, which would increase the stability of the core in the X-Y plane.

Provisions for protection against nonsymmetric perturbations in the X-Y power distribution that could result from equipment malfunctions are made in the protection system design. This includes control rod drop, rod misalignment, and asymmetric loss-of-coolant flow.

A more detailed discussion of the power distribution control in PWR cores is presented in Reference 3.

4.3.2.9 Vessel Irradiation

It is beyond the scope of this section to present methods and analyses used in the determination of neutron and gamma flux attenuation between the core and the pressure vessel other than a brief review as given below. A more complete discussion on the pressure vessel irradiation and surveillance program is given in Section 5.4.3.6.

The primary shielding material that serves to attenuate high-energy neutron and gamma flux originating in the core consists primarily of the core baffle, the core barrel, the neutron pads, and the associated water annuli, all of which are within the region between the core and the pressure vessel.

In general, few group neutron diffusion theory codes are used to determine flux and fission power density distributions within the active core, and the accuracy of these analyses is verified

by incore measurements on operating reactors. Outside the active core, methods such as those that use multigroup space-dependent slowing-down codes described in Section 5.4.3.6.2 are used. Region-wise power-sharing information from the core calculations is often used as reference source data for the multigroup codes.

The neutron flux distribution and spectrum in the various structural components vary significantly from the core to the pressure vessel. Representative values of the neutron flux distribution and spectrum are presented in Table 4.3-5. The values listed are based on first-core cycle reactor core parameters and power distributions, and thus, are suitable estimates for long-term neutron irradiation projections and for correlation with radiation damage estimates.

As discussed in Section 5.4.3.6, the irradiation surveillance program uses actual test samples to verify the accuracy of the calculated fluxes at the vessel.

4.3.3 Analytical Methods (PDQ Two-Zone/NOMAD)

Calculations required in nuclear design consist of three distinct types, which are performed in sequence:

1. Determination of effective fuel temperatures
2. Generation of macroscopic few-group parameters
3. Space-dependent, few-group diffusion calculations

The purpose of this section is to describe the PDQ Two-Zone and NOMAD computational models used for reactor physics analyses, and to describe the accuracy of these models.

4.3.3.1 Fuel Temperature (Doppler) Calculations

Fuel temperature data is obtained using the EPRI ESCORE code. Fuel pin construction, power level, and burnup data are input to the code for determination of the best estimate volume averaged fuel pin temperature as a function of burnup and power level. The volume averaged temperatures are adjusted by determining a single uniform temperature which results in the same resonance absorption as the more detailed 10 ring ESCORE temperature distribution.

The fuel temperature calculation considers the effect of radial variation of pellet conductivity, expansion-coefficient and heat-generation rate, elastic deflection of the clad, and a gap conductance that depends on the initial fill gas, the hot open-gap dimension, and the fraction of the pellet over which the gap is closed. The fraction of the gap assumed closed represents an empirical adjustment used to produce good agreement with observed reactivity data at beginning of life. Further gap closure occurs with burnup and accounts for the decrease in Doppler defect with burnup that has been observed in operating plants.

ESCORE predictions of fuel temperature have been validated against test data as described in the EPRI ESCORE code manual (References 28 & 29). Use of these predicted fuel temperatures within the PDQ and NOMAD core design models has resulted in good agreement

with measured reactivity parameters (critical boron concentration, estimated critical rod position, etc.) as discussed in Section 4.3.3.3.

4.3.3.2 **Macroscopic Group Constants**

The primary source of the basic nuclear cross section data is the ENDF/B-V library used in the EPRI CELL2 code. The library contains cross sections for 68 fast energy groups ranging from 0.414 eV to 10 MeV and 35 thermal energy groups ranging from 0.000253 eV to 1.855 eV. Additional details of the library are available in Reference 22.

The CELL2 code is used to calculate composition-dependent energy spectra and then collapse the fine-energy group cross sections to produce two-group cross sections for each unit cell. CELL2 calculates two-group spectrum-weighted cross sections for each type of unit cell used to represent the reactor core. A unit cell can be either a fuel rod, a control rod guide tube, or a burnable poison rod, the moderator associated with each type of rod, and an extra region around the cell to account for the impact of other assembly materials. A supercell is defined as the combined flux weighted homogenization of all the regions comprising a unit cell. For the PDQ two zone model (Reference 27), the fuel unit cell consists of a fuel rod, the cladding, moderator, and an extra region to account for guide tubes (with or without BP rods) and moderator gaps between assemblies. The supercell option is used to represent the fuel assembly in the PDQ two zone model because only a homogenized assembly can be represented due to the coarse mesh structure used. The homogenization is performed in a manner that results in all the mesh blocks within each zone initially having the same material composition. All fuel cross sections (not burnable poison or control rods) used in the PDQ two zone model are based on the CELL2 supercell data. A more detailed description of the theory and use of the CELL2 code is available in References 22 and 23.

The neutron energy spectrum calculated by CELL2 depends on the material concentrations in the unit cell. The material concentrations change during the operation of the reactor as a result of:

1. Depletion of the fuel nuclides
2. Changes in the soluble boron
3. Changes in moderator temperature (density)
4. Removal or addition of BP rods

The neutron spectrum is also dependent on the temperature of the fuel due to Doppler broadening of the resonance absorption peaks. CELL2 is used to calculate the effect of changes in both the material concentrations and the fuel and moderator temperatures on the neutron spectrum and spectrum-weighted two-group cross sections.

To provide a base of fuel cross section data comprehensive enough for development of a thorough HARMONY tableset, CELL2 fuel cell cases are run over a wide variety of core operating conditions.

After identification of significant cross section sensitivities the cross sections are formatted into HARMONY tableset format.

4.3.3.2.1 BP Cross Section Generation

Because CELL2 cannot represent both BP rods and fuel rods in their actual geometry simultaneously, a two stage approach is used. The unit cell for the BP model consists of the BP absorber, clad, moderator, and two extra regions consisting of fuel and moderator homogenized. The fuel and moderator homogenization is performed in such a way that the flux spectrum in the fuel region nearest the BP pin is reasonably representative of the fuel pin cell spectrum. The neutron absorption rate of the BP pin is calculated and properly volume averaged for use as input to the CELL2 fuel pin cell model for determining the sensitivity of fuel cross sections to BP neutron absorption. The BP cell model is also used to provide BP microscopic absorption cross sections and flux depression factors which are input to the HARMONY tableset as a function of fuel isotopics, boron, moderator temperature or specific volume, and BP B10 number density.

4.3.3.2.2 Cross Section Representation

Sets of HARMONY cross section tables based on these CELL2 calculations are prepared by the ETHIL code. These tables represent:

1. Microscopic fast and thermal energy group absorption, fission and transport cross sections for each material or isotope.
2. Fast and thermal Nu and Kappa for each fissioning isotope.
3. The macroscopic removal cross section.
4. Multiple G-factor tables applied to (1) and (3) above to model any important cross section dependences not accounted for in the cross section tables. The G-factor tables also model number density dependences (such as soluble boron as a function of moderator density) and flux depression factors (for BP or control rods).

4.3.3.2.3 Normalization to KENO-V.a, Benchmark Cases

Prior experience with reactor core modeling has indicated that adjusting the predictions of PDQ (and by extension the cross section generation code) to higher order Monte Carlo predictions often improves the agreement between prediction and measurement. The Monte Carlo program used by Virginia Power for this purpose is the KENO-V.a code run using the SCALE3 driver package with the 218 group ENDF/B-IV (Reference 25) cross section set. The PDQ two zone HARMONY tablesets contain adjustment factors to normalize BP worth, soluble boron worth, and overall reactivity predictions to target predictions. In the KENO model each fuel pin, guide tube and BP rod is explicitly modeled including clad and voids. A bias is assigned to the KENO

eigenvalues on the basis of the results from several modeled critical experiments. Appropriate consideration is given to the statistical uncertainty of the KENO predictions. The normalization process is applied separately to each fuel enrichment in the HARMONY tableset.

4.3.3.2.4 KENO-V.a Control Rod Cross Sections

A KENO-V.a (Reference 26) model is also used to generate control rod cross sections for the PDQ two zone model. The geometry used is a checkerboard assembly arrangement in which every other assembly can contain a control rod. The 27 group ENDF/B-IV cross section library is used because it contains fission products needed to simulate burned fuel. The cross sections are appropriately volume weighted and added to the HARMONY tableset as microscopic cross sections and G-factors. A checkerboard PDQ two zone model is used in an iterative process to determine the correct flux depression factor to be applied to the control rod cross sections in each energy group so that the overall reactivity effect produced agrees well with the KENO predictions. Comparisons of measured and predicted integral and differential control rod worths indicate excellent overall agreement using this model.

4.3.3.2.5 Reflector and Baffle Cross Sections

Determination of coarse mesh baffle and reflector constants for the PDQ two zone geometry is done by appropriately volume weighting and then adjusting the coarse mesh constants to better match the power distribution and flux ratios predicted by a very fine mesh PDQ model. Cross section data for the stainless steel region is obtained by editing the clad region of a CELL2 stainless steel clad fuel cell. Water and boron mixture cross sections are generated using the CELL2 non-fuel option. PDQ quarter core fine and coarse mesh runs are made so that the relative power distributions and the flux ratios near the baffle can be compared. Small adjustments to the baffle constants are made until the agreement between the models for a variety of conditions is judged acceptable.

A similar procedure is used to determine the axial reflector representation.

As discussed in Section 4.3.3.3 macroscopic cross-section within the PDQ and NOMAD core design models has resulted in good agreement with measured reactivity parameters (critical boron concentration, estimated critical rod position, etc.).

4.3.3.3 **Spatial Few-Group Diffusion Calculations**

Virginia Power employs a coarse mesh (five non-uniform mesh per fuel assembly), three-dimensional (26 non-uniform axial mesh), two neutron energy group diffusion-depletion (with thermal-hydraulic feedback) calculational package, designated as the PDQ two zone calculational model. The “two zone” designation refers to the use of two separate material zones to represent each fuel assembly in the X-Y dimension - one zone where no lumped burnable poison rods or control rods exist and one zone in which the poison rods or control rods are homogenized with the fuel materials. The PDQ two zone model uses the Virginia Power computer codes SHUFL and PDQV2, as well as input from the EPRI ARMP-02, CELL2 (References 22

& 23) and NUPUNCHER (Reference 23) codes, the Virginia Power ETHIL code, the EPRI ESCORE (Reference 24) code, and the SCALE3 (Reference 25) package from ORNL (including KENO-V.a). In addition, pin power distributions and instrument thimble fluxes are reconstructed with the Virginia Power computer codes PCF and RECON.

The types of calculations that can be performed by the PDQ two zone model include:

1. Reactor Physics Analysis
   a. Three-dimensional assembly average radial power distributions, relative radial peaking factors ($F_{XY}(Z)$), enthalpy rise hot channel factors ($F_{\Delta H}(X,Y)$), assembly average axial power distribution, core average-axial power distribution (P(Z)), and heat flux hot channel factor ($F_Q(X,Y,Z)$).
   b. Critical soluble boron concentrations.
   c. Nuclide concentrations.
   d. Integral and differential control rod bank worths.
   e. Abnormally positioned control rod bank worths.
   f. Moderator and Doppler coefficients and defects.
2. Fuel Management Analysis
   a. Batch power and burnup sharing.
   b. Fuel isotopics as a function of burnup.
   c. Scoping studies for the evaluation of alternative future cycle designs and fuel loadings.

Through comparisons with measurements taken at Surry Unit Nos. 1 and 2 and North Anna Unit Nos. 1 and 2 the accuracy of the PDQ two zone model has been demonstrated for each of the following production calculations: (1) critical boron concentrations, (2) control rod bank worths (integral and differential), (3) assemblywise power distributions (both axial and radial) and (4) reactivity coefficients for final production calculations to support reactor operations or safety analysis (Reference 27). Based on comparison with measured data it is estimated that the accuracy of current analytical methods is as summarized in Table 4.3-6.

NOMAD is a one-dimensional (axial), two energy group, diffusion theory computer code with thermal-hydraulic feedback, and a calculational model designated as the Virginia Power NOMAD model. The code is designed to perform both reload design analyses and core operation evaluations.

Virginia Power developed an enhanced version of the NOMAD model. Consistent with the intent stated in VEP-NFE-1A, the enhanced version of the NOMAD model is a result of a

continuing effort to verify and improve the model. All model inputs to NOMAD come either directly or indirectly from PDQ 3-D model calculations. These inputs include cross sections, reference isotopics, $F_{XY}(Z)$'s and radial bucklings.

The benefit of the strong connection between the NOMAD and PDQ 3-D models has been demonstrated through a comparison of NOMAD predictions to a wide variety of measurements, including startup physics data; axial power shapes and peaking factors; temperature, power, and xenon transients; and Estimated Critical Position (ECP) calculations. Comparison of NOMAD uncertainty factors to Nuclear Reliability Factors (NRF) for F_Z, F_Q, differential boron worth, critical boron concentration, isothermal temperature coefficients, differential rod worth and integral rod worth verify the accuracy of the NOMAD model and the applicability of the NRF for NOMAD calculations.

NOMAD calculations were compared to measurements for a wide range of cycle designs and parameters to demonstrate the capabilities of the model and to determine appropriate uncertainty factors for use with NOMAD. Tables 4.3-7 through 4.3-9 summarize the statistical results for these comparisons. Note that all statistical uncertainties met their respective VEP-FRD-45A limits (Table 4.3-6), design tolerances or administrative limits.

In addition to the statistical results, NOMAD was benchmarked to various transients, including the S2C2 load follow, two N1C3 return to power scenarios, the N1C6 pipe inspection transient, the N1C9 MTC measurement, and the N1C11 initial ramp to power. NOMAD was compared to measured axial offset (or ΔI), boron concentration and/or axial power (F_Z) and showed good agreement for all transients. This demonstrates the accuracy of the model for a variety of factors including Doppler temperature effects, moderator temperature effects, boron concentration, control rod position, and xenon.

These results show NOMAD meets the required reliability factors and is capable of performing axial power calculations, including FAC and RPDC calculations, RSAC calculations, normal operation transient evaluations including load follow simulations, differential and integral rod worth predictions, ECP calculations, xenon worth calculations, reactivity coefficient calculations, axial offset control, peaking factor analyses, and axial burnup distributions. Based on the qualification results described, NOMAD has been shown to be acceptable using present uncertainty factors and design tolerances.

4.3.4 Analytical Methods (CMS)

Calculations required in nuclear design consist of three distinct types, which are performed in sequence:

1. Determination of effective fuel temperatures
2. Generation of macroscopic few-group parameters
3. Space-dependent, few-group nodal calculations

The purpose of this section is to describe the Studsvik Core Management System (CMS) computational model (comprised principally of the CASMO-4, CMS-LINK and SIMULATE-3 codes) used for reactor physics analyses and to describe the accuracy of this model.

4.3.4.1 **Fuel Temperature (Doppler) Calculations**

Fuel temperature data is obtained using the EPRI ESCORE code. Fuel pin construction, power level, and burnup data are input to the code for determination of the best estimate volume averaged fuel pin temperature as a function of burnup and power level. The volume averaged temperatures are adjusted by determining a single uniform temperature which results in the same resonance absorption as the more detailed 10 ring ESCORE temperature distribution.

The fuel temperature calculation considers the effect of radial variation of pellet conductivity, expansion-coefficient and heat-generation rate, elastic deflection of the clad, and a gap conductance that depends on the initial fill gas, the hot open-gap dimension, and the fraction of the pellet over which the gap is closed. The fraction of the gap assumed closed represents an empirical adjustment used to produce good agreement with observed reactivity data at beginning of life. Further gap closure occurs with burnup and accounts for the decrease in Doppler defect with burnup that has been observed in operating plants.

ESCORE predictions of fuel temperature have been validated against test data as described in the EPRI ESCORE code manual (References 28 & 29). Use of these predicted fuel temperatures within the SIMULATE core design model has resulted in good agreement with measured reactivity parameters (critical boron concentration, estimated critical rod position, etc.) as discussed in Section 4.3.4.3.

4.3.4.2 **Macroscopic Group Constants**

The primary source of the basic nuclear cross section data is the ENDF/B-4 library (although some data come form other sources) used in the CASMO-4 code. The library contains cross sections for 70 energy groups. Additional details of the library are available in Reference 42.

CASMO-4 (CASMO) is a multigroup two-dimensional transport theory code for burnup calculations on BWR and PWR assemblies or simple pin cells. The code handles a geometry consisting of cylindrical fuel rods of varying composition in a square pitch array. Fuel rods may be loaded with integral poisons such as gadolinium or boron. The fuel assembly model may contain burnable absorber rods, cluster control rods, in-core instrument channels, water gaps, boron steel curtains, and cruciform control rods in the regions separating fuel assemblies. Typical fuel storage rack geometries can also be handled. Some characteristics of CASMO are listed below:

1. Nuclear data are collected in a library containing microscopic cross sections in 70 energy groups. Neutron energies cover the range 0 to 10 MeV.
2. CASMO can accommodate non-symmetric fuel bundles containing up to 25 by 25 rods. Full, half, quadrant or octant symmetry (mirror symmetry) can be utilized in the calculations.

3. Absorber rods or water holes covering 1 x 1, 2 x 2 pin cell positions or larger areas are allowed in the assembly.
4. Effective resonance cross sections are calculated individually for each fuel pin.
5. A fundamental mode calculation is performed to account for leakage effects.
6. The microscopic depletion is calculated in each fuel and burnable absorber pin. Isotopic depletion as a function of irradiation is calculated for each fuel pin and for each region containing a burnable absorber.
7. Discontinuity factors are calculated at the boundary between bundles and for reflector regions.

In order to generate a neutronic data library for SIMULATE-3 a series of CASMO depletions and branch cases is required. This series of calculations is defined within CMS as the "SIMULATE-3 Case Matrix." This case matrix consists of a series of depletions and instantaneous branch cases vs. exposure as a function of varied boron concentration, moderator temperature, fuel temperature, and shutdown cooling time, as well as cases with control rods and without removable burnable poison in guide tube locations.

4.3.4.2.1 Cross Section Representation

CMS-LINK (Reference 43) is a linking code that processes CASMO card image files into a binary formatted nuclear data library for use by SIMULATE-3. The code collects the following data from CASMO card image files:

- Two-group macroscopic cross sections
- Two-group discontinuity factors
- Fission product data
- Detector data
- Pin power reconstruction data
- Kinetics data
- Isotopics data
- Spontaneous fission data

Functional dependencies for key core condition variables are predefined in the code. A diverse set of CASMO cases provide data covering a range of reactor conditions between hot or cold shutdown and full power operation. Branch cases include changes in soluble boron, moderator temperature, fuel temperature, insertion and removal of burnable poison rods, insertion of control rods, and isotopic decay after shutdown. The cumulative effect of long term changes in

individual variables such as soluble boron, moderator temperature or fuel temperature are treated as “history” effects by CMS-LINK and subsequently in SIMULATE.

4.3.4.3 Spatial Few-Group Nodal Calculations

SIMULATE-3 (SIMULATE) is an advanced two-group nodal code for the analysis of both PWRs and BWRs. The code is based on the QPANDA neutronics model (Reference 44) which employs fourth-order polynomial representations of the intranodal flux distributions in both the fast and thermal groups. Key features of SIMULATE are:

1. Pin power reconstruction
2. No normalization required against higher order calculations
3. Explicit representation of the reflector region
4. Coupled neutronics/thermal-hydraulics
5. Internal calculation of the effect of spacer grids on axial power distributions
6. Calculation of intra-nodal axial power distribution effect on F_Q

The types of calculations that can be performed by the CMS model include:

1. Three-dimensional assembly power and flux distributions, relative radial peaking factors ($F_{xy}(Z)$), enthalpy rise hot channel factors ($F_{\Delta H}(X,Y)$), assembly average axial power distribution, core average axial power distribution (F(Z)), and heat flux hot channel factor ($F_Q(X,Y,Z)$)
2. Soluble boron concentration and boron worth
3. Fuel and burnable poison nuclide concentrations as a function of fuel burnup
4. Integral and differential control rod bank worths
5. Abnormally positioned control rod worths
6. Moderator and Doppler temperature coefficients and defects
7. Power coefficients and defects
8. Operational transient simulation
9. Delayed neutron parameters and prompt neutron lifetime
10. Detector reaction rates, coupling coefficients, and peaking factors for flux map analysis
11. Fuel burnup
12. Scoping studies for the evaluation of alternative fuel management strategies, fuel design changes, burnable poison product changes, and alternate control rod designs

Comparison of CASMO/SIMULATE and Monte Carlo code calculations of pin-to-box ratios and flux thimble instrument reaction rate ratios are used in combination with normalized

flux map reaction rate comparisons to determine appropriate peaking factor ($F_{\Delta H}$ and F_Q) uncertainty factors. Comparison of pin-to-box ratios and flux thimble reaction rate ratios (W-primes) exercises the entire CMS system (CASMO, CMS-LINK, and SIMULATE). Pin-to-box ratios are defined here to be the ratio of pin power to assembly average power. W-prime is defined as the normalized ratio of assembly power to flux thimble instrument reaction rate.

SIMULATE predictions were compared against measurements from 29 North Anna and 33 Surry cycles (Reference 36). The types of core measurements used for model benchmarking include:

1. Critical boron concentration

   Hot full power (HFP)
   Hot zero power (HZP) beginning of cycle (BOC)
   HZP for restarts following reactor trips or mid-cycle outages

2. Startup Physics Tests (HZP, BOC)

   Integral control rod worth (via boron dilution and rod swap methods)
   Differential control rod worth (boron dilution method)
   Isothermal temperature coefficient (ITC)
   Differential boron worth (DBW)

3. Estimated Critical Position (ECP)

   Return to HZP critical conditions following an outage
   Verification of reactivity effect of control rods, power defect, soluble boron, xenon and other isotopic changes

4. Flux maps

   Instrument thimble reaction rates

5. Operational transients (Similar to load follow maneuvers)

   Verification of reactivity effects (critical boron vs. time)
   Verification of correct axial power distribution effects (axial offset or delta-I versus time)
   Verification of undamped xenon oscillation axial power distribution behavior (correct balance between Doppler feedback and axial xenon oscillations)

Through the comparisons with measured data, the accuracy of the SIMULATE model has been demonstrated. Based on the comparisons with measured data, reliability factors for CMS were developed (Reference 36) and are summarized in Table 4.3-10.

4.3 REFERENCES

1. *Reload Nuclear Design Methodology*, VEP-FRD-42, Rev. 2.1-A, August 2003.
2. *Westinghouse Anticipated Transients Without Reactor Trip Analysis*, WCAP-8330, 1974.
3. J. S. Moore, *Power Distribution Control of Westinghouse Pressurized Water Reactors*, WCAP-7208 (Westinghouse Proprietary), 1968, and WCAP-7811, 1971.
4. F. L. Langford and R. J. Nath, Jr., *Evaluation of Nuclear Hot Channel Factor Uncertainties*, WCAP-7308-L (Westinghouse Proprietary), 1969, and WCAP-7810, 1971.
5. A. F. McFarlane, *Core Power Capability in Westinghouse PWRs*, WCAP-7267-L (Westinghouse Proprietary), 1969, and WCAP-7809, 1971.
6. J. M. Hellman, editor, *Fuel Densification Experimental Results and Model for Reactor Application*, WCAP-8218-P-A (proprietary), 1975, and WCAP-8219-A (nonproprietary), 1975.
7. J. M. Hellman and J. W. Yank, *Effects of Fuel Densification Power Spikes on Clad Thermal Transients*, WCAP-8359, 1974.
8. T. Morita, et al., *Topical Report, Power Distribution Control and Load Following Procedures*, WCAP-8385 (proprietary), 1974, and WCAP-8403 (nonproprietary), 1974.
9. A. F. McFarlane, *Power Peaking Factors*, WCAP-7912-P-A (proprietary), 1975, and WCAP-7912-A (nonproprietary), 1975.
10. S. Altomare and R. F. Barry, *The TURTLE 24.0 Diffusion Depletion Code*, 7213-P-A (proprietary), 1975, and WCAP-7758-A (nonproprietary), 1975.
11. J. O. Cermak, et al., *Pressurized Water Reactor pH - Reactivity Effect*, Final Report, WCAP-3696-8 (EURAEC-2074), 1968.
12. J. E. Outzs, *Plant Startup Test Report, H. B. Robinson Unit No. 2*, WCAP-7844, 1972.
13. Letter from W. R. Cartwright (Vepco) to U.S. Nuclear Regulatory Commission, Serial No. 88-603, September 30, 1988.
14. C. G. Poncelet and A. M. Christie, *Xenon-Induced Spatial Instabilities in Large PWRs*, WCAP-3680-20 (EURAEC-1974), 1968.
15. F. B. Skogen and A. F. McFarlane, *Control Procedures for Xenon-Induced X-Y Instabilities in Large PWRs*, WCAP-3680-21 (EURAEC-2111), 1969.
16. F. B. Skogen and A. F. McFarlane, *Xenon-Induced Spatial Instabilities in Three-Dimensions*, WCAP-3680-22 (EURAEC-2116), 1969.
17. J. C. Lee, et al., *Axial Xenon Transient Tests at the Rochester Gas and Electric Reactor*, WCAP-7964, 1971.

18. R. F. Barry, et al., *The PANDA Code*, WCAP-7048-P-A (proprietary), 1975, and WCAP-7757-A (nonproprietary), 1975.

19. R. F. Barry, *LEOPARD - A Spectrum-Dependent Non-Spatial Depletion Code for the IBM-7094*, WCAP-3269-26, 1963.

20. T. R. England, *CINDER - A One-Point Depletion and Fission Product Program*, WAPD-TM-334, 1962.

21. M. H. Davis, et al., *Safety-Related Research and Development for Westinghouse Pressurized Water Reactors, Program Summaries, Fall 1974*, WCAP-8485, 1975.

22. R. E. MacFarlane, et al., *Description of the CELL-2 Fast and Thermal Cross Section Libraries,* Part II, Chapter 2, ARMP-02, EPRI-NP-4574, (October 1987).

23. G. R. Poetschat, et al., *EPRI-PRESS, Volume 2: User's Manual,* Part II, Chapter 5, ARMP-02, EPRI NP-4574, (August 1986).

24. R. B. Fancher, et al., *Escore—the EPRI Steady-State Core Reload Evaluator Code: General Description*, EPRI-NP-5100, (February 1987).

25. *Scale: A Modular Code System for Performing Standardized Computer Analyses for Licensing Evaluation*, ORNL-NUREG-CSD-VI-R3, (December 1984).

26. *Keno V.a—An Improved Monte Carlo Criticality Program with Supergrouping,* Oak Ridge National Laboratory, ORNL-NUREG-CSD-2-VI-R2, (December 1984).

27. *The PDQ Two Zone Model,* VEP-NAF-1, R. A. Hall, July 1990.

28. EPRI-NP-4492-CCMP, *ESCORE: The EPRI Steady-State Core Reload Evaluator Code,* dated August 1986.

29. L. E. Strawbridge and R. F. Barry, "Criticality Calculations for Uniform Water-Moderated Lattices," *Nuclear Science and Engineering*, Vol. 23, 1965.

30. R. J. Nodvik, *Saxton Core 2, Fuel Performance Evaluation, Part II,* WCAP-3385-56, 1970.

31. R. D. Leamer, et al., *PUO_2-UO_2 Fueled Critical Experiments*, WCAP-3726-1, 1967.

32. *Westinghouse Reload Safety Evaluation Methodology*, WCAP-9272.

33. Letters from B. C. Buckley and L. B. Engle (U.S. NRC) to W. L. Stewart (Virginia Electric and Power Company), *Surry, Units 1 and 2, and North Anna, Units 1 and 2 - Removal of 45,000 MWD/MTU Batch Average Burnup Restriction (TAC Nos. M87767, M87768, M87812, and M87813)*, December 14, 1993 and April 20, 1994.

34. *Relaxed Power Distribution Control Methodology and Associated Fq Surveillance Technical Specifications*, VEP-NE-1-Rev. 0.1-A, August 2003.

35. Letter from W. L. Stewart (Vepco) to H. R. Denton (NRC), Serial No. 450, August 20, 1982.

36. *Qualification of the Studsvik Core Management System Reactor Physics Methods for Application to North Anna and Surry Power Stations,* DOM-NAF-1-Rev. 0.0-P-A (June 2003).

37. S. L. Davidson, et al., *Assessment of Clad Flattening and Densification Power Spike Factor Elimination in Westinghouse Nuclear Fuel,* WCAP-13589-A, (Proprietary) March 1995.

38. Letter from A. C. Thadani (USNRC) to Mr. C. R. Lehmann (ESCORE Users Group Chairman), *Acceptance for Referencing of Licensing Topical Report,* EPRI-NP-5100, *ESCORE—The EPRI Steady-State Core Reload Evaluator Code: General Description,* dated May 23, 1990.

39. *Westinghouse Spent Fuel Rack Criticality Analysis Methodology,* WCAP-14416-NP-A, Rev. 1, 1996.

40. Letter from L. N. Hartz (Virginia Electric and Power Company) to USNRC, Serial No. 00-491, September 27, 2000.

41. Letter from Stephen Monarque (USNRC) to D. A. Christian (Virginia Electric and Power Company), *North Anna Power Station, Units 1 and 2 - Issuance of Amendments re: Technical Specifications Changes to Increase Fuel Enrichment and Spent Fuel Pool Soluble Boron and Fuel Burnup Credit (TAC Nos. MB0197 and MB0198),* June 15, 2001.

42. D. Knott, B. H. Forssen, CASMO-4, *A Fuel Assembly Burnup Program, Methodology,* Studsvik of America, STUDSVIK/SOA-95/2 Revision 0, September 1995.

43. T. Bahadir, J. Umbarger, M. Edenius, *CMS-LINK User's Manual,* Studsvik of America, SOA-97/04 Revision 2, April 1999.

44. J. T. Cronin, K. S. Smith, D. M. Ver Planck, J. A. Umbarger, M. Edenius, *SIMULATE-3 Methodology,* Studsvik of America, SOA-95/18 Revision 0, October 1995.

Table 4.3-1
REACTOR CORE DESCRIPTION
(FIRST CYCLE)

Active Core	
Equivalent diameter	119.7 in.
Core average active fuel height, first core (hot)	143.7 in.
Height-to-diameter ratio	1.20
Total cross-section area	78.14 ft^2
H_2O/U molecular ratio, lattice (cold)	2.41
Reflector Thickness and Composition	
Top - water plus steel	10 in.
Bottom - water plus steel	10 in.
Side - water plus steel	15 in.
Fuel Assemblies	
Number	157
Rod array	17 x 17
Rods per assembly	264
Rod pitch	0.496 in.
Overall transverse dimensions	8.426 in. x 8.426 in.
Fuel weight (as UO_2)	181,205 lb
Zircaloy weight	38,230 lb
Number of grids per assembly	8-R type
Composition of grids	Inconel 718
Weight of grids (effective in core)	1885 lb
Number of guide thimbles per assembly	24
Composition of guide thimbles	Zircaloy-4
Diameter of guide thimbles (upper part)	0.450 in. i.d. x 0.482 in. o.d.
Diameter of guide thimbles (lower part)	0.397 in. i.d. x 0.429 in. o.d.
Diameter of instrument guide thimbles	0.450 in. i.d. x 0.482 in. o.d.
Fuel Rods	
Number	41,448
Outside diameter	0.374 in.
Diameter gap	0.0065 in.
Clad thickness	0.0225 in.
Clad material	Zircaloy-4
Fuel Pellets	
Material	UO_2 sintered
Density (% of theoretical)	95

Table 4.3-1 (continued)
REACTOR CORE DESCRIPTION
(FIRST CYCLE)

Fuel Pellets (continued)	
Fuel enrichments, wt%	
Region 1	2.10
Region 2	2.60
Region 3	3.10
Diameter	0.3225 in.
Length	0.530 in.
Mass of UO_2 per ft of fuel rod	0.364 lb
Rod Cluster Control Assemblies	
Neutron absorber	Ag-In-Cd
Composition	80%, 15%, 5%
Diameter	0.341 in.
Density	0.367 lb/in^3
Cladding material	SS 304, cold-worked
Clad thickness	0.0185 in.
Number of clusters	
Full-length	48
Part-length	5[a]
Number of absorber rods per cluster	24
Full-length assembly weight (dry)	157 lb
Burnable Poison Rods (First Core)	
Number	1072
Material	Borosilicate glass
Outside diameter	0.381 in.
Inner tube, o.d.	0.1815 in.
Clad material	Stainless steel
Inner tube material	Stainless steel
Boron loading (wt% B_2O_3 in glass rod)	12.5
Weight of boron - 10 per ft of rod	0.000419 lb/ft
Initial reactivity worth ($\Delta\rho$)	7.0% (hot), ~5.5% (cold)
Excess Reactivity	
Maximum fuel assembly k_∞ (cold, clean, unborated water)	<1.6
Maximum core reactivity (cold, zero power, beginning of cycle)	1.25

a. Part-length control rods have been removed.

Table 4.3-2
NUCLEAR DESIGN PARAMETERS
(FIRST CYCLE)

Core Average Linear Power (kW/ft), Including Densification Effects	5.44
Total Heat Flux Hot Channel	2.32
Nuclear Enthalpy Rise Hot Channel, $F^N_{\Delta H}$	1.55
Reactivity Coefficients	
Doppler coefficient	See Figures 4.3-27 and 4.3-28
Moderator temperature coefficient at operating conditions[a]	0 to -40 pcm/°F
Boron coefficient in primary coolant[a]	-16 to -8 pcm/ppm
Rodded moderator density coefficient at operating conditions	$\leq +0.43 \times 10^5$ pcm/gm/cc
Delayed Neutron Fraction and Lifetime	
β_{eff} beginning of life, (end of life)	0.0075, (0.0044)
λ^*, beginning of life, (end of life)	19.4 (18.1) μsec
Control Rod Worths	
Rod requirements	See Table 4.3-3
Maximum bank worth	<2300 pcm
Maximum ejected-rod worth	See Chapter 15
Boron Concentrations	
Refueling	2000
$k_{eff} \leq 0.95$, cold, rod cluster control assemblies in	1271
Zero power, $k_{eff} = 0.99$, cold rod cluster control assemblies out	1455
Zero power, $k_{eff} = 0.99$, hot, rod cluster control assemblies out	1430
Full power, no xenon, $k_{eff} = 1.0$, hot, rod cluster control assemblies out	1198
Full power, equilibrium xenon, $k_{eff} = 1.0$, hot, rod cluster control assemblies out	905
Reduction with fuel burnup	
First cycle, ppm/GWd/MTU[b]	See Figure 4.3-3
Reload cycle, ppm/GWd/MTU	100

a. 1 pcm = 1 percent millirho = 1×10^{-5} $\Delta\rho$, where $\Delta\rho$ is calculated from two statepoint values of k_{eff} by $\ln(k_x/k_1)$.

b. Gigawatt day (GWd) = 1000 megawatt days (1000 MWd).

Table 4.3-3
REACTIVITY REQUIREMENT FOR ROD CLUSTER CONTROL ASSEMBLIES

Reactivity Effects (%)	Beginning of Life (First Cycle)	End of Life (First Cycle)	End of Life (Equilibrium Cycle) (Typical)
1. Control requirements			
Fuel temperature (Doppler),% Δρ	1.30	1.20	1.30
Moderator temperature,% Δρ	0.5	1.17	1.25
Void,% Δρ	0.05	0.05	0.05
Redistribution,% Δρ	0.50	0.85	0.85
Rod insertion allowance,% Δρ	0.50	0.50	0.50
2. Total Control, % Δρ	2.85	3.77	3.95
3. Estimated rod cluster control assembly worth (48 rods)			
All assemblies inserted,% Δρ	9.88	9.57	8.50
All but one (highest worth) assemblies inserted,% Δρ	7.85	7.81	6.64
4. Estimated rod cluster control assembly credit with 10% adjustment to accommodate uncertainties,% Δρ	7.06	7.03	5.97
5. Shutdown margin available (4-2),% Δρ	4.21	3.26	2.02[a]

a. The design-basis minimum shutdown is 1.77%.

Table 4.3-4
AXIAL STABILITY INDEX, PWR CORE WITH A 12-FT HEIGHT

Burnup (MWd/T)	F_Z	C_B (ppm)	Stability Index (hr^{-1}) Exp.	Calc.
1550	1.34	1065	-0.041	-0.032
7700	1.27	700	-0.014	-0.006
		Difference:	+0.027	+0.026

Table 4.3-5
TYPICAL FIRST CORE NEUTRON FLUX LEVELS (N/CM^2-SEC) AT FULL POWER

	E >1.0 MeV	5.53 KeV <E ≤1.0 MeV	.625 eV ≤E 5.53 KeV	E <.625 eV $(nv)_O$
Core center	6.51×10^{13}	1.12×10^{14}	8.50×10^{13}	3.00×10^{13}
Core outer radius at midheight	3.23×10^{13}	5.74×10^{13}	4.63×10^{13}	8.60×10^{12}
Core top, on axis	1.53×10^{13}	2.42×10^{13}	2.10×10^{13}	1.63×10^{13}
Core bottom, on axis	2.36×10^{13}	3.94×10^{13}	3.50×10^{13}	1.46×10^{13}
Pressure vessel inner wall, azimuthal peak, core midheight	2.77×10^{10}	5.75×10^{10}	6.03×10^{10}	8.38×10^{10}

Table 4.3-6
SUMMARY OF PDQ TWO-ZONE/NOMAD
NUCLEAR RELIABILITY FACTORS (NRF)

Parameter	VEP-FRD-45A NRF
Doppler Temperature Coefficient	× 1.10
Individual Integral Bank Worth	× 1.10
Cumulative Integral Bank Worth	× 1.10
Differential Bank Worth	2 pcm/step
Critical Boron Concentration	50 ppm
Differential Boron Worth	× 1.05
Moderator Temperature Coefficient	3 pcm/°F
$F_{\Delta H}$	× 1.05
F_Q	× 1.075

Table 4.3-7
NOMAD ECP RESULTS

Maximum Overprediction (pcm)	Maximum Underprediction (pcm)	Mean (pcm)	Standard Deviation (pcm)
+336	-74	+134	129

Note: Includes 14 ECPs: 4 N1C9, 6 S2C11, and 4 S2C13.

Table 4.3-8
NOMAD STARTUP PHYSICS TESTING RESULTS

Parameter	Maximum Overprediction	Maximum Underprediction	Mean	Standard Deviation
Endpoints (ppm)	-36	+17	-21	17
Boron Worth (%)	+1.38	-4.13	-2.17	2.32
ITC (pcm/°F)	-1.45	+0.52	-0.15	0.60
IRW (rod swap) (%)	+11.36	-7.84	2.99	5.14
IRW (dilution) (%)	+7.12	-6.73	-0.58	4.36

Notes:

1. Boron difference is (M-P).
2. Boron worth difference is (M-P)/M*100%.
3. ITC difference is (M-P).
4. Rod worth difference is (P-M)M*100%.
5. Includes 6 cycles (N1C3, N1C6, N1C9, S2C2, S2C11, and S2C13).

Table 4.3-9
NOMAD FQ AND FZ RESULTS

Parameter	Maximum Overprediction (%)	Maximum Underprediction (%)	Mean (%)	Standard Deviation (%)
F_Z	1.92	-6.73	-2.41	1.96
F_Z (HFP only)	1.71	-5.79	-2.44	1.89
F_Q	22.75(4)	-7.75	0.44(4)	6.67(4)
F_Q (HFP only)	1.77	-7.75	-3.02	1.89

Notes:

1. Database includes 2 maps at HZP, 1 map at 30% power, 1 map at 75% power, and 20 maps between 96% and 100% power with D-bank at various rod insertions. Data is for S2C2 (5 maps), S2C13 (5 maps), N1C3 (6 maps), N1C6 (4 maps), and N1C11 (4 maps).
2. Total database has 134 F_Q and F_Z comparisons at axial points midway between spacer grid positions.
3. HFP only database has a total of 112 F_Q and F_Z comparisons at axial points midway between spacer grid positions.
4. These values reflect the use of a conservative part power multiplier applied to the HFP F_{XY} values used in the calculation of F_Q. The multiplier used is governed by Technical Specification and currently is set to linearly increase with decreasing power from 1.0 at HFP (or higher) to 1.3 at HZP.
5. The calculated 95%/95% one sided uncertainty factors are: F_Q: 6.91% and F_Z: 6.13%.

Table 4.3-10
SUMMARY OF CMS NUCLEAR RELIABILITY FACTORS (NRF)

Parameter	NRF Upper	Lower
Integral Control Rod Bank Worth (Individual banks)	× 1.1	× 0.9
Integral Control Rod Bank Worth (Total of all banks)	× 1.1	× 0.9
Differential Control Rod Bank Worth	× 1.15	× 0.8
Critical Boron Concentration	+ 50 ppm	- 50 ppm
Differential Boron Worth	× 1.05	× 0.95
Isothermal and Moderator Temperature Coefficient	+ 2 pcm/°F	- 2 pcm/°F
Doppler Temperature Coefficient	× 1.10	× 0.90
Doppler Power Coefficient	× 1.10	× 0.90
Effective Delayed Neutron Fraction	× 1.05	× 0.95
Prompt Neutron Lifetime	× 1.05	× 0.95
FDH	× 1.04	N/A
FQ	× 1.04	N/A

Figure 4.3-1
FUEL LOADING ARRANGEMENT

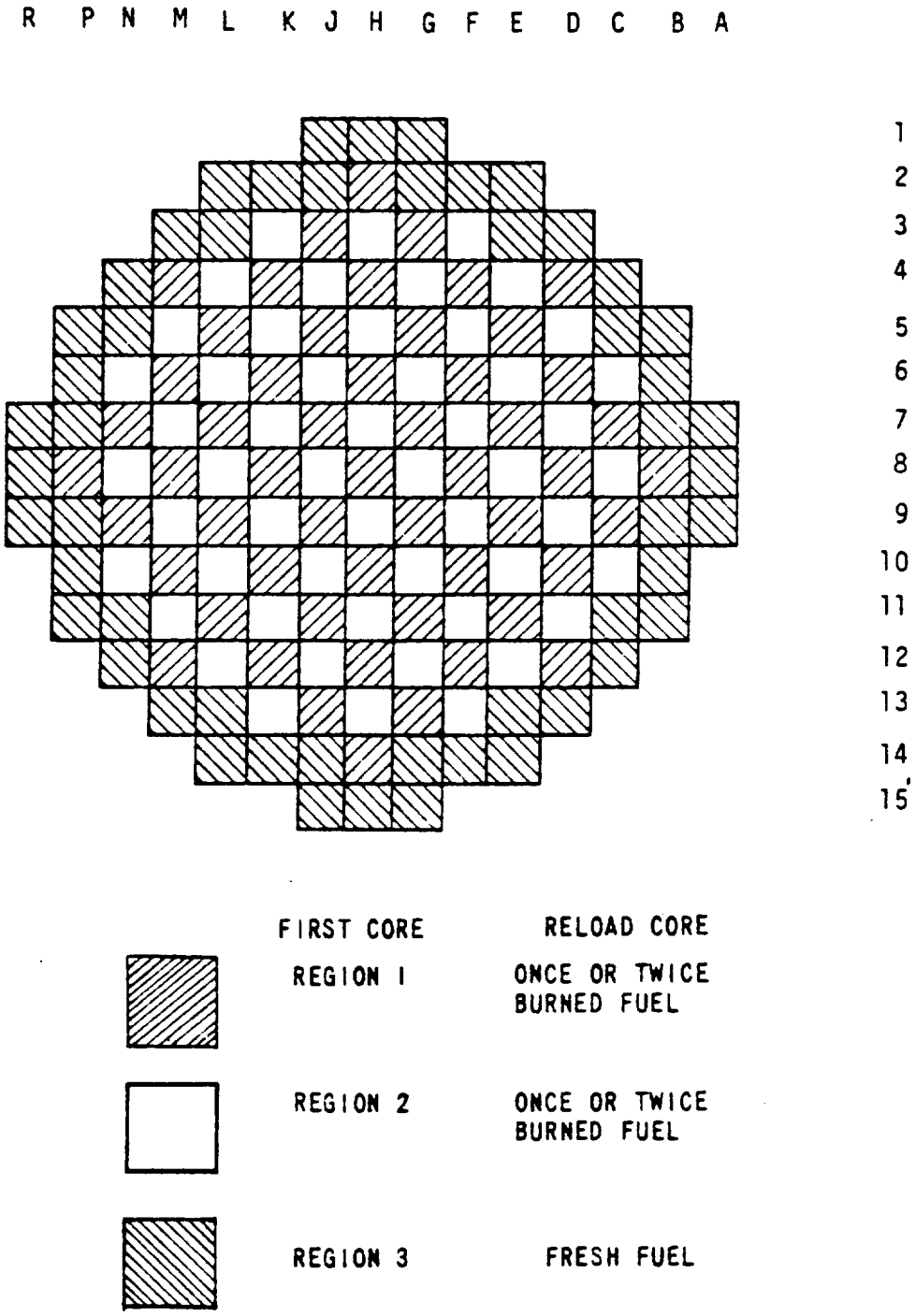

N0403001

Fuel Loading Arrangement

Figure 4.3-2
PRODUCTION AND CONSUMPTION OF HIGHER ISOTOPES

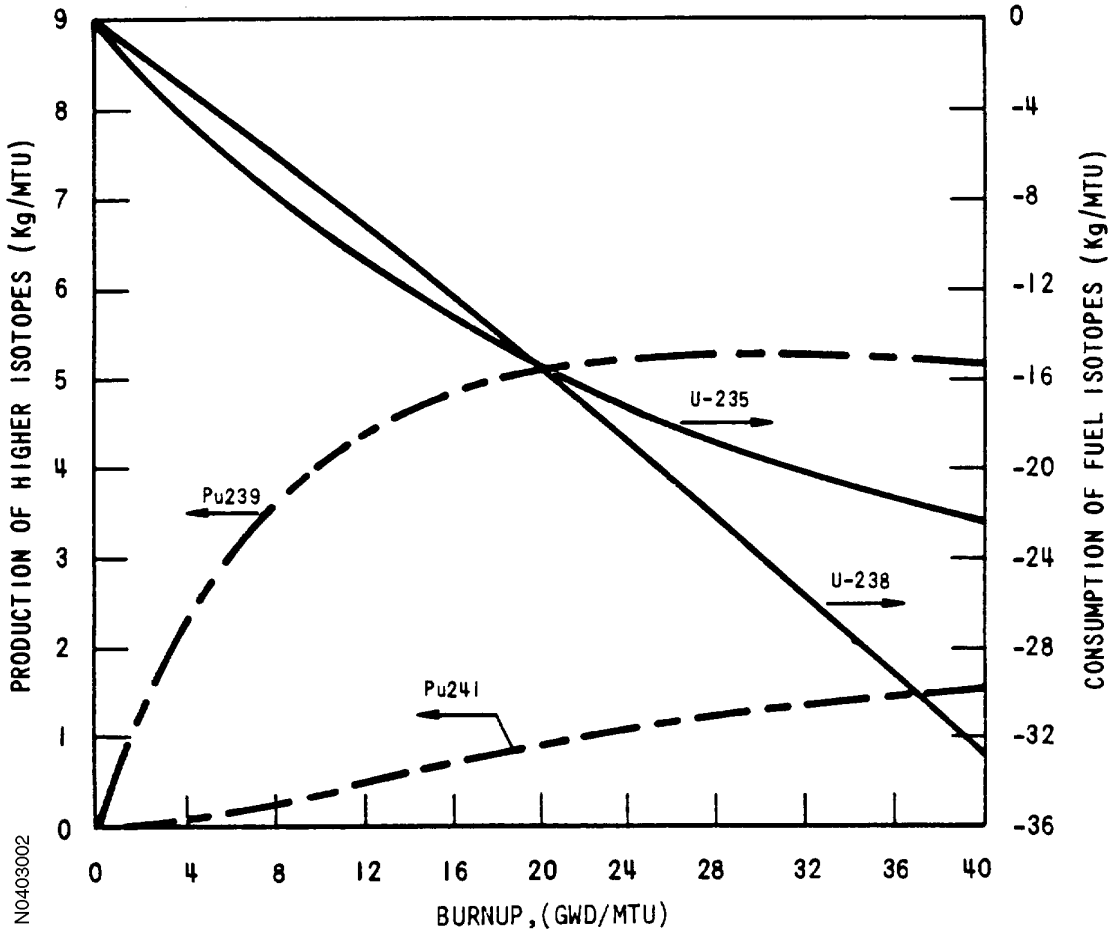

Figure 4.3-3
BORON CONCENTRATION VERSUS FIRST CYCLE BURNUP
WITH AND WITHOUT BURNABLE POISON RODS

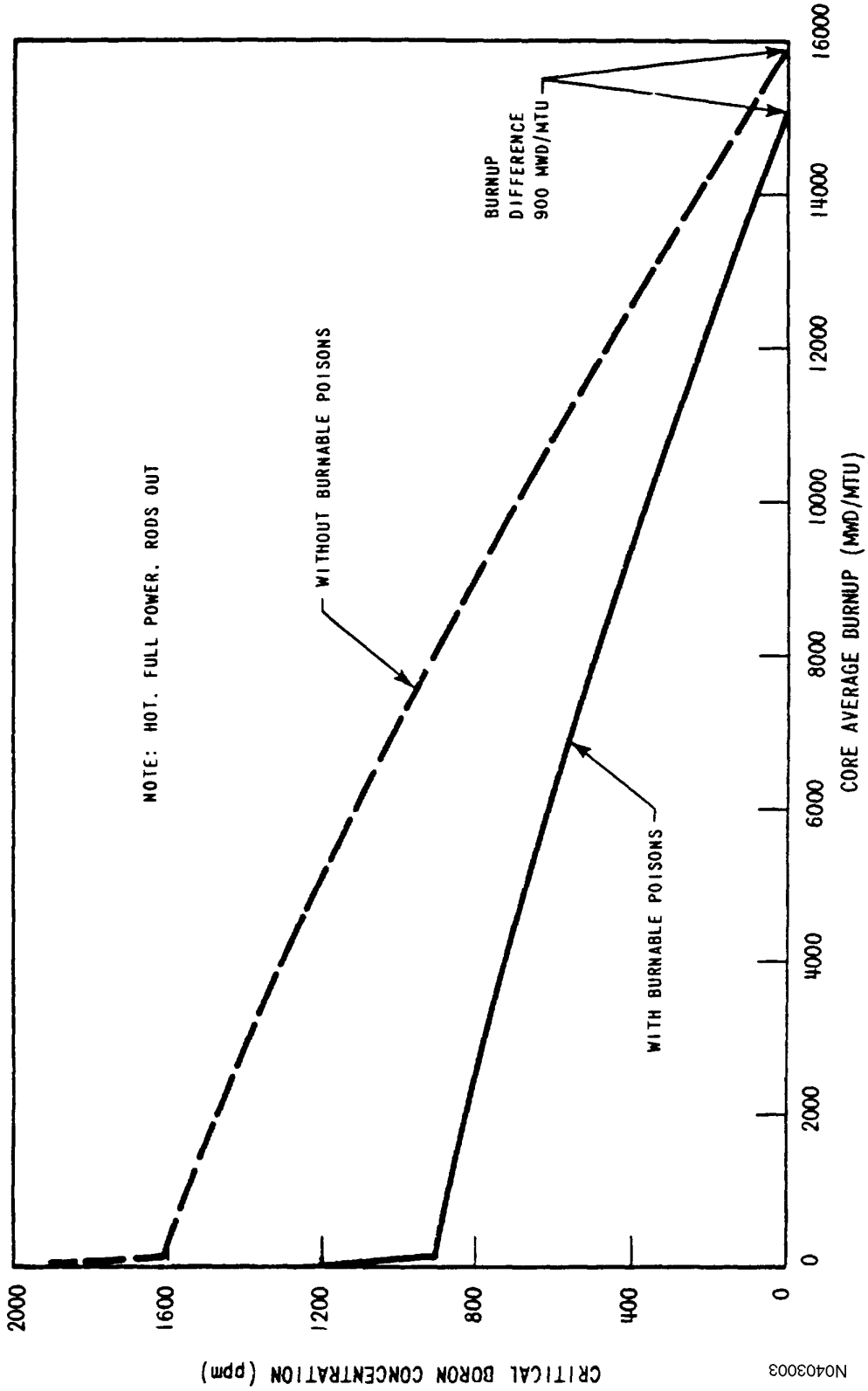

Figure 4.3-4
SAMPLE BURNABLE POISON ROD ARRANGEMENT WITHIN AN ASSEMBLY

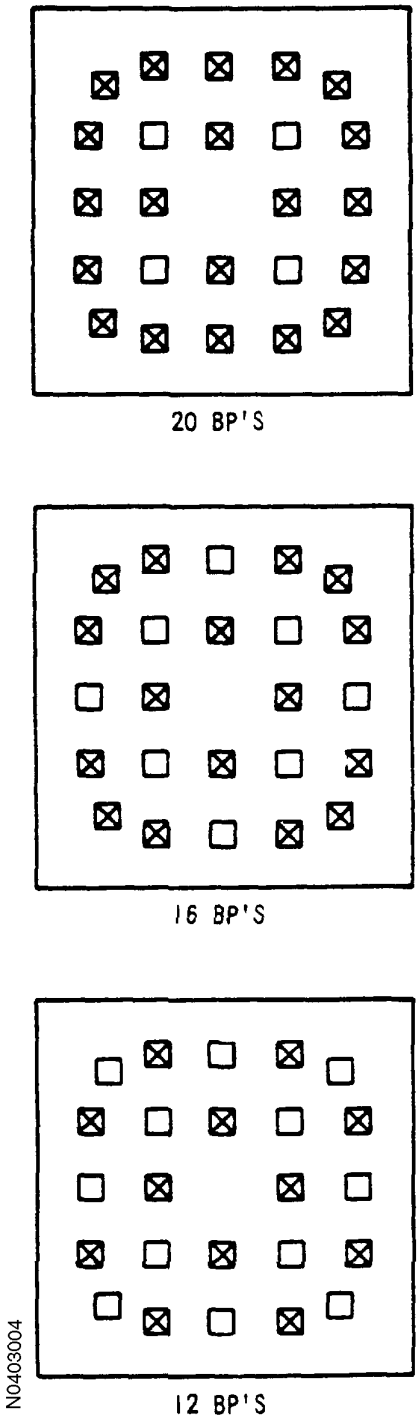

Figure 4.3-5
BURNABLE POISON LOADING PATTERN
UNIT NO. 1 (FIRST CYCLE)

	R	P	N	M	L	K	J	H	G	F	E	D	C	B	A
1															
2							16 P		16						
3					12	16		12 S		16	12				
4					16		16		16		16				
5			12	16		16		20		16		16	12		
6			16		16		16		16		16		16		
7		16		16		16		20		16		16		16	
8			12		20		20		20		20		12		
9		16		16		16		20		16		16		16	
10			16		16		16		16		16		16		
11			12	16		16		20		16		16	12		
12					16		16		16		16				
13					12	16		12 S		16	12				
14							16		16 P						
15															

N0403005

NUMBER INDICATES NUMBER OF BURNABLE POISON RODS
S INDICATES SECONDARY SOURCE RODS
P INDICATES PRIMARY SOURCE RODS

Figure 4.3-6
BURNABLE POISON LOADING PATTERN
UNIT NO. 2 (FIRST CYCLE)

	R	P	N	M	L	K	J	H	G	F	E	D	C	B	A	
1																
2							16 P		16							
3					12	16		12		16	12					
4					16		16	S	16		16					
5			12	16		16		20		16		16	12			
6			16		16		16		16		16		16			
7		16		16		16		20		16		16		16		
8			12		20		20		20		20		12			
9		16		16		16		20		16		16		16		
10			16		16		16		16		16		16			
11			12	16		16		20		16		16	12			
12					16		16	S	16		16					
13					12	16		12		16	12					
14							16		16 P							
15																

N0403006

NUMBER INDICATES NUMBER OF BURNABLE POISON RODS
S INDICATES SECONDARY SOURCE RODS
P INDICATES PRIMARY SOURCE RODS

Figure 4.3-7
NORMALIZED POWER DENSITY DISTRIBUTION NEAR BEGINNING OF LIFE, UNRODDED CORE, HOT FULL POWER, NO XENON

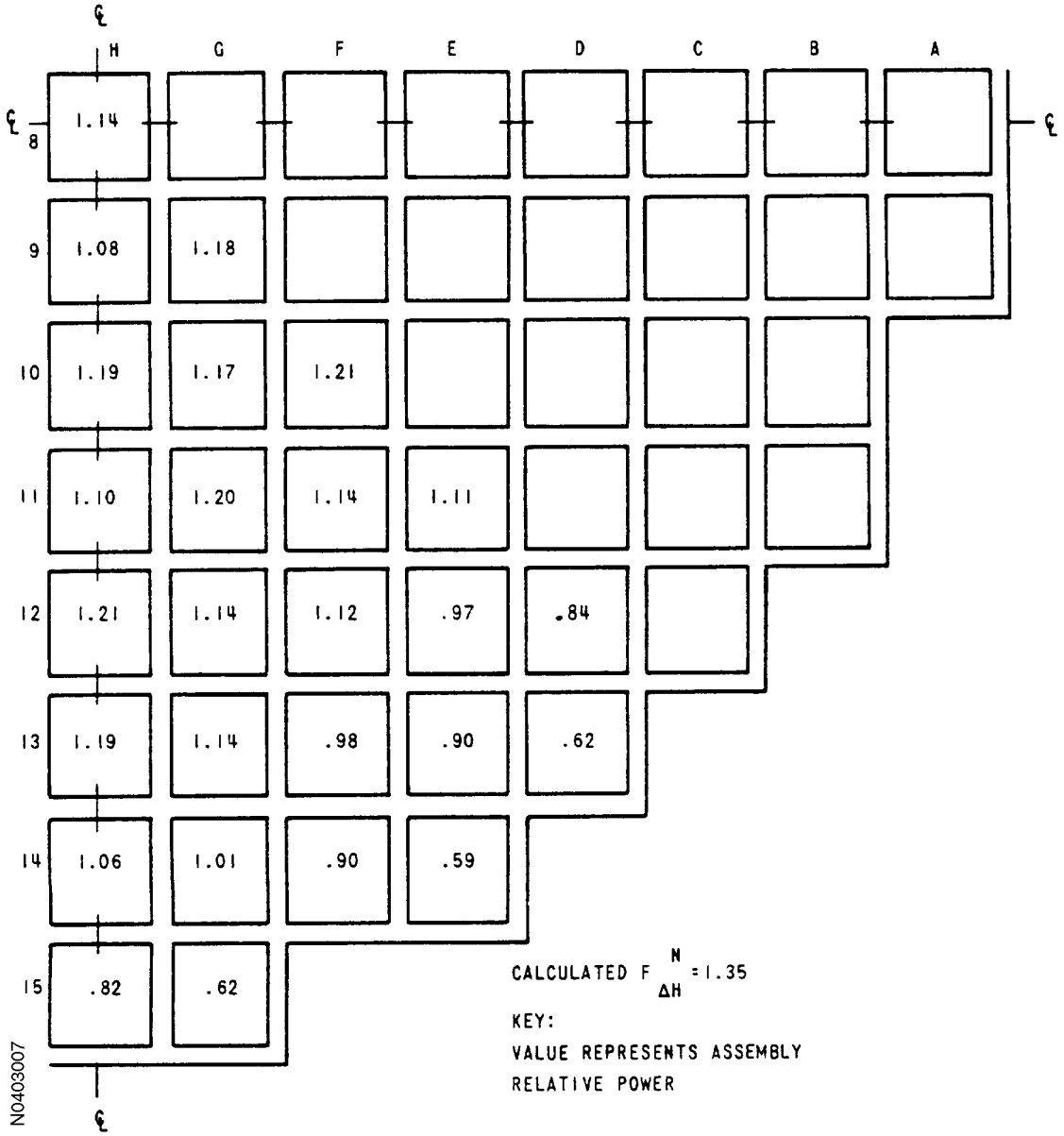

Figure 4.3-8
NORMALIZED POWER DENSITY DISTRIBUTION NEAR BEGINNING OF LIFE, UNRODDED CORE, HOT FULL POWER, EQUILIBRIUM XENON

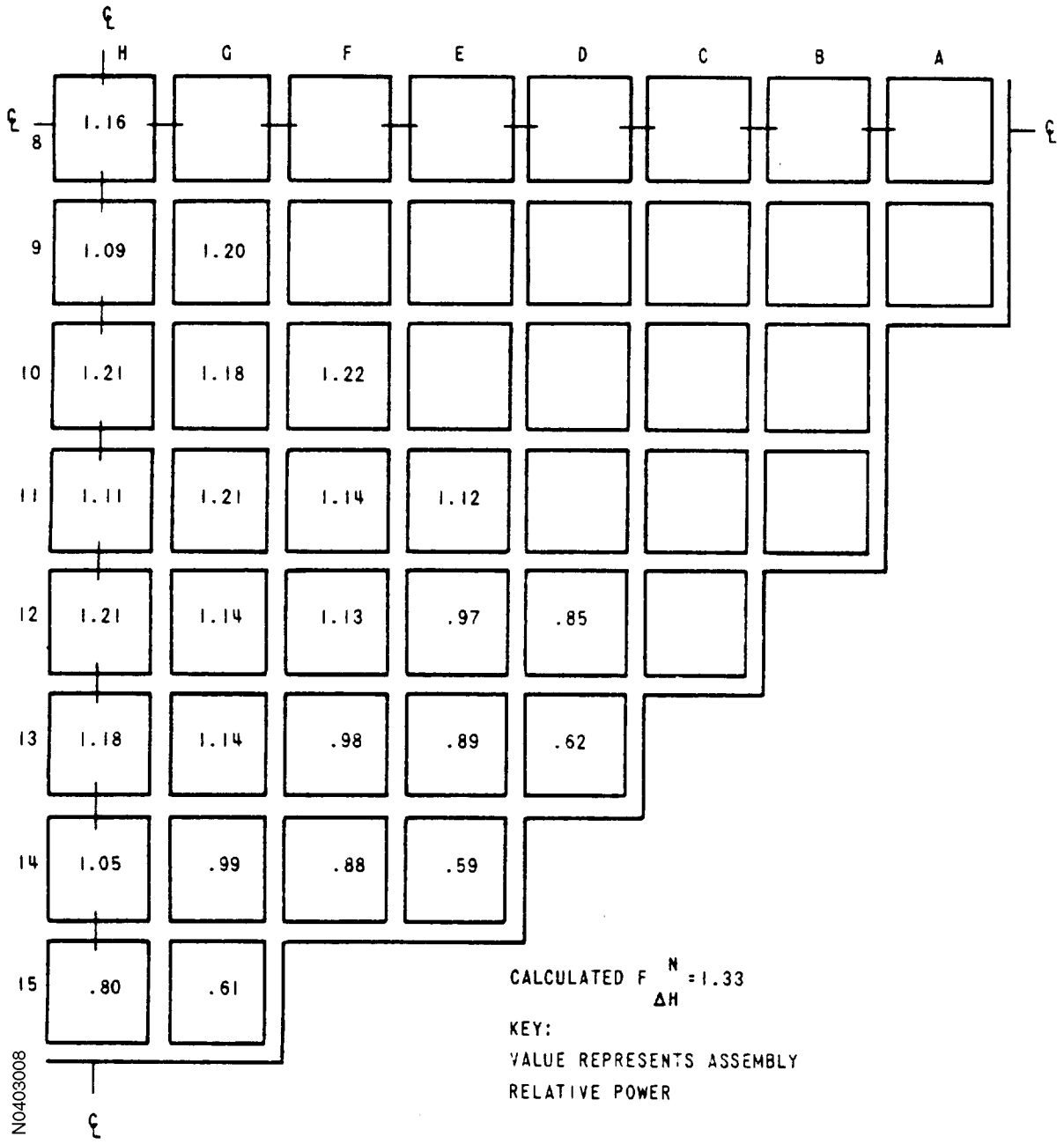

Figure 4.3-9
NORMALIZED POWER DENSITY DISTRIBUTION NEAR BEGINNING OF LIFE, GROUP D 30%, HOT FULL POWER, EQUILIBRIUM XENON

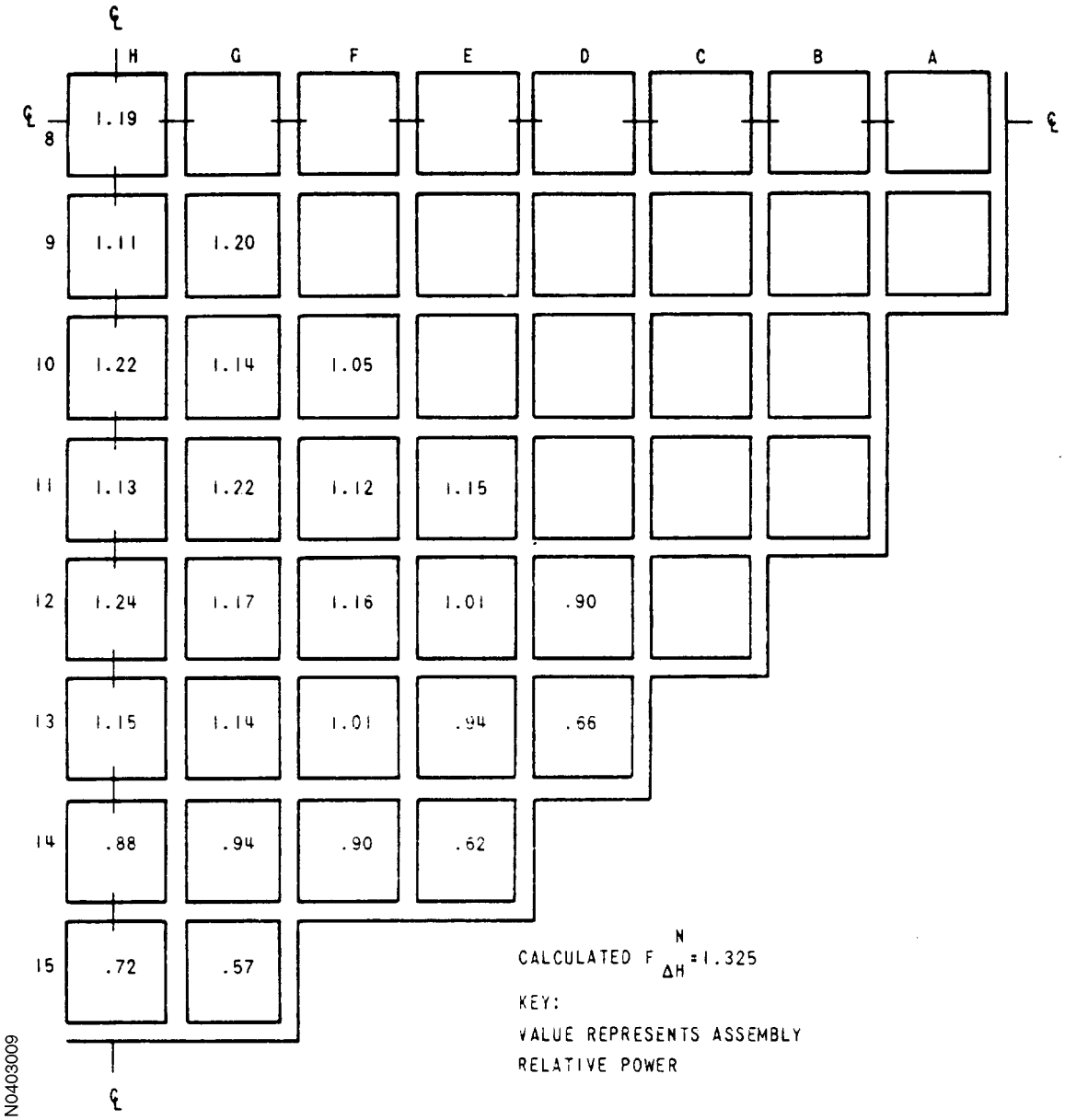

Figure 4.3-10
NORMALIZED POWER DENSITY DISTRIBUTION NEAR MIDDLE OF LIFE, UNRODDED CORE, HOT FULL POWER, EQUILIBRIUM XENON

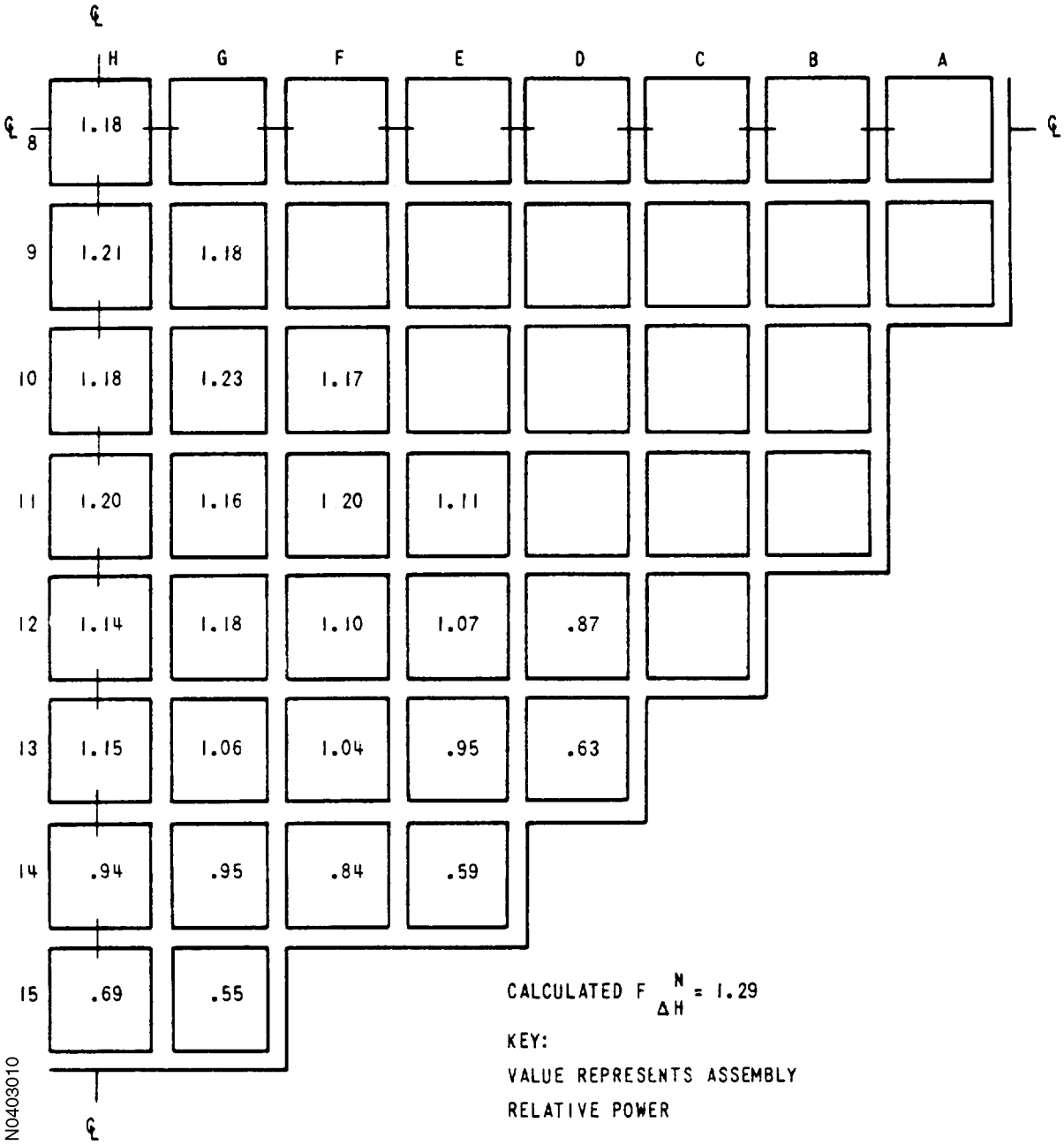

Figure 4.3-11
NORMALIZED POWER DENSITY DISTRIBUTION NEAR END OF LIFE, UNRODDED CORE, HOT FULL POWER, EQUILIBRIUM XENON

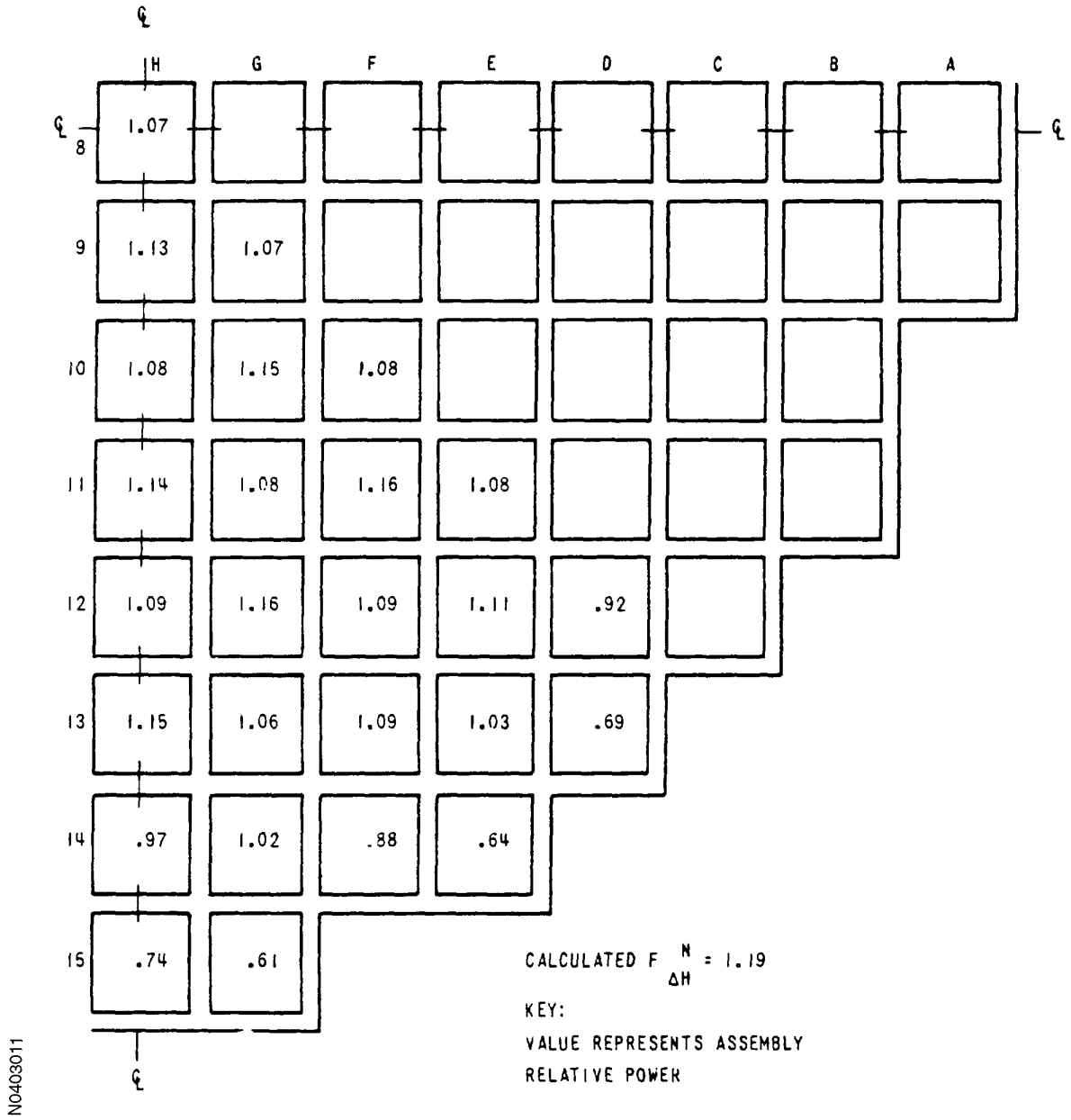

Figure 4.3-12
RODWISE POWER DISTRIBUTION IN A TYPICAL ASSEMBLY
(ASSEMBLY G-9) NEAR BEGINNING OF LIFE, HOT FULL POWER,
EQUILIBRIUM XENON, UNRODDED CORE

1.08																
1.08	1.10															
1.09	1.11	1.15														
1.09	1.13	1.20	X													
1.09	1.15	1.21	1.24	1.24												
1.10	1.17	X	1.25	1.26	X											
1.09	1.15	1.22	1.22	1.23	1.26	1.24										
1.09	1.15	1.22	1.22	1.23	1.27	1.25	1.25									
1.10	1.18	X	1.24	1.26	X	1.27	1.28	X								
1.10	1.16	1.22	1.22	1.24	1.27	1.25	1.26	1.28	1.26							
1.10	1.16	1.22	1.23	1.24	1.27	1.25	1.26	1.28	1.26	1.26						
1.11	1.18	X	1.26	1.27	X	1.28	1.28	X	1.28	1.28	X					
1.11	1.16	1.23	1.26	1.26	1.28	1.25	1.25	1.28	1.26	1.26	1.29	1.27				
1.11	1.15	1.22	X	1.27	1.27	1.24	1.24	1.27	1.25	1.25	1.28	1.28	X			
1.11	1.14	1.17	1.22	1.24	X	1.25	1.25	X	1.25	1.25	X	1.26	1.24	1.19		
1.11	1.12	1.14	1.16	1.18	1.21	1.19	1.20	1.22	1.20	1.20	1.22	1.19	1.18	1.16	1.15	
1.11	1.11	1.12	1.12	1.13	1.14	1.14	1.15	1.16	1.15	1.15	1.15	1.14	1.14	1.13	1.13	1.14

N0403012

Figure 4.3-13
RODWISE POWER DISTRIBUTION IN A TYPICAL ASSEMBLY
(ASSEMBLY G-9) NEAR END OF LIFE, HOT FULL POWER,
EQUILIBRIUM XENON, UNRODDED CORE

1.00																
.99	1.00															
1.00	1.02	1.05														
1.01	1.04	1.09	X													
1.02	1.05	1.11	1.13	1.11												
1.02	1.08	X	1.13	1.13	X											
1.02	1.06	1.10	1.09	1.10	1.12	1.10										
1.02	1.06	1.10	1.09	1.09	1.12	1.10	1.10									
1.03	1.08	X	1.11	1.12	X	1.12	1.12	X								
1.02	1.06	1.10	1.09	1.09	1.12	1.10	1.10	1.12	1.10							
1.02	1.06	1.10	1.09	1.10	1.12	1.10	1.10	1.12	1.10	1.10						
1.02	1.08	X	1.13	1.13	X	1.12	1.12	X	1.12	1.12	X					
1.02	1.05	1.11	1.13	1.11	1.13	1.10	1.10	1.12	1.10	1.10	1.13	1.12				
1.01	1.04	1.09	X	1.13	1.13	1.09	1.09	1.12	1.09	1.09	1.13	1.13	X			
1.00	1.02	1.05	1.09	1.11	X	1.11	1.10	X	1.10	1.11	X	1.11	1.09	1.05		
1.00	1.00	1.02	1.04	1.05	1.08	1.06	1.06	1.08	1.06	1.06	1.08	1.06	1.04	1.02	1.01	
1.00	1.00	1.00	1.01	1.02	1.03	1.03	1.03	1.03	1.03	1.03	1.03	1.02	1.01	1.00	1.00	1.00

N0403013

Figure 4.3-14
TYPICAL AXIAL POWER SHAPES OCCURRING AT START OF LIFE
(See Section 4.1 concerning part length control rods)

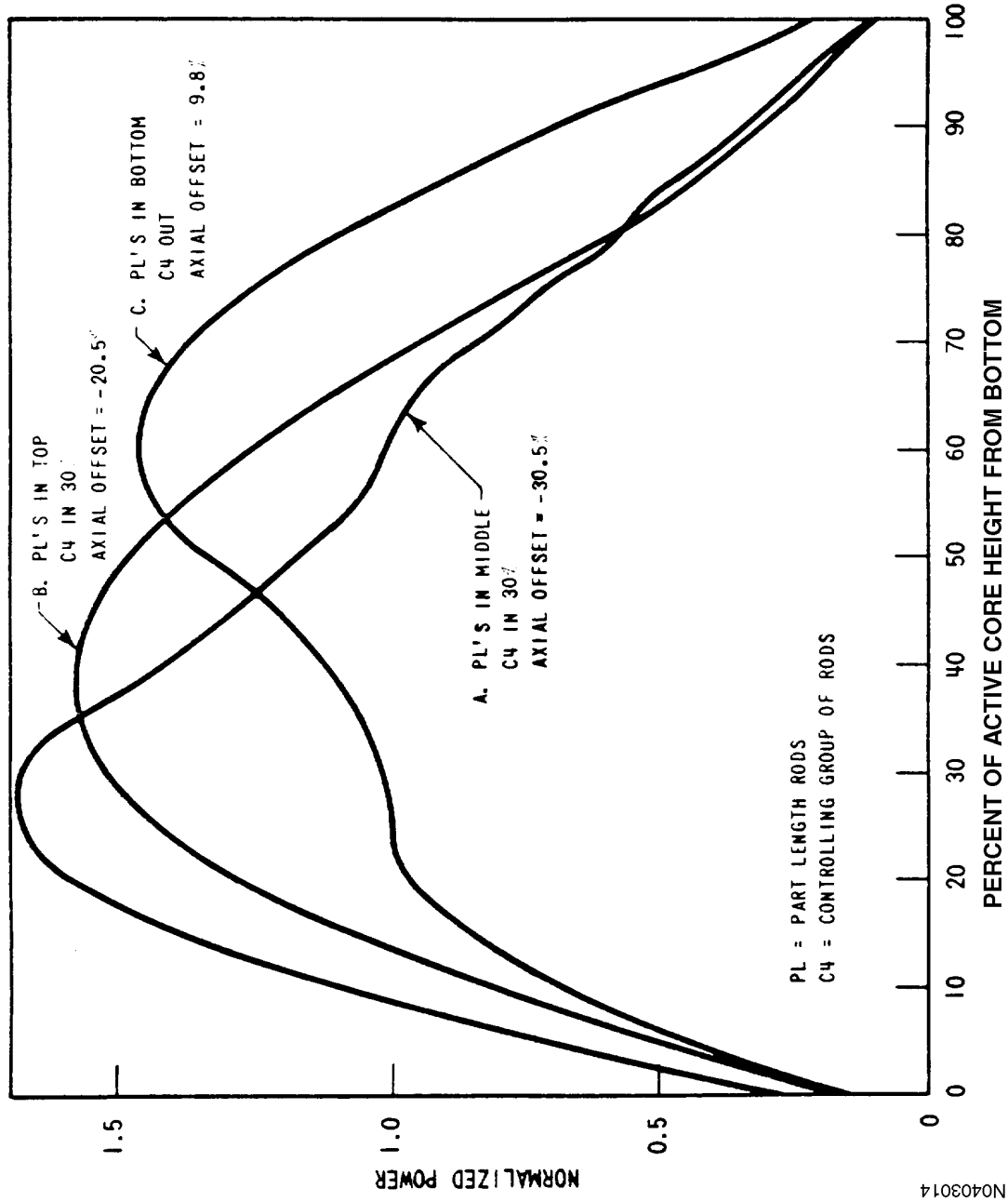

Figure 4.3-15
TYPICAL AXIAL POWER SHAPES OCCURRING AT MIDDLE OF LIFE
(See Section 4.1 concerning part length control rods)

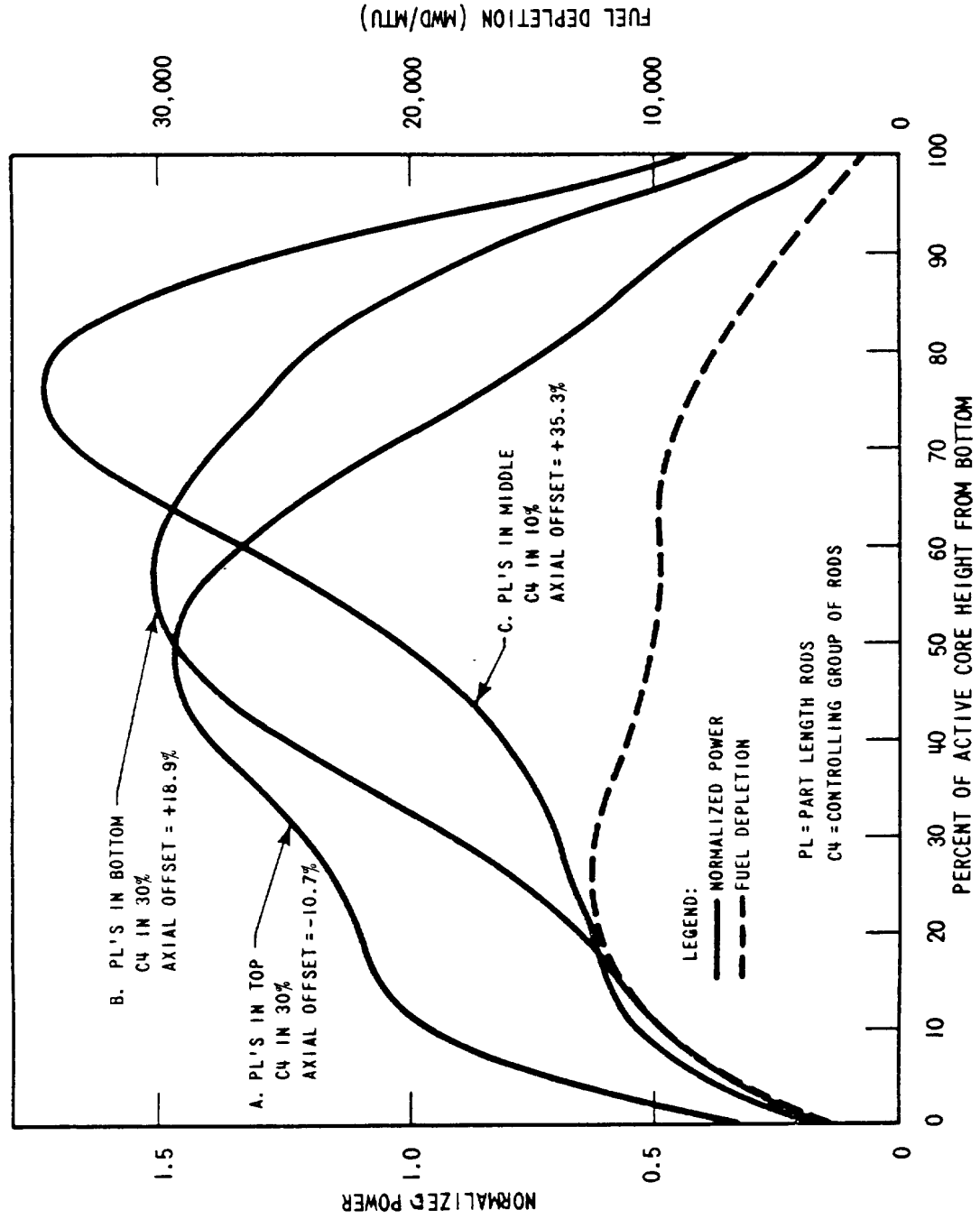

N040301 5

Figure 4.3-16
TYPICAL AXIAL POWER SHAPES OCCURRING AT END OF LIFE
(See Section 4.1 concerning part length control rods)

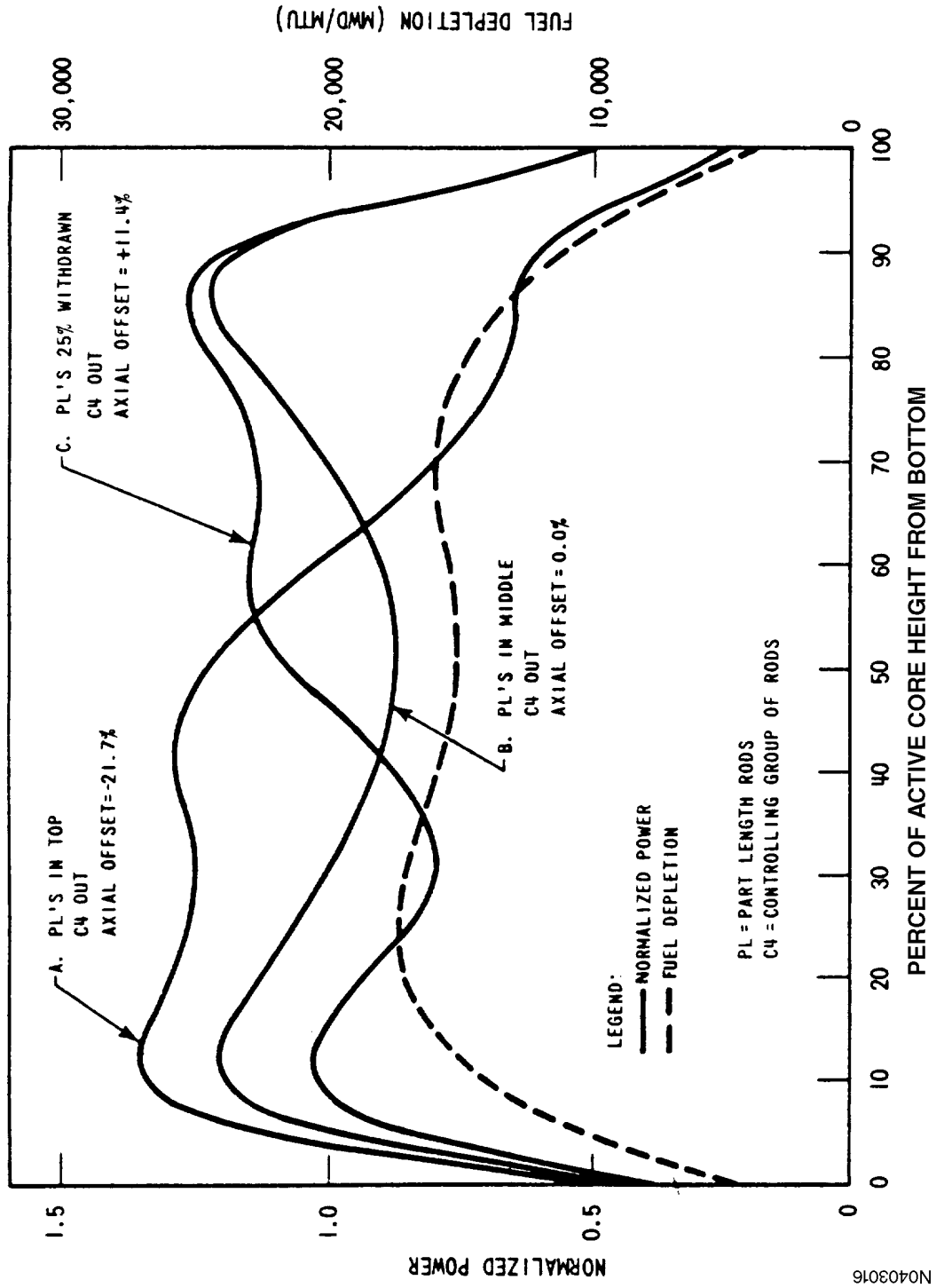

Figure 4.3-17
COMPARISON OF ASSEMBLY AXIAL POWER DISTRIBUTION WITH CORE AVERAGE AXIAL DISTRIBUTION, BANK SLIGHTLY INSERTED PART LENGTH AT MID-PLANE
(See Section 4.1 concerning part length control rods)

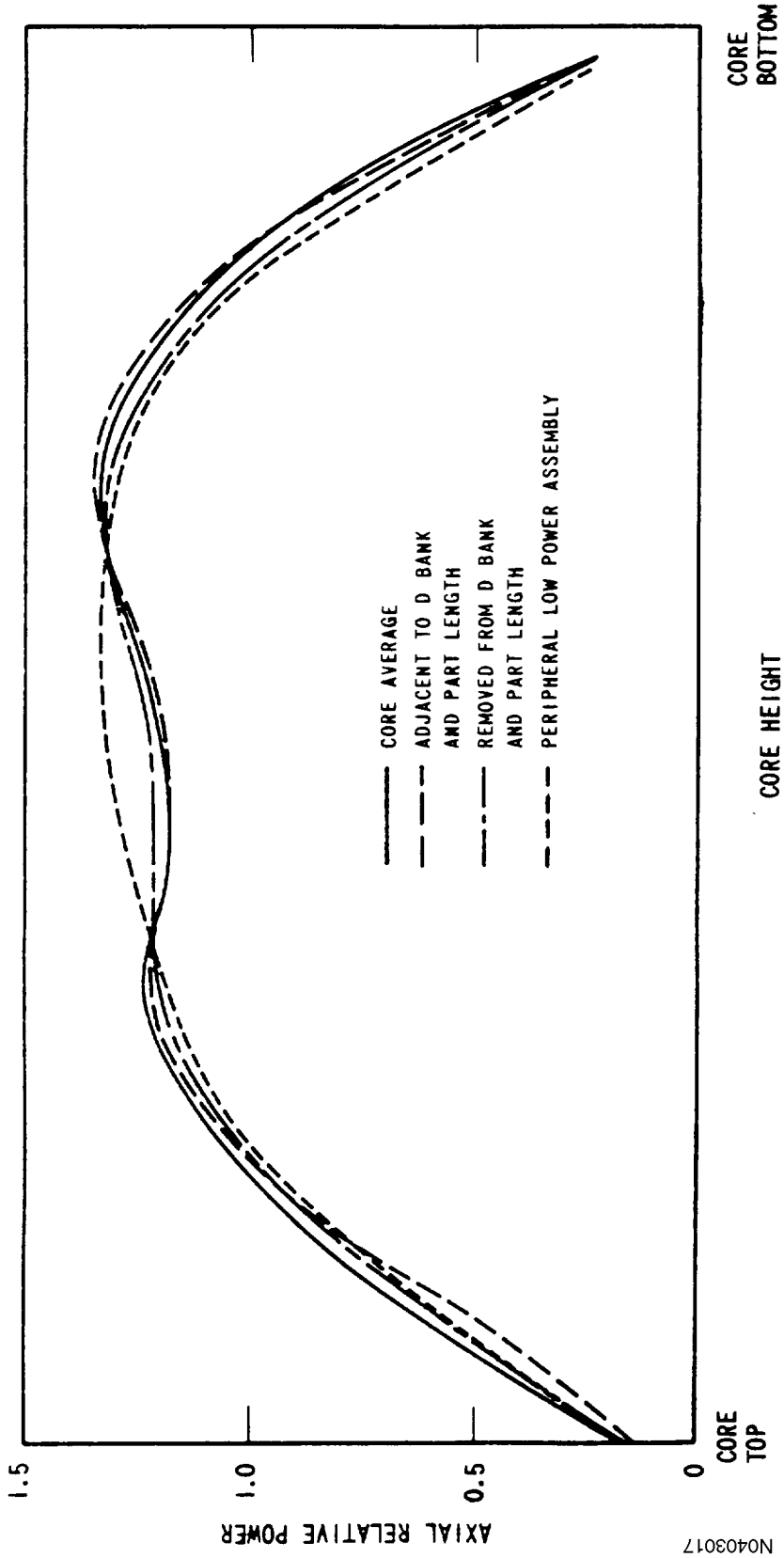

Figure 4.3-18
FLOW CHART FOR DETERMINING THE DENSIFICATION SPIKE FACTOR[a]

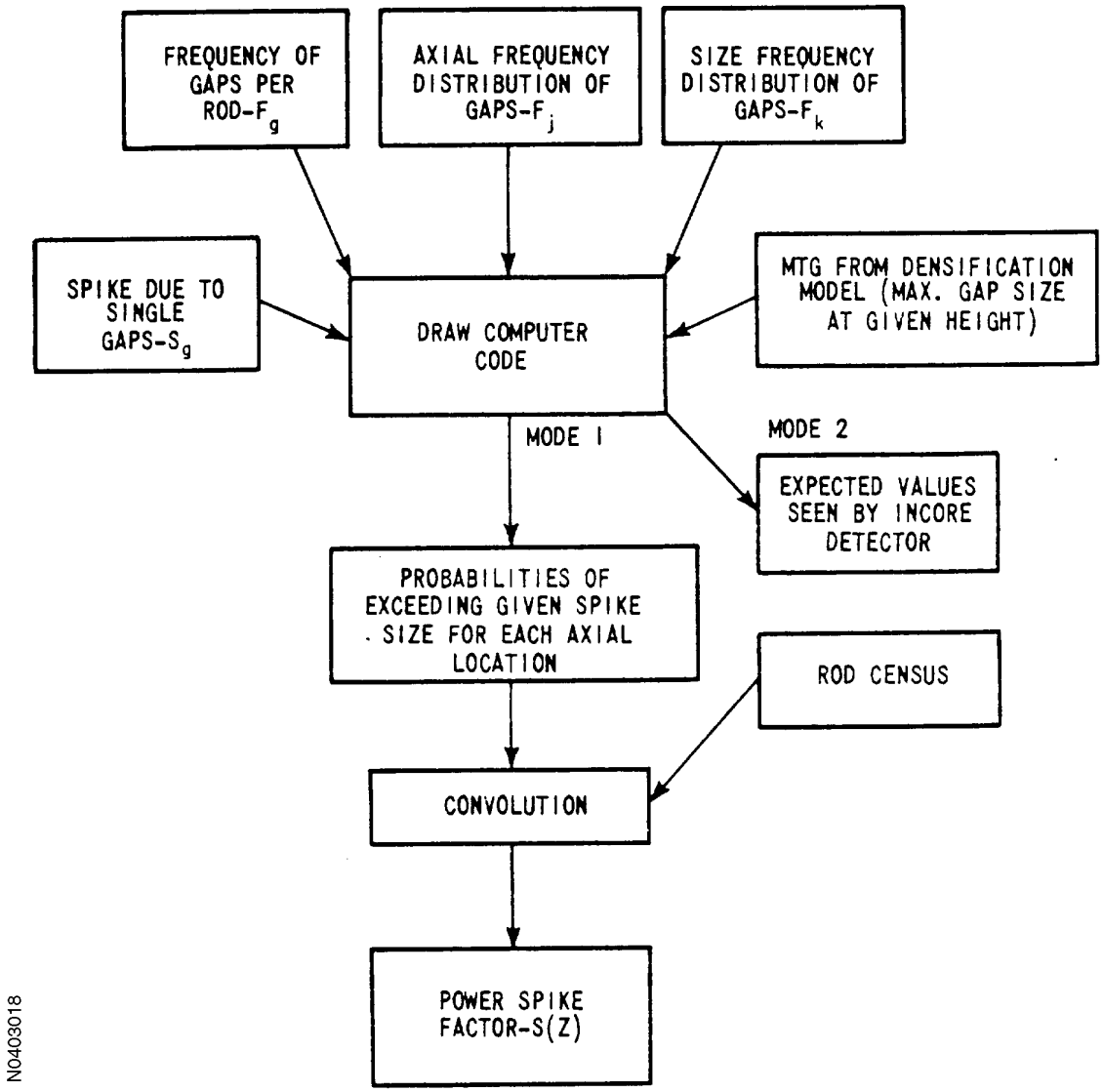

a. Use of the power spike densification factor is no longer required in North Anna nuclear design calculations.

Figure 4.3-19
PREDICTED POWER SPIKE DUE TO SINGLE
NONFLATTENED GAP IN THE ADJACENT FUEL[a]

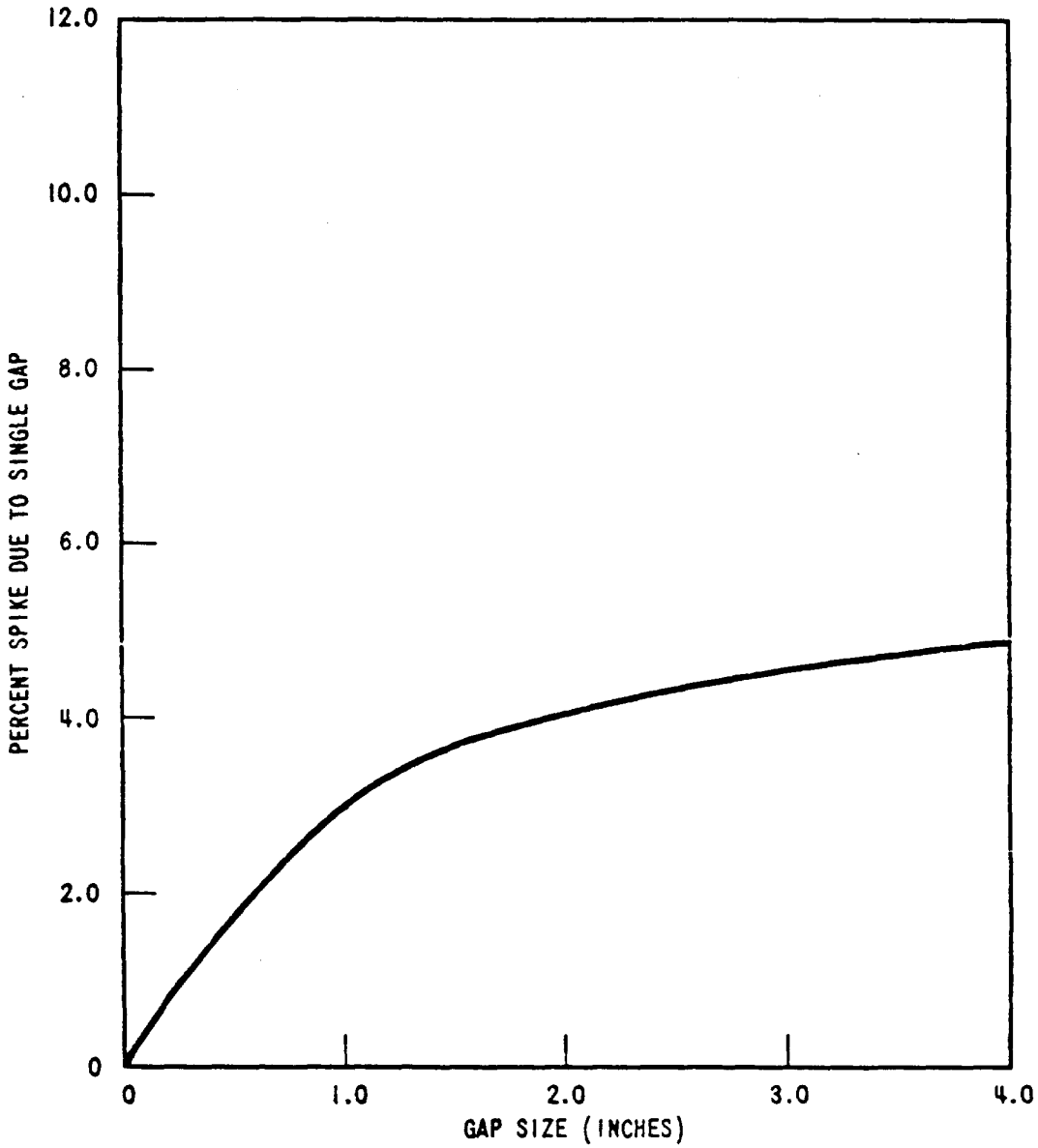

N0403019

a. Use of the power spike densification factor is no longer required in North Anna nuclear design calculations.

Figure 4.3-20
POWER SPIKE FACTOR AS A FUNCTION OF AXIAL POSITION[a]

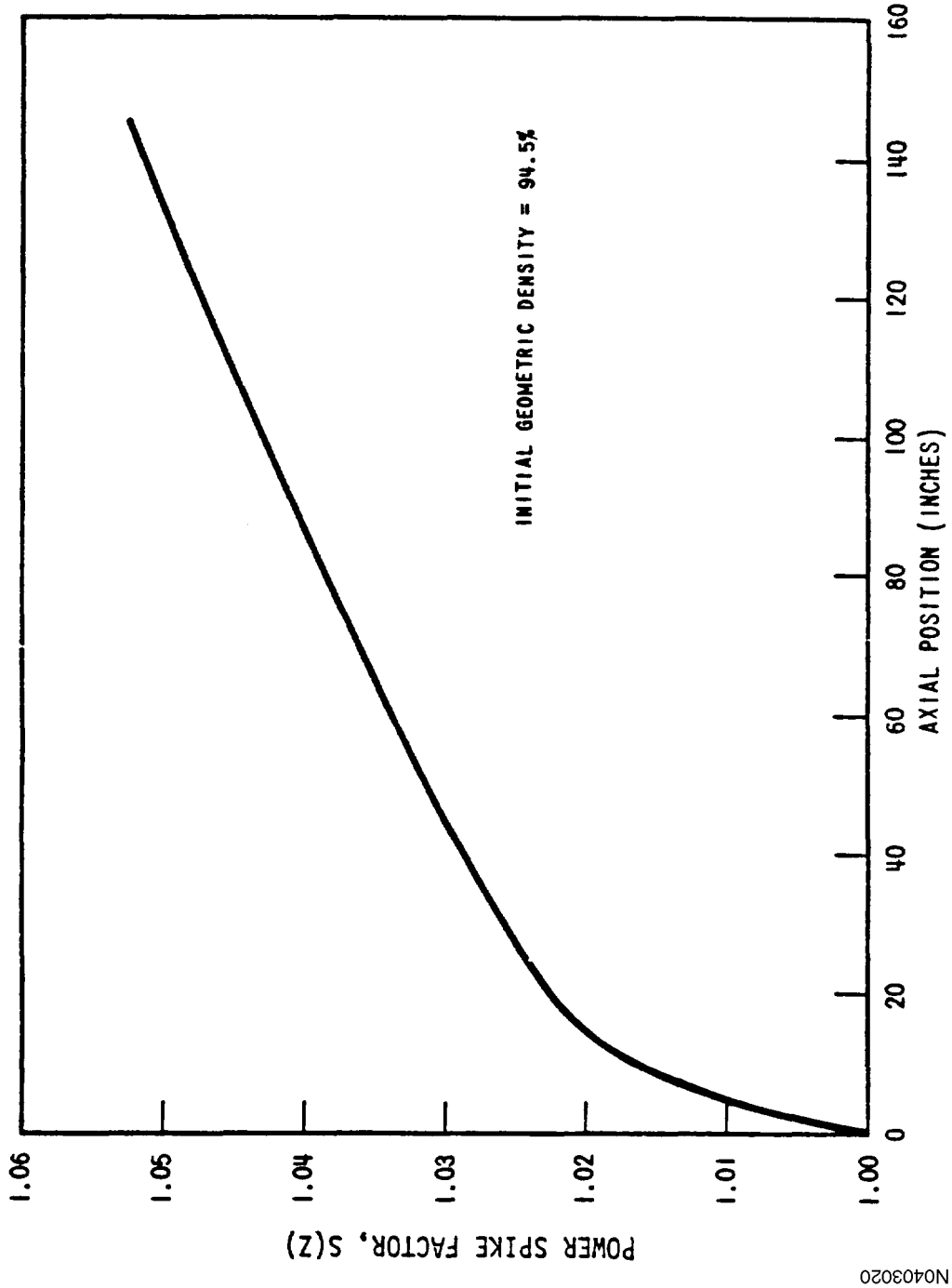

a. Use of the power spike densification factor is no longer required in North Anna nuclear design calculations.

Figure 4.3-21
MAXIMUM F_Q x POWER VERSUS AXIAL HEIGHT DURING NORMAL OPERATION
(For specific F_Q values see the Technical Specifications)

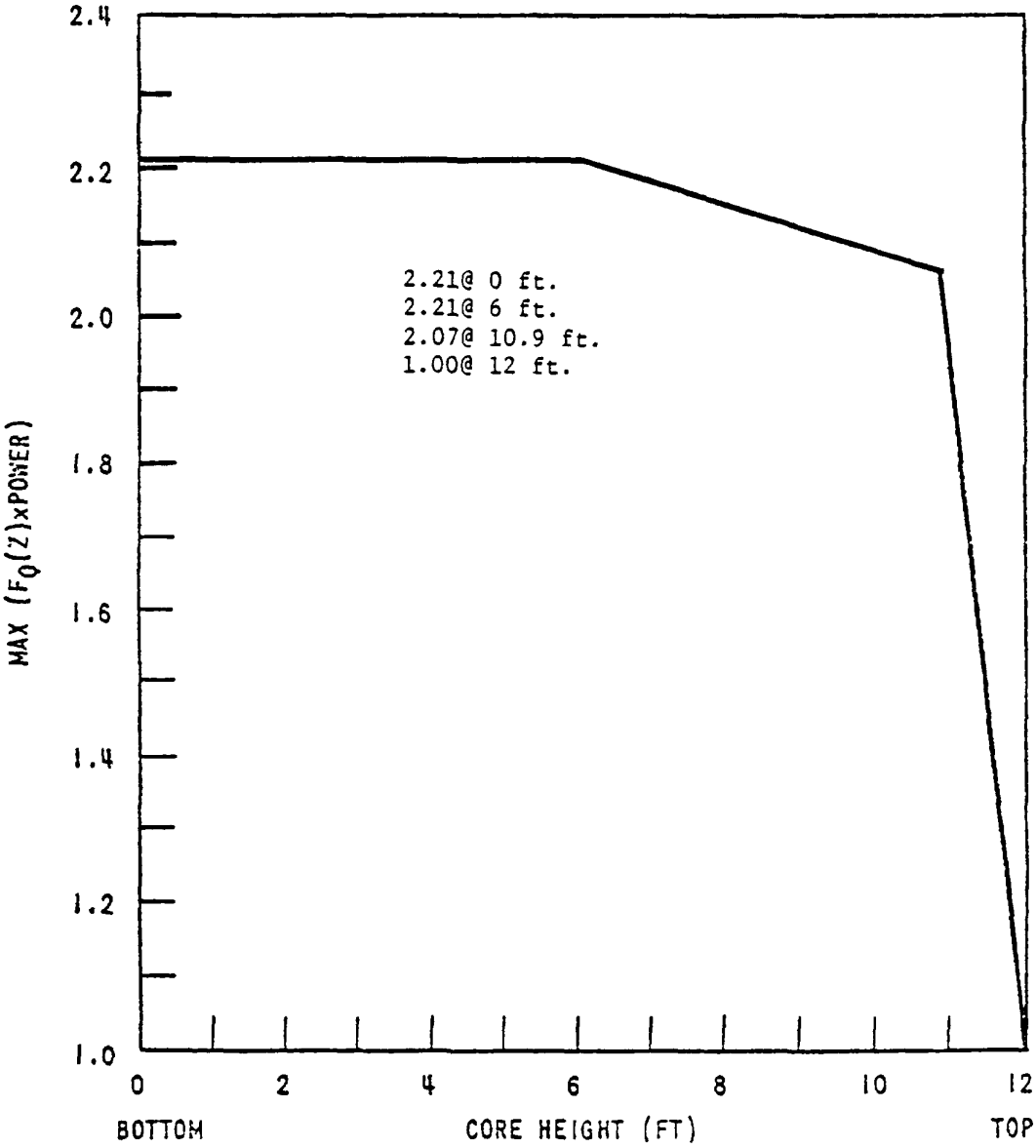

N0403021

(a) For specific F_Q values see the Technical Specifications

Figure 4.3-22
PEAK POWER DURING CONTROL ROD MALFUNCTION OVERPOWER TRANSIENTS

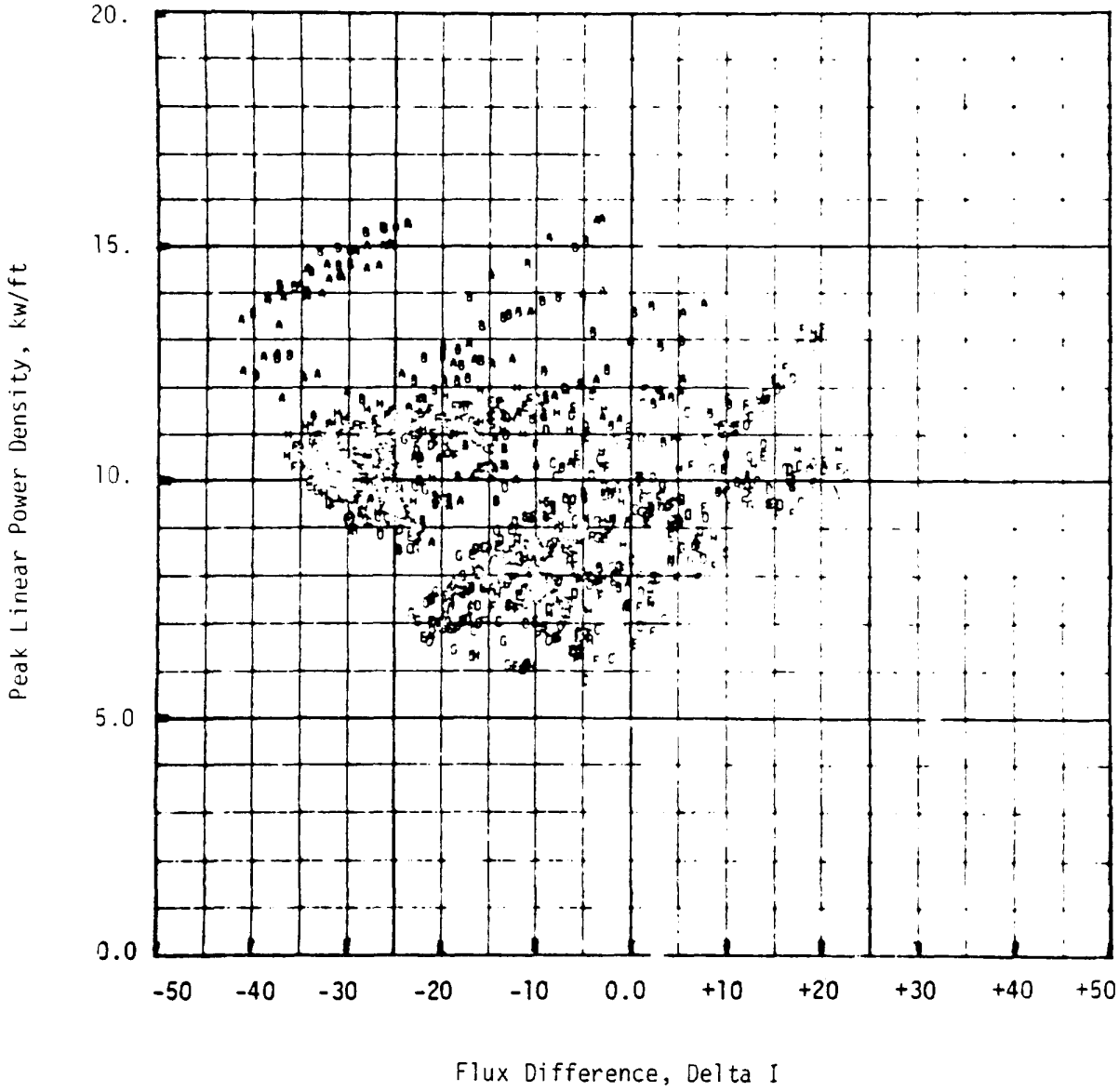

N0403022

Figure 4.3-23
TYPICAL PEAK POWER DURING BORATION/DILUTION OVERPOWER TRANSIENTS

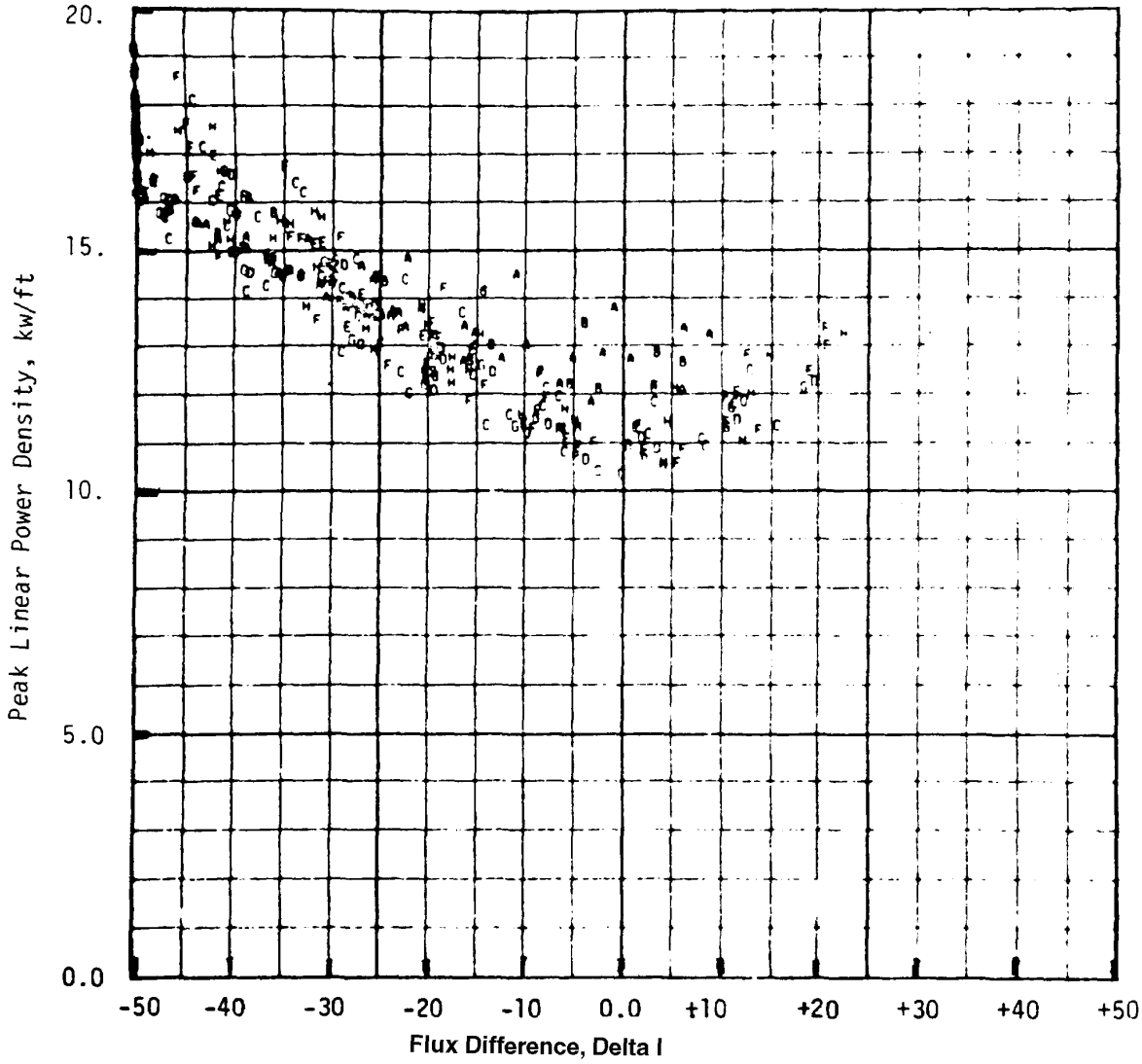

N0403023

Figure 4.3-24
COMPARISON BETWEEN CALCULATED AND MEASURED
RELATIVE FUEL ASSEMBLY POWER DISTRIBUTION

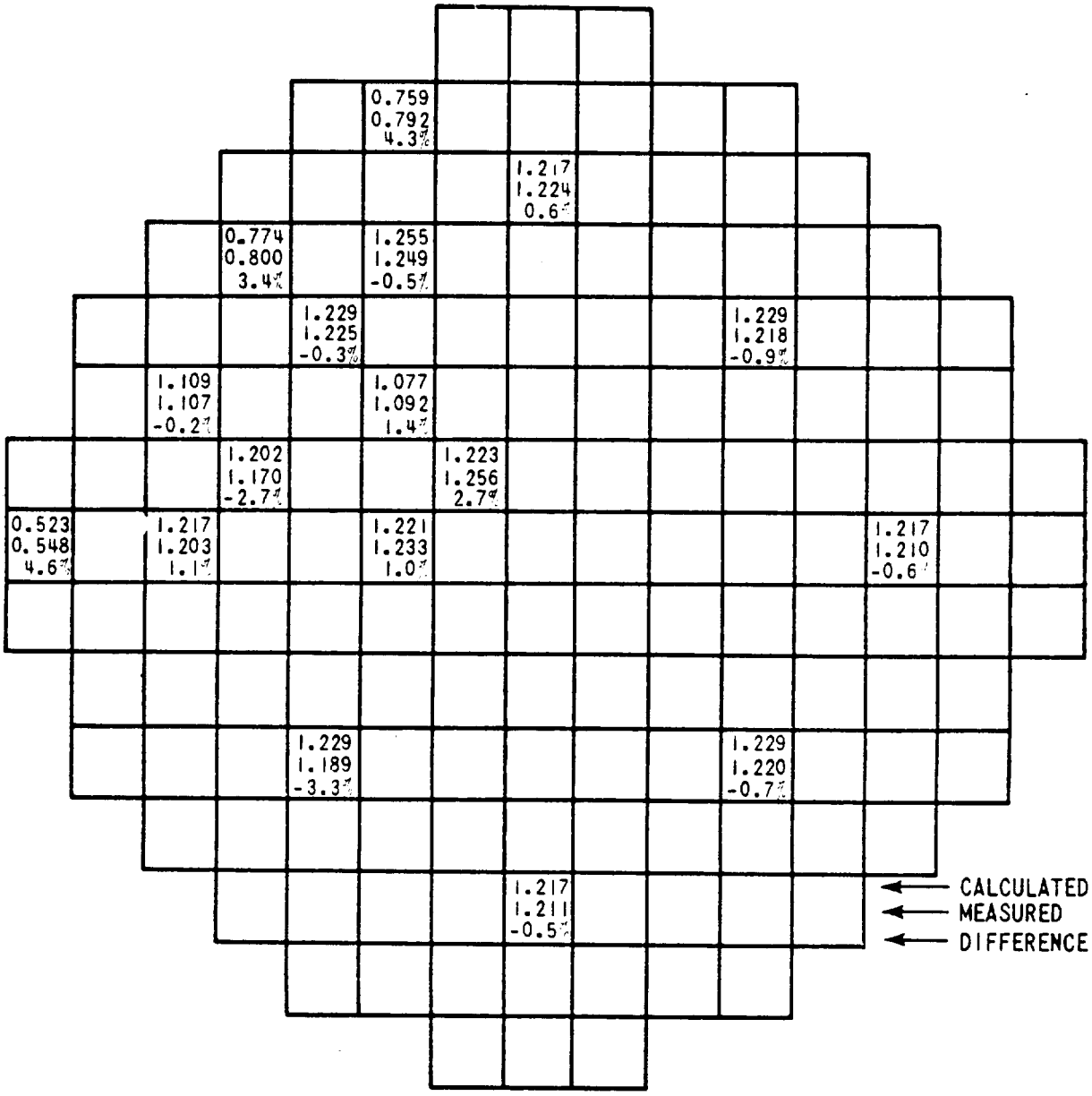

PEAKING FACTORS

$\bar{F}_z$ = 1.5

$F^N_{\Delta H}$ = 1.357

F^N_Q = 2.07 LOCATED AT M-8 SOUTH

N0403024

Figure 4.3-25
COMPARISON OF CALCULATED AND MEASURED AXIAL SHAPE

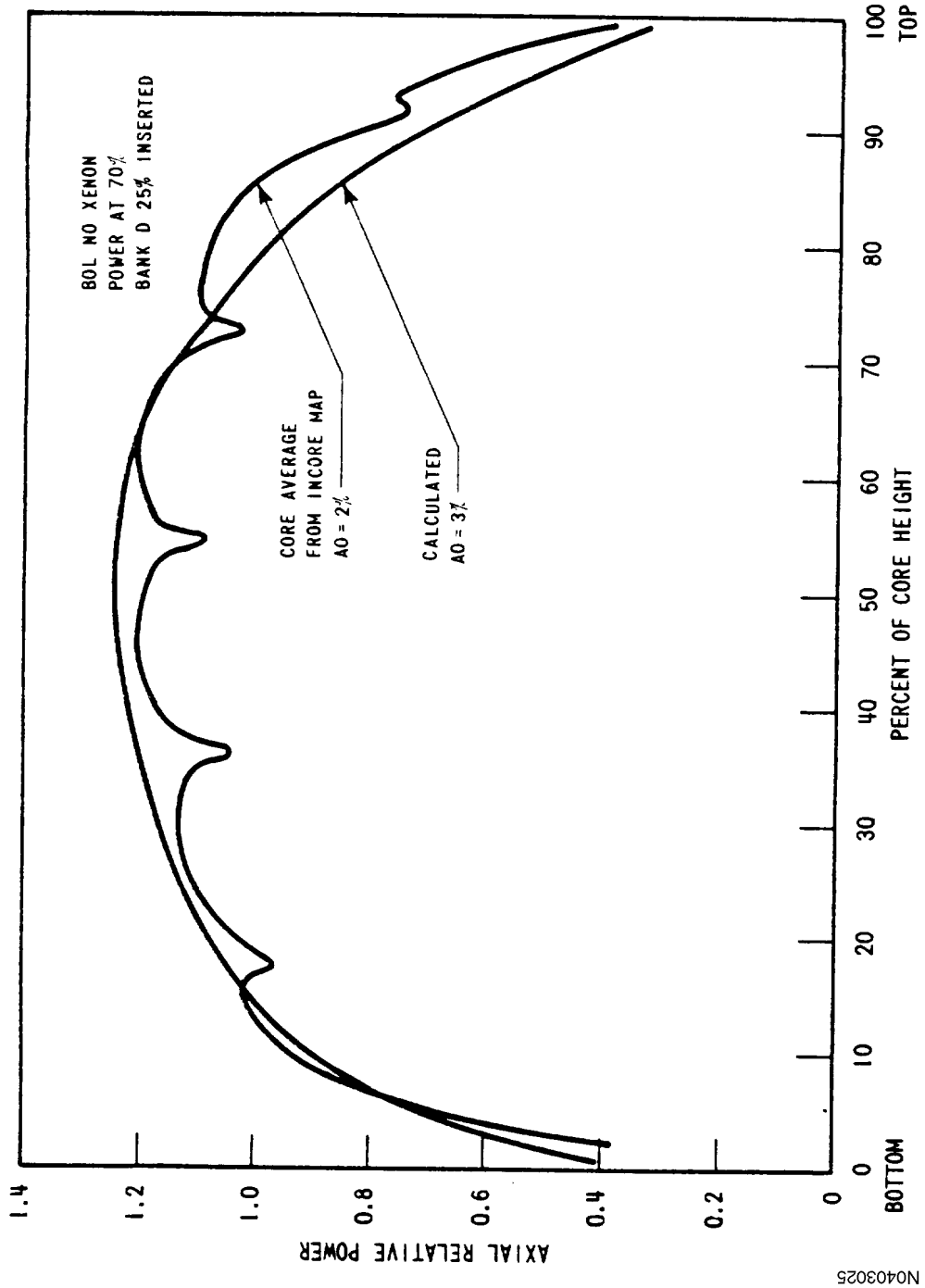

Figure 4.3-26
MEASURED VALUES OF F_Q FOR FULL POWER ROD CONFIGURATIONS

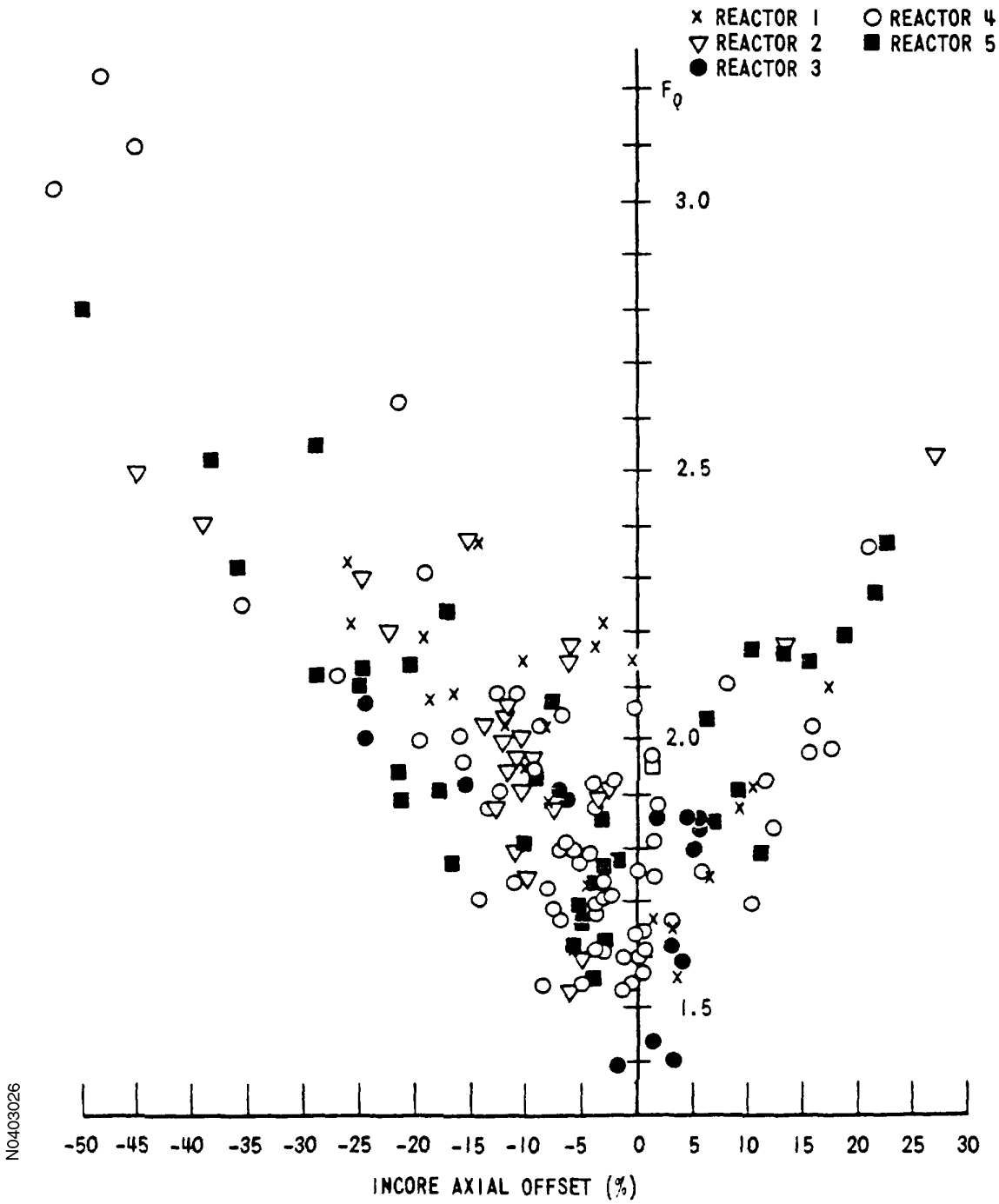

Figure 4.3-27
DOPPLER TEMPERATURE COEFFICIENT AT BOL AND EOL CYCLE 1

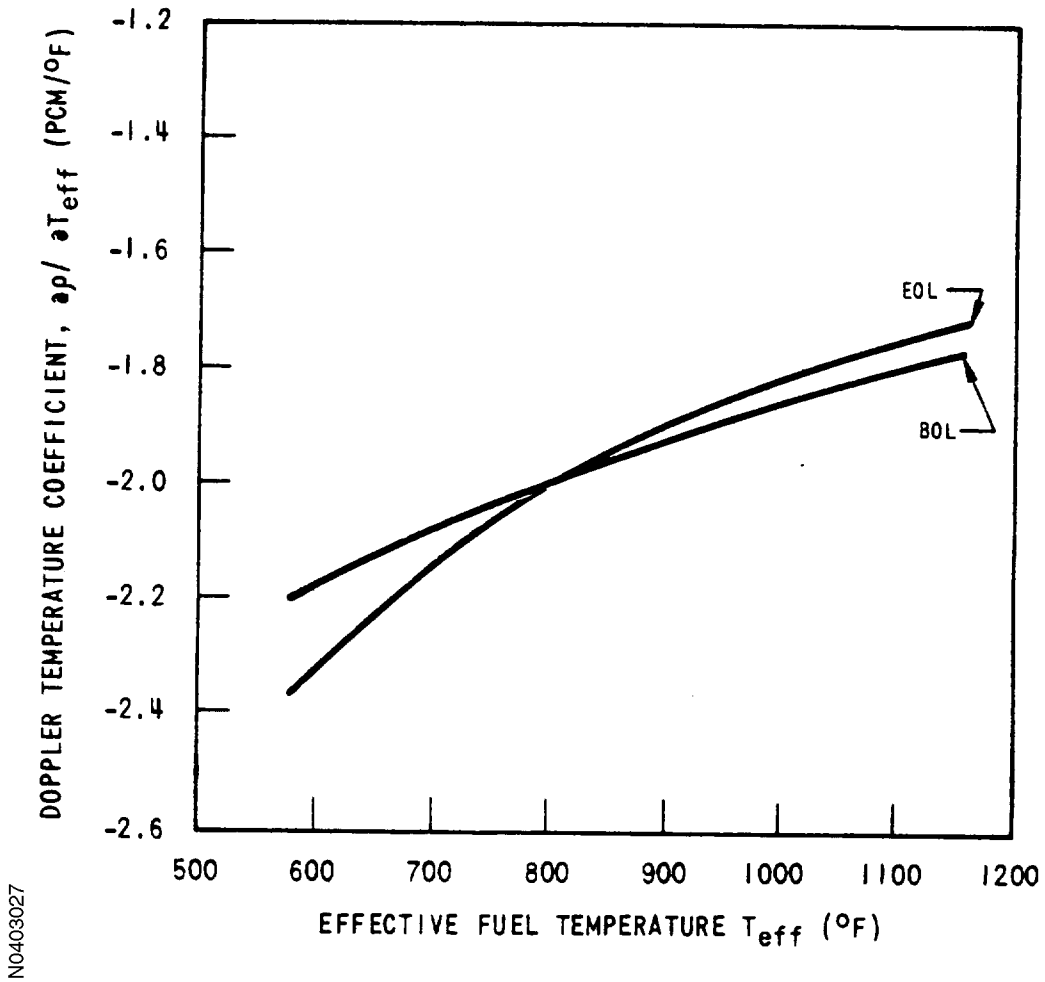

Figure 4.3-28
DOPPLER - ONLY POWER COEFFICIENT - BOL, EOL CYCLE 1

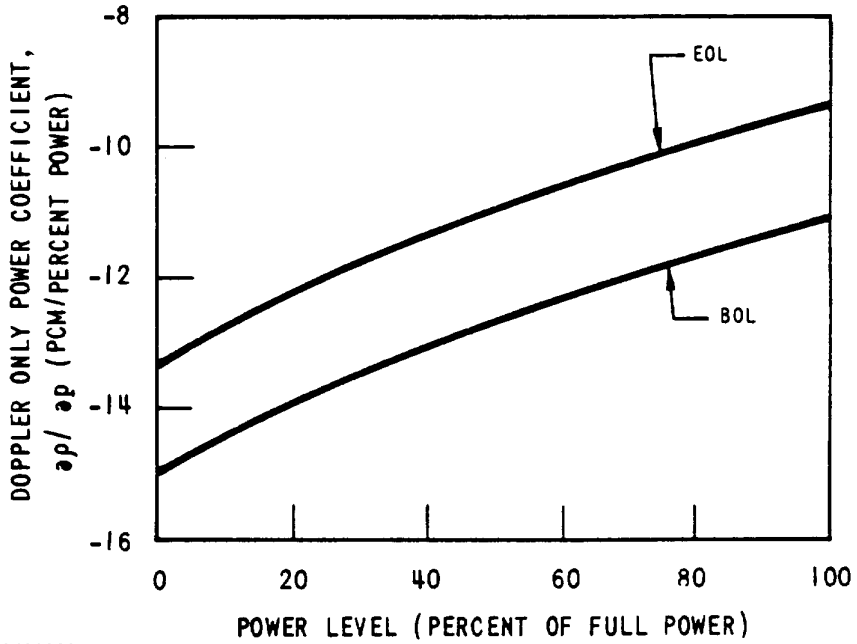

N0403028

Figure 4.3-29
DOPPLER - ONLY POWER DEFECT- BOL, EOL CYCLE 1

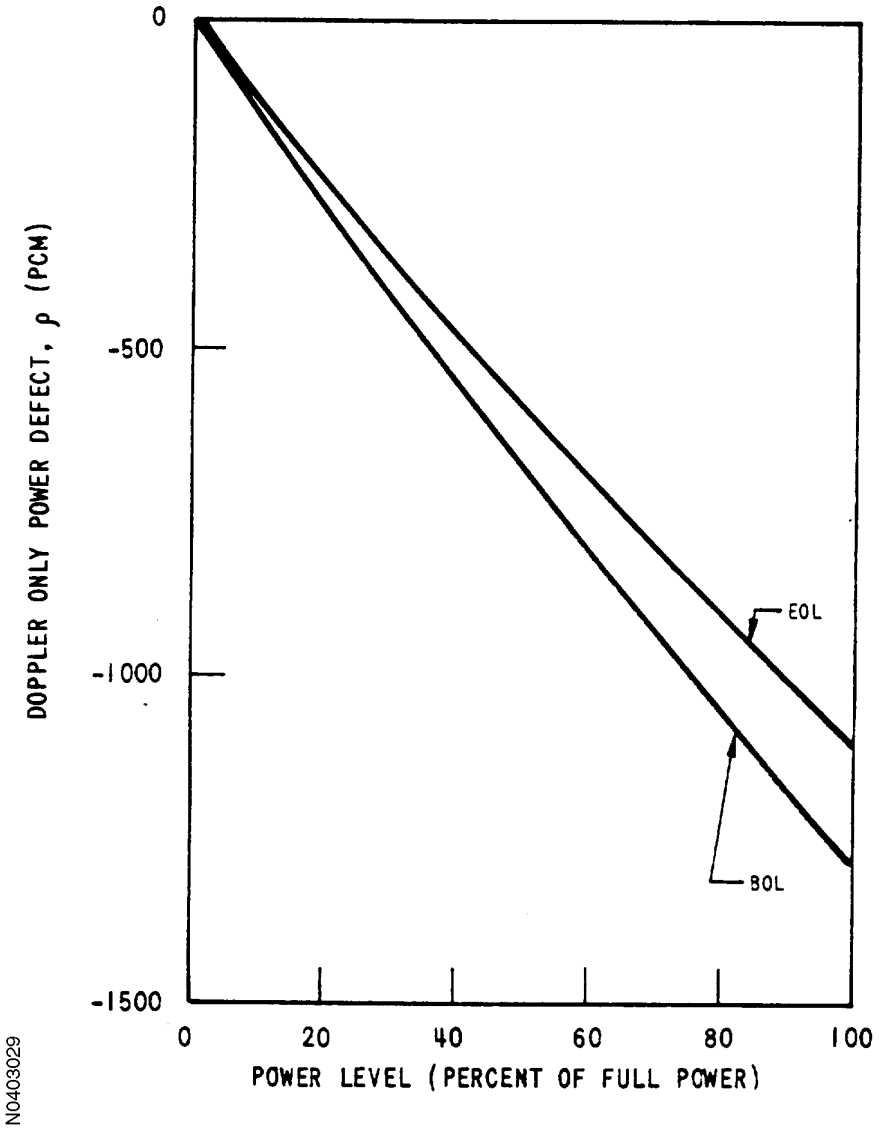

Figure 4.3-30
MODERATOR TEMPERATURE COEFFICIENT - BOL, CYCLE 1, NO RODS

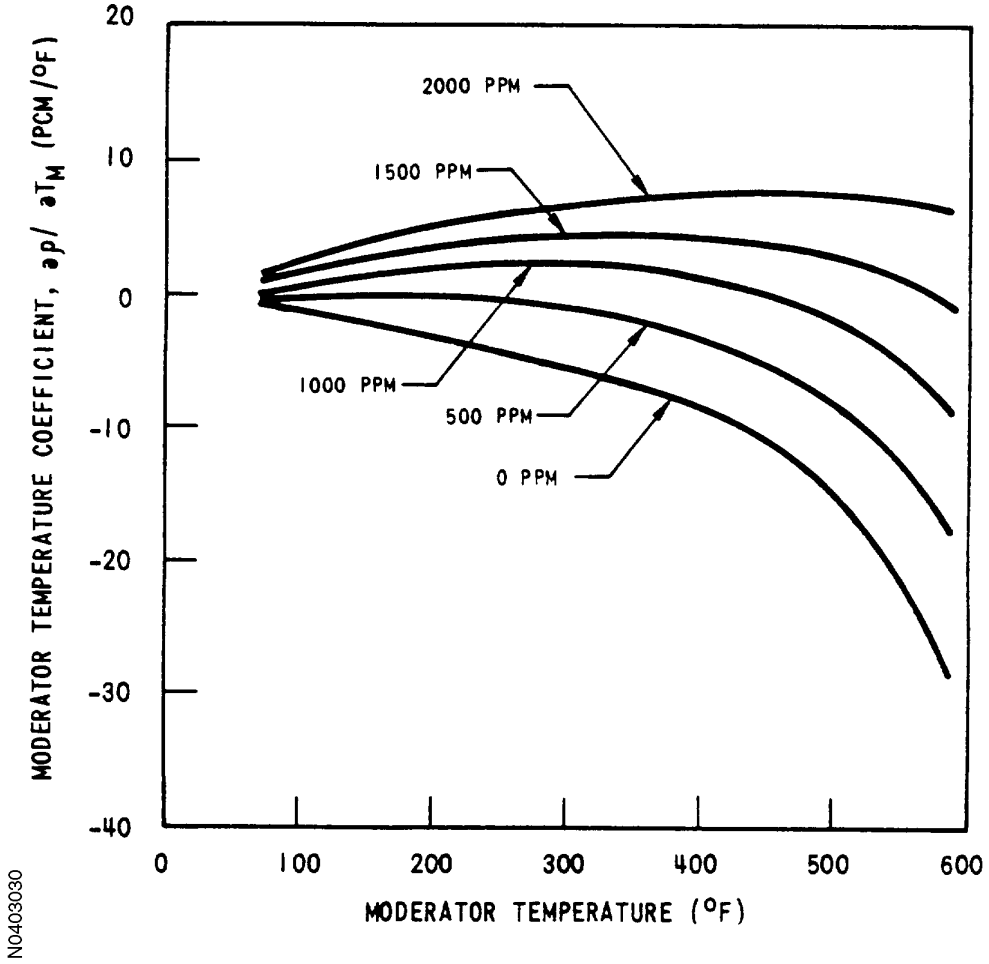

Figure 4.3-31
MODERATOR TEMPERATURE COEFFICIENT - EOL, CYCLE 1

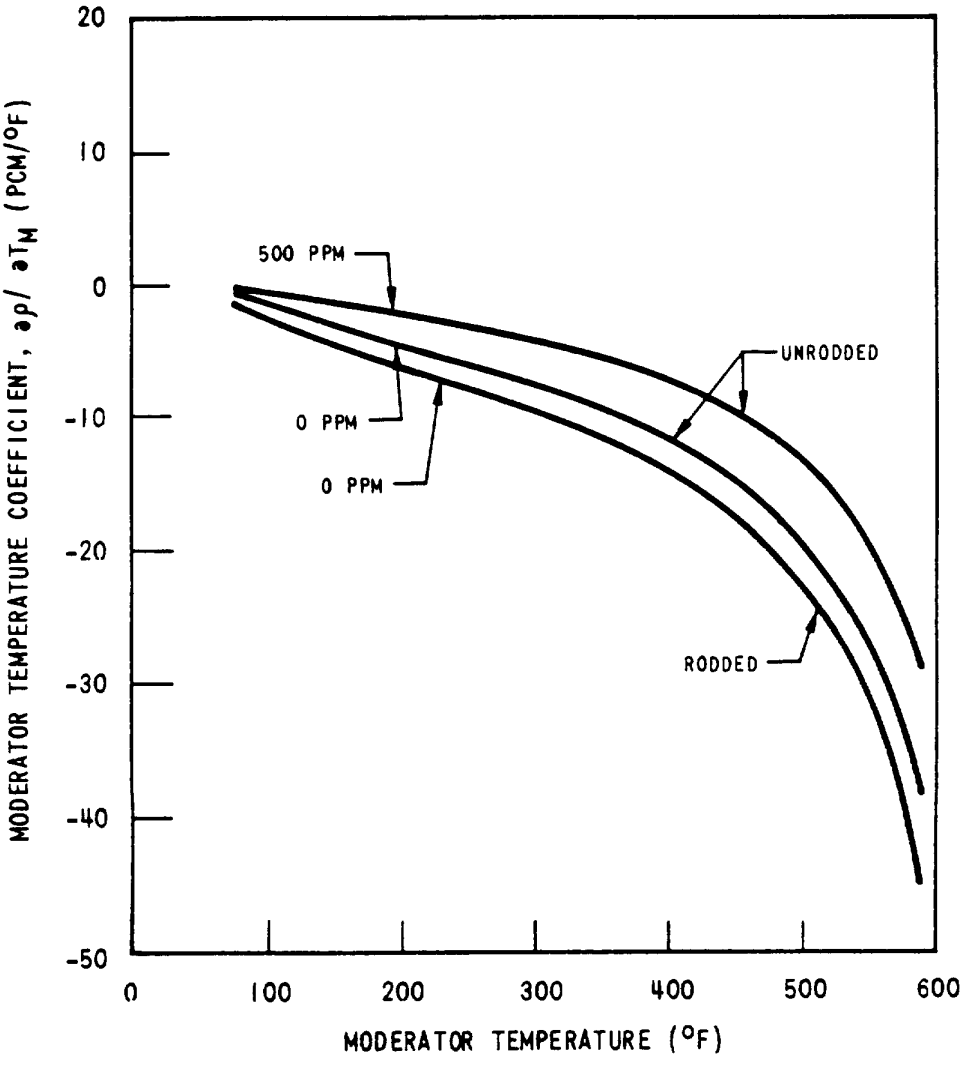

Figure 4.3-32
MODERATOR TEMPERATURE COEFFICIENT AS A FUNCTION OF BORON CONCENTRATION - BOL CYCLE 1, NO RODS

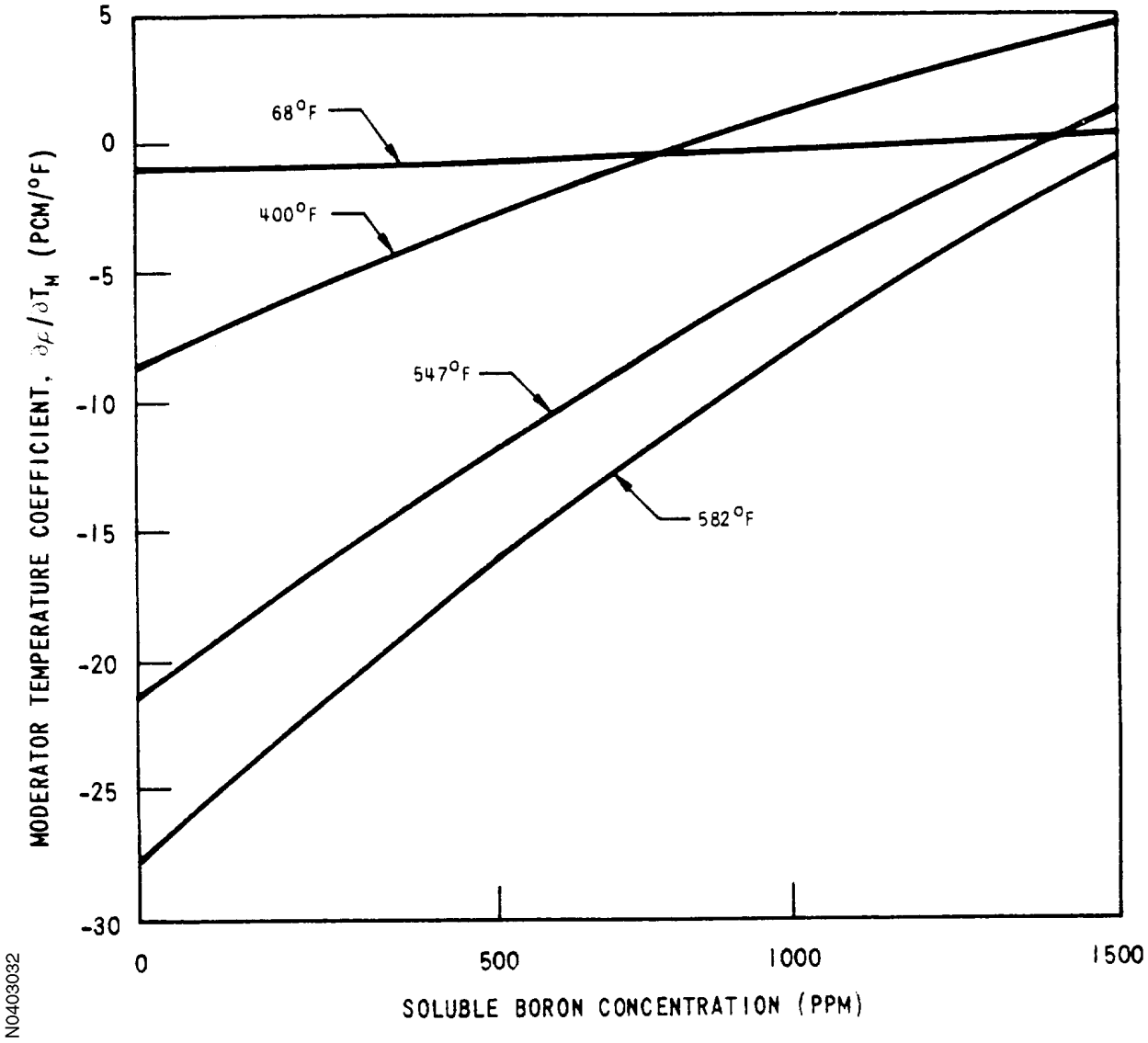

Figure 4.3-33
HOT FULL POWER TEMPERATURE COEFFICIENT
DURING CYCLE 1 FOR THE CRITICAL BORON CONCENTRATION

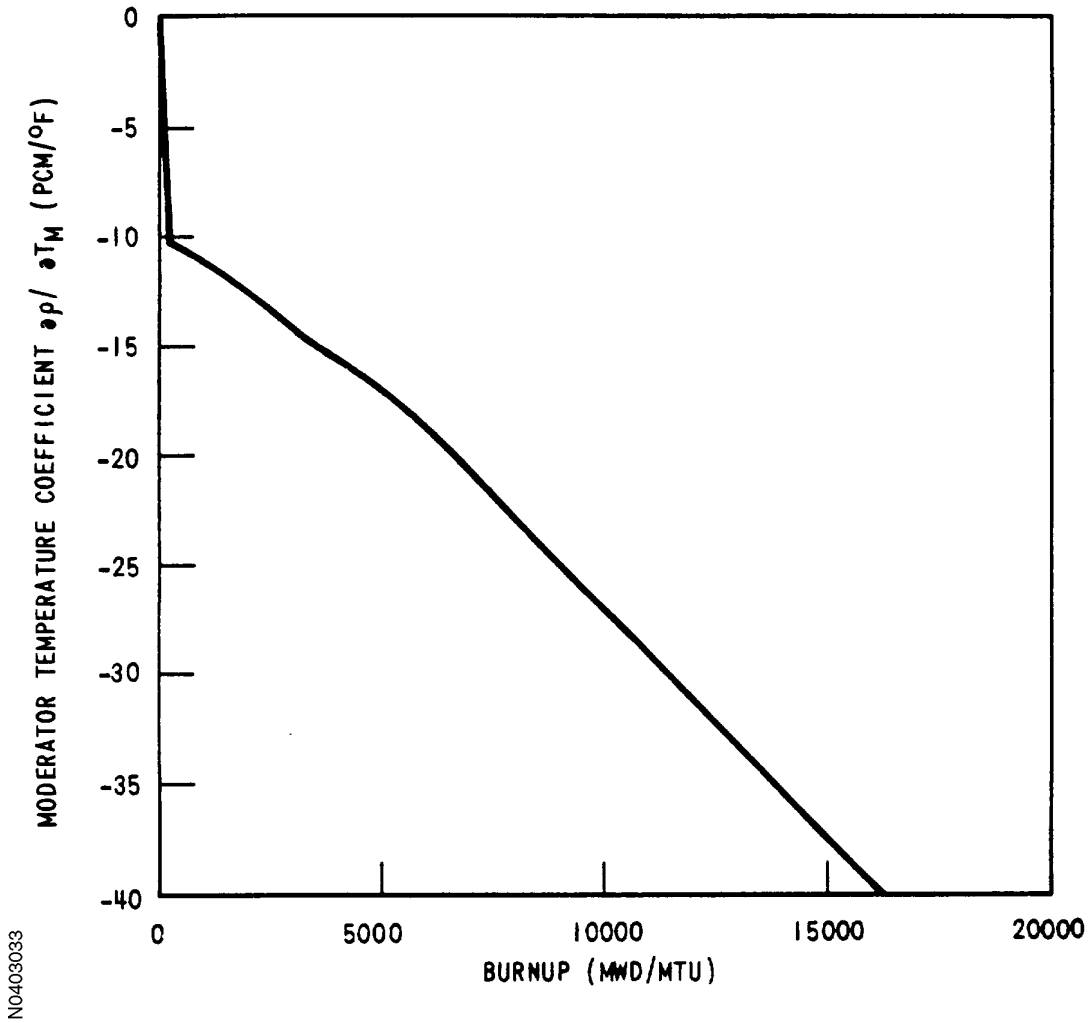

Figure 4.3-34
TOTAL POWER COEFFICIENT - BOL, EOL, CYCLE 1

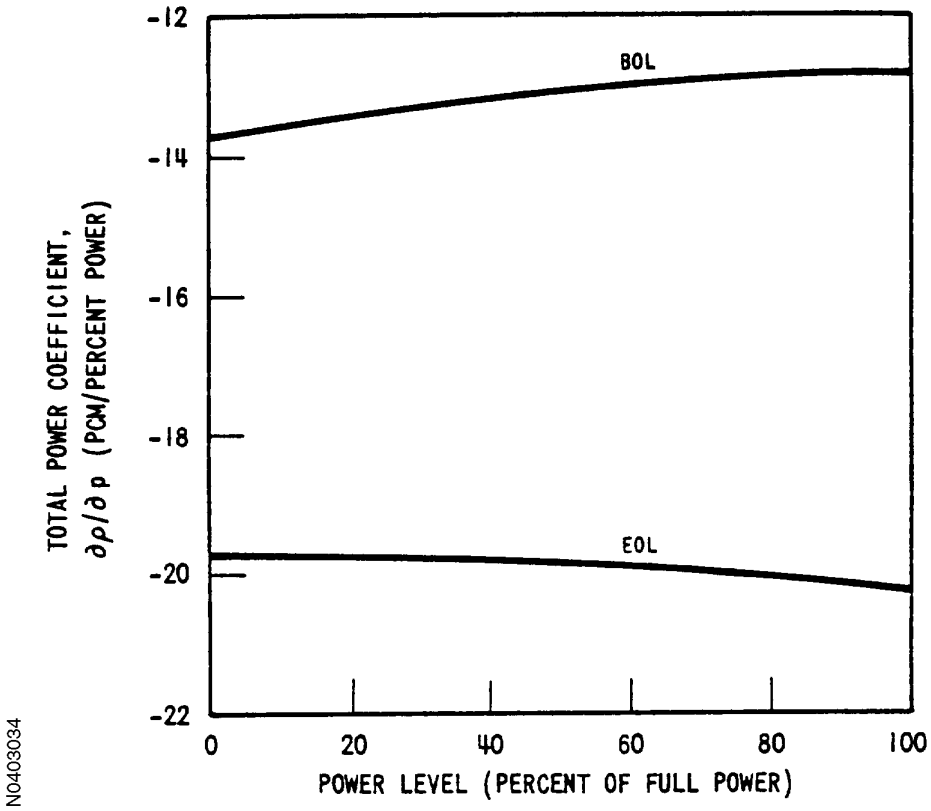

Figure 4.3-35
TOTAL POWER DEFECT- BOL, EOL CYCLE 1

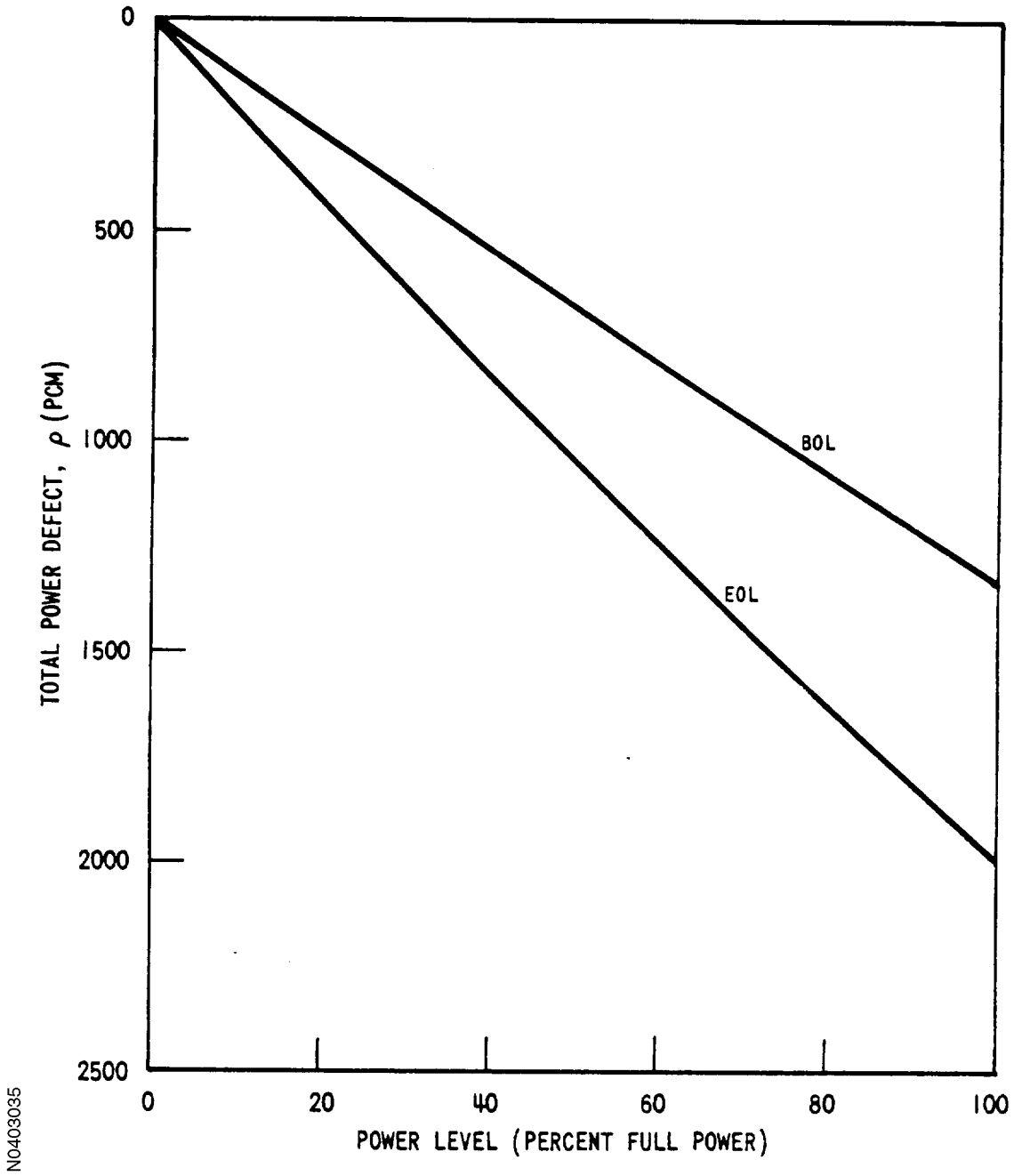

Figure 4.3-36
ROD CLUSTER CONTROL ASSEMBLY PATTERN

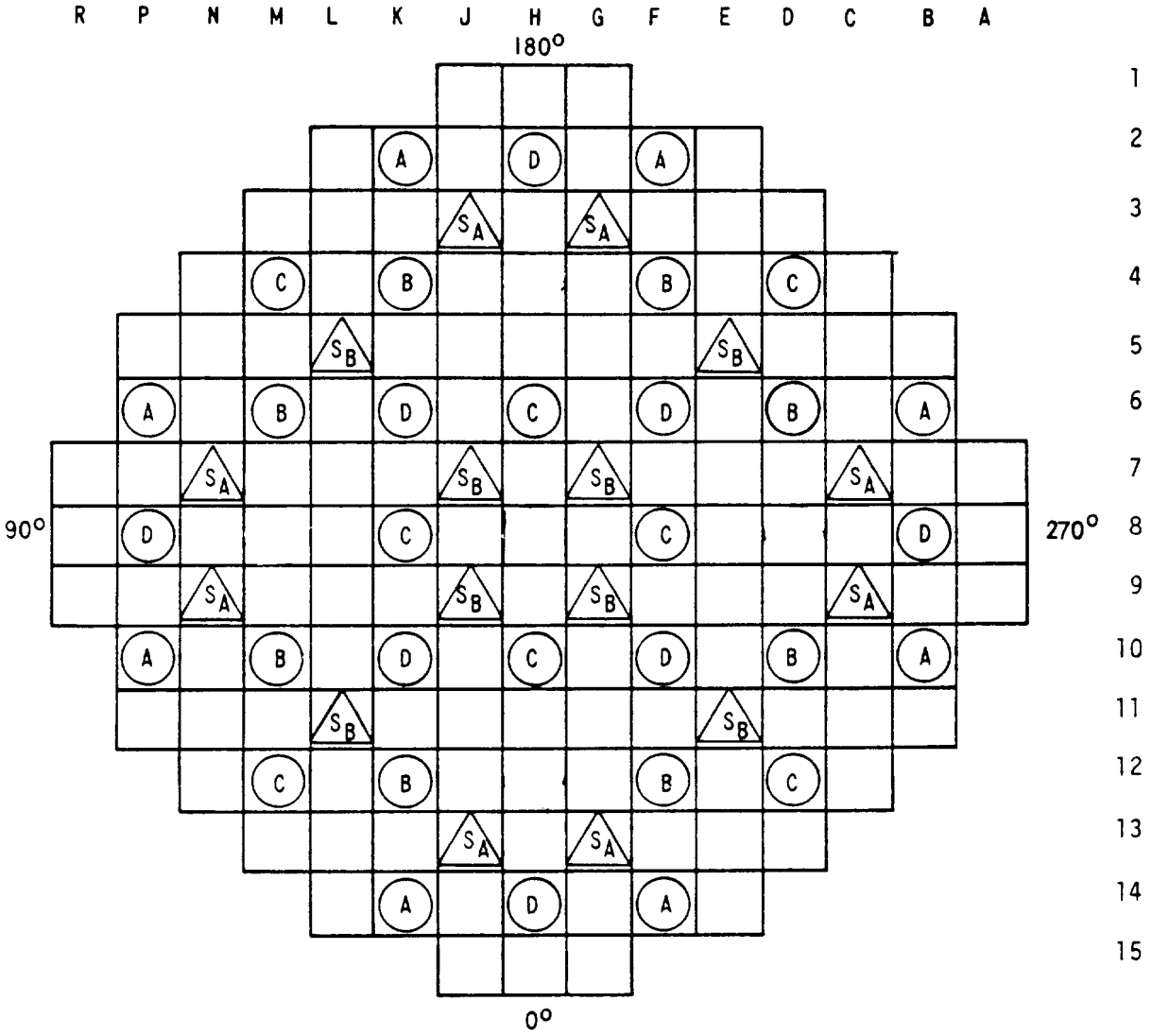

FUNCTION	NUMBER OF CLUSTERS
CONTROL BANK D	8
CONTROL BANK C	8
CONTROL BANK B	8
CONTROL BANK A	8
SHUTDOWN BANK S_B	8
SHUTDOWN BANK S_A	8

N0403036

Figure 4.3-37
ACCIDENTAL SIMULTANEOUS WITHDRAWAL OF TWO CONTROL BANKS, EOL, HZP BANKS A AND B MOVING IN THE SAME PLANE, PL AT 140 STEPS
(See Section 4.1 concerning part length control rods)

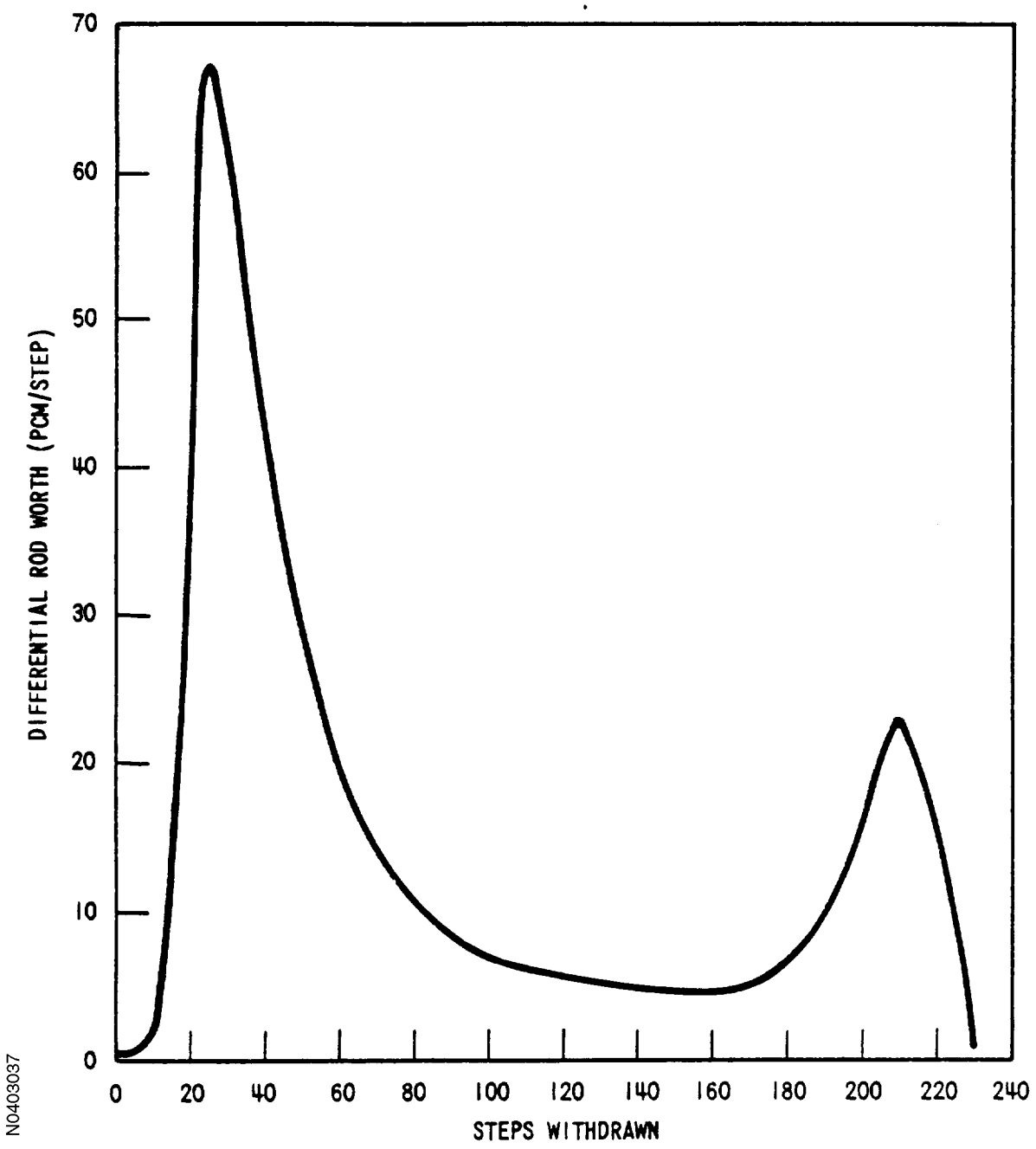

Figure 4.3-38
AXIAL OFFSET VERSUS TIME PWR CORE
WITH A 12-FT. HEIGHT AND 121 ASSEMBLIES

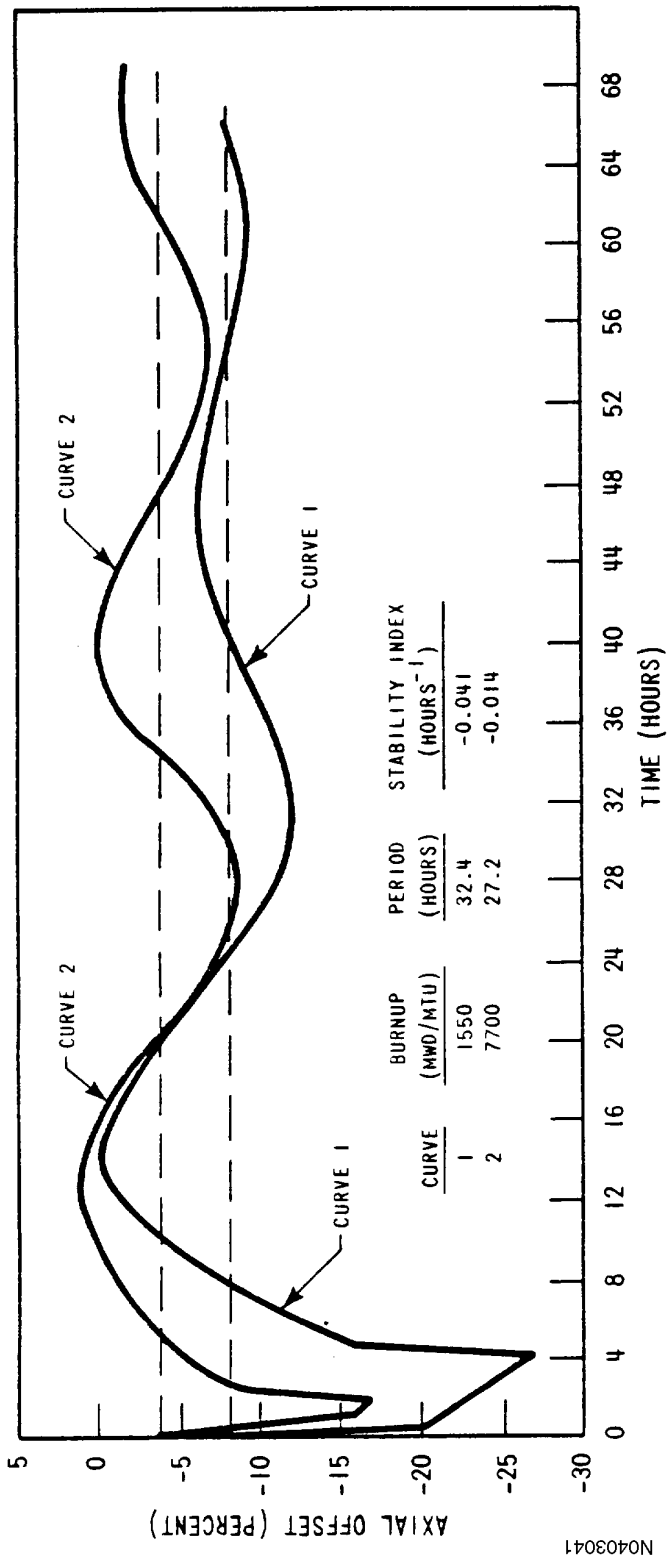

Figure 4.3-39
X-Y XENON TEST THERMOCOUPLE RESPONSE
QUADRANT TILT DIFFERENCE VERSUS TIME

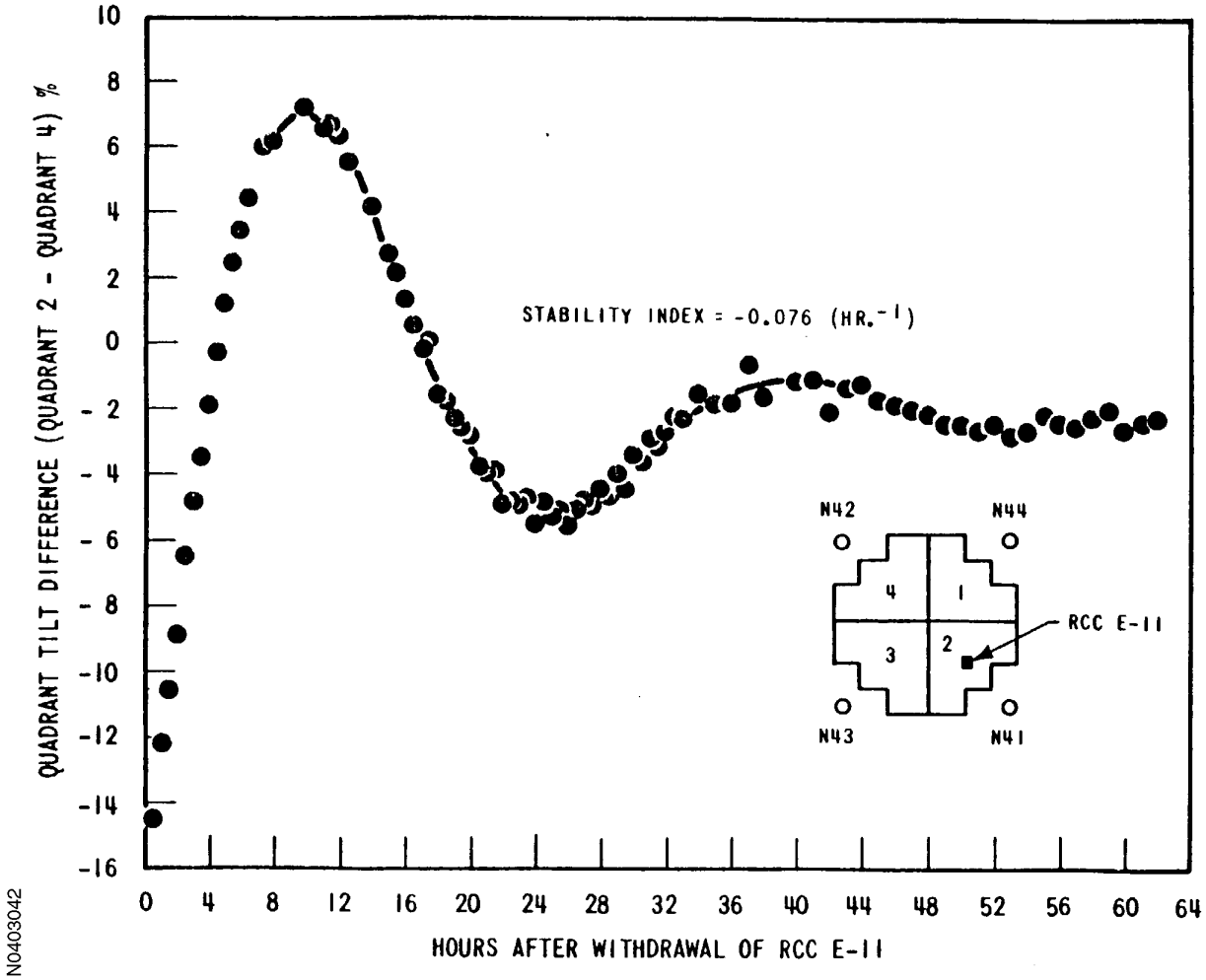

Intentionally Blank

4.4 THERMAL AND HYDRAULIC DESIGN

4.4.1 Design Basis

The overall objective of the thermal and hydraulic design of the reactor core is to provide adequate heat transfer, compatible with the heat generation distribution in the core, so that heat removal by the reactor coolant system or the emergency core cooling system (when applicable) ensures that the following performance and safety criteria requirements are met:

1. Fuel damage[1] is not expected during normal operation and operational transients (Condition I) or any transient conditions arising from faults of moderate frequency (Condition II). It is not possible, however, to preclude a very small number of rod failures. These will be within the capability of the plant cleanup system and are consistent with the plant design bases.
2. The reactor can be brought to a safe state following a Condition III event with only a small fraction of fuel rods damaged,[1] although sufficient fuel damage might occur to preclude resumption of operation without considerable outage time.
3. The reactor can be brought to a safe state and the core can be kept subcritical with acceptable heat transfer geometry following transients arising from Condition IV events.

In order to satisfy the above criteria, the following design bases have been established for the thermal and hydraulic design of the reactor core.

4.4.1.1 Departure from Nucleate Boiling Design Basis

Basis

Departure from nucleate boiling (DNB) will not occur on at least 95% of the limiting fuel rods during normal operation and operational transients, and any transient conditions arising from faults of moderate frequency (Conditions I and II events) at a 95% confidence level. Historically, this criterion has been conservatively met by adhering to the following thermal design basis: there must be at least a 95% probability that the minimum departure from nucleate boiling ratio (DNBR) of the limiting power rod during Condition I and II events is greater than or equal to the DNBR limit of the DNB correlation being used. The DNBR limit for the correlation is established based on the variance of the correlation such that there is a 95% probability with 95% confidence that DNB will not occur when the calculated DNBR is at the DNBR limit.

Discussion

Historically this DNBR limit has been 1.30 for Westinghouse applications with the W-3 correlation. More recently, the WRB-1 correlation (References 1 & 97) has been employed. With the significant improvement in the accuracy of the critical heat flux prediction with the WRB-1

1. Fuel damage as used here is defined as the penetration of the fission product barrier (i.e., the fuel rod clad).

correlation over previous DNB correlations a DNBR limit of 1.17 is applicable in this application based on the NRC evaluation and approval of this correlation (References 1 & 97).

The design method employed during the 1986 core uprating to meet the DNB design basis is the "Improved Thermal Design Procedure" (Reference 2). This method was later superceded for the Chapter 15 accident analyses by Virginia Power's "Statistical DNBR Evaluation Methodology" (Reference 83). In both methodologies, uncertainties in plant operating parameters, nuclear and thermal parameters, and fuel fabrication parameters are considered statistically such that there is at least a 95 percent probability that DNB will not occur for the limiting power rod. Plant parameter uncertainties are used to determine the plant DNBR uncertainty. This DNBR uncertainty, combined with the DNBR limit, establishes a design DNBR value which must be met in plant safety analyses. Since the parameter uncertainties are considered in determining the design DNBR value, the plant safety analyses are performed using values of input parameters without uncertainties. For the application of Virginia Power's *Statistical DNBR Evaluation Methodology,* the design DNBR value is 1.26. The phenomenon of fuel rod bowing, as described in References 84 and 85, must be accounted for in the DNBR safety analysis.

It should be noted that a design value of 1.46 or more was employed in all safety analyses. The margin available between the design DNBR used in the safety analyses and the limiting design DNBR value is more than enough to offset any rod bow penalties. Any excess margin is not required for adequate design but will be used for flexibility in the design and operation of the plant.

By preventing DNB, adequate heat transfer is ensured between the fuel clad and the reactor coolant, thereby preventing clad damage as a result of inadequate cooling. Maximum fuel rod surface temperature is not a design basis, as it will be within a few degrees of coolant temperature during operation in the nucleate boiling region. Limits provided by the nuclear control and protection systems are such that this design basis will be met for transients associated with Condition II events, including overpower transients. There is an additional large DNBR margin at rated power operation and during normal operating transients.

4.4.1.2 **Fuel Temperature Design Basis**

Basis

During modes of operation associated with Condition I and Condition II events, the maximum fuel temperature shall be less than the melting temperature of UO_2. The UO_2 melting temperature for at least 95% of the peak kW/ft fuel rods will not be exceeded at the 95% confidence level. The melting temperature of UO_2 is taken as 5080°F (Reference 3) unirradiated and reducing 58°F per 10,000 MWd/MTU. By precluding UO_2 melting, the fuel geometry is preserved and possible adverse effects of molten UO_2 on the cladding are eliminated. To preclude center melting and as a basis for overpower protection system setpoints, a calculated centerline

fuel temperature of 4700°F has been selected as the overpower limit. This provides sufficient margin for uncertainties in the thermal evaluations as described in Section 4.4.2.10.1.

Discussion

Fuel rod thermal evaluations are performed at rated power, maximum overpower, and during transients at various burnups. These analyses ensure that this design basis, as well as the fuel integrity design basis given in Section 4.2, are met. They also provide input for the evaluation of Condition III and Condition IV faults given in Chapter 15.

4.4.1.3 Core Flow Design Basis

Basis

A minimum percentage of the thermal flow rate will pass through the fuel rod region of the core and be effective for fuel rod cooling. Coolant flow through the thimble tubes as well as the leakage from the core barrel-baffle region into the core are not considered effective for heat removal.

Discussion

Core-cooling evaluations are based on the thermal flow rate (minimum flow) entering the reactor vessel. A maximum value is allotted as bypass flow. This includes rod control cluster guide thimble cooling flow, head cooling flow, baffle leakage, and leakage to the vessel outlet nozzle.

4.4.1.4 Hydrodynamic Stability Design Basis

Modes of operation associated with Condition I and II events shall not lead to hydrodynamic instability.

4.4.1.5 Other Considerations

The above design bases together with the fuel clad and fuel assembly design bases given in Section 4.2.1.1 are sufficiently comprehensive so that additional limits are not required.

Fuel rod diametral gap characteristics, moderator-coolant flow velocity and distribution, and moderator void are not inherently limiting. Each of these parameters is incorporated into the thermal and hydraulic models used to ensure that the above-mentioned design criteria are met. For instance, the fuel rod diametral gap characteristics change with time (and the fuel rod integrity is evaluated on that basis). The effect of the moderator flow velocity and distribution (Section 4.4.2.6) and moderator void distribution (Section 4.4.2.5) are included in the core thermal evaluation and thus affect the design bases.

Meeting the fuel clad integrity criteria covers possible effects of clad temperature limitations. As noted in Section 4.2.1.3.1, the fuel rod conditions change with time. A single clad temperature limit for Condition I or Condition II events is not appropriate since, of necessity, it

would be overly conservative. A clad temperature limit is applied to the loss-of-coolant accident (LOCA) (Section 15.4.1) and control-rod-ejection accident (Reference 82).

These design bases are equally applicable to cores with Zircaloy and ZIRLO cladding and skeleton components (Reference 93). The thermal and hydraulic design methods and correlations described in subsequent sections are also applicable for the use of both alloys.

4.4.1.6 Use of Reconstituted Fuel

The design bases described herein are applicable for fuel rod reconstitution. The thermal-hydraulic evaluation of reconstituted fuel assemblies is performed in accordance with NRC approved codes and methods which are in subsequent sections.

Fuel rod reconstitution affects predictions of departure from nucleate boiling (DNB) in hot channels due to a local power reduction and the resultant effects of enthalpy and flow. Westinghouse demonstrated in Reference 94 that it is conservative to model a reconstituted assembly as a regular fuel assembly in DNB analyses for Westinghouse reconstituted assemblies with mixing vane grid designs. Reference 95 demonstrated that the results of Reference 94 were also applicable to Virginia Power methods and models.

For reload cores using reconstituted fuel assemblies, a cycle specific evaluation is performed to confirm that the exact configuration and associated core power distribution of the reconstituted assemblies do not introduce a change in radial gradients in the flow and enthalpy distribution that could invalidate the applicability of the critical heat flux (CHF) correlation (Reference 96). It is also confirmed that the reconstituted fuel assembly is bounded by a regular fuel assembly in DNB analyses.

4.4.2 Description

4.4.2.1 Summary Comparison

Table 4.4-1 provides a comparison of the design parameters for North Anna with the original 15 x 15 fuel design at 2775 MWt and 580.3°F T_{avg} and the 17 x 17 standard fuel design at 2775 MWt and 580.3°F T_{avg}. Table 4.4-2 provides a comparison of the design parameters for North Anna with the 17 x 17 standard fuel design at uprated temperature conditions of 2775 MWt and 587.8°F T_{avg}, and the 17 x 17 NAIF fuel design at the uprated power conditions at 2893 MWt and 586.8°F T_{avg}.

The inability to make a direct comparison of all plant operating parameters in Tables 4.4-1 and 4.4-2 results from the significant advances and improvements made in the method of analysis of core performance for this application. The standard core was analyzed on a worst case basis for all parameters involved in determining limiting setpoints. The North Anna uprated core is demonstrated to meet all design bases by considering the values of plant parameters and the uncertainties in these parameters in a more realistic fashion through the use of the Statistical DNBR Evaluation Methodology. The justification for the analytical techniques used in

determining the values presented for the North Anna uprated core are presented in the relevant chapters in this document.

The original design of the North Anna Power Station used the W-3 DNB correlation with the modified spacer factor ("R" grid DNB correlation) and a multiplier of 0.865. The results of the 17 x 17 geometry DNB tests (References 4 & 38) indicated that a less conservative multiplier of 0.88 was required for the W-3 DNB correlation with the modified spacer factor ("R" grid DNB correlation).

When the North Anna core thermal rating was increased from 2775 MW to 2893 MW (References 89 & 90) the analyses were performed with the WRB-1 correlation and the ITDP methodology (Reference 2). (ITDP has since been superceded by Virginia Power's Statistical DNBR Evaluation Methodology.) Both the W-3 and WRB-1 correlations will be discussed below. Fuel densification has been considered in the fuel temperature evaluations as discussed in Sections 4.4.2.2, 4.4.2.10.1, and 4.4.3.4.2. Fuel densification has been considered in the DNB evaluations using the methods and models described in detail in References 6 and 99.

4.4.2.2 Fuel and Cladding Temperatures

Consistent with the thermal-hydraulic design bases described in Section 4.4.1, the following discussion pertains mainly to fuel pellet temperature evaluation. Fuel clad integrity is discussed in Section 4.2.1.3.1.

The thermal-hydraulic design ensures that the maximum fuel temperature is below the melting point of UO_2. To preclude center melting and as a basis for overpower protection system setpoints, a calculated centerline fuel temperature of 4700°F has been selected as the overpower limit. The temperature distribution within the fuel pellet is predominantly a function of the local power density and the UO_2 thermal conductivity. However, the computation of radial fuel temperature distributions combines crud, oxide, clad, gap, and pellet conductances. The factors that influence these conductances, such as gap size (or contact pressure), internal gas pressure, gas composition, pellet density, and radial power distribution within the pellet, were combined into a semiempirical thermal model (Section 4.2.1.3.1) with the model modifications for time-dependent fuel densification given in Reference 6. This thermal model enables the determination of these factors and their net effects on temperature profiles. The temperature predictions were compared to inpile fuel temperature measurements (References 7, 9, 100, & 101) with good results.

Effect of Fuel Densification on Fuel Rod Temperatures

Fuel densification results in fuel pellet shrinkage. This affects the fuel temperatures in the following ways:

1. Pellet radial shrinkage increases the pellet diametral gap, which results in increased thermal resistance of the gap, and thus, higher fuel temperatures (Section 4.2.1.3.1).

2. Pellet axial shrinkage may produce pellet-to-pellet gaps that result in local power spikes, described in Section 4.3.2.2.1, and thus, higher total heat flux hot-channel factor, F_Q, and local fuel temperatures.
3. Pellet axial shrinkage will result in a fuel stack height reduction and an increase in the linear power generation rate (kW/ft) for a constant core power level. For the fuel rod specifications listed in Table 4.3-1, the increase in linear power is less than 0.2% (Reference 98).

Fuel rod thermal evaluations (fuel centerline, average and surface temperatures) are determined throughout the fuel rod lifetime with consideration of burnup-dependent densification. To determine the maximum fuel temperatures, various burn-up rods, including the highest burnup rod, are analyzed over the rod linear power range of interest. Analyses have shown that the maximum fuel temperatures typically occur near the beginning of life. Figure 4.4-1 illustrates the relationship between fuel average and surface temperatures and the linear power density (kW/ft). The temperatures shown represent typical values of the peak temperatures that are attained during the operating lifetime of the fuel. Specific values may change for reload fuel, and are assessed on a cycle specific basis.

Figure 4.4-2 similarly illustrates the relationship between fuel centerline temperatures and the linear power density (kw/ft). The temperatures shown represent typical values of the peak temperatures that are attained during the operating lifetime of the fuel. As for the fuel average and surface temperatures, specific values of the centerline temperatures may change for reload fuel, and are assessed on a cycle specific basis. The maximum pellet temperatures at the hot spot during full-power steady-state and at the peak linear power for determination of protection setpoints are shown in Table 4.4-1 for the original North Anna design. The principal factors that were employed in the determination of the fuel temperature are discussed below.

4.4.2.2.1 UO_2 Thermal Conductivity

The thermal conductivity of uranium dioxide was evaluated from data reported by Howard et al. (Reference 10), Lucks et al. (Reference 11), Danial et al. (Reference 12), Feith (Reference 13), Vogt et al. (Reference 14), Nishijima et al. (Reference 15), Ainscough et al. (Reference 16), Godfrey et al. (Reference 17), Stora et al. (Reference 18), Bush (Reference 19), Asamoto et al. (Reference 20), Kruger (Reference 21), and Gyllander (Reference 22).

At the higher temperatures, thermal conductivity is best obtained by using the integral conductivity to melt; that can be determined with more certainty. From an examination of the data, it was concluded that the best estimate for the value of $\int_0^{2800°C} k dt$ is 93 W/cm. This conclusion was based on the integral values reported by Gyllander (Reference 22), Lyons et al. (Reference 23), Coplin et al. (Reference 24), Duncan (Reference 8), Bain (Reference 25), and Stora (Reference 26).

The design curve for the thermal conductivity is shown in Figure 4.4-3. The section of the curve at temperatures between 0° and 1300°C is in excellent agreement with the recommendation

of the IAEA panel (Reference 27). The section of the curve above 1300°C was derived for an integral value of 93 W/cm (References 8, 22 & 26).

Thermal conductivity for UO_2 at 95% theoretical density can be represented best by the following equation:

$$K = \frac{1}{11.8 + 0.0238T} + 8.775\times10^{-13}T^3 \qquad (4.4\text{-}1)$$

where:

K = W/cm-°C

T = °C

4.4.2.2.2 Radial Power Distribution in UO_2 Fuel Rods

An accurate description of the radial power distribution as a function of burn-up is needed in determining the power level for incipient fuel melting and other important performance parameters such as pellet thermal expansion, fuel swelling, and fission gas release rates.

This information on radial power distributions in UO_2 fuel rods was determined with the neutron transport theory code, LASER. The LASER code was validated by comparing the code predictions on radial burn-up and isotopic distributions with measured radial microdrill data (References 28 & 29). A "radial power depression factor," f, was determined using radial power distributions predicted by LASER. The factor f enters into the determination of the pellet centerline temperature, T_c, relative to the pellet surface temperature, T_s, through the expression:

$$\int_{T_s}^{T_c} k(T)\,dT = \frac{q'f}{4\pi} \qquad (4.4\text{-}2)$$

where:

k(T) = the thermal conductivity for UO_2 with a uniform density distribution

q' = the linear power generation rate

f = radial power depression factor.

4.4.2.2.3 Gap Conductance

The temperature drop across the pellet-clad gap is a function of the gap size and the thermal conductivity of the gas in the gap. The gap-conductance model was selected such that, when combined with the UO_2 thermal conductivity model, the calculated fuel centerline temperatures reflect the inpile temperature measurements.

The temperature drop across the gap is calculated by assuming an annular gap-conductance model of the following form:

$$h = \frac{K_{gas}}{\left(\frac{\delta}{2}\right)(GMF) + \delta_r} \tag{4.4-3}$$

or an empirical correlation derived from thermocouple and melt radius data

$$h = 1500\ K_{gas} + \frac{4.0}{0.006 + 12\delta} \tag{4.4-4}$$

where:

K_{gas} = thermal conductivity of the gas mixture including a correlation factor (Reference 30) for the accommodation coefficient for light gases (e.g., helium), Btu/hr-ft-°F

δ = diametral gap size, ft

δ_r = effective gap spacing due to surface roughness, ft

GMF = a gap multiplication factor to eliminate bias between predicted and measured values

The larger gap-conductance value from these two equations is used to calculate the temperature drop across the gap for finite gaps.

For evaluations in which the pellet-clad gap is closed, a contact conductance is calculated. The contact conductance between UO_2 and the cladding was measured and found to be dependent on the contact pressure, composition of the gas at the interface, and the surface roughness (References 30 & 31). This information together with the surface roughness found in Westinghouse reactors leads to the following correlation:

$$h = 0.6P + \frac{K_{gas}}{\delta_r} \tag{4.4-5}$$

where:

h = contact conductance, Btu/hr-ft^2-°F

P = contact pressure, psi

K_{gas} = thermal conductivity of gas mixture at the interface including a correction factor (Reference 30) for the accommodation coefficient for light gases (e.g., helium), Btu/hr-ft-°F

4.4.2.2.4 Surface Heat Transfer Coefficients

The fuel rod surface heat transfer coefficients during subcooled forced convection and nucleate boiling are presented in Section 4.4.2.8.1.

4.4.2.2.5 Fuel Clad Temperatures

The outer surface of the fuel rod at the hot spot operates at a temperature of approximately 660°F for steady-state operation at rated power throughout core life due to the onset of nucleate boiling. Initially (beginning of life), this temperature is that of the clad metal surface.

During operation over the life of the core, the buildup of oxides and crud on the fuel rod surface causes the temperature of the outer surface of the clad metal to increase. Allowance is made in the fuel center melt evaluation for this temperature rise. Since the thermal-hydraulic design basis limits DNB, adequate heat transfer was provided between the fuel clad and the reactor coolant so that the core thermal output was not limited by considerations of the clad temperature. Figure 4.4-4 shows the axial variation of average clad temperature for a typical (average power) rod both at beginning of life and after 20,000 EFPH of operation.

4.4.2.2.6 Treatment of Peaking Factors

The total heat flux hot-channel factor, F_Q, is defined by the ratio of the maximum to core average heat flux. As presented in Table 4.3-2 and discussed in Section 4.3.2.2.6, the design value F_Q for normal operation is defined in the plant Technical Specifications and is evaluated for its impact on thermal and hydraulic design criteria for each reload core.

As described in Section 4.3.2.2.6, the peak local power at the maximum overpower trip point is 21.1 kW/ft. The centerline temperature at this kW/ft must be below the UO_2 melt temperature over the lifetime of the rod, including allowances for uncertainties. The melt temperature of unirradiated UO_2 is 5080°F (Reference 3) and decreases by 58°F per 10,000 MWd/MTU. The centerline temperature is evaluated for each cycle to confirm that the maximum overpower trip point is below the power required to produce melting. Fuel centerline and average temperatures at rated (100%) power and at the maximum overpower trip point are presented in Table 4.4-2.

4.4.2.3 Critical Heat Flux Ratio or Departure from Nucleate Boiling Ratio and Mixing Technology

The minimum DNBRs for the rated power, design overpower, and anticipated transient conditions for the original North Anna design are given in Table 4.4-1. A comparison of uprated conditions (References 89 & 90) and the increased T_{ave} operating conditions (References 86 & 87) is included in Table 4.4-2. The core average DNBR is not a safety-related item, as it is not directly related to the minimum DNBR in the core, which occurs at some elevation in the limiting flow channel. Similarly, the DNBR at the hot spot is not directly safety-related. The minimum DNBR in the limiting flow channel will be downstream of the peak heat flux location (hot spot) due to the increased downstream enthalpy.

DNBRs were calculated by using the correlations and definitions described in Sections 4.4.2.3.1 and 4.4.2.3.2. The COBRA and THINC-IV computer codes (discussed in

Section 4.4.3.4.1) were used to determine the flow distribution in the core and the local conditions in the hot channel for use in the DNB correlation. The use of hot-channel factors is discussed in Section 4.4.3.2.1 (nuclear hot-channel factors) and in Section 4.4.2.3.4 (engineering hot-channel factors).

4.4.2.3.1 Departure from Nucleate Boiling Technology

Early experimental studies of DNB were conducted with fluid flowing inside single heated tubes or channels and with single annulus configurations with one or both walls heated. The results of the experiments were analyzed using many different physical models for describing the DNB phenomenon, but all resultant correlations are highly empirical in nature. The evolution of these correlations is given by Tong (References 32 & 33), including the W-3 correlation that is in wide use in the PWR industry.

As testing methods progressed to the use of rod bundles instead of single channels, it became apparent that the bundle average flow conditions cannot be used in DNB correlations. As outlined by Tong (Reference 34), test results showed that correlations based on average conditions were not accurate predictors of DNB heat flux. This indicated that a knowledge of the local subchannel conditions within the bundle is necessary.

In order to determine the local subchannel conditions, the THINC (References 35 & 60) and COBRA (Reference 66) computer codes were developed. In these codes, a rod bundle is considered to be an array of subchannels each of which includes the flow area formed by four adjacent rods. The subchannels are also divided into axial steps so that each may be treated as a control volume. By solving simultaneously the mass, energy, and momentum equations, the local fluid conditions in each control volume are calculated. The W-3 correlation, developed from single-channel data, can be applied to rod bundles by using the subchannel local fluid conditions calculated by the codes.

It was shown by Tong (Reference 34) that the above approach yielded conservative predictions, particularly in rod bundles with mixing vane grid spacers. Hence, a correlation factor was developed to adapt the W-3 correlation (which was developed based on single-channel data) to rod bundles with spacer grids. This correction factor, termed the “Spacer Factor,” was developed as a multiplier on the W-3 correlation.

A “Modified Spacer Factor” was developed from rod bundle DNB test results conducted in the Westinghouse high-pressure water loop at Columbia University. These tests were conducted on non-uniform axial heat flux test sections to determine the DNB performance of a low parasitic, top-split mixing-vane grid design, referred to as the “R” grid. A description of this test program and a summary of the results are given below. The grid used in the 17 x 17 fuel assembly is similar in design to the “R” grid.

"R" grid rod bundle DNB tests (References 36 & 37) were conducted over a wide range of simulated reactor conditions applicable to present PWR designs. These conditions were the following:

Axial grid spacing	20 in., 26 in., and 32 in.
Local DNB quality	-15 to +15%
Local mass velocity	1.6×10^6 to 3.7×10^6 lb/hr-ft^2
Local inlet temperature	440 to 620°F
Pressure	1490 to 2440 psi
Local heat flux	0.3×10^6 to 1.1×10^6 Btu/hr-ft^2
Axial heat flux distribution	Non-uniform (cos u and u sin u)
Heated length	8 ft and 14 ft
Heater rod o.d.	0.422 in.

The experimental program consisted of a DNB test series for both an all-channel and partial-channel surface-heated condition in a 16-rod bundle arranged in a 4 x 4 array. A radial power profile was simulated by operating the central heated rods of the bundle at approximately 15% higher power than the other rods. Two test series were conducted on 26-inch axial grid spacing: (1) all-channel surface-heated condition (typical cell), and (2) partial-channel surface-heated condition (thimble "cold-wall" cell).

For the thimble cold-wall test series, one of the central four heater rods was replaced by an unheated rod. The simulated unheated thimble was made up of a thin steel rod over which were placed ceramic cylinders with an outer diameter equal to the thimble outer diameter. This thimble was attached to the grid in the same manner as in the reactor core using a sleeve brazed into the grid and then bulged out above and below the grid to connect to the thimble.

These rod bundle DNB data were analyzed and a "modified" spacer factor (References 36 & 37) was developed to conservatively incorporate the "R" mixing-vane grid benefit for both typical and cold-wall cells. This modified spacer factor is:

$$F'_S = \left(\frac{P}{225.896}\right)^{0.5} (1.445 - 0.0371L)(e^{(x+0.2)^2} - 0.73) + K_S\left(\frac{G}{10^6}\right)\left(\frac{TDC}{0.019}\right)^{0.35} \qquad (4.4\text{-}6)$$

where:

P = primary system pressure, psia

L = total heated core length, ft

x = local quality expressed in fractional form

G = local mass velocity, lb/hr-ft^2

TDC = thermal diffusion coefficient

K_S= axial grid spacing coefficient that has the following values:

Grid Spacing (in.)	K_S
32	0.027
26	0.046
20	0.066

Figure 4.4-5 presents all "R" grid typical cell data. Figure 4.4-6 shows all the "R" grid thimble cell data. The predicted heat flux in Figures 4.4-5 and 4.4-6 incorporates the modified spacer factor per Equation 4.4-7 for typical cells and Equation 4.4-8 for thimble cold-wall cells:

$$q''_{PRED} = q''_{\substack{DNB,N \\ W-3}} \times F'_S \qquad (4.4\text{-}7)$$

where:

$q''_{\substack{DNB,N \\ W-3}}$ =predicted non-uniform DNB heat flux using the W-3 correlation as described in Reference 40

$$q''_{PRED} = q''_{\substack{DNB,N,CW \\ W-3}} \times F'_S \qquad (4.4\text{-}8)$$

where:

$q''_{\substack{DNB,N,CW \\ W-3}}$ =predicted non-uniform DNB heat flux with flow cell having a cold (unheated) wall evaluated with the W-3 cold-wall correlation described in Section 4.4.2.3.2 and Reference 33

F'_S defined in Equation 4.4-6 is the same in both Equations 4.4-7 and 4.4-8 for both typical and thimble cold-wall cells.

Effect of 17 x 17 Geometry on DNB

The initial 17 x 17 fuel assembly design incorporated seven grids, two end-grids and five mixing vane grids, and a grid spacing of approximately 26 inches. A DNB test program similar to the one described for the "R" grid was conducted at the Westinghouse high-pressure water loop at Columbia University (Reference 4). In this test program, DNB data were obtained for 17 x 17 fuel assembly geometry in a 5 x 5 rod bundle array. Test results were obtained for typical cells (all walls heated) in 8-foot and 14-foot bundles with uniform axial heat flux, and for thimble cold-wall cells in 8-foot bundles with uniform axial heat flux.

The final 17 x 17 fuel assembly design incorporated an additional mixing vane grid with a nominal grid spacing of 22 inches. An additional DNB test program was conducted to provide data applicable to the 17 x 17 fuel assembly with 22-inch axial grid spacing (Reference 38). In this test program, DNB data were obtained for 17 x 17 fuel assembly geometry in a 5 x 5 rod bundle array. Test results were obtained for typical cells (all walls heated) in 8-foot and 14-foot bundles with uniform axial heat flux, and for 14-foot typical and thimble cold-wall cells with non-uniform axial heat flux. All bundles were for mixing-vane spacings of 22 inches. The actual 17 x 17 fuel assembly geometry incorporated in the design of this plant includes nominal grid spans of approximately 20 inches.

The data obtained in these test programs were analyzed with the existing "R" grid DNB correlation described above to determine the effect on DNB of the 17 x 17 fuel assembly geometry. Plots of ratio of measured to predicted DNB heat flux versus flow parameters showed that the "R" grid correlation properly accounts for local fluid parameters. However, the "R" grid correlation consistently overpredicted the DNB heat flux. Hence, a multiplier of 0.88 on the modified spacer factor F'_s is required to correctly predict the magnitude of the DNB heat flux for 17 x 17 geometry.

Figures 4.4-7 and 4.4-8 show the 17 x 17 data obtained in these test programs. The predicted heat flux includes the 0.88 multiplier on the modified spacer factor, Equation 4.4-6, as noted above.

Westinghouse applied the design criterion that DNB will not occur at a 95% probability with a 95% confidence level to the DNB test data from the testing with mixing vane spacings of 22 inches to obtain a DNBR limit for application to the actual 17 x 17 fuel assembly geometry (approximately 20 inch grid spacing) incorporated in the design of this plant. The DNB design criterion is discussed in Section 4.4.1.1. In order to meet this criterion, a limiting value of DNBR was determined by the method of Owen (Reference 39). Owen has prepared tables that give values of kp such that "at least a proportion P of the population is greater than $M/P_{-kp}s$ with confidence γ," where M/P and s are the sample mean and standard deviation, respectively. When this method was carried out using the data in Figure 4.4-7, the results indicated that a reactor core using this geometry may operate with a minimum DNBR of 1.28 and satisfy the design criterion. However, a minimum DNBR of 1.30 is used in design calculations for the 17 x 17 fuel assembly geometry for which the W-3 correlation with the Modified Spacer Factor and 0.88 multiplier is the applicable DNB correlation.

4.4.2.3.2 Definition of Departure from Nucleate Boiling Ratio

4.4.2.3.2.1 *W-3 Correlation.* The DNB heat flux ratio (DNBR) as applied to the 17 x 17 design when all flow cell walls are heated (typical cell) is:

$$DNBR = \frac{q''_{DNB,N} \times 0.88 \times F'_s}{q''_{loc}} \qquad (4.4\text{-}9)$$

where:

$$q''_{DNB,\,N} = \frac{q''_{DNB,\,EU}}{F} \tag{4.4-10}$$

and $q''_{DNB,\,EU}$ is the uniform DNB heat flux as predicted by the W-3 DNB correlation (Reference 40) when all flow cell walls are heated.

F is the flux shape factor to account for non-uniform axial heat flux distributions (Reference 40) with the "C" term modified as in Reference 33.

F'_S is the modified spacer factor defined by Equation 4.4-6 in Section 4.4.2.3.1 and using an axial grid spacing coefficient, Ks = 0.046, and a thermal diffusion coefficient (TDC) of 0.038, based on the 26-inch grid-spacing data previously described. Since the actual grid spacing is approximately 20 inches, these values are conservative, since the DNB performance was found to improve, and TDC increases as axial grid spacing decreases (References 36 & 41).

q''_{loc} is the actual local heat flux.

The DNB heat flux ratio as applied to this design when a cold wall is present is:

$$DNBR = \frac{q''_{DNB,\,N,\,CW} \times 0.88 \times F'_s}{q''_{loc}} \tag{4.4-11}$$

where:

$$q''_{DNB,\,N,\,CW} = \frac{q''_{DNB,\,EU,\,Dh} \times CWF}{F} \tag{4.4-12}$$

where:

$q''_{DNB,\,EU,\,Dh}$ = uniform DNB heat flux as predicted by the W-3 cold-wall DNB correlation (Reference 33) when not all flow cell walls are heated (thimble cold-wall cell).

$$\text{CWF (Reference 33)} = 1.0 - Ru\left[13.76 - 1.372e^{1.78X} - 4.732\frac{G}{10^6}^{-0.0535} - 0.0619\left(\frac{P}{1000}\right)^{0.14} - 8.509Dh^{0.107}\right] \tag{4.4-13}$$

and Ru = 1 - De/Dh.

F'_s as defined by Equation 4.4-6 in Section 4.4.2.3.1 is the same as used for a typical cell.

Values of minimum DNB using the W-3 correlation for the original design are the limiting values obtained by applying the above two definitions of DNBR to the appropriate cell (typical cell with all walls heated, or a thimble cold-wall cell with a partial heated wall condition).

The procedures used in the evaluation of DNB margin for the original design showed that the calculated minimum DNBR for the peak rod or rods in the core will be above 1.30 during Class I and II incidents, even when all the engineering hot-channel factors described in Section 4.4.2.3.4 occur simultaneously in these channels. In reality, the probability of this simultaneous occurrence is negligibly small and substantial increases in local heat flux or coolant temperature could be tolerated without violation of the design basis.

4.4.2.3.2.2 *WRB-1 Correlation.* The WRB-1 Correlation (Reference 1), was developed exclusively from Westinghouse rod mixing vane grid bundle data based on local fluid conditions. This correlation accounts directly for both typical and thimble cold wall cell effects, uniform and non-uniform heat flux profiles, and variations in rod heated length and in grid spacing.

The DNB heat flux ratio (DNBR) as applied to the 17 x 17 design when all flow cell walls are heated (typical cell) and when a cold wall is present (thimble cell) is:

$$DNBR = \frac{q''_{DNB,N}}{q''_{loc}} \tag{4.4-14}$$

where:

$$q''_{DNB,N} = \frac{q''_{DNB,EU}}{F} \tag{4.4-15}$$

and $q''_{DNB,N,EU}$ is the uniform DNB heat flux as predicted by the WRB-1 DNB correlation (Reference 1) and q''_{loc} is the actual local heat flux. F is the flux shape factor to account for non-uniform axial heat flux distributions (Reference 40 with the "C" term modified as in Reference 33).

The applicable range of variables for the WRB-1 correlation is:

Pressure	$1440 \le P \le 2490$ psia
Local Mass Velocity	$0.9 \le G_{loc}/10^6 \le 3.7$ lb/ft^2-hr
Local Quality	$-0.2 \le X_{loc} \le 0.3$
Heated Length[1]	$L_h \le 14$ feet
Grid Spacing	$13 \le g_{sp} \le 32$ inches
Equivalent Hydraulic Diameter	$0.37 \le d_e \le 0.60$ inches
Equivalent Heated Hydraulic Diameter	$0.46 \le d_h \le 0.59$ inches

Figure 4.4-9 shows measured critical heat flux plotted against predicted critical heat flux using the WRB-1 Correlation.

1. Inlet to CHF location.

Included in the data used to develop the WRB-1 Correlation is the DNB data obtained from the test program for the 17 x 17 fuel assembly with 22-inch grid spacing (Reference 38). Test results were obtained for typical cells (all walls heated) in 8-foot and 14-foot bundles with uniform axial heat flux and for 14-foot typical and thimble cold wall cells with nonuniform axial heat flux.

As stated in Section 4.4.1.1 Westinghouse chose the DNBR limit of the DNB correlation such that there is a 95% probability with 95% confidence that DNB will not occur when the calculated DNBR is at the DNBR limit. In order to meet this criterion, the DNBR limit value is determined by the method of Owen (Reference 39).

4.4.2.3.3 Mixing Technology

The rate of heat exchange by mixing between flow channels is proportional to the difference in the local mean fluid enthalpy of the respective channels, the local fluid density, and flow velocity. The proportionality is expressed by the dimensionless thermal diffusion coefficient, TDC, which is defined as:

$$TDC = \frac{w'}{\rho V a} \tag{4.4-16}$$

where:

w' = flow exchange rate per unit length, lb/ft-sec

ρ = fluid density, lbm/ft^3

V = fluid velocity, ft/sec

a = lateral flow area between channels per unit length, ft^2/ft

As a part of a research and development program, Westinghouse sponsored and directed mixing tests at Columbia University (Reference 41). These series of tests, using the “R” mixing-vane grid design on 13-inch, 26-inch, and 32-inch grid spacing, were conducted in pressurized-water loops at Reynolds numbers similar to that of a PWR core under the following single- and two-phase (subcooled boiling) flow conditions.

Pressure	1500 to 2400 psia
Inlet temperature	331 to 619°F
Mass velocity	0.945 to 3.8 × 10^6 lb$_m$/hr-ft^2
Reynolds number	1.34 to 7.69 × 10^5
Bulk outlet quality	-52.1 to -13.5%

TDC was determined by comparing the THINC code predictions with the measured subchannel exit temperatures. Data for 26-inch axial grid spacing are presented in Figure 4.4-10 where the thermal diffusion coefficient is plotted versus the Reynolds number. TDC was found to

be independent of Reynolds number, mass velocity, pressure, and quality over the ranges tested. The two-phase data (local, subcooled boiling) fell within the scatter of the single-phase data. The effect of two-phase flow on the value of TDC has been demonstrated by Cadek et al. (Reference 41), Rowe and Angle (References 42 & 43), and Gonzalez-Santalo and Griffith (Reference 44). In the subcooled boiling region, the values of TDC were indistinguishable from the single-phase values. In the quality region, Rowe and Angle showed that in the case with rod spacing similar to that in PWR reactor core geometry, the value of TDC increased with quality to a point and then decreased, but never below the single-phase value. Gonzalez-Santalo and Griffith showed that the mixing coefficient increased as the void fraction increased.

The data from the tests on the 15 x 15 “R” grid in Reference 41 showed that a design TDC value of 0.038 (for 26-inch grid spacing) can be used in determining the effect of coolant mixing in the THINC analysis.

A mixing test program similar to the one described above was conducted at Columbia University for the 17 x 17 geometry and mixing-vane grids on 26-inch spacing (Reference 45). The mean value of TDC obtained from these tests was 0.059, and all data was well above the design value of 0.038.

Since the actual reactor grid spacing for the final 17 x 17 fuel assembly geometry is approximately 20 inches, additional margin is available for this design, since the value of TDC increases as the axial grid spacing decreases.

4.4.2.3.4 Hot-Channel Factors

The total hot-channel factors for heat flux and enthalpy rise are defined as the maximum-to-core-average ratios of these quantities. The heat flux hot-channel factor considers the local maximum linear heat generation rate at a point (the hot spot), and the enthalpy rise hot-channel factor involves the maximum integrated value along a channel (the hot-channel).

Each of the total hot-channel factors considers a nuclear hot-channel factor (Section 4.4.3.2), describing the neutron power distribution, and an engineering hot-channel factor, which allows for variations in flow conditions and fabrication tolerances. The engineering hot-channel factors are made up of subfactors that account for the influence of the variations of fuel pellet diameter, density, enrichment, and eccentricity; fuel rod diameter, pitch, and bowing; inlet flow distribution; flow redistribution; and flow mixing.

4.4.2.3.4.1 *kW/ft Engineering Hot-Channel Factor,* F_Q^E . The kW/ft engineering hot channel factor is used to evaluate the maximum linear heat generation rate in the core. This subfactor is determined by statistically combining the fabrication variations for fuel pellet diameter, density, and enrichment, and has a value of 1.03 at the 95% probability level with 95% confidence. As shown in Reference 46, no DNB penalty need be taken for the short relatively low intensity heat flux spikes caused by variations in the above parameters, as well as fuel pellet eccentricity and fuel rod diameter variation.

4.4.2.3.4.2 *Enthalpy Rise Engineering Hot-Channel Factor,* $F^E_{\Delta H}$. The following effects of fabrication tolerances and variations in flow conditions are considered in the core thermal subchannel analysis (Section 4.4.3.4.1).

1. Pellet Diameter, Density, and Enrichment

   The effect of variations in pellet diameter, density, and enrichment is employed in the subchannel analyses as an engineering factor on the enthalpy rise ($F^E_{\Delta H}$). This factor is accounted for by increasing the relative power of the hot fuel rod. This factor ($F^E_{\Delta H}$) has a value of 1.02 for use in non-statistical DNB analyses. In the statistical DNB methodologies, the variations in pellet diameter, density, and enrichment are considered statistically in establishing the design DNBR limit (Section 4.4.1.1).

   Design values employed in the subchannel analyses related to the above fabrication variations are based on applicable limiting tolerances such that these design values are met for 95% of the limiting channels at a 95% confidence level. Measured manufacturing data on Westinghouse 17 x 17 fuel show that the tolerances are conservative. In addition, each fuel assembly is checked to ensure that the channel spacing design criteria are met.

2. Fuel Rod Diameter, Pitch, and Bowing

   The fuel rod diameter, pitch, and bowing variations, including inpile effects, are covered by the rod bow penalty.

   A request for a rod bow penalty reduction which was based upon a revised rod bow evaluation methodology (Reference 84) was submitted to the NRC. Previously, the rod bow penalty was met by a combination of retained DNBR margin and a Technical Specification penalty upon ($F^N_{\Delta H}$). The NRC approval (Reference 91) of the submittal permitted the removal of the Technical Specification ($F^N_{\Delta H}$) penalty, since the revised rod bow penalty was entirely accommodated by the retained DNBR margin. The NRC subsequently approved a reduction in the burn-up at which the DNBR penalties and peaking factor uncertainties are calculated, from 33,000 to 24,000 MWD/MTU (Reference 92).

3. Inlet Flow Maldistribution

   The consideration of inlet flow maldistribution in core thermal performances is discussed in Section 4.4.3.1.2. Inlet maldistribution is considered in the subchannel analysis by using an inlet flow reduction to the hot assembly. A 5% reduction in coolant flow to the hot assembly is used in design calculations.

4. Flow Redistribution

   Flow redistribution is the reduction in flow in the hot channel resulting from the high flow resistance in the channel due to the local or bulk boiling. The effect of the non-uniform flow distribution is inherently considered in the subchannel analysis by including boiling and cross flow effects between subchannels.

5. Flow Mixing

   Flow mixing is considered in the subchannel analysis by using a thermal diffusion coefficient (TDC) determined from subchannel mixing tests. The subchannel mixing model incorporated in the codes and used in reactor design is based on this experimental data as discussed in Sections 4.4.2.3.3 and 4.4.2.10.8. The mixing vanes incorporated in the spacer grid design induce additional flow mixing between the various flow channels in a fuel assembly as well as between adjacent assemblies. This mixing reduces the enthalpy rise in the hot channel resulting from local power peaking or unfavorable mechanical tolerances.

4.4.2.4 Flux Tilt Considerations

Significant quadrant power tilts are not anticipated during normal operation since this phenomenon is caused by some asymmetric perturbation. A dropped or misaligned rod cluster control assembly could cause changes in hot-channel factors; however, these events are analyzed separately in Chapter 15. This discussion will be confined to flux tilts caused by x-y xenon transients, inlet temperature mismatches, enrichment variations within tolerances, and so forth.

The design value of the enthalpy rise hot channel factor $F_{\Delta H}$ as discussed in Section 4.3.2.2.7 together with the uncertainty accounted for in the Statistical DNBR Evaluation Methodology is assumed to be sufficiently conservative that flux tilts up to and including the alarm point (see the Technical Specifications) will not result in values of $F^N_{\Delta H}$ greater than that assumed in the analysis. The design value of F_Q does not include a specific allowance for quadrant flux tilts.

4.4.2.5 Void Fraction Distribution

The calculated core average and the hot-subchannel maximum and average void fractions are presented in Table 4.4-4 for operation at full power with design hot-channel factors. The void fraction distribution in the core at various radial and axial locations is presented in Reference 47. The void models are described in Section 4.4.2.8.3.

Since void formation due to subcooled boiling is an important promoter of interassembly flow redistribution, a sensitivity study was performed with THINC-IV using the void model referenced above (Reference 47).

The results of this study showed that because of the realistic crossflow model, the minimum DNBR in the hot channel is relatively insensitive to variations in this model. The range of variations considered in this sensitivity study covered the maximum uncertainty range of the data used to develop each part of the void fraction correlation.

4.4.2.6 Core Coolant Flow Distribution

Assembly average coolant mass velocity and enthalpy at various radial and axial core locations for a representative loading are given below. Coolant enthalpy rise and flow distributions

are shown for the 4-foot elevation (one-third of core height) in Figure 4.4-11, and 8-foot elevation (two-thirds of core height) in Figure 4.4-12, and at the core exit in Figure 4.4-13. These distributions are for the full-power conditions as given in Table 4.4-1 and for the radial power density distribution shown in Figure 4.3-8. The THINC code analysis for this case used a uniform core inlet enthalpy and inlet flow distribution.

4.4.2.7 **Core Pressure Drops and Hydraulic Loads**

4.4.2.7.1 Core Pressure Drops

The analytical model and experimental data used to calculate the pressure drops shown in Tables 4.4-1 and 4.4-2 are described in Section 4.4.2.8. The core pressure drop includes the fuel assembly, lower core plate, and upper core plate pressure drops. The full-power operation pressure drop values shown in Tables 4.4-1 and 4.4-2 are the unrecoverable pressure drops across the vessel, including the inlet and outlet nozzles, and across the core. The pressure drops in Tables 4.4-1 and 4.4-2 are based on either the thermal-design or the best-estimate flow for actual plant operating conditions as described in Section 5.1.2. Section 5.1.2 defines and describes the best estimate flow which is the most likely value for the actual plant operating condition, the thermal design flow (minimum flow) which is the basis for reactor core thermal performance (except as noted in Section 5.1.2) and the mechanical design flow (maximum flow) which is used in the mechanical design of the reactor vessel internals and fuel assemblies. Since the best-estimate flow is that flow which is most likely to exist in an operating plant, the calculated core pressure drops using the best-estimate flow are more representative of the actual pressure drops than those using the thermal design flow.

Uncertainties associated with the core pressure drop values are discussed in Section 4.4.2.10.2.

The pressure drops quoted in Table 4.4-1 for the original 17 x 17 design are based on seven grids and conservatively estimated grid pressure loss coefficients. Fuel assembly pressure drop testing was conducted in a single assembly vessel, isothermal flow loop, known as D Loop. Phase 1 of the D-loop tests (Reference 5) resulted in a measured core pressure drop of magnitude sufficiently lower than the predicted pressure drop. The pressure drops quoted in Table 4.4-1 for the original 17 x 17 design were determined to be conservative even with the addition of an eighth grid. This result was reaffirmed by later phases of the D-loop tests. The conservatively estimated grid pressure loss coefficients used in the calculation of the predicted pressure drop in Reference 5 are the same conservatively estimated grid pressure loss coefficients used for the Table 4.4-1 pressure drop calculations for the original 17 x 17 design. Thus, it was expected that the calculated pressure drop would be conservative (larger) relative to the measured value.

The fuel assembly loss coefficients and pressure drops are determined for all significant changes to the fuel assembly and reactor operating conditions.

4.4.2.7.2 Hydraulic Loads

The fuel assembly triple leaf hold-down springs, shown on Figure 4.2-2, are designed to keep the fuel assemblies in contact with the lower core plate under all Condition I and II events with the exception of the turbine overspeed transient associated with a loss of external load. The hold-down springs are designed to tolerate the possibility of an overdeflection associated with fuel assembly lift-off for this case and provide contact between the fuel assembly and the lower core plate following this transient. More adverse flow conditions can occur during a LOCA. These conditions are presented in Section 15.4.1.

Hydraulic loads at normal operating conditions are calculated considering the mechanical design flow that is described in Section 5.1 and accounting for the minimum core bypass flow based on manufacturing tolerances. Core hydraulic loads at cold plant start-up conditions are also based on this flow but are adjusted to account for the coolant density difference. Conservative core hydraulic loads for a pump overspeed transient, which could possibly create flow rates 20% greater than the mechanical design flow, are evaluated to be approximately twice the fuel assembly weight.

Core hydraulic loads were measured during the prototype assembly tests described in Section 1.5. Reference 5 contains a detailed discussion of the results.

Lift forces are directly proportional to the pressure drop. The lift force on an eight-grid assembly is thus less than 5% greater than the lift force on a seven-grid assembly for the same flow rate. Reference 5 shows that lift-off of an eight-grid fuel assembly (5% greater than the seven-grid assembly shown) is not predicted to occur during a postulated pump overspeed transient even though it is not necessary to preclude lift-off. The effect of start-up and shutdown transients is shown to be inconsequential in Reference 5.

The fuel assembly lift forces are determined for all significant changes to the fuel assembly and reactor operating conditions and demonstrated to meet the design constraints discussed in this section.

4.4.2.8 **Correlation and Physical Data**

4.4.2.8.1 Surface Heat Transfer Coefficients

Forced convection heat transfer coefficients are obtained from the familiar Dittus-Boelter correlation (Reference 48), given below, with the properties evaluated at bulk fluid conditions,

$$\frac{hD_e}{K} = 0.023\frac{D_eG}{\mu}^{0.8}\frac{C_p\mu}{K}^{0.4} \qquad (4.4\text{-}17)$$

where:

h = heat transfer coefficient, Btu/hr-ft^2-°F

D_e = equivalent diameter, ft

K = thermal conductivity, Btu/hr-ft-°F

G = mass velocity, lb/hr-ft^2

μ= dynamic viscosity, lb/ft-hr

C_p = heat capacity, Btu/lb-°F

This correlation has been shown to be conservative (Reference 49) for rod bundle geometries with pitch-to-diameter ratios in the range used by PWRs.

The onset of nucleate boiling occurs when the clad wall temperature reaches the amount of superheat predicted by Thom's (Reference 50) correlation. After this occurrence, the outer clad wall temperature is determined by the Thom's correlation in the fuel rod thermal evaluations (References 98, 102, & 106).

$$\Delta T_{sat} = [0.072 \exp(-P/1260)]\,(q'')^{0.5} \qquad (4.4\text{-}18)$$

where:

ΔT_{sat} = wall superheat, T_w - T_{sat}, °F

q" = wall heat flux, Btu/hr-ft^2

P = pressure, psia

T_w = outer clad wall temperature, °F

T_{sat} = saturation temperature of coolant at P, °F

THINC-IV (References 47 & 58) uses the Thom's correlation to predict the inception of nucleate boiling and to select the void fraction correlation (see Section 4.4.2.8.3). The COBRA IIIC/MIT computer code (Reference 88), however, uses the Jens and Lottes correlation (Reference 103) to predict the inception of nucleate boiling.

4.4.2.8.2 Total Core and Vessel Pressure Drop

Unrecoverable pressure losses occur as a result of viscous drag (friction) and/or geometry changes (form) in the fluid flow path. The flow field is assumed to be incompressible, turbulent, single-phase water. These assumptions apply to the core and vessel pressure drop calculations for the purpose of establishing the primary loop flow rate. Two-phase considerations are neglected in the vessel pressure drop evaluation because the core average void is negligible (see Section 4.4.2.5 and Table 4.4-4). Two-phase flow considerations in the core thermal subchannel analyses are considered and the models are discussed in Section 4.4.3.1.3. Core and vessel pressure losses are calculated by equations of the form:

$$P_L = \left(K + f\frac{L}{D_e}\right)\frac{\rho\ V^2}{2\ g_c(144)} \qquad (4.4\text{-}19)$$

where:

P_L = unrecoverable pressure drop, lb_f/in^2

ρ = fluid density, lbm/ft^3

L = length, ft

D_e = equivalent diameter, ft

V = fluid velocity, ft/sec

$$g_c = 32.174 \frac{lb_m - ft}{lb_f - second^2}$$

K = form loss coefficient, dimensionless

f = friction loss coefficient, dimensionless

Fluid density is assumed to be constant at the appropriate value for each component in the core and vessel. Because of the complex core and vessel flow geometry, precise analytical values for the form and friction loss coefficients were not available. Therefore, experimental values for these coefficients were obtained from geometrically similar models.

Values are quoted in Tables 4.4-1 and 4.4-2 for unrecoverable pressure loss across the reactor vessel, including the inlet and outlet nozzles, and across the core. The results of full-scale tests of core components and fuel assemblies were used in developing the core pressure loss characteristic. The pressure drop for the vessel was obtained by combining the core loss with correlation of one-seventh scale model hydraulic test data on a number of vessels (References 51 & 52) and form loss relationships (Reference 53). Moody (Reference 54) curves were used to obtain the single- phase friction factors.

Core pressure drops were confirmed by Phase 1 and later phases of the D-loop tests (Reference 5) for the original 17 x 17 design. These hydraulic verification tests included hydraulic head losses and effects of velocity changes as well as unrecoverable pressure losses. The effects of velocity changes are small, since the static pressure taps are located at elevations of approximately equal flow areas (and therefore approximately equal velocities). When wall static pressure taps are used near ambient fluid conditions, it can be shown analytically that the elevation head losses do not contribute to the measured core pressure drops. Therefore, data from the hydraulic verification tests can be directly applied to confirm the pressure drop values for the original 17 x 17 design quoted in Table 4.4-1, which are based on unrecoverable pressure losses only.

In addition, as discussed in Section 4.4.4.1, tests on the RCS were made before initial criticality to demonstrate that a conservative RCS coolant flow rate had been used in the original design and analyses of the plant, and tests are performed on a periodic basis to ensure that the measured RCS flow continues to meet the applicable requirements. This ensures that the pressure losses calculated by the method described here are conservative.

4.4.2.8.3 Void Fraction Correlation

There are three separate void regions considered in the flow boiling calculation in the THINC-IV computer code (References 47 & 58). These are illustrated in Figure 4.4-14. They are the wall void region (no bubble detachment), the subcooled boiling region (bubble detachment), and the bulk boiling region. In the wall void region, the point where local boiling begins is determined when the clad temperature reaches the amount of superheat predicted by Thom's (Reference 50) correlation (discussed in Section 4.4.2.8.1). The void fraction in this region is calculated using Maurer's (Reference 55) relationship. The bubble detachment point, where the superheated bubbles break away from the wall, is determined by using Griffith's (Reference 56) relationship. The void fraction in the subcooled boiling region (i.e., after the detachment point) is calculated from the Bowring (Reference 57) correlation. This correlation predicts the void fraction from the detachment point to the bulk boiling region. The void fraction in the bulk boiling region is predicted by using homogeneous flow theory and assuming no slip. The void fraction in this region is therefore a function only of the thermodynamic quality.

Void fractions are predicted in the COBRA IIIC/MIT Computer Code (Reference 88) using the Smith void fraction correlation (Reference 104) in conjunction with the Levy subcooled void model (Reference 105). The Levy model uses local heat flux and fluid conditions in predicting the true (non-equilibrium) quality. This true quality is then used in the Smith correlation to predict the void fraction in both the subcooled and bulk boiling regions.

4.4.2.9 **Thermal Effects of Operational Transients**

DNB core safety limits are generated as a function of coolant temperature, pressure, core power, and the axial and radial power distributions. Operation within these DNB safety limits insures that the DNB design basis is met for both steady-state operation and for anticipated operational transients that are slow with respect to fluid transport delays in the primary system. In addition, for fast transients, e.g., uncontrolled rod bank withdrawal at power incident, specific protection functions are provided as described in Chapter 7 and the use of these protection functions are described in Chapter 15. The thermal response of the fuel is discussed in Section 4.4.3.7.

4.4.2.10 **Uncertainties in Estimates**

4.4.2.10.1 Uncertainties in Fuel and Clad Temperatures

As discussed in Section 4.4.2.2, the fuel temperature is a function of crud, oxide, clad, gap, and pellet conductances. Uncertainties in the fuel temperature calculation are essentially of two types: (1) fabrication uncertainties such as variations in the pellet and clad dimensions and the pellet density, and (2) model uncertainties such as variations in the pellet conductivity and the gap conductance. For the current thermal model (Reference 102), these uncertainties were quantified by comparison of the thermal model predictions with inpile thermocouple measurements The uncertainties are also based on out-of-pile measurements of the fuel and clad properties, and measurements of the fuel and clad dimensions during fabrication. The resulting uncertainties are

then used in evaluations involving the fuel temperature. The effect of densification on fuel temperature uncertainties is discussed in Reference 6, and the fuel densification model used in current fuel temperature calculations is presented in Reference 98.

In addition to the temperature uncertainty described above, the measurement uncertainty in determining the local power and the effect of density and enrichment variations on the local power are considered in establishing the heat flux hot-channel factor. These uncertainties are described in Section 4.3.2.2.1.

Reactor trip setpoints as specified in the Technical Specifications include allowance for instrument and measurement uncertainties such as calorimetric error, instrument drift and channel reproducibility, temperature measurement uncertainties, noise, and heat capacity variations.

Uncertainty in determining the cladding temperature results from uncertainties in the crud and oxide thickness. Because of the excellent heat transfer between the surface of the rod and the coolant, the film temperature drop does not appreciably contribute to the uncertainty.

4.4.2.10.2 Uncertainties in Pressure Drops

Core and vessel pressure drops are quoted in Tables 4.4-1 and 4.4-2. The uncertainties quoted are based on the uncertainties in both the test results and the analytical extension of these values to the reactor application.

A major use of the core and vessel pressure drops is to determine the reactor coolant system (RCS) coolant flow rates, as discussed in Section 5.1. In addition, as discussed in Section 4.4.4.1, tests on the RCS were made before initial criticality to demonstrate that a conservative RCS coolant flow rate had been used in the original design and analyses of the plant, and are performed on a periodic basis to ensure that the measured RCS flow continues to meet the applicable requirements.

4.4.2.10.3 Uncertainties Due to Inlet Flow Maldistribution

The effects of uncertainties in the inlet flow maldistribution criteria used in the core thermal analyses are discussed in Section 4.4.3.1.2.

4.4.2.10.4 Uncertainty in DNB Correlation

The uncertainty in the DNB correlation can be written as a statement on the probability of not being in DNB based on the statistics of the DNB data as discussed in Section 4.4.2.3.

4.4.2.10.5 Uncertainties in DNBR Calculations

The uncertainties in the DNBRs due to uncertainties in the nuclear peaking factors were accounted for by applying an 8% uncertainty factor in the design basis for the radial power factor (see Section 4.3.2.2.6). This 8% consists of 4% calculational uncertainty and 4% measurement uncertainty. For statistical DNBR analysis, the 4% calculational uncertainty is added to the predicted value and the 4% measurement uncertainty is included in the determination of the

statistical DNBR design limit (see Section 4.4.1.1). For non-statistical DNB analysis, the full 8% uncertainty is added to the predicted value. Values for the engineering hot-channel factors are used in the DNBR calculations as discussed in Section 4.4.2.3.4. The results of a sensitivity study (Reference 47) with THINC-IV showed that the minimum DNBR in the hot channel is relatively insensitive to variations in the corewide radial power distribution (for the same value of $F^N_{\Delta H}$).

The ability of the THINC-IV computer code to accurately predict flow and enthalpy distributions in rod bundles is discussed in Section 4.4.3.4.1 and in Reference 58. Studies have been performed (Reference 47) to determine the sensitivity of the minimum DNBR in the hot channel to the void fraction correlation (see also Section 4.4.2.8.3); the inlet velocity and exit pressure distributions assumed as boundary conditions for the analysis; and the grid pressure loss coefficients. The results of these studies show that the minimum DNBR in the hot channel is relatively insensitive to variations in these parameters. The range of variations considered in these studies covered the range of possible variations in these parameters.

4.4.2.10.6 Uncertainties in Flow Rates

Section 5.1.2 describes three flow rates that are used in the core thermal performance calculations: minimum measured flow, lower-bounding design flow, and thermal design flow. The minimum measured flow is the minimum allowable RCS Total Flow Rate and is less than the best-estimate flow rate. The minimum measured flow, as stated in Section 15.1.2.2, is used to analyze those events for which the Virginia Power Statistical Evaluation Methodology is the governing DNB methodology. The lower-bounding design flow is less than the minimum measured flow by an amount which accommodates the uncertainty associated with the methods used to measure, and confirm, the minimum allowable RCS Total Flow Rate. The lower-bounding design flow is greater than the thermal design flow and is used to analyze other DNBR-related transients and events which are limited by considerations such as heat sink or pressurization criteria. The thermal design flow is the basis for the original core thermal performance evaluation and is the basis for the reactor core thermal performance (except as noted above), the steam generator thermal performance, and the nominal plant parameters used throughout the design. In addition, a portion of the assumed design flow is assumed to be ineffective for the purposes of core heat removal capability because it bypasses the core. The various available vessel flow paths considered in the calculation of the core bypass flow are described in Section 4.4.3.1.1.

4.4.2.10.7 Uncertainties in Hydraulic Loads

As discussed in Section 4.4.2.7.2, hydraulic loads on the fuel assembly were evaluated for a pump overspeed transient that creates flow rates 20% greater than the mechanical design flow. The mechanical design flow, as stated in Section 5.1, is greater than the best-estimate or most likely flow rate value for the actual plant operating condition (by approximately 2%).

4.4.2.10.8 Uncertainty in Mixing Coefficient

The value of the mixing coefficient, TDC, used in original THINC analyses for North Anna was 0.038. The mean value of TDC obtained in the "R" grid mixing tests described in Section 4.4.2.3.1 was 0.042 (for 26-inch grid spacing; seven grid fuel assembly). The value of 0.038 is one standard deviation below the mean value; and approximately 90% of the data gives values of TDC greater than 0.038 (Reference 41).

The results of the mixing tests done on 17 x 17 geometry, as discussed in Section 4.4.2.3.3, for a 22-inch grid spacing (eight grid fuel assembly) had a mean value of TDC of 0.059 and standard deviation of $\sigma = 0.007$.

4.4.2.11 **Plant Configuration Data**

Plant configuration data for the thermal-hydraulic and fluid systems external to the core are provided in the appropriate chapters (5, 6, and 9). Implementation of the emergency core cooling system is discussed in Chapter 15. Some specific areas of interest are the following:

1. Total coolant flow rates for the reactor coolant system and each loop are provided in Table 5.1-1. Flow rates employed in the evaluation of the core are presented in Section 4.4.
2. Total reactor coolant system volume including pressurizer and surge line, and reactor coolant system liquid volume including pressurizer water at steady-state power conditions are given in Table 5.1-1.
3. Physical data for each component of the reactor coolant system is presented in Section 5.5. The components of the reactor coolant system are water-filled during power operation, with the pressurizer being approximately 63% water- filled.
4. Components of the emergency core cooling system are located so as to meet the criteria for net positive suction head described in Section 6.3.
5. Line lengths and sizes for the safety injection system are determined so as to guarantee a total system resistance that will provide, as a minimum, the fluid delivery rates assumed in the safety analyses described in Chapter 15.
6. The minimum flow areas for components of the reactor coolant system are presented in Section 5.5.
7. The steady-state pressure drops and temperature distributions through the reactor coolant system are presented in Table 5.1-1.

4.4.3 Evaluation

4.4.3.1 Core Hydraulics

4.4.3.1.1 Flow Paths Considered in Core Pressure Drop and Thermal Design

The following vessel flow paths or core bypass flow were considered:

1. Flow through the spray nozzles into the upper head for head-cooling purposes.
2. Flow entering into the rod cluster control guide thimbles to cool the control rods.
3. Leakage flow from the vessel inlet nozzle directly to the vessel outlet nozzle through the gap between the vessel and the barrel.
4. Flow entering into the core from the barrel-baffle region through the gaps between the baffle plates.
5. Flow passing between the peripheral fuel assemblies and the baffle.

The above contributions were evaluated to confirm that the design value of the core bypass flow is met. The design value of core bypass flow for a standard plant is equal to 4.5% of the total vessel flow. Of the total allowance, 2.5% is associated with the internals (items 1, 3, 4, and 5 above) and 2.0% for the core (item 2 above). Calculations were performed for the standard plant using drawing tolerances on a worst-case basis and accounting for uncertainties in pressure losses. Based on these calculations, the core bypass flow for the standard plant is less than or equal to 4.5%.

The bypass flow value for the original North Anna design matched that of the standard plant. The implementation of statistical DNBR methods at North Anna redefined the bypass flow criteria as best estimate and design bypass flow. The statistical DNBR methods utilized a best estimate bypass flow of 3.0%. The non-statistical DNBR methods continued to use the design bypass flow of 4.5%. The removal of the thimble plugs at North Anna, in conjunction with the implementation of the North Anna Improved Fuel product, resulted in an increase in bypass flow. The best estimate bypass flow increased to 4.5% and the design bypass flow increased to 6.5%. North Anna Unit 1 has since been modified for up flow conversion. The bypass flow resulting from the upflow conversion has been evaluated and found to be acceptable.

Flow model test results for the flow path through the reactor are discussed Section 4.4.2.8.2.

4.4.3.1.2 Inlet Flow Distributions

Data has been considered from several one-seventh scale hydraulic reactor model flow tests, References 51, 52, and 59, in arriving at the core inlet flow maldistribution criteria to be used in the code analyses (see Section 4.4.3.4.1). Analyses using this data indicated that a conservative design basis is to consider 5% reduction in the flow to the hot assembly, Reference 60. The same design basis of 5% reduction to the hot assembly inlet are used in THINC-IV and COBRA analyses.

The experimental error estimated in the inlet velocity distribution has been considered as outlined in Reference 47, where the sensitivity of changes in inlet velocity distributions to hot-channel thermal performance is shown to be small. Studies (Reference 47) made with the improved THINC model (THINC-IV) showed that it is adequate to use the 5% reduction in inlet flow to the hot assembly for a loop out of service based on the experimental data in References 51 and 52.

The effect of the total flow rate on the inlet velocity distribution was studied in the experiments of Reference 51. As was expected, on the basis of the theoretical analysis, no significant variation could be found in inlet velocity distribution with reduced flow rate.

4.4.3.1.3 Empirical Friction Factor Correlations

Two empirical friction factor correlations were used in the THINC-IV computer code (described in Section 4.4.3.4.1).

The friction factor in the axial direction, parallel to the fuel rod axis, was evaluated using the Novendstern-Sandberg correlation (Reference 61). This correlation consists of the following:

1. For isothermal conditions, this correlation uses the Moody (Reference 54) friction factor including surface roughness effects.
2. Under single-phase heating conditions, a factor is applied based on the values of the coolant density and viscosity at the temperature of the heated surface and at the bulk coolant temperature.
3. Under two-phase flow conditions, the homogeneous flow model proposed by Owens (Reference 62) is used with a modification to account for a mass velocity and heat flux effect.

The flow in the lateral directions, normal to the fuel rod axis, views the reactor core as a large tube bank. Thus, the lateral friction factor proposed by Idel'chick (Reference 53) is applicable. This correlation is of the form:

$$F_L = A\ Re_L^{-0.2} \qquad (4.4\text{-}20)$$

where:

A = function of the rod pitch and diameter as given in Reference 53

Re_L = lateral Reynolds number based on the rod diameter

Extensive comparisons of THINC-IV predictions using these correlations to experimental data are given in Reference 58, and they verify the applicability of these correlations in PWR design. In contrast to THINC-IV, COBRA-IIIc/MIT code (described in Section 4.4.3.4.1) uses an isothermal friction factor correlation in conjunction with a wall viscosity correlation and a correlation for predicting two-phase friction multipliers in computing single and two-phase pressure drops. These correlations are described in detail in Reference 96.

4.4.3.2 Influence of Power Distribution

The core power distribution that is largely established at beginning of life by fuel enrichment, loading pattern, and core power level is also a function of variables such as control rod worth and position and fuel depletion throughout lifetime. Radial power distributions in various planes of the core are often illustrated for general interest; however, the core radial enthalpy rise distribution as determined by the integral of power up each channel is of greater importance for DNB analyses. These radial power distributions, characterized by $F^N_{\Delta H}$ (defined in Section 4.3.2.2.2), as well as axial heat flux profiles, are discussed in the following two sections.

4.4.3.2.1 Nuclear Enthalpy Rise Hot-Channel Factor, $F^N_{\Delta H}$

Given the local power density q' (kW/ft) at a point x, y, z in a core with N fuel rods and height H,

$$F^N_{\Delta H} = \frac{\text{Hot rod power}}{\text{average rod power}} = \frac{\text{Max}\int_o^H q'(x_o,y_o,z)dz}{\frac{1}{N}\sum_{\substack{\text{all}\\ \text{rods}}}\int_o^H q'(x,y,z)dz} \tag{4.4-21}$$

The way in which $F^N_{\Delta H}$ is used in the DNB calculation is important. The location of minimum DNBR depends on the axial profile, and the value of DNBR depends on the enthalpy rise to that point. Basically, the maximum value of the rod integral is used to identify the most likely rod for minimum DNBR. An axial power profile is obtained which, when normalized to the design value of $F^N_{\Delta H}$, recreates the axial heat flux along the limiting rod. The surrounding rods are assumed to have the same axial profile, with rod average powers that are typical of distributions found in hot assemblies. In this manner, worst-case axial profiles can be combined with worst-case radial distributions for reference DNB calculations.

It should be noted again that $F^N_{\Delta H}$ is an integral and is used as such in the DNB calculations. Local heat fluxes are obtained by using hot-channel and adjacent-channel explicit power shapes that take into account variations in horizontal power shapes throughout the core. The sensitivity of the THINC-IV analysis to radial power shapes is discussed in Reference 47.

For operation at a fraction P of full power, the design $F^N_{\Delta H}$ used (Reference 107) is given by:

$$F^N_{\Delta H} \leq \text{CFDH}\,[1 + \text{PFDH}\,(1 - P)] \tag{4.4-22}$$

where: CFDH = $F^N_{\Delta H}$ at Rated Thermal Power

PFDH = Power Fraction Multiplier for $F^N_{\Delta H}$

$$P = \frac{\text{THERMAL POWER}}{\text{RATED THERMAL POWER}}$$

For the current values CFDH and PFDH, see the Core Operating Limits Report.

The permitted relaxation of $F^N_{\Delta H}$ is included in the DNB protection setpoints and allows radial power shape changes with rod insertion to the insertion limits (Reference 63), thus allowing greater flexibility in the nuclear design.

4.4.3.2.2 Axial Heat Flux Distributions

As discussed in Section 4.3.2.2.4, the axial heat flux distribution can vary as a result of rod motion, power change, or spatial xenon transients that may occur in the axial direction. Consequently, it is necessary to measure the axial power imbalance by means of the ex-core nuclear detectors (as discussed in Section 4.3.2.2.4) and protect the core from excessive axial power imbalance. The reference axial shape used in establishing core DNB limits (that is Overtemperature ΔT protection system setpoints) is a chopped cosine with a peak to average value of 1.55. The Reactor Trip System provides automatic reduction of the trip setpoints on excessive axial power imbalance, i.e., when an extremely large axial offset corresponds to an axial shape that could lead to a DNBR that is less than that calculated for the reference DNB design axial shape. To determine the magnitude of the setpoint reduction, the reference shape is supplemented by other axial shapes skewed to the bottom or top of the core.

The course of those accidents in which DNB is a concern is analyzed in Chapter 15 assuming that the protection setpoints have been set on the basis of these shapes. In many cases the axial power distribution in the hot channel changes throughout the course of the accident due to rod motion, coolant temperature and power level changes.

4.4.3.3 **Core Thermal Response**

A general summary of the steady-state thermal-hydraulic design parameters including thermal output, flow rates, etc., is provided in Tables 4.4-1 and 4.4-2 for all loops in operation for various design conditions. Table 4.4-3 provides these parameters for operation with one coolant loop out of service. Technical Specifications prohibit this mode of operation, but this data was used in the previously applicable two-loop rod withdrawal from power (RWAP) accident described in Chapter 15 (based on the original nominal core heat output of 2775 MWt).

As stated in Section 4.4.1, the design bases of the reactor core are to prevent DNB and to prevent fuel melting for Conditions I and II events. The protective systems described in Chapter 7 are designed to meet these bases. The response of the core to Condition II transients is given in Chapter 15.

4.4.3.4 **Analytical Techniques**

4.4.3.4.1 Core Analysis

The objective of reactor core thermal design is to determine the maximum heat removal capability in all flow subchannels and show that the core safety limits, as presented in the Technical Specifications, are not exceeded while compounding engineering and nuclear effects. The thermal design takes into account local variations in dimensions, power generation, flow redistribution, and mixing. THINC-IV is a realistic three-dimensional matrix model that has been developed to account for hydraulic and nuclear effects on the enthalpy rise in the core (References 47 & 58). The behavior of the hot assembly is determined by superimposing the power distribution among the assemblies upon the inlet flow distribution while allowing for flow mixing and flow distribution between assemblies. The average flow and enthalpy in the hottest assembly is obtained from the corewide, assembly-by-assembly analysis. The local variations in power, fuel rod and pellet fabrication, and mixing within the hottest assembly are then superimposed on the average conditions of the hottest assembly in order to determine the conditions in the hot channel.

The NRC has approved Reference 88 for the use of the Virginia Power version of the COBRA-IIIc/MIT code as an alternative approach for performing steady state and transient reactor core thermal-hydraulic analysis. In contrast to the THINC code described below, the Virginia Power model uses a single-pass method for predicting the thermal and hydraulic behavior of the core, and for calculating DNB ratios. The critical heat flux or DNBR and Mixing Technology described in Section 4.4.2.3 is applied within the COBRA analysis in an analogous manner. The NRC staff found Reference 88 “to be acceptable for referencing by Virginia Power in future reload licensing submittals for North Anna, Surry and future plants of the same design.”

The following sections describe the use of the THINC-IV code in the thermal-hydraulic design evaluation to determine the conditions in the hot channel and to ensure that the safety-related design bases are not violated.

Steady-State Analysis

The THINC-IV computer program determines coolant density, mass velocity, enthalpy, vapor void, static pressure, and DNBR distributions along parallel flow channels within a reactor core under all expected operating conditions. The core region being studied is considered to be made up of a number of contiguous elements in a rectangular array extending the full length of the core. An element may represent any region of the core from a single assembly to a subchannel.

The momentum and energy exchange between elements in the array are described by the equations for the conservation of energy and mass, the axial momentum equation, and two lateral momentum equations that couple each element with its neighbors. The momentum equations used in THINC-IV are similar to the Euler equations (Reference 64), except that frictional loss terms have been incorporated that represent the combined effects of frictional and form drag due to the

presence of grids and fuel assembly nozzles in the core. The crossflow resistance model used in the lateral momentum equations was developed from experimental data for flow normal to tube banks (References 53 & 65). The energy equation for each element also contains additional terms that represent the energy gain or loss due to the crossflow between elements.

The unique feature in THINC-IV is that lateral momentum equations, which include both inertial and crossflow resistance terms, have been incorporated into the calculational scheme. This differentiates THINC-IV from other thermal-hydraulic programs in which only the lateral resistance term is modeled. Another important consideration in THINC-IV is that the entire velocity field is solved, en masse, by a field equation, while in other codes such as THINC-I (Reference 35) and COBRA-III (Reference 66), the solutions are obtained by stepwise integration throughout the array.

The resulting formulation of the conservation equations is more rigorous for THINC-IV; therefore, the solution is more accurate. In addition, the solution method is complex and some simplifying techniques must be employed. Since the reactor flow is chiefly in the axial direction, the core flow field is primarily one-dimensional, and it is reasonable to assume that the velocities and the parameter gradients are larger in the axial direction than the lateral direction. Therefore, a perturbation technique can be used to represent the axial and lateral parameters in the conservation equations. The lateral velocity components are regarded as perturbed quantities that are smaller than the unperturbed axial velocity. The core parameters are split into an unperturbed and a perturbed component, with the unperturbed component equaling the core average value at a given elevation and the perturbed value being the difference between the local value and the unperturbed component. Since the magnitudes of the unperturbed and perturbed parameters are significantly different, they can be solved separately. The unperturbed equations are one-dimensional and can be solved with the resulting solutions becoming the coefficients of the perturbed equations. An iterative method is then used to solve the system of perturbed equations that couples all the elements in the array.

Three THINC-IV computer runs constitute one design run: a corewide analysis, a hot-assembly analysis, and a hot-subchannel analysis. While the calculational method is identical for each run, the elements that are modeled by THINC-IV change from run to run. In the corewide analysis, the computational elements represent full fuel assemblies; in the second computation, the elements represent a quarter of the hot assembly. For the last computation, a quarter of the hot assembly is analyzed and each individual subchannel is represented as a computational element.

The first computation is a corewide, assembly-by-assembly analysis that uses an inlet velocity distribution modeled from experimental reactor models (References 51, 52 & 59) (Section 4.4.3.1.2). In the corewide analysis, the core is considered to be made up of a number of contiguous fuel assemblies divided axially into increments of equal length. The system of perturbed and unperturbed equations is solved for this array, giving the flow, enthalpy, pressure drop, temperature, and void fraction in each assembly. The system of equations is solved using the specified inlet velocity distribution and a known exit pressure condition at the top of the core. This

computation determines the interassembly energy and flow exchange at each elevation for the hot assembly. THINC-IV stores this information, and then uses it for the subsequent hot assembly analysis.

In the second computation, each computational element represents one-fourth of the hot assembly, which is considered to be at the core center for all design DNBR calculations. The inlet flow and the amount of momentum and energy interchange at each elevation is known from the previous corewide calculation. The same solution technique is used to solve for the local parameters in the hot one-quarter assembly.

While the second computation provides an overall analysis of the thermal and hydraulic behavior of the hot quarter assembly, it does not consider the individual channels in the hot assembly. The third computation further divides the hot assembly into channels consisting of individual fuel rods to form flow channels. The local variations in power, fuel rod and pellet fabrication, and fuel rod spacing and mixing (engineering hot-channel factors) within the hottest assembly are imposed on the average conditions of the hottest fuel assembly in order to determine the conditions in the hot channel. The engineering hot-channel factors are described in Section 4.4.2.3.4.

Experimental Verification

An experimental verification (Reference 58) of the THINC-IV analysis for corewide assembly-to-assembly enthalpy rises, as well as enthalpy rise in a non-uniformly heated rod bundle, have been obtained. In these experimental tests, the system pressure, inlet temperature, mass flow rate, and heat fluxes were typical of present PWR core designs.

During the operation of a reactor, various incore monitoring systems obtain measured data indicating the core performance. Assembly power distributions and assembly mixed mean temperature are measured and can be converted into the proper three-dimensional power input needed for the THINC programs. These data can then be used to verify the Westinghouse thermal-hydraulic design codes.

One standard start-up test is the natural circulation test in which the core is held at a very low power (approximately 2%) and the pumps are turned off. The core will then be cooled by the natural circulation currents created by the power differences in the core. During natural circulation, a thermal siphoning effect occurs, resulting in the hotter assemblies gaining flow, thereby creating significant interassembly crossflow. As described in the preceding section, the most important feature of THINC-IV is the method by which crossflow is evaluated. Thus, tests with significant crossflow are of more value in the code verification. Interassembly crossflow is caused by radial variations in pressure. Radial pressure gradients are in turn caused by variations in the axial pressure drops in different assemblies. Under normal operating conditions (subcooled forced convection), the axial pressure drop is due mainly to friction losses. Since all assemblies have the same geometry, all assemblies have nearly the same axial pressure drops, and crossflow velocities are small. However, under natural circulation conditions (low flow), the axial pressure

drop is due primarily to the difference in elevation head (or coolant density) between assemblies (axial velocity is low, and therefore axial friction losses are small). This phenomenon can result in relatively large radial pressure gradients, and therefore higher crossflow velocities than at normal reactor operating conditions.

The incore instrumentation was used to obtain the assembly-by-assembly core power distribution during a natural circulation test. Assembly exit temperatures during the natural circulation test on a 157-assembly, three-loop plant were predicted using THINC-IV. The predicted data points were plotted as assembly temperature rise versus assembly power, and a least-squares fitting program used to generate an equation that best fit the data. The result is the straight line presented in Figure 4.4-15. The measured assembly exit temperatures are reasonably uniform, as indicated in this figure, and are predicted closely by the THINC-IV code. This agreement verifies the lateral momentum equations and the crossflow resistance model used in THINC-IV. The larger crossflow resistance used in THINC-I reduces flow redistribution, so that THINC-IV gives better agreement with the experimental data.

Data have also been obtained for Westinghouse plants operating from 67 to 101% of full power. A representative cross section of the data obtained from a two-loop reactor and a three-loop reactor were analyzed to verify the THINC-IV calculational method. The THINC-IV predictions were compared with the experimental data as shown in Figures 4.4-16 and 4.4-17. The predicted assembly exit temperatures were compared with the measured exit temperatures for each data run. The standard deviation of the measured and predicted assembly exit temperatures were calculated and compared for both THINC-IV and THINC-I and are given in Table 4.4-5. As the standard deviations indicate, THINC-IV generally fits the data somewhat more accurately than THINC-I. For the core inlet temperatures and powers examined, the coolant flow is essentially single-phase. Thus, one would expect little interassembly crossflow and quite small differences between THINC-IV and THINC-I predictions, as seen in the tables. Both codes are conservative and predict exit temperatures higher than measured values for the higher-powered assemblies.

An experimental verification of the THINC-IV subchannel calculation method has been obtained from exit temperature measurements in a non-uniformly heated rod bundle (Reference 67). The inner nine heater rods were operated at approximately 20% more power than the outer rods to create a typical PWR intra-assembly power distribution. The rod bundle was divided into 36 subchannels and the temperature rise was calculated by THINC-IV using the measured flow and power for each experimental test.

Figure 4.4-18 shows, for a typical run, a comparison of the measured and predicted temperature rises as a function of the power density in the channel. The measurements represent an average of two to four measurements taken in various quadrants of the bundle. It is seen that the THINC-IV results predict the temperature gradient across the bundle very well. In Figure 4.4-19, the measured and predicted temperature rises are compared for a series of runs at different pressures, flows, and power levels.

Extensive additional experimental verification is presented in Reference 58.

Transient Analysis

The THINC-IV thermal-hydraulic computer code does not have a transient capability.

The Virginia Power version of the COBRA-IIIc/MIT code is used for performing transient reactor core thermal-hydraulic analysis as approved by the NRC in Reference 88.

The Virginia Power version of the COBRA-IIIc/MIT code does not have the capability for evaluating fuel rod thermal response. This is treated by the methods described in Section 15.1.9.

4.4.3.4.2 Fuel Temperatures

As discussed in 4.4.2.2, the fuel rod behavior is evaluated using a semiempirical thermal model that considers in addition to the thermal aspects such items as clad creep, fuel swelling, fission gas release, release of absorbed gases, cladding corrosion and elastic deflection, and helium solubility (References 98 & 106).

A detailed description of the thermal model can be found in Reference 102 with the modifications for time-dependent densification given in Reference 98.

4.4.3.4.3 Hydrodynamic Instability

The analytical methods used to access hydraulic instability are discussed in Section 4.4.3.5.

4.4.3.5 **Hydrodynamic and Flow Power Coupled Instability**

Boiling flows may be susceptible to thermohydrodynamic instabilities (Reference 68). These instabilities are undesirable in reactors since they may cause a change in thermohydraulic conditions that may lead to a reduction in the DNB heat flux relative to that observed during a steady flow condition or to undesired forced vibrations of core components. Therefore, a thermohydraulic design was developed which states that modes of operation under Condition I and II events shall not lead to thermohydrodynamic instabilities.

Two specific types of flow instabilities are considered for W PWR operation. These are the Ledinegg or flow excursion type of static instability and the density wave type of dynamic instability.

A Ledinegg instability involves a sudden change in flow rate from one steady state to another. This instability occurs (Reference 68) when the slope of the reactor coolant system pressure $\left(\frac{\partial \Delta P}{\partial G_{\text{internal}}}\right)$ becomes algebraically smaller than the loop supply (pump head) pressure drop-flow rate curve $\left(\frac{\partial \Delta P}{\partial G_{\text{external}}}\right)$.

The criterion for stability is thus $\left(\frac{\partial \Delta P}{\partial_{G\ internal}}\right) > \left(\frac{\partial \Delta P}{\partial_{G\ external}}\right)$. The W pump head curve has a negative slope ($\partial\Delta P/\ \partial G/\text{external} < 0$) whereas the reactor coolant system pressure drop-flow curve has a positive slope ($\partial\Delta P/\ \partial G$ internal > 0) over the Condition I and Condition II operational ranges. Thus, the Ledinegg instability will not occur.

The mechanism of density wave oscillations in a heated channel has been described by Lahey and Moody (Reference 69). Briefly, an inlet flow fluctuation produces an enthalpy perturbation. This perturbs the length and the pressure drop of the single phase region and causes quality or void pertubations in the two-phase regions which travel up the channel with the flow. The quality and length pertubations in the two-phase region create two-phase pressure drop perturbations. However, since the total pressure drop across the core is maintained by the characteristics of the fluid system external to the core, then the two-phase pressure drop perturbation feeds back to the single phase region. These resulting perturbations can be either attenuated or self-sustained.

A simple method has been developed by Ishii (Reference 70) for parallel closed channel systems to evaluate whether a given condition is stable with respect to the density wave type of dynamic instability. This method has been used to assess the stability of typical W reactor designs (References 71, 72 & 73) under Condition I and II operation. The results indicate that a large margin to density wave instability exists, e.g., increases on the order of 200% of rated reactor power would be required for the predicted inception of this type of instability.

The application of the method of Ishii (Reference 70) to W reactor designs is conservative due to the parallel open channel feature of Westinghouse PWR cores. For such cores, there is little resistance to lateral flow leaving the flow channels of high power density. There is also energy transfer from channels of high power density to lower power density channels. This coupling with cooler channels has led to the opinion that an open channel configuration is more stable than the above closed channel analysis under the same boundary conditions. Flow stability tests (Reference 74) have been conducted where the closed channel systems were shown to be *less* stable than when the same channels were cross connected at several locations. The cross connections were such that the resistance to channel to channel cross flow and enthalpy perturbations would be greater than that which would exist in a PWR core which has a relatively low resistance to cross flow.

Flow instabilities which have been observed have occurred almost exclusively in closed channel systems operating at low pressures relative to the W PWR operating pressures. Kao, Morgan and Parker (Reference 75) analyzed parallel closed channel stability experiments simulating a reactor core flow. These experiments were conducted at pressures up to 2200 psia. The results showed that for flow and power levels typical of power reactor conditions, no flow oscillations could be induced above 1200 psia.

Additional evidence that flow instabilities do not adversely affect thermal margin is provided by the data from the rod bundle DNB tests. Many W rod bundles have been tested over wide ranges of operating conditions with no evidence of premature DNB or of inconsistent data which might be indicative of flow instabilities in the rod bundle.

In summary, it is concluded that thermohydrodynamic instabilities will not occur under Condition I and II modes of operation for Westinghouse PWR reactor designs. A large power margin, greater than doubling rated power, exists to predicted inception of such instabilities. Analysis has been performed which shows that minor plant to plant differences in W reactor designs such as fuel assembly arrays, core power to flow ratios, fuel assembly length, etc. will not result in gross deterioration of the above power margins.

4.4.3.6 **Temperature Transient Effects Analysis**

Waterlogging damage of a fuel rod could occur as a consequence of a power increase on a rod after water has entered the fuel rod through a clad defect. Water entry will continue until the fuel rod internal pressure is equal to the reactor coolant pressure. A subsequent power increase raises the temperature and, hence, could raise the pressure of the water contained within the fuel rod. The increase in hydrostatic pressure within the fuel rod then drives a portion of the water from the fuel rod through the water entry defect. Clad distortion and/or rupture can occur if the fuel rod internal pressure increase is excessive due to insufficient venting of water to the reactor coolant. This occurs when there is both a rapid increase in the temperature of the water within the fuel rod and a small defect. Zircaloy-clad fuel rods that have failed due to waterlogging (References 76 & 77) indicate that very rapid power transients are required for fuel failure. Testing on waterlogged rods (Reference 76) showed that the fuel enthalpy increase required to rupture the cladding significantly exceeds the enthalpy increase associated with normal operational transients. Release of the internal fuel rod pressure is expected to have a minimal effect on the reactor coolant system (Reference 76) and is not expected to result in the failure of additional fuel rods (Reference 77). The ejection of fuel pellet fragments into the coolant stream is not expected (References 76 & 77). A clad breech due to waterlogging is thus expected to be similar to any fuel rod failure mechanism that exposes fuel pellets to the reactor coolant stream. Waterlogging has not been identified as the mechanism for clad distortion or perforation of any Westinghouse Zircaloy-4 or ZIRLO clad fuel rods.

An excessively high fuel rod internal gas pressure could cause clad failure. One of the fuel rod design bases (Section 4.2.1.1.1) is that the internal pressure of the lead rod in the reactor will be limited to a value below that which could cause the diametral gap to increase due to outward creep during steady-state operation. During operational transients, fuel rod clad rupture due to high internal gas pressure is precluded by meeting the above design basis.

4.4.3.7 Potentially Damaging Temperature Effects During Transients

The fuel rod experiences many operational transients (intentional maneuvers) during its residence in the core. A number of thermal effects must be considered when analyzing the fuel rod performance.

The clad can be in contact with the fuel pellet at some time in the fuel lifetime. Local stress and strain increases may occur if the fuel pellet temperature is increased after the clad is in contact with the pellet. Clad-pellet interaction is discussed in Section 4.2.1.3.1.

Increasing the fuel temperature results in an increased fuel rod internal pressure. One of the fuel rod design bases is that the fuel rod internal pressure does not exceed a value that could cause the diametral gap to increase due to outward creep during steady-state operation (Section 4.2.1.1.1).

The potential effects of operation with waterlogged fuel are discussed in Section 4.4.3.6, which concluded that waterlogging is not a concern during operational transients.

Clad flattening, as noted in Section 4.2.1.3.1, has been observed in some operating power reactors. It is possible that, during a transient, axial thermal expansion of the fuel stack against a flattened section of clad could cause failure of the clad. However, no cladding failures have been attributed to this mechanism, and clad flattening is now precluded during the fuel residence in the core as part of the fuel rod design (Section 4.2.1.3.1).

There can be a differential thermal expansion between the fuel rods and the guide thimbles during a transient. Excessive bowing of the fuel rods could occur if the grid assemblies did not allow axial movement of the fuel rods relative to the grids. Thermal expansion of the fuel rods is considered in the grid design so that axial loads imposed on the fuel rods during a thermal transient will not result in excessively bowed fuel rods (Section 4.2.1.2.2).

4.4.3.8 Energy Release During Fuel Element Burnout

As discussed in Section 4.4.3.3, the core is protected from going through DNB over the full range of possible operating conditions. At full-power nominal operation, the minimum DNBR was found to be 2.29. In the extremely unlikely event that DNB should occur, the clad temperature will rise due to the steam blanketing at the rod surface and the consequent degradation in heat transfer. During this time there is a potential for chemical reaction between the cladding and the coolant. However, because of the relatively good film-boiling heat transfer following DNB, the energy release resulting from this reaction is insignificant compared to the power produced by the fuel.

DNB With Physical Burnout

Westinghouse (Reference 67) has conducted DNB tests in a 25-rod bundle where physical burnout occurred with one rod. After this occurrence, the 25-rod test section was used for several days to obtain more DNB data from the other rods in the bundle. The burnout and deformation of

the rod did not affect the performance of neighboring rods in the test section during the burnout or the validity of the subsequent DNB data points as predicted by the W-3 correlation. No occurrences of flow instability or other abnormal operation were observed.

DNB With Return to Nucleate Boiling

Additional DNB tests have been conducted by Westinghouse (Reference 78) in 19- and 21-rod bundles. In these tests, DNB without physical burnout was experienced more than once on single rods in the bundles for short periods of time. Each time, a reduction in power of approximately 10% was sufficient to reestablish nucleate boiling on the surface of the rod. During these and subsequent tests, no adverse effects were observed on this rod or any other rod in the bundle as a consequence of operating in DNB.

4.4.3.9 Energy Release or Rupture of Waterlogged Fuel Elements

A full discussion of waterlogging including energy release is contained in Section 4.4.3.6. It is noted that the resulting energy release is not expected to affect neighboring fuel rods.

4.4.3.10 Fuel Rod Behavior Effects From Coolant Flow Blockage

Coolant flow blockages can occur within the coolant channels of a fuel assembly or external to the reactor core. The effects of fuel assembly blockage within the assembly on fuel rod behavior is more pronounced than external blockages of the same magnitude. In both cases the flow blockages cause local reductions in coolant flow. The amount of local flow reduction, where it occurs in the reactor, and how far along the flow stream the reduction persists are considerations that will influence the fuel rod behavior. The effects of coolant flow blockages in terms of maintaining rated core performance are determined both by analytical and experimental methods. The experimental data are usually used to augment analytical tools such as computer programs similar to the THINC-IV program. Inspection of the DNB correlation (Section 4.4.2.3 and Reference 40) shows that the predicted DNBR is dependent upon the local values of quality and mass velocity.

The THINC-IV code is capable of predicting the effects of local flow blockages on DNBR within the fuel assembly on a subchannel basis, regardless of where the flow blockage occurs. In Reference 58, it is shown that for a fuel assembly similar to the Westinghouse design, THINC-IV accurately predicts the flow distribution within the fuel assembly when the inlet nozzle is completely blocked. Full recovery of the flow was found to occur about 30 inches downstream of the blockage. With the reference reactor operating at the nominal full-power conditions specified in Table 4.4-1, the effects of an increase in enthalpy and decrease in mass velocity in the lower portion of the fuel assembly would not result in the reactor reaching the DNBR limit.

From a review of the open literature, it was concluded that flow blockage in open-lattice cores similar to the Westinghouse cores causes flow perturbations that are local to the blockage. For instance, Ohtsubo et al. (Reference 79) show that the mean bundle velocity is approached asymptotically about 4 inches downstream from a flow blockage in a single-flow cell. Similar

results were also found for two and three cells completely blocked. Basmer et al. (Reference 80) tested an open-lattice fuel assembly in which 41% of the subchannels were completely blocked in the center of the test bundle between spacer grids. Their results showed that the stagnant zone behind the flow blockage essentially disappears after 1.65 L/De, or about 5 inches, for their test bundle. They also found that leakage flow through the blockage tended to shorten the stagnant zone or, in essence, the complete recovery length. Thus, local flow blockages within a fuel assembly have little effect on subchannel enthalpy rise. The reduction in local mass velocity is then the main parameter that affects the DNBR. If the North Anna units were operating at full power and nominal steady-state conditions as specified in Table 4.4-2, a significant reduction in local mass velocity would be required to reduce the minimum DNBR to the design limit DNBR.

The above mass velocity effect on the DNB correlation was based on the assumption of fully developed flow along the full channel length. In reality, a local flow blockage is expected to promote turbulence and thus would likely not affect DNBR at all.

Coolant flow blockages induce local crossflows as well as promote turbulence. Fuel rod behavior is changed under the influence of a sufficiently high crossflow component. Fuel rod vibration could occur, caused by this crossflow component, through vortex shedding or turbulent mechanisms. If the crossflow velocity exceeds the limit established for fluid elastic stability, large amplitude whirling results. The limits for a controlled vibration mechanism are established from studies of vortex shedding and turbulent pressure fluctuations. The crossflow velocity required to exceed fluid elastic stability limits is dependent on the axial location of the blockage and the characterization of the crossflow (jet flow or not). These limits are greater than those for vibratory fuel rod wear. Crossflow velocity above the established limits can lead to mechanical wear of the fuel rods at the grid support locations. Fuel rod wear due to flow-induced vibration is considered in the fuel rod fretting evaluation (Section 4.2).

4.4.4 Testing and Verification

4.4.4.1 Tests Before Initial Criticality

A reactor coolant flow test, as noted in Table 14.1-2, was performed following fuel loading but before initial criticality. Coolant-loop elbow-tap differential pressure drop data were obtained in this test. These data in conjunction with coolant pump performance information allowed a determination of the coolant flow rates at reactor operating conditions. This test verified that proper coolant flow rates were used in the original core thermal and hydraulic analysis.

Additional testing is performed on a periodic basis to measure the reactor coolant system total flow rate. This testing satisfies the requirements of the Technical Specifications. The periodic measurement of the reactor coolant system total flow rate is adequate to detect flow degradation and ensure correlation of the flow indication channels (coolant-loop elbow-taps) with measured flow such that the indicated percent flow will provide sufficient verification of flow rate for the reactor protection system. The results of this testing also verify that the proper coolant flow rates continue to be used in the core thermal and hydraulic analysis.

4.4.4.2 Initial Power and Plant Operation

Core power distribution measurements are made at several core power levels (Section 4.3.2.2.8). These tests are used to ensure that conservative peaking factors are used in the core thermal and hydraulic analysis.

Additional demonstration of the overall conservatism of the THINC analysis was obtained by comparing THINC predictions to incore thermocouple measurements. These measurements were performed on the Zion reactor (Reference 81). No further in-reactor testing is required.

4.4.4.3 Component and Fuel Inspections

Inspections performed on the manufactured fuel are delineated in Section 4.2.1.4. Fabrication measurements critical to thermal and hydraulic analysis are obtained to verify that the engineering hot-channel factors employed in the design analysis (Section 4.4.2.3.4) are met.

4.4.5 Instrumentation Application

4.4.5.1 Incore Instrumentation

Instrumentation is provided to determine core power distribution. Radial, axial, and azimuthal core characteristics may be obtained for all core quadrants with information obtained by the moveable detector system.

The incore instrumentation system is comprised of thermocouples positioned to measure fuel assembly coolant outlet temperatures at preselected positions, and moveable detectors that can be positioned in guide thimbles that run the length of selected fuel assemblies to measure the neutron flux distribution. Figures 4.4-20 and 4.4-21 show the number and location of instrumented assemblies in the Unit 1 and Unit 2 cores.

The incore instrumentation system is described in more detail in Section 7.7.1.9.

The incore instrumentation system is provided to obtain data from which fission power density distribution in the core, coolant enthalpy distribution in the core, and fuel burnup distribution may be determined.

The core exit thermocouple system, in conjunction with core inlet temperature data, is provided for indication of radial distributions of coolant enthalpy rise across representative regions of the core. This function is a part of the inadequate core cooling monitor system (ICCM). The ICCM is discussed in Section 7.9.

4.4.5.2 Overtemperature and Overpower Delta T Instrumentation

The overtemperature delta T trip protects the core against low DNBR. The overpower delta T trip protects against excessive power (fuel rod rating protection).

As discussed in Section 7.2.1.1.2, factors included in establishing the overtemperature delta T and overpower delta T trip setpoints include the reactor coolant temperature in each loop

and the axial distribution of core power through the use of the two section ex-core neutron detectors.

4.4.5.3 Instrumentation to Limit Maximum Power Output

The output of the three ranges (source, intermediate, and power) of detectors, with the electronics of the nuclear instruments, is used to limit the maximum power output of the reactor within their respective ranges.

There are six radial locations containing a total of eight neutron flux detectors installed around the reactor in the primary shield. Two proportional counters for the source range are installed on opposite “flat” portions of the core containing the primary start-up sources, at an elevation approximately one-quarter of the core height. Two compensated ionization chambers for the intermediate range, located in the same instrument wells and detector assemblies as the source-range detectors, are positioned at an elevation corresponding to one-half of the core height. Four dual-section uncompensated ionization chamber assemblies for the power range are installed vertically at the four corners of the core and located equidistant from the reactor vessel at all points and, to minimize neutron flux pattern distortions, within 1 foot of the reactor vessel. Each power range detector provides two signals corresponding to the neutron flux in the upper and in the lower sections of a core quadrant. The three ranges of detectors are used as inputs to monitor neutron flux from a completely shutdown condition to 120% of full power with the capability of recording overpower excursions up to 200% of full power.

The difference in neutron flux between the upper and lower sections of the power-range detectors is used to limit the overtemperature delta T and overpower delta T trip setpoints, and to provide the operator with an indication of the core power axial offset. In addition, the output of the power range channels is used for the following:

1. The rod speed control function.
2. To alert the operator to an excessive power imbalance between the quadrants.
3. Protect the core against rod-ejection accidents.
4. Protect the core against adverse power distributions resulting from dropped rods.

Details of the neutron detectors and nuclear instrumentation design and the control and trip logic are given in Chapter 7. The limits on neutron flux operation and allowable values are given in the Technical Specifications. The trip setpoints are given in the Technical Requirements Manual.

4.4 REFERENCES

1. Motley, F. E., et al., *New Westinghouse Correlation WRB-1 for Predicting Critical Heat Flux in Rod Bundles with Mixing Vane Grids*, WCAP-8762-P-A (proprietary) and WCAP-8763 (non-proprietary), Westinghouse Nuclear Energy Systems, July 1984.
2. Chelemer, H., et al., *Improved Thermal Design Procedures*, WCAP-8567, July 1975.
3. J. A. Christensen, R. J. Allio, and A. Biancheria, *Melting Point of Irradiated* UO_2, WCAP-6065, 1965.
4. K. W. Hill, F. E. Motley, F. F. Cadek, and A. H. Wenzel, *Effect of 17 x 17 Fuel Assembly Geometry on DNB,* WCAP-8296-A (proprietary), 1975, and WCAP-8297-A (non-proprietary), 1975.
5. S. Nakazato and E. E. DeMario, *Hydraulic Flow Test of the 17 x 17 Fuel Assembly*, WCAP-8278 (proprietary), 1974, and WCAP-8279 (nonproprietary), 1974.
6. J. M. Hellman, editor, *Fuel Densification Experimental Results and Model for Reactor Application*, WCAP-8218-P-A (proprietary), 1975, and WCAP-8219-A (nonproprietary), 1975.
7. C. R. Hann, et al., *Data Report for the NRC/PNL Halden Assembly IFA-431,* PNL-2494, April 1978.
8. R. N. Duncan, *Rabbit Capsule Irradiation of* UO_2, CVTR Project, CVNA-142, 1962.
9. C. R. Hann, et al., *Data Report for the NRC/PNL Halden Assembly IFA-432,* NUREG/CR-0560, PNL-2673, 1978.
10. V. C. Howard and T. G. Gulvin, *Thermal Conductivity Determinations on Uranium Dioxide by a Radial Flow Method*, UKAEA IG-Report 51, 1960.
11. C. F. Lucks and H. W. Deem, *Thermal Conductivity and Electrical Conductivity of* UO_2, in *Progress Reports Relating to Civilian Applications*, BMI-1448 (Rev.) for June 1960; BMI-1489 (Rev.) for December 1960; and BMI-1518 (Rev.) for May 1961.
12. J. L. Daniel, J. Matolich, Jr., and H. W. Deem, *Thermal Conductivity of* UO_2, HW-69945, 1962.
13. A. D. Feith, *Thermal Conductivity of* UO_2 *by a Radial Heat Flow Method*, TID-21668, 1962.
14. J. Vogt, L. Grandell, and U. Runfors, *Determination of the Thermal Conductivity of Unirradiated Uranium Dioxide*, AB Atomenergi Report RMB-527, 1964, quoted in IAEA Technical Report Series No. 59, *Thermal Conductivity of Uranium Dioxide*.
15. T. Nishijima, T. Kawanda, and A. Ishihata, *Thermal Conductivity of Sintered* UO_2 *and* $A1_2O_3$ *at High Temperatures*, *Journal of the American Ceramic Society*, Vol. 48, pp. 31-34, 1965.

16. J. B. Ainscough and M. J. Wheeler, *The Thermal Diffusivity and Thermal Conductivity of Sintered Uranium Dioxide*, in *Proceedings of the Seventh Conference of Thermal Conductivity*, National Bureau of Standards, Washington, 1968, p. 467.

17. T. G. Godfrey, W. Fulkerson, T. G. Killie, J. P. Moore, and D. L. McElroy, *Thermal Conductivity of Uranium Dioxide and Armco Iron by an Improved Radial Heat Flow Technique*, ORNL-3556, 1964.

18. J. P. Stora et al., *Thermal Conductivity of Sintered Uranium Oxide Under In-Pile Conditions*, EURAEC-1095, 1964.

19. A. J. Bush, *Apparatus for Measuring Thermal Conductivity to 2500°C,* Westinghouse Research Laboratories Report 64-1P6-401-R3 (proprietary), 1965.

20. R. R. Asamoto, F. L. Anselin, and A. E. Conti, *The Effect of Density on the Thermal Conductivity of Uranium Dioxide*, GEAP-5493, 1968.

21. O. L. Kruger, *Heat Transfer Properties of Uranium and Plutonium Dioxide*, Paper 11-N-68F, *Nuclear Division of the American Ceramic Society*, Pittsburgh, Fall 1968.

22. J. A. Gyllander, *In-Pile Determination of the Thermal Conductivity of UO_2 in the Range 500-2500°C,* AE-411, 1971.

23. M. F. Lyons et al., *UO_2 Powder and Pellet Thermal Conductivity During Irradiation*, GEAP-5100-1, 1966.

24. D. H. Coplin et al., *The Thermal Conductivity of UO_2 by Direct In-Reactor Measurements*, GEAP-5100-6, 1968.

25. A. S. Bain, *The Heat Rating Required to Produce Center Melting in Various UO_2 Fuels*, ASTM Special Technical Publication, No. 306, Philadelphia, Pa., 1962, pp. 30-46.

26. J. P. Stora, *In-Reactor Measurements of the Integrated Thermal Conductivity of UO_2 - Effect of Porosity*, *Transactions of ANS*, Vol. 13, pp. 137-138, 1970.

27. International Atomic Energy Agency, *Thermal Conductivity of Uranium Dioxide*, IAEA Technical Reports Series, No. 59, Vienna, 1966.

28. C. G. Poncelet, *Burnup Physics of Heterogeneous Reactor Lattices*, WCAP-6069, 1965.

29. R. J. Nodvick, *Saxton Core II Fuel Performance Evaluation*, WCAP-3385-56, Part II, *Evaluation of Mass Spectrometric and Radiochemical Analyses of Irradiated Saxton Plutonium Fuel,* 1970.

30. R. A. Dean, *Thermal Contact Conductance Between UO_2 and Zircaloy-2*, CVNA-127, 1962.

31. A. M. Ross and R. L. Stoute, *Heat Transfer Coefficient Between UO_2 and Zircaloy-2*, AECL-1552, 1962.

32. L. S. Tong, *Boiling Heat Transfer and Two-Phase Flow*, John Wiley & Sons, New York, 1965.

33. L. S. Tong, *Boiling Crisis and Critical Heat Flux*, AEC Critical Review Series, TID-25887, 1972.

34. L. S. Tong, *Critical Heat Fluxes on Rod Bundles in Two-Phase Flow and Heat Transfer in Rod Bundles*, ASME, New York, 1969, pp. 31-41.

35. H. Chelemer, J. Weisman, and L. S. Tong, *Subchannel Thermal Analysis of Rod Bundle Cores*, WCAP-7015, Revision 1, 1969.

36. F. E. Motley and F. F. Cadek, *DNB Test Results for New Mixing Vane Grids (R)*, WCAP-7695-P-A (proprietary), 1975, and WCAP-7958-A (nonproprietary), 1975.

37. F. E. Motley and F. F. Cadek, *DNB Test Results for R Grid Thimble Cold Wall Cells*, WCAP-7695-Addendum 1-P-A (proprietary), 1975, and WCAP-7958-Addendum 1-A (nonproprietary), 1975.

38. Motley, F. E., Wehzel, A. H., and Cadek, F. F., *Critical Heat Flux Testing of 17 x 17 Fuel Assembly Geometry w/22 Inch Grid Spacing*, WCAP-8536, May 1975 (Proprietary) and WCAP-8537, May 1975 (Non-Proprietary).

39. Owen, D. B., *Factors for One Sided Tolerance Limits and for Variables Sampling Plans*, SCR-607, March 1963.

40. L. S. Tong, *Prediction of Departure from Nucleate Boiling for an Axially Non-Uniform Heat Flux Distribution*, *Journal of Nuclear Energy*, Vol. 21, pp. 241-248, 1967.

41. F. F. Cadek, F. E. Motley, and D. P. Dominicis, *Effect of Axial Spacing on Interchannel Thermal Mixing with the R Mixing Vane Grid*, WCAP-7941-P-A (proprietary), 1975, and WCAP-7959-A (nonproprietary), 1975.

42. D. S. Rowe and C. W. Angle, *Crossflow Mixing Between Parallel Flow Channels During Boiling, Part II Measurement of Flow and Enthalpy in Two Parallel Channels*, BNWL-371, Part 2, 1967.

43. D. S. Rowe and C. W. Angle, *Crossflow Mixing Between Parallel Flow Channels During Boiling, Part III Effect of Spacers on Mixing Between Two Channels*, BNWL-371, Part 3, 1969.

44. J. M. Gonzalez-Santalo and P. Griffith, *Two-Phase Flow Mixing in Rod Bundle Subchannels,* ASME Paper 72-WA/NE-19.

45. F. E. Motley, A. H. Wenzel, and F. F. Cadek, *The Effect of 17 x 17 Fuel Assembly Geometry on Interchannel Thermal Mixing*, WCAP-8298-P-A (proprietary), 1975, and WCAP-8299-A (nonproprietary), 1975.

46. Hill, K. W., Motley, F.E., and Cadek, F. F., *Effect of Local Heat Flux Spikes on DNB in Non-Uniform Heated Rod Bundles*, WCAP-8174-P-A, February 1975 (Proprietary) and WCAP-8202-A, February 1975 (Non-Proprietary).

47. L. E. Hochreiter, *Application of the THINC IV Program to PWR Design*, WCAP-8054-P-A (proprietary), February 1989, and WCAP-8195-A (nonproprietary), February 1989.

48. F. W. Dittus and L. M. K. Boelter, *Heat Transfer in Automobile Radiators of the Tubular Type*, *California University Publication in Engineering*, Vol. 2, No. 13, pp. 443-461, 1930.

49. J. Weisman, *Heat Transfer to Water Flowing Parallel to Tube Bundles*, *Nuclear Science Engineering*, Vol. 6, pp. 78-79, 1959.

50. J. R. S. Thom, W. M. Walker, T. A. Fallon, and G. F. S. Reising, *Boiling in Sub-cooled Water During Flowup Heated Tubes or Annuli*, *Proceedings of the Institute of Mechanical Engineers*, Vol. 180, Pt. C, 1955-1966, pp. 226-46.

51. G. Hetsroni, *Hydraulic Tests of the San Onofre Reactor Model*, WCAP-3269-8, 1964.

52. G. Hetsroni, *Studies of the Connecticut-Yankee Hydraulic Model*, NYO-3250-2, 1965.

53. I. E. Idel'chik, *Handbook of Hydraulic Resistance*, AEC-TR-6630, 1960.

54. L. F. Moody, *Friction Factors for Pipe Flow*, *Transactions of the American Society of Mechanical Engineers*, Vol. 66, pp. 671-684, 1944.

55. G. W. Maurer, *A Method of Predicting Steady State Boiling Vapor Fractions in Reactor Coolant Channels*, WAPD-BT-19, 1960, pp. 59-70.

56. P. Griffith, J. A. Clark, and W. M. Rohsenow, *Void Volumes in Subcooled Boiling Systems*, ASME Paper No. 58-HT-19.

57. R. W. Bowring, *Physical Model, Based on Bubble Detachment, and Calculation of Steam Voidage in the Subcooled Region of a Heated Channel*, HPR-10, 1962.

58. L. E. Hochreiter, H. Chelemer, and P. T. Chu, *THINC-IV, An Improved Program for Thermal-Hydraulic Analysis of Rod Bundle Cores*, WCAP-7956-A, February 1989.

59. F. D. Carter, *Inlet Orificing of Open PWR Cores*, WCAP-9004 (proprietary), 1969, and WCAP-7836 (nonproprietary), 1972.

60. J. Shefcheck, *Application of the THINC Program to PWR Design*, WCAP-7359-L (proprietary), 1969, and WCAP-7838 (nonproprietary), 1972.

61. E. H. Novendstern and R. O. Sandberg, *Single Phase Local Boiling and Bulk Boiling Pressure Drop Correlations*, WCAP-2850 (proprietary), 1966, and WCAP-7916 (nonproprietary), 1972.

62. W. L. Owens, Jr., *Two-Phase Pressure Gradient*, in *International Developments in Heat Transfer, Part II*, ASME, New York, 1961, pp. 363-368.

63. A. F. McFarlane, *Power Peaking Factors*, WCAP-7912-P-A (proprietary), 1975, and WCAP-7912-A (nonproprietary), 1975.

64. H. R. Vallentine, *Applied Hydrodynamics*, Buttersworth Publishers, London, 1959.

65. W. M. Kays and A. L. London, *Compact Heat Exchangers*, National Press, Palo Alto, 1955.

66. D. S. Rowe, *COBRA-III, A Digital Computer Program for Steady State and Transient Thermal-Hydraulic Analysis of Rod Bundle Nuclear Fuel Elements*, BNWL-1695, March 1973.

67. J. Weisman, A. H. Wenzel, L. S. Tong, D. Fitzsimmons, W. Thorne, and J. Batch, *Experimental Determination of the Departure from Nucleate Boiling in Large Rod Bundles at High Pressures*, *Chem. Eng. Prog. Symp. Ser. 64*, No. 82, 1968, pp. 114-125.

68. J. A. Boure, A. E. Berglus, and L. S. Tong, *Review of Two-Phase Flow Instability*, Nucl. Engr. Design 25 (1973) p. 165-192.

69. R. T. Lahey and F. J. Moody, *The Thermal Hydraulics of a Boiling Water Reactor*, American Nuclear Society, 1977.

70. P. Saha, M. Ishii, and N. Zuber, *An Experimental Investigation of the Thermally Induced Flow Oscillations in Two-Phase Systems*, J. of Heat Transfer, Nov. 1976, pp. 616-622.

71. Virgil C. Summer FSAR, Docket #50-395.

72. Byron/Braidwood FSAR, Docket #50-456.

73. South Texas FSAR, Docket #50-498.

74. S. Kakac, T. N. Veziroglu, K. Akyuzlu, O. Berkol, *Sustained and Transient Boiling Flow Instabilities in a Cross-Connected Four-Parallel-Channel Upflow System*, Proc of 5th International Heat Transfer Conference, Tokyo, Sept. 3-7, 1974.

75. H. S. Kao, C. D. Morgan, and W. B. Parker, *Prediction of Flow Oscillation in Reactor Core Channel*, Trans. ANS, Vol. 16, 1973, pp. 212-213.

76. L. A. Stephan, *The Effects of Cladding Material and Heat Treatment on the Response of Waterlogged UO_2 Fuel Rods to Power Bursts*, IN-ITR-111, 1970.

77. Letters from Western New York Nuclear Research Center to the AEC, dated February 11, 1971, and August 27, 1971, Docket No. 50-57.

78. L. S. Tong et al., *Critical Heat Flux (DNB) in Square and Tri-Angular Array Rod Bundles*, *Japan Society of Mechanical Engineers Semi-International Symposium*, Tokyo, Japan, September 4-8, 1967, pp. 25-34.

79. A. Ohtsubo and S. Uruwashi, *Stagnant Fluid Due to Local Flow Blockage*, *Journal of Nuclear Science Technology*, Vol. 9, No. 7, pp. 433-434, 1972.

80. P. Basmer, D. Kirsh, and G. F. Schultheiss, *Investigation of the Flow Pattern in the Recirculation Zone Downstream of Local Coolant Blockages in Pin Bundles*, *Atomwirtschaft*, Vol. 17, No. 8, pp. 416-417, 1972.

81. T. M. Burke, C. E. Meyer, and J. Shechek, *Analysis of Data from the Zion (Unit 1) THINC Verification Test*, WCAP-8453-A (proprietary), May 1976, and WCAP-8454-A (nonproprietary), May 1976.

82. J. G. Miller and J. O. Erb, *VEPCO Evaluation of the Control Rod Ejection Transient,* VEP-NFE-2-A, December 1984.

83. R. C. Anderson, *Statistical DNBR Evaluation Methodology*, VEP-NE-2-A, June 1987.

84. Skaritka, J. (Ed.), *Fuel Rod Bow Evaluation*, WCAP-8691, Rev. 1 (Proprietary) and WCAP-8692, Rev. 1 (Non-Proprietary), July 1979.

85. *Partial Response to Request Number 1 for Additional Information on WCAP-8691, Rev. 1*, letter E. P. Rahe, Jr., (Westinghouse) to J. R. Miller (NRC), NS-EPR-2515, dated October 9, 1981; *Remaining Response to Request Number 1 for Additional Information on WCAP-8691, Rev. 1* letter, E. P. Rahe, Jr. (Westinghouse) to J. R. Miller (NRC), NS-EPR-2572, dated March 16, 1982.

86. L. B. Engle (NRC) to W. L. Stewart (Virginia Power), 587.8°F Tave approval for North Anna 1, March 13, 1984.

87. L. B. Engle (NRC) to W. L. Stewart (Virginia Power), 587.8°F Tave approval for North Anna 2, October 15, 1984.

88. F. W. Sliz & K. L. Basehore, *Virginia Power Reactor Core Thermal-Hydroulic Analysis Using the COBRA IIIC/MIT Computer Code*, VEP-FRD-33-A, October 1983.

89. Letter from W. L. Stewart (Virginia Power) to Harold R. Denton (NRC), Amendment to Operating Licenses NPF-4 and NPF-7 for Rated Thermal Power of 2893 MWt, serial No. 85-077, May 2, 1985.

90. Letter from L. B. Engle (NRC) to W. L. Stewart (Virginia Power), 2893 MWt Rated Thermal Power approval for North Anna Units 1 and 2, August 25, 1986.

91. Letter from L. B. Engle (NRC) to W. L. Stewart (VP), Serial #85-775, dated October 24, 1985.

92. Letter from C. Berlinger (NRC) to E. P. Rahe, Jr. (Westinghouse), *Request for Reduction in Fuel Assembly Burnup Limit for Calculation of Maximum Rod Bow Penalty*, June 18, 1986.

93. Davidson, S. L. and Ryan, T. L. (Eds.), *VANTAGE+ Fuel Assembly Reference Core Report,* WCAP-12610-A (Proprietary), April 1995.

94. Slagle, W. H. (Editor), *Westinghouse Fuel Assembly Reconstitution Evaluation Methodology,* WCAP-13060-P-A (Proprietary), July 1993.

95. Letter from W. L. Stewart (Virginia Electric and Power Company) to U.S. Nuclear Regulatory Commission, *North Anna Power Station Units 1 and 2 - Proposed Technical Specifications Changes - Reconstituted Fuel Assemblies,* Serial Number 93-706, November 19, 1993.

96. Letter from L. B. Engle (NRC) to J. P. O'Hanlon (Virginia Electric and Power Company), *North Anna Units 1 and 2 - Issuance of Amendments Re: Fuel Assembly Reconstitution (TAC Nos. M88364 and M88365)*, August 9, 1994.

97. R. C. Anderson and N. P. Wolfhope, *Qualification of the WRB-1 CHF Correlation in the Virginia Power COBRA Code,* VEP-NE-3-A, Virginia Power, July 1990.

98. R. A. Weiner et al., *Improved Fuel Performance Models for Westinghouse Fuel Rod Design and Safety Evaluations,* WCAP-10851-P-A (Proprietary), August 1988.

99. S. L. Davidson, R. L. Oelrich, and P. J. Kersting, *Assessment of Clad Flattening and Densification Power Spike Factor Elimination in Westinghouse Nuclear Fuel,* WCAP-13589-P-A (Proprietary), March 1995.

100. E. R. Bradley et al., *Data Report for the NRC/PNL Halden Assembly IFA-432: April 1978-May 1980,* NUREG/CR-1950, PNL-3709, April 1981.

101. E. R. Bradley et al., *Data Report for the Instrumented Fuel Assembly IFA-513,* NUREG/CR-1838, PNL-3637, August 1981.

102. W. J. Leech, D. D. Davis, and M. S. Benzvi, *Revised PAD Code Thermal Safety Model,* WCAP-8720-A2 (Proprietary), October 1982.

103. W. H. Jens and P. A. Lottes, *Analyses of Heat Transfer, Burnout, Pressure Drop, and Density Data for High Pressure Water,* USAEC Report ANL-4627, Argonne National Laboratory (1951).

104. S. L. Smith, *Void Fractions in Two-Phase Flow: A Correlation Based Upon an Equal Velocity Head Model,* Proceedings of the Institution of Mechanical Engineers, Vol. 184, part 1, No. 36, P. 547 (1969-70).

105. S. Levy, *Forced Convection Subcooled Boiling - Prediction of Vapor Volumetric Fraction,* GEAP-5157, General Electric Company (April 1966).

106. J. P. Foster et al., *Westinghouse Improved Performance Analysis and Design Model (PAD 4.0)*, WCAP-15063-P-A, Revision 1, with Errata (Proprietary), July 2000.

107. Letter from L. B. Engle (NRC) to W. L. Stewart (VEPCO), *North Anna Units 1 and 2 - Issuance of Amendments Re: Core Operating Limits Report (TAC Nos. 76828 and 76829),* Serial Number 91-341, June 7, 1991.

Table 4.4-1
REACTOR DESIGN COMPARISON TABLE (ORIGINAL DESIGN)

Thermal and Hydraulic Design Parameters	17 x 17 with Densification	15 x 15 without Densification
Reactor core heat output	2775 MWt	2775 MWt
Reactor core heat output	9471.1×10^6 Btu/hr	9471.1×10^6 Btu/hr
Heat generated in fuel	97.4%	97.4%
System pressure, nominal	2250 psia	2250 psia
System pressure, minimum steady-state	2220 psia	2220 psia
Minimum DNBR at nominal conditions		
Typical flow channel	2.15	2.05
Thimble (cold-wall) flow channel	1.77	1.75
Minimum DNBR for design transients	1.30	1.30
DNB correlation	"R" (W-3 with modified spacer factor	"L" (W-3 with modified spacer factor
Coolant flow		
Total thermal flow rate	105.2×10^6 lb/hr	105.2×10^6 lb/hr
Effective flow rate for heat transfer	100.5×10^6 lb/hr	100.5×10^6 lb/hr
Effective flow area for heat transfer	41.5 ft^2	41.8 ft^2
Average velocity along fuel rods	15.1 ft/sec	15.1 ft/sec
Average mass velocity	2.42×10^6 lb/hr-ft^2	2.41×10^6 lb/hr-ft^2
Coolant temperature		
Nominal inlet	546.8°F	546.8°F
Average rise in vessel	67.0°F	67.0°F
Average rise in core	69.8°F	69.8°F
Average in core	583.4°F	583.4°F
Average in vessel	580.3°F	580.3°F
Heat transfer		
Active heat transfer surface area	48,600 ft^2	42,460 ft^2
Average heat flux	189,800 Btu/hr-ft^2	217,300 Btu/hr-ft^2
Maximum heat flux for normal operation	440,500 Btu/hr-ft^2 [(a)]	521,400 Btu/hr-ft^2
Average thermal output	5.44 kW/ft	7.03 kW/ft
Maximum thermal output for normal operation	12.6 kW/ft [(a)]	15.6 kW/ft
Maximum thermal output at maximum overpower trip point (118% power) and Peak linear power for determination of protection setpoints	18.0 kW/ft	21.1 kW/ft

a. This limit is associated with the value of $F_Q = 2.32$.

Table 4.4-1 (continued)
REACTOR DESIGN COMPARISON TABLE (ORIGINAL DESIGN)

Thermal and Hydraulic Design Parameters	17 x 17 with Densification	15 x 15 without Densification
Fuel central temperature (BOL)		
Peak at 100% power	3,250°F	3,750°F
Peak at maximum thermal output for maximum overpower trip point	4,150°F	4,500°F
Pressure drop		
Across core	23.7 ± 4.7 psi [b]	20.9 ± 1.2 psi [c]
Across vessel, including nozzle	44.1 ± 6.6 psi	38.9 ± 5.8 psi

b. Based on best-estimate flow rate (Section 5.1).
c. Based on thermal design flow rate (Section 5.1).

Table 4.4-2
REACTOR DESIGN COMPARISON TABLE (CURRENT OPERATING CONDITIONS)

Thermal and Hydraulic Design Parameters	Uprated Power 17 x 17 NAIF Design	Uprated T_{avg} (587.8°F) 17 x 17 LOPAR Design
Reactor core heat output	2898 MWt [a]	2775 MWt
Reactor core heat output	9888×10^6 Btu/hr	9471.1×10^6 Btu/hr
Heat generated in fuel	97.4%	97.4%
System pressure, nominal	2250 psia	2250 psia
System pressure, minimum steady-state	2250 psia	2220 psia
Minimum DNBR at nominal conditions		
Typical flow channel	2.42	>1.30
Thimble (cold-wall) flow channel	2.29	>1.30
Minimum DNBR for design transients	1.46	>1.30
DNB correlation	WRB-1	"R" (W-3 with modified spacer factor)
Coolant flow		
Total thermal flow rate	108.2×10^6 lb/hr [b]	106.3×10^6 lb/hr
Effective flow rate for heat transfer	105.0×10^6 lb/hr	101.5×10^6 lb/hr
Effective flow area for heat transfer	41.5 ft^2	41.5 ft^2
Average velocity along fuel rods	15.9 ft/sec	15.6 ft/sec
Average mass velocity	2.53×10^6 lb/hr-ft^2	2.44×10^6 lb/hr-ft^2
Coolant temperature		
Nominal inlet	553.5°F	555.5°F
Average rise in vessel	66.6°F	64.5°F
Average rise in core	68.4°F	67.2°F
Average in core	589.7°F	591.1°F
Average in vessel	586.8°F	587.8°F
Heat transfer		
Active heat transfer surface area	48,600 ft^2	48,600 ft^2
Average heat flux	198,218 Btu/hr-ft^2	189,800 Btu/hr-ft^2
Maximum heat flux for normal operation	434,100 Btu/hr-ft^2 [c]	440,350 Btu/hr-ft^2 [d]
Average thermal output	5.69 kW/ft	5.44 kW/ft
Maximum thermal output for normal operation	12.46 kW/ft [c]	12.6 kW/ft [d]

a. These parameters are for a core rated thermal power of 2898 MWt, which bounds the current licensed maximum core power of 2893 MWt.
b. Value used in DNB analyses. (ITDP Transients).
c. These parameter values are associated with an F_Q value of 2.19.
d. These parameter values are associated with an F_Q value of 2.32.

Table 4.4-2 (continued)
REACTOR DESIGN COMPARISON TABLE (CURRENT OPERATING CONDITIONS)

Thermal and Hydraulic Design Parameters	Uprated Power 17 x 17 NAIF Design	Uprated T_{avg} (587.8°F) 17 x 17 LOPAR Design
Heat transfer (continued)		
Maximum thermal output at maximum overpower trip point (118% power) and Peak linear power for determination of protection setpoints	21.1 kW/ft	21.1 kW/ft
Fuel central temperature (BOL)		
Peak at 100% power	3200°F	3250°F
Peak at maximum thermal output for maximum overpower trip point	4150°F	4150°F
Pressure drop		
Across core	18.3 psi [e]	23.7 ± 4.7 psi [f]
Across vessel, including nozzle	34.71 psi	44.1 ± 6.6 psi

e. Based on thermal design flow rate (Section 5.1).
f. Based on best-estimate reactor flow rate (Section 5.1).

Table 4.4-3
THERMAL-HYDRAULIC DESIGN PARAMETERS
FOR ONE OF THREE COOLANT LOOPS OUT OF SERVICE[a]

	One Loop Isolated
Total core heat output	1805 MWt
Total core heat output	6160×10^6 Btu/hr
Heat generated in fuel	97.4%
Nominal system pressure	2250 psia
Coolant flow	
Effective thermal flow rate for heat transfer	72.4×10 lb/hr
Effective flow area for heat transfer	41.5 ft^2
Average velocity along fuel rods	10.7 ft/sec
Average mass velocity	1.74×10 lb/hr-ft^2
Coolant temperature	
Design nominal inlet	537.4°F
Average rise in core	65.1°F
Average in core	571.3°F
Heat transfer	
Active heat transfer surface area	48,600 ft^2
Average heat flux	123,500 Btu/hr-ft^2
Minimum DNBR at nominal operating conditions	>1.77
Minimum DNBR for design and anticipated transients	≥1.30

a. Plant operation with one loop out of service is prohibited by the Plant Technical Specifications

Table 4.4-4
VOID FRACTIONS AT NOMINAL REACTOR CONDITIONS
WITH DESIGN HOT-CHANNEL FACTORS

	Average	Maximum
Core	0.66%	-
Hot subchannel	4.6%	17.5%

Table 4.4-5
COMPARISON OF THINC-IV AND THINC-I PREDICTIONS WITH DATA
FROM REPRESENTATIVE WESTINGHOUSE TWO- AND THREE-LOOP REACTORS

Reactor	Power (MWt)	Percent Full Power	Measured Inlet Temp (°F)	rms(°F) THINC-I	(°F) THINC-IV	Improvement for THINC-IV over THINC-I
Ginna	847	65.1	543.7	1.97	1.83	0.14
	854	65.7	544.9	1.56	1.46	0.10
	857	65.9	543.9	1.97	1.82	0.15
	947	72.9	543.8	1.92	1.74	0.18
	961	74.0	543.7	1.97	1.79	0.18
	1091	83.9	542.5	1.73	1.54	0.19
	1268	97.5	542.0	2.35	2.11	0.24
	1284	98.8	540.2	2.69	2.47	0.22
	1284	98.9	541.0	2.42	2.17	0.25
	1287	99.0	544.4	2.26	1.97	0.29
	1294	99.5	540.8	2.20	1.91	0.29
	1295	99.6	542.0	2.10	1.83	0.27
Robinson	1427.0	65.1	548.0	1.85	1.88	0.03
	1422.6	64.9	549.4	1.39	1.39	0.00
	1529.0	88.0	550.0	2.35	2.34	0.01
	2207.3	100.7	534.0	2.41	2.41	0.00
	2213.9	101.0	533.8	2.52	2.44	0.08

Figure 4.4-1
FUEL AVERAGE AND SURFACE TEMPERATURES VERSUS LINEAR POWER:
TYPICAL PEAK VALUES DURING FUEL ROD LIFETIME

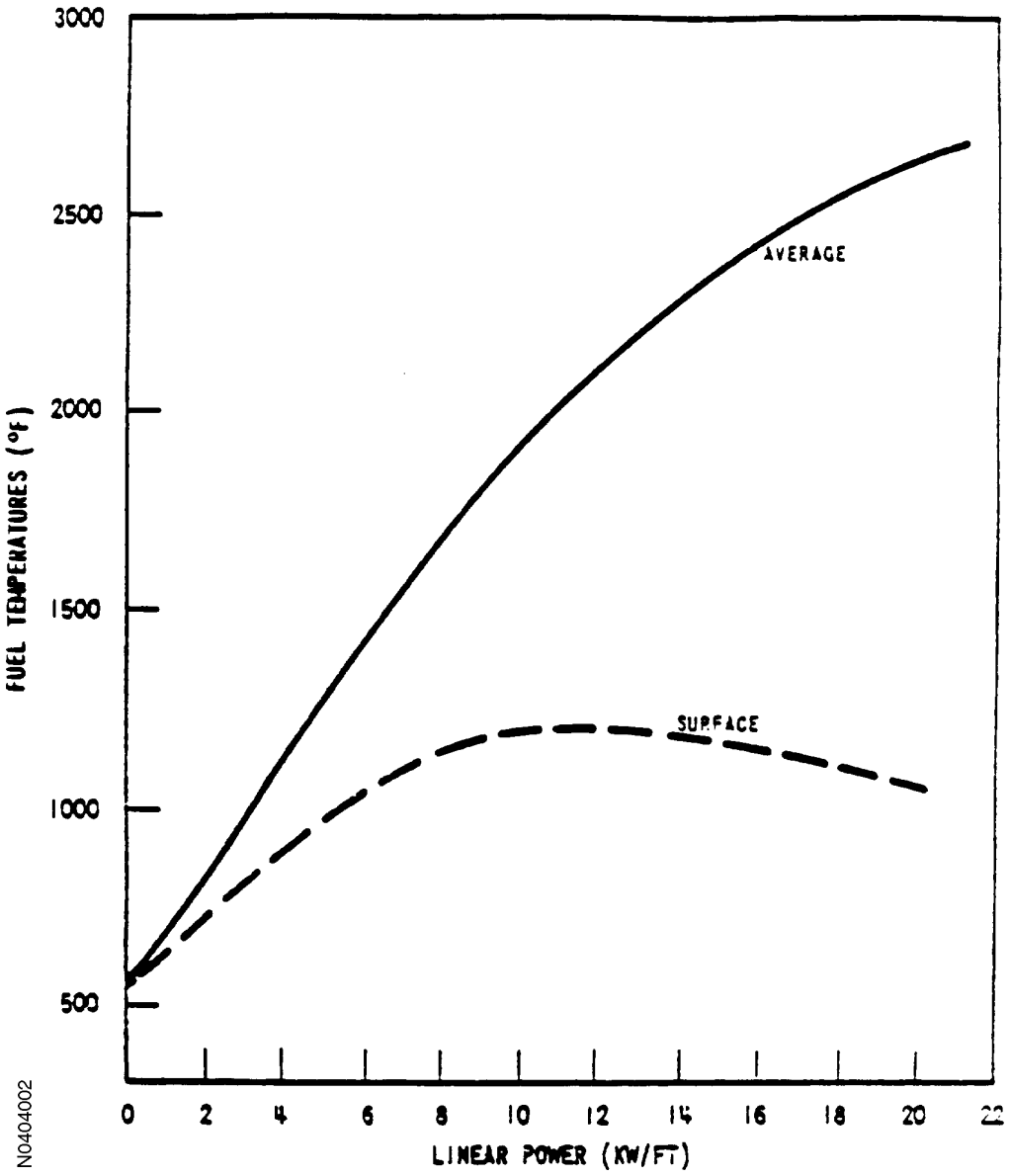

Figure 4.4-2
FUEL CENTERLINE TEMPERATURE VERSUS LINEAR POWER:
TYPICAL PEAK VALUES DURING FUEL ROD LIFETIME

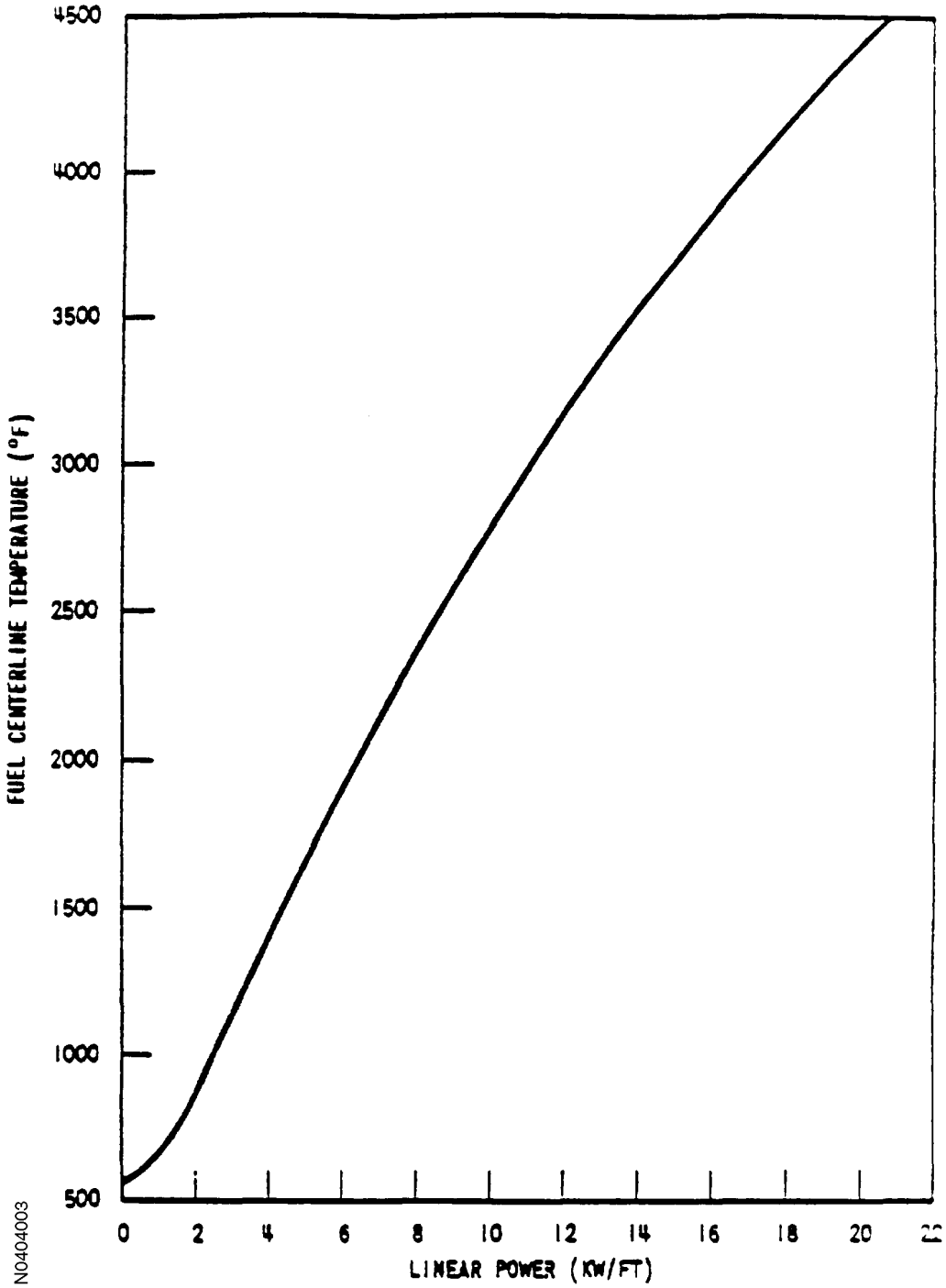

Figure 4.4-3
THERMAL CONDUCTIVITY OF UO_2 (DATA CORRECTED TO 95% THEORETICAL DENSITY)

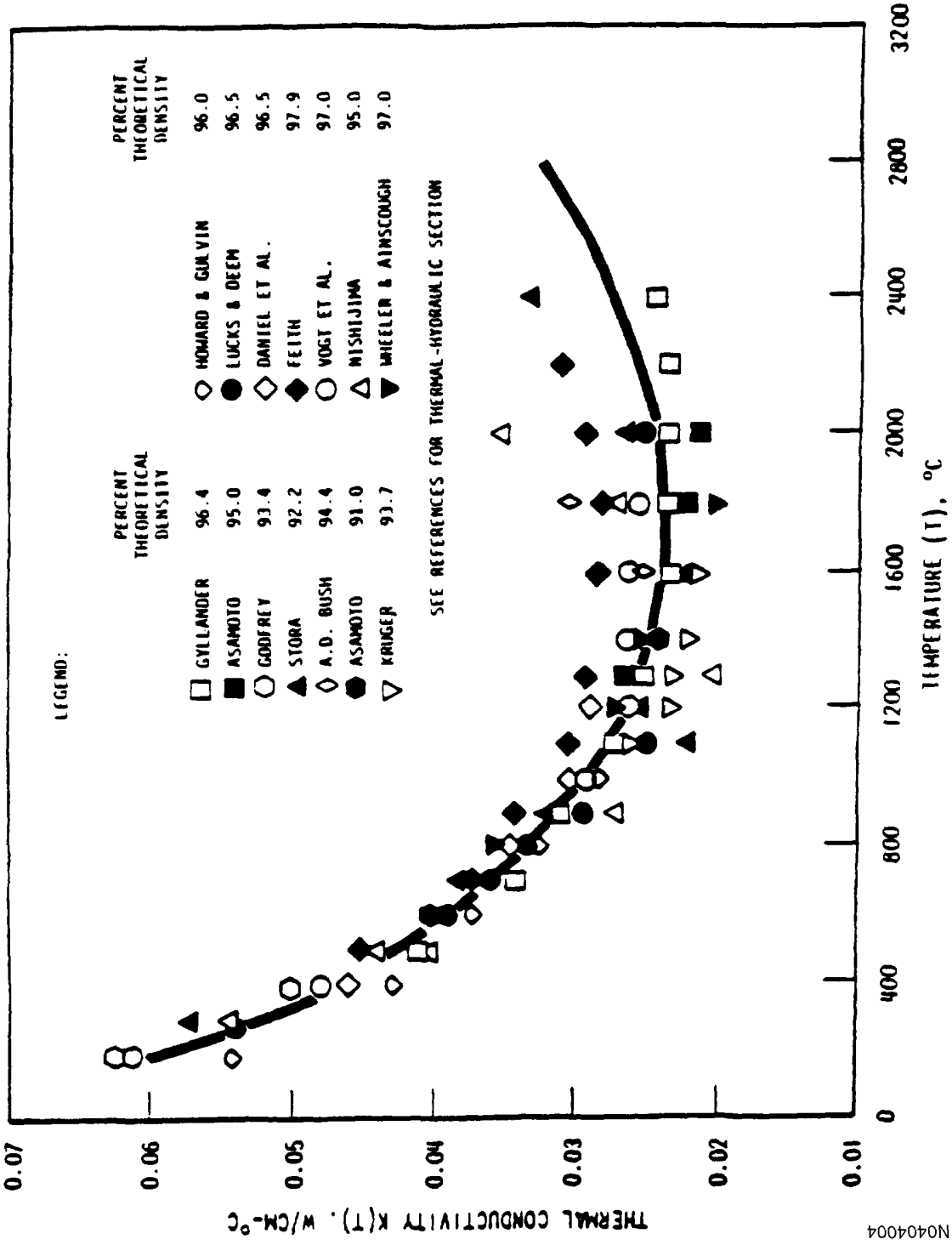

N040400 4

Figure 4.4-4
AXIAL VARIATION OF AVERAGE CLAD TEMPERATURE
FOR ROD OPERATING AT 5.43 KW/FT

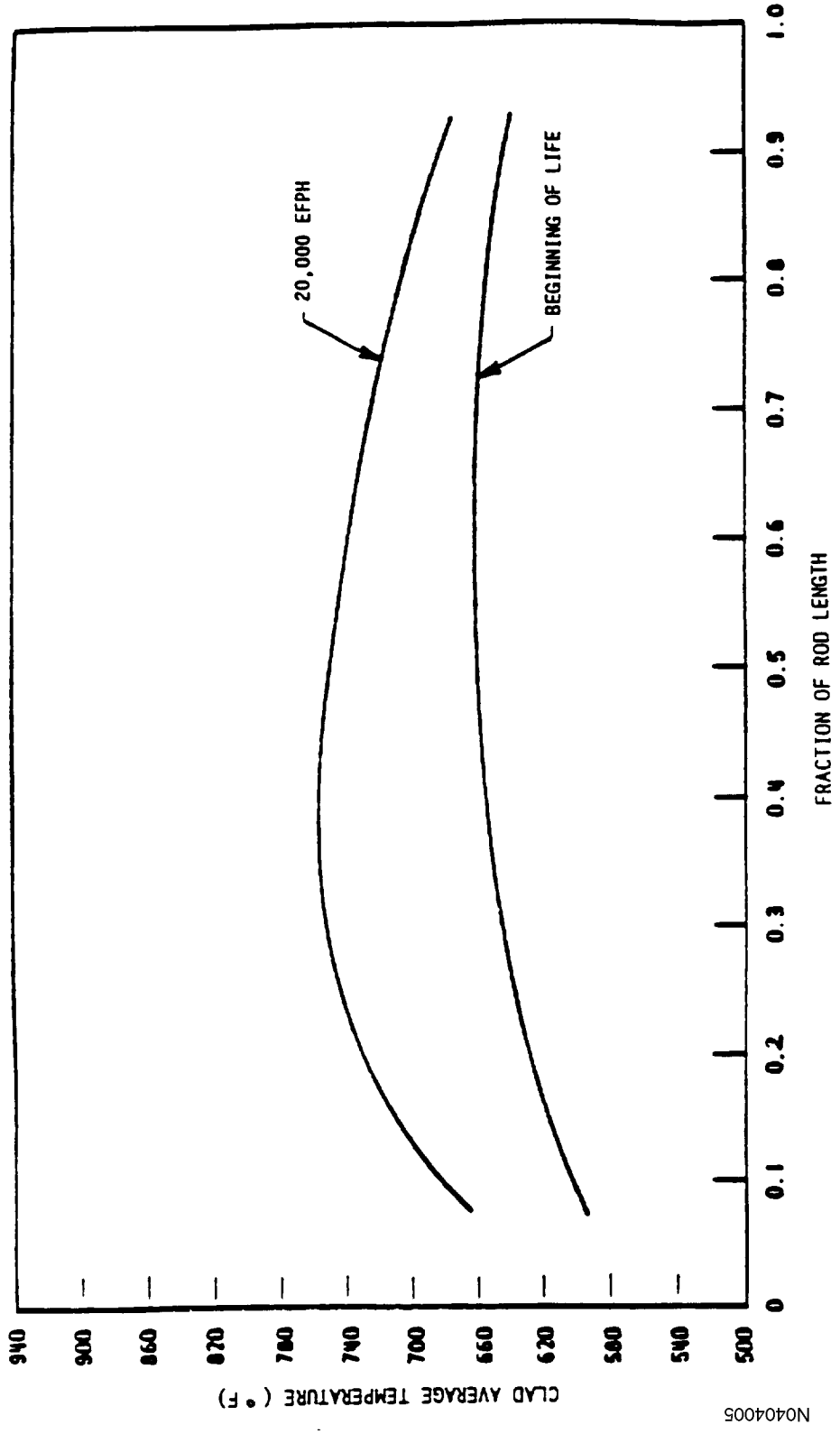

Figure 4.4-5
COMPARISON OF ALL "R" GRID DATA FOR TYPICAL CELL

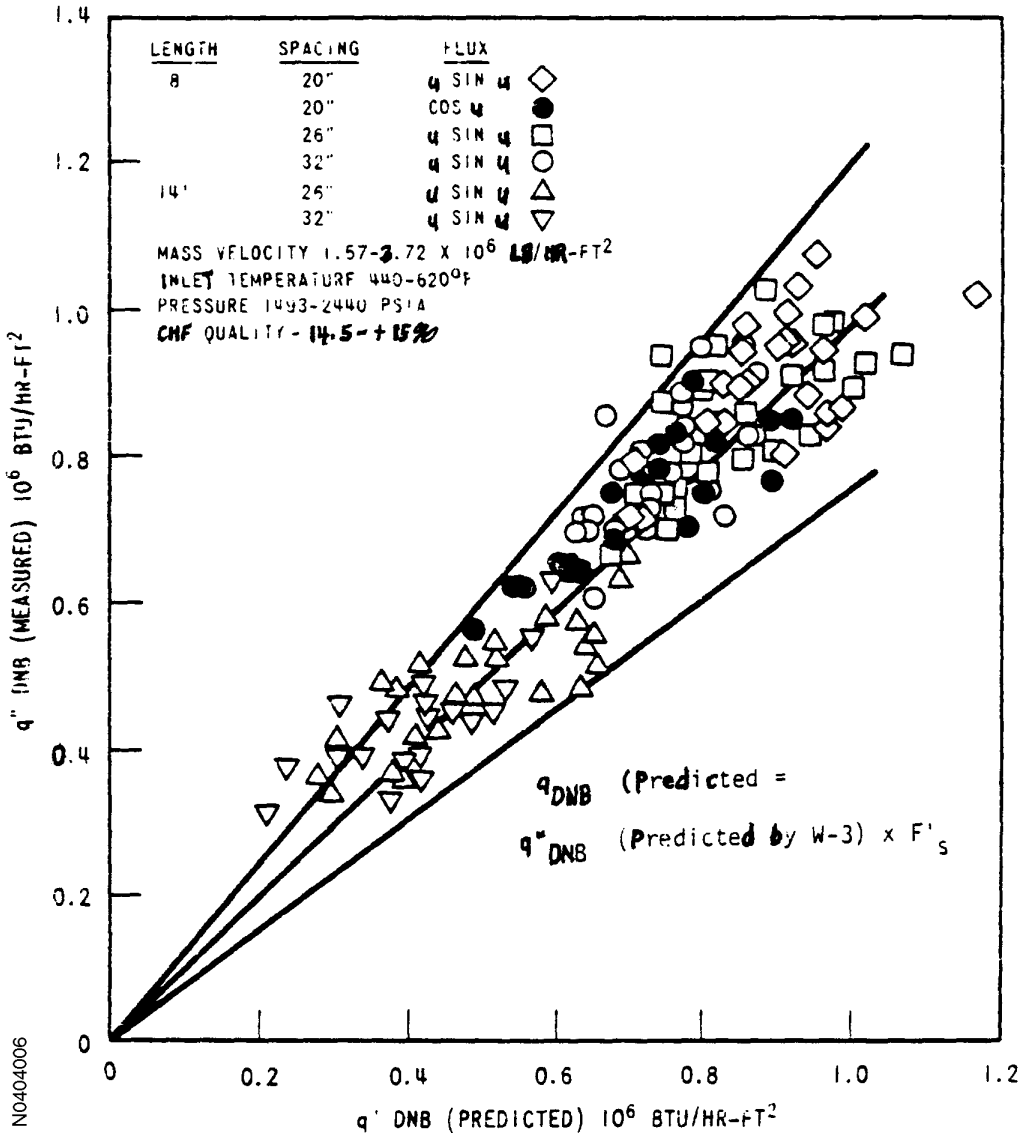

Figure 4.4-6
COMPARISON OF ALL "R" GRID DATA FOR THIMBLE CELLS

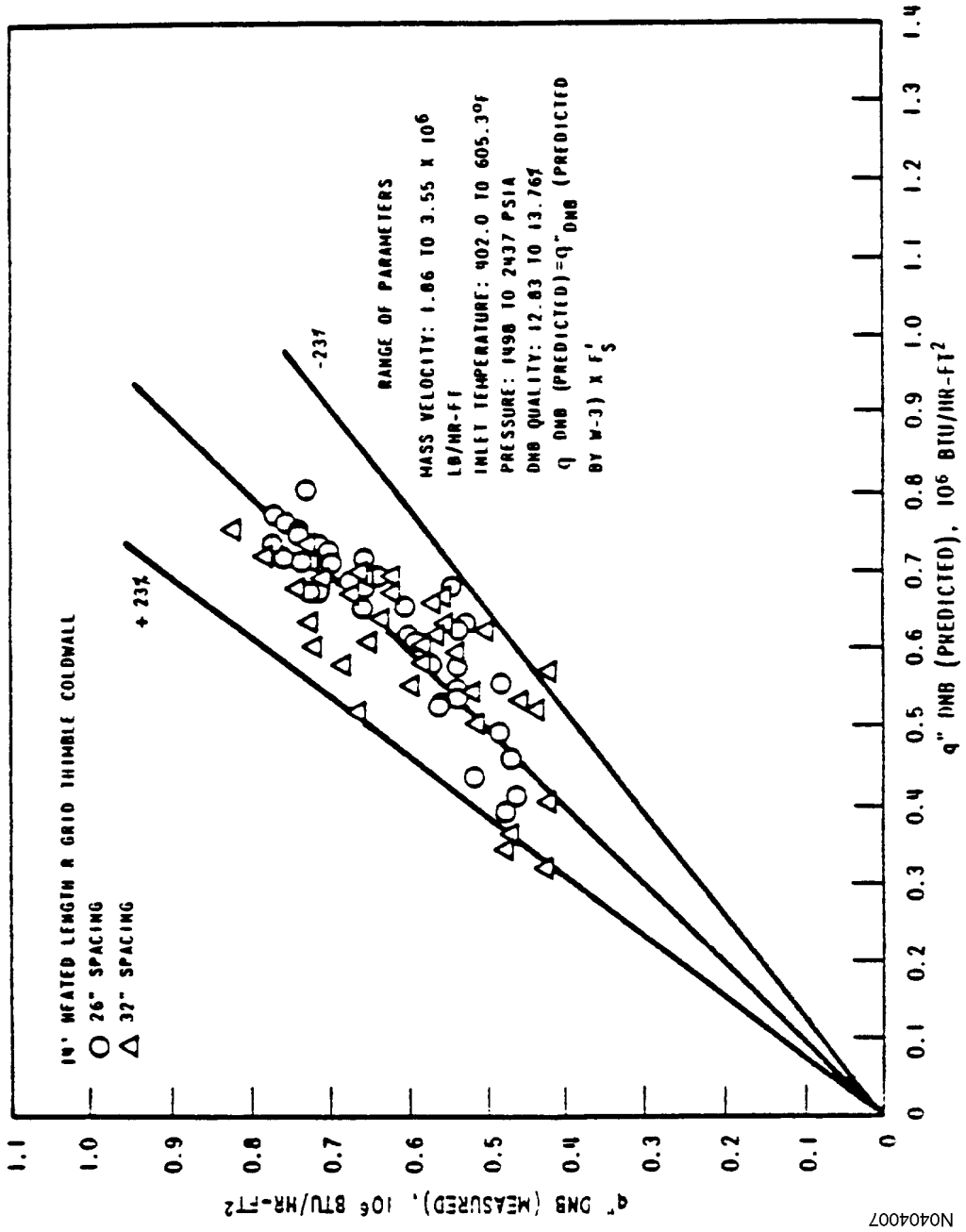

N040400T

Figure 4.4-7
COMPARISON OF 17 X 17 DNB DATA WITH GRID SPACING OF 26 INCHES

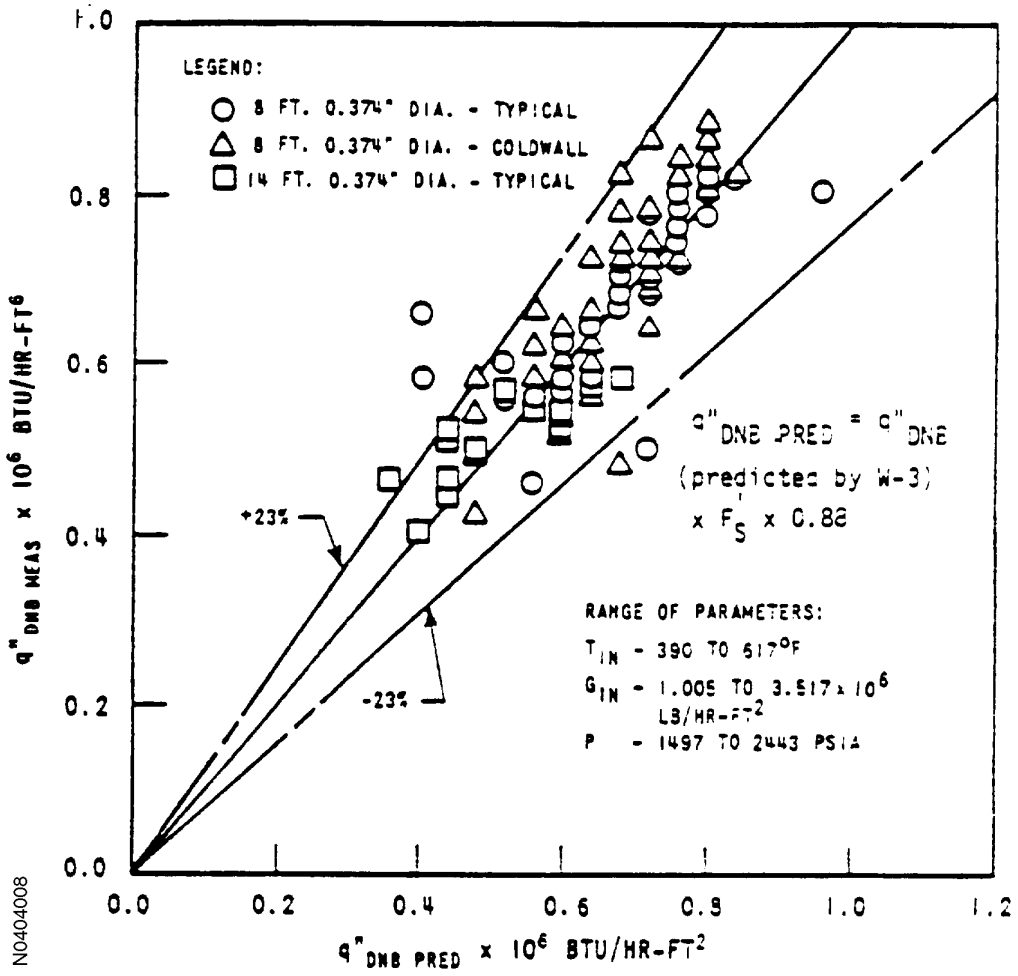

Figure 4.4-8
COMPARISON OF MEASURED TO PREDICTED CHF
WITH GRID SPACING OF 22 INCHES

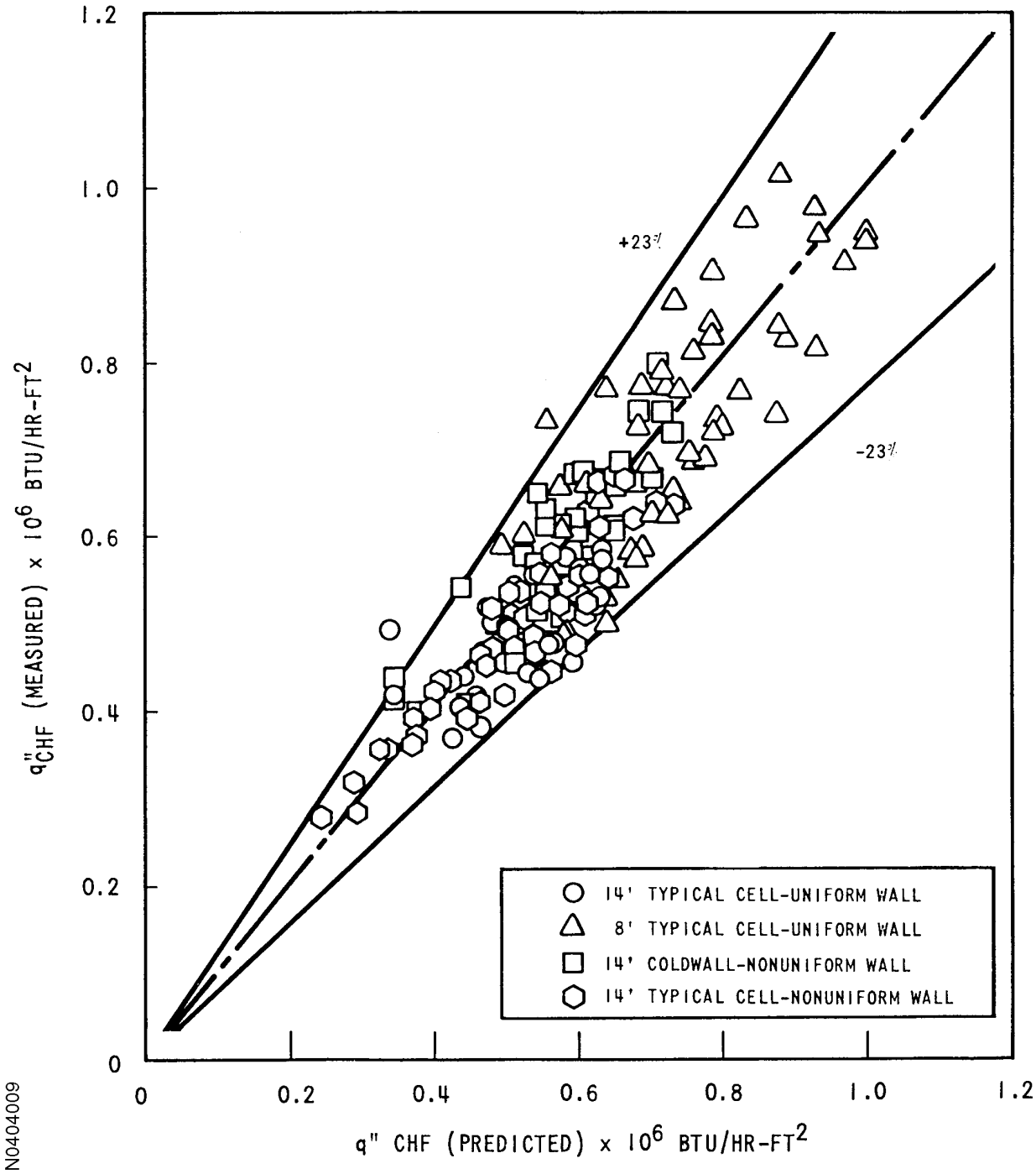

Figure 4.4-9
MEASURED VERSUS PREDICTED CRITICAL HEAT FLUX - WRB-I CORRELATION

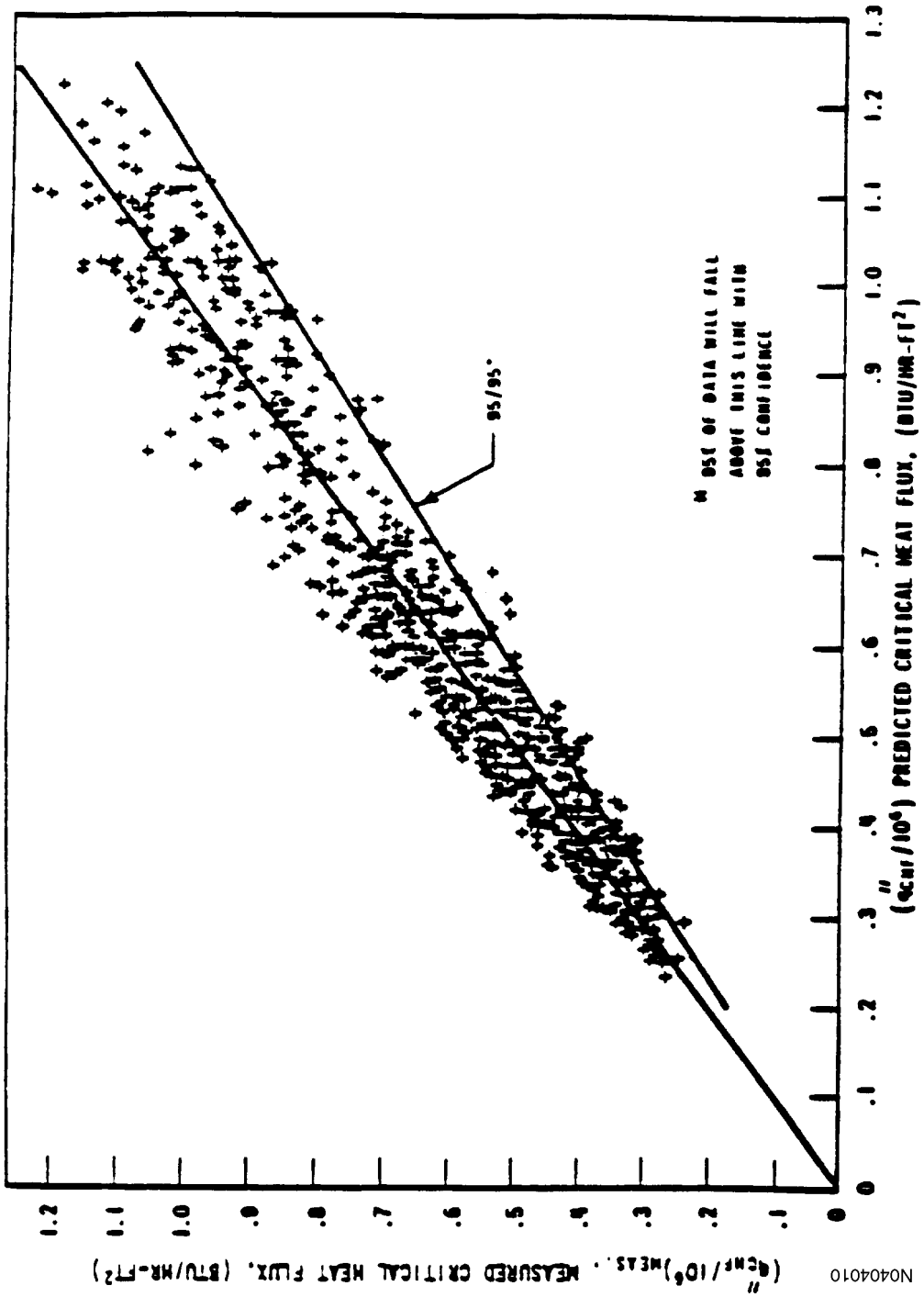

Figure 4.4-10
TDC VERSUS REYNOLDS NUMBER FOR 26-IN. GRID SPACING

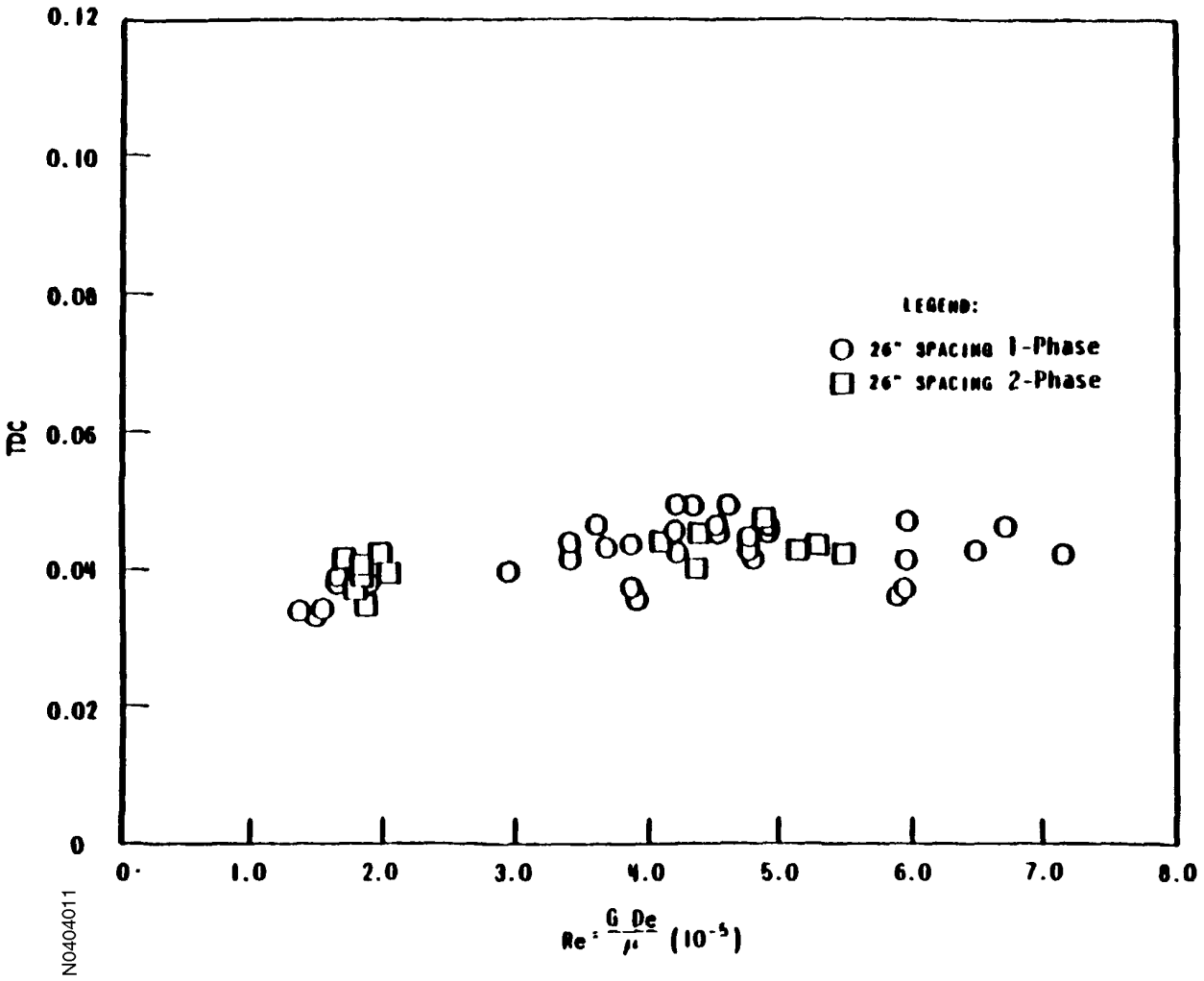

Figure 4.4-11
NORMALIZED RADIAL FLOW AND ENTHALPY
DISTRIBUTION AT 4-FT ELEVATION (REPRESENTATIVE)

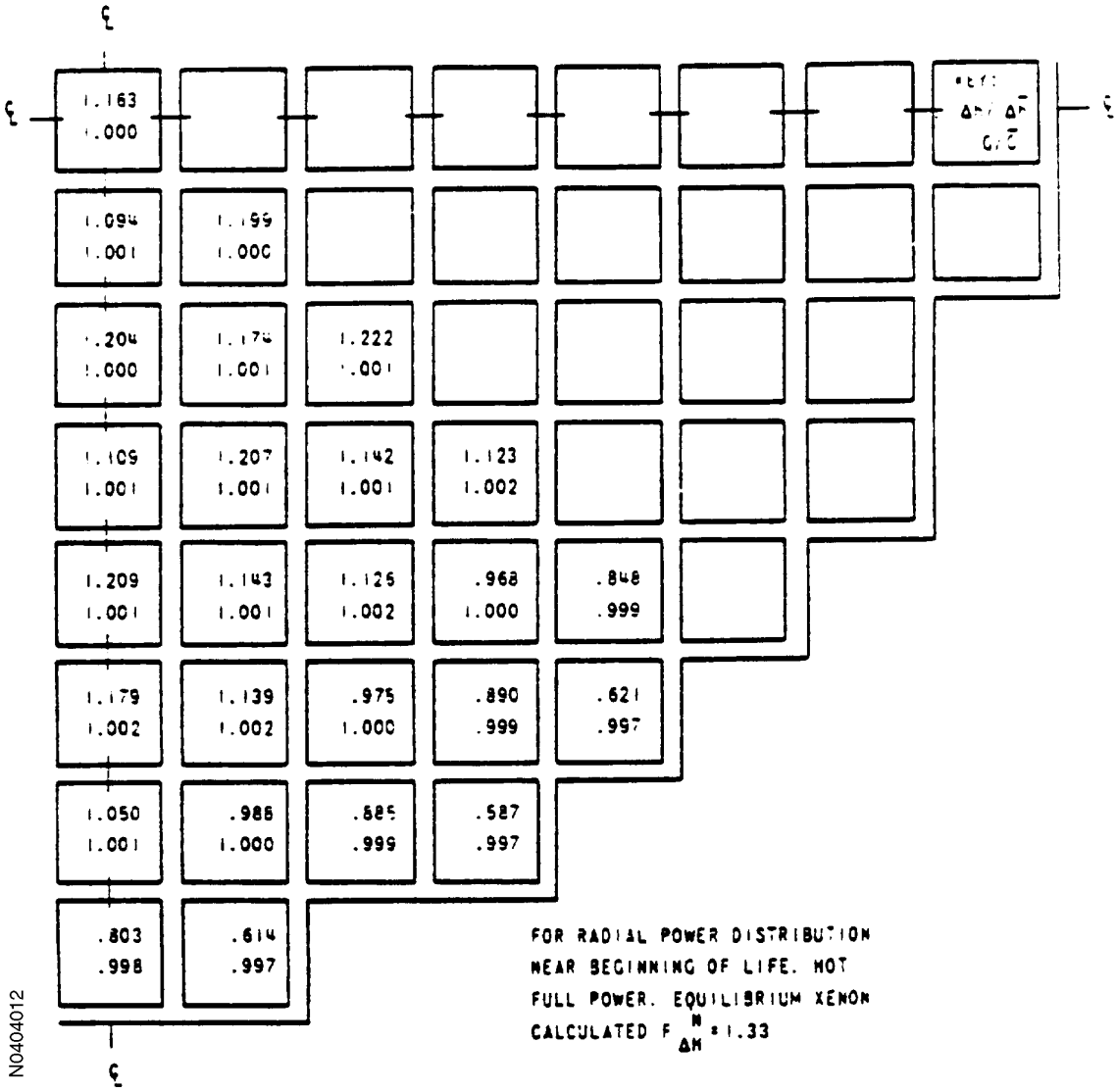

Figure 4.4-12
NORMALIZED RADIAL FLOW AND ENTHALPY
DISTRIBUTION AT 8-FT ELEVATION (REPRESENTATIVE)

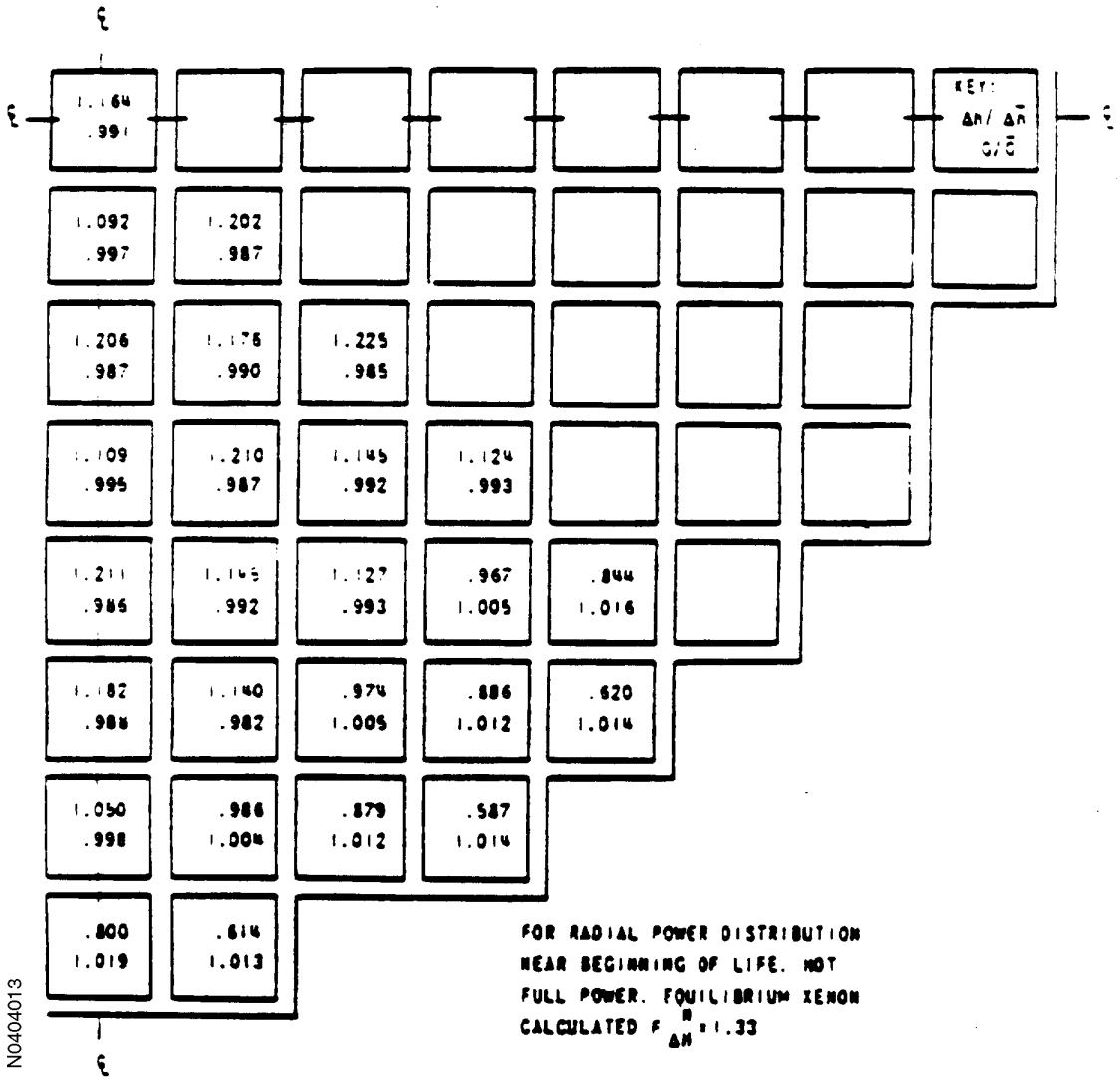

Figure 4.4-13
NORMALIZED RADIAL FLOW AND ENTHALPY
DISTRIBUTION AT 12-FT ELEVATION - CORE EXIT (REPRESENTATIVE)

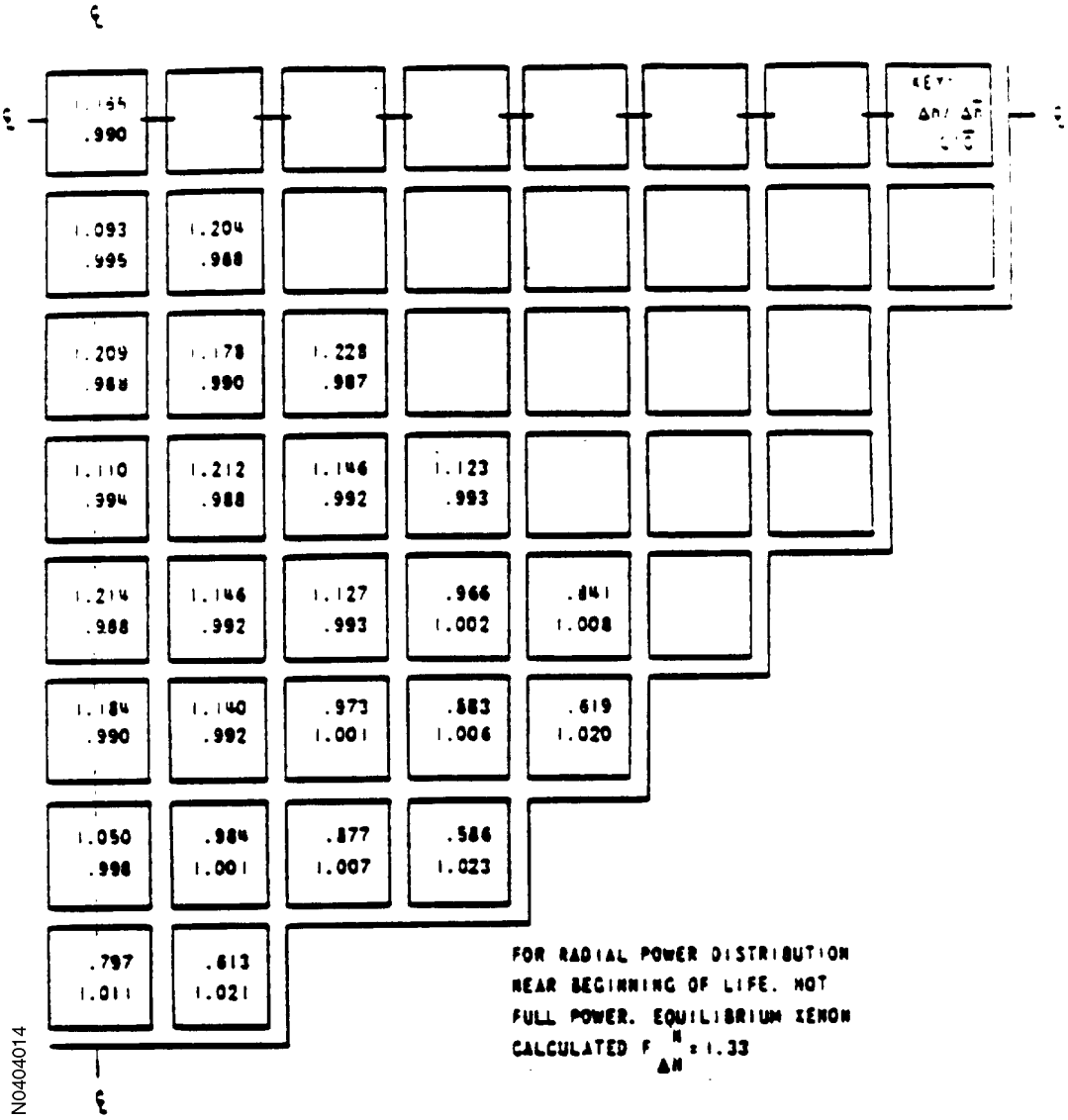

Figure 4.4-14
THERMODYNAMIC QUALITY, $X = H - H_{sat} / H_g - H_{sat}$
VOID FRACTION VERSUS THERMODYNAMIC QUALITY $H - H_{sat}/H_g - H_{sat}$

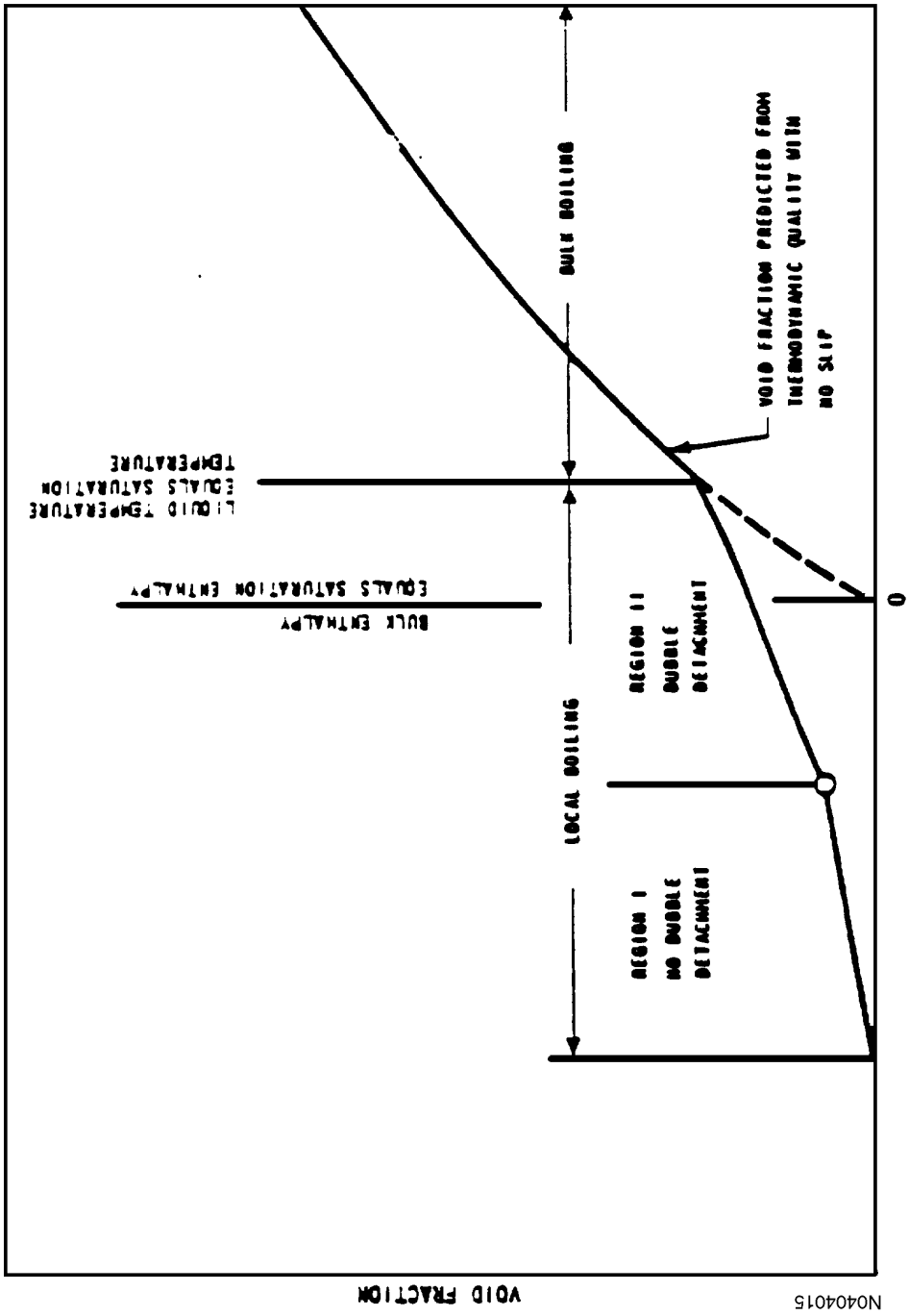

Figure 4.4-15
PWR NATURAL CIRCULATION TEST

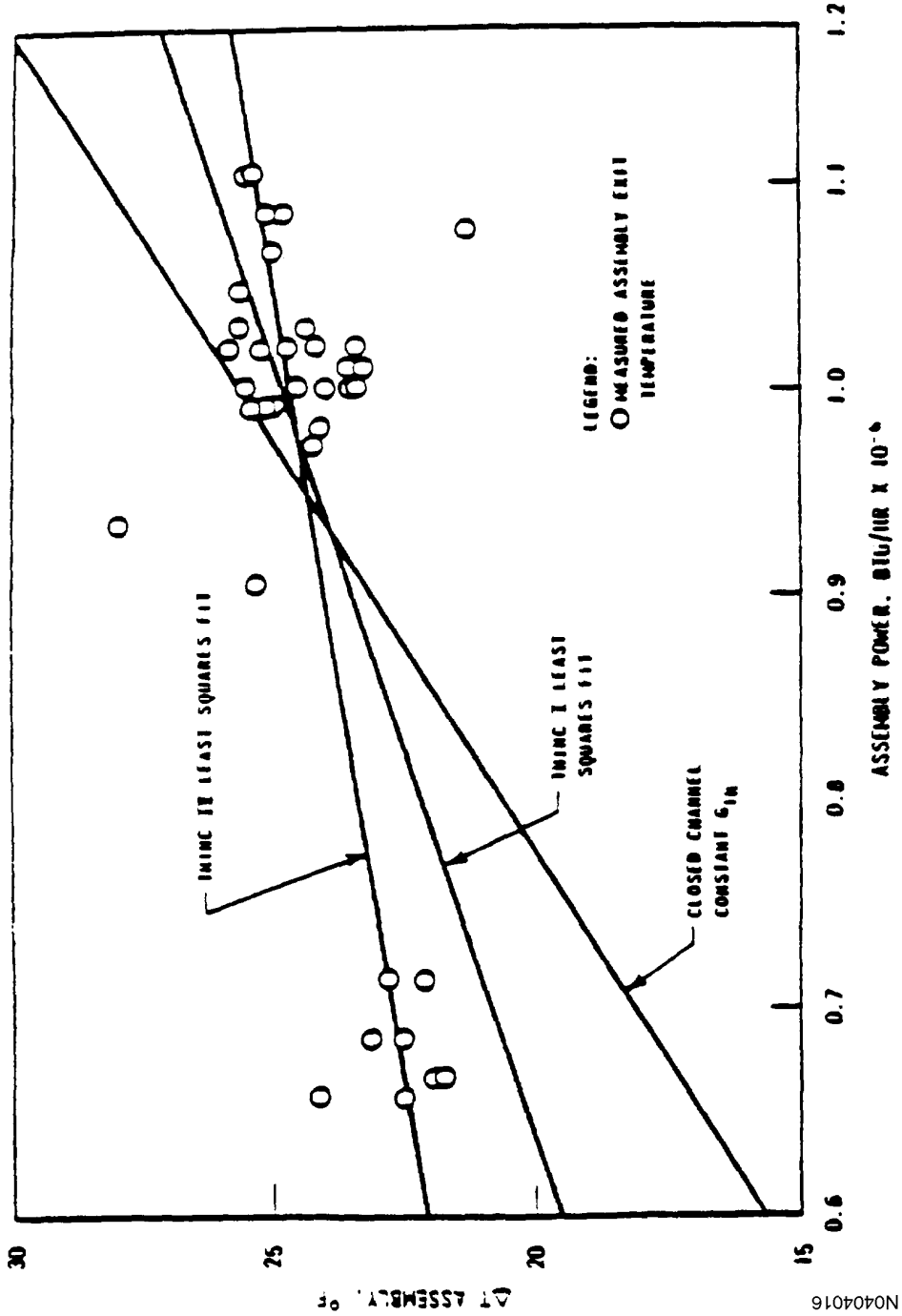

N040401G

Figure 4.4-16
COMPARISON OF A REPRESENTATIVE W TWO-LOOP REACTOR INCORE THERMOCOUPLE MEASUREMENTS WITH THINC-IV PREDICTIONS

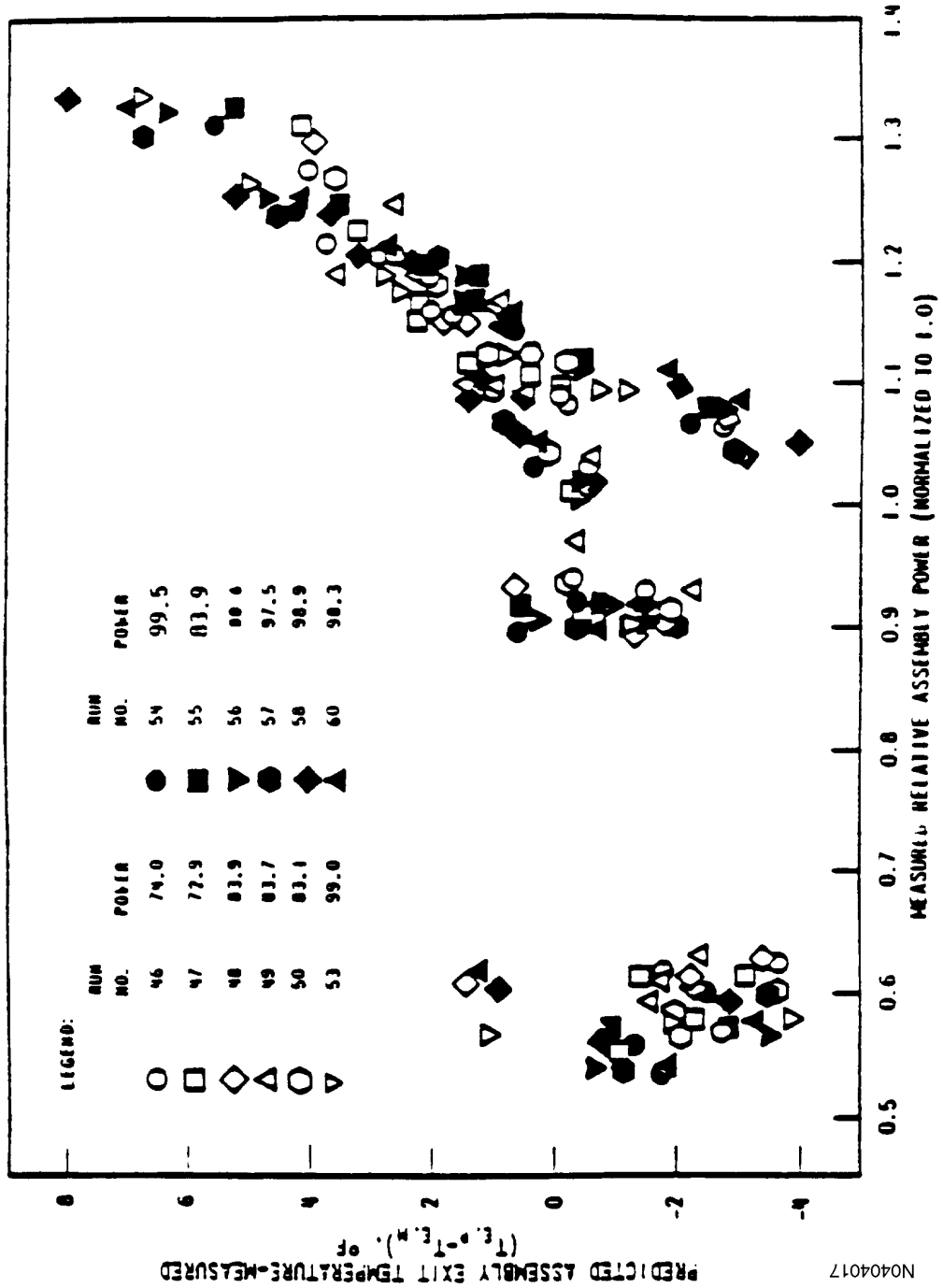

Figure 4.4-17
COMPARISON OF A REPRESENTATIVE W THREE-LOOP REACTOR INCORE THERMOCOUPLE MEASUREMENTS WITH THINC-IV PREDICTIONS

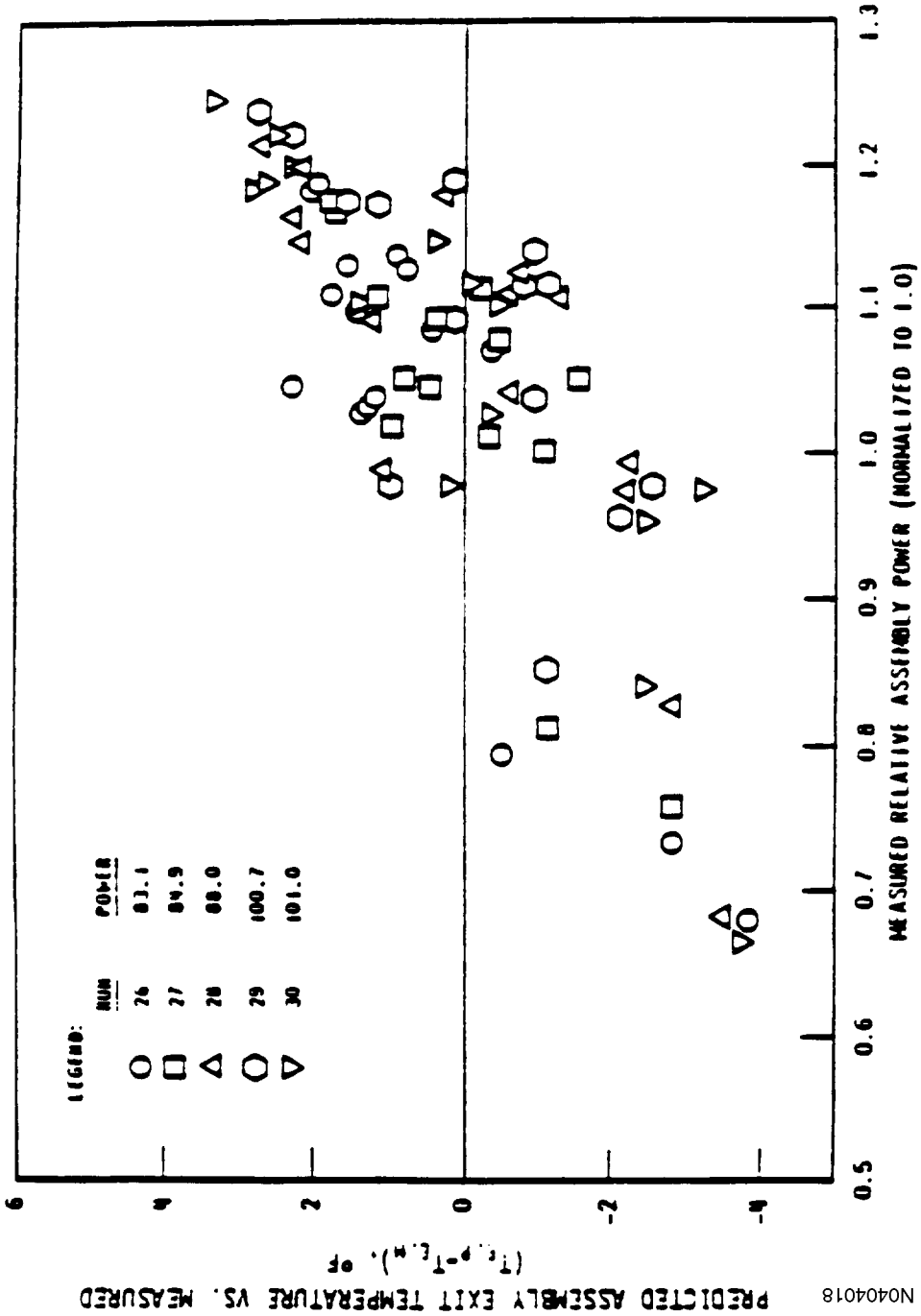

N040401 8

Figure 4.4-18
HANFORD SUBCHANNEL TEMPERATURE DATA COMPARISON WITH THINC-IV

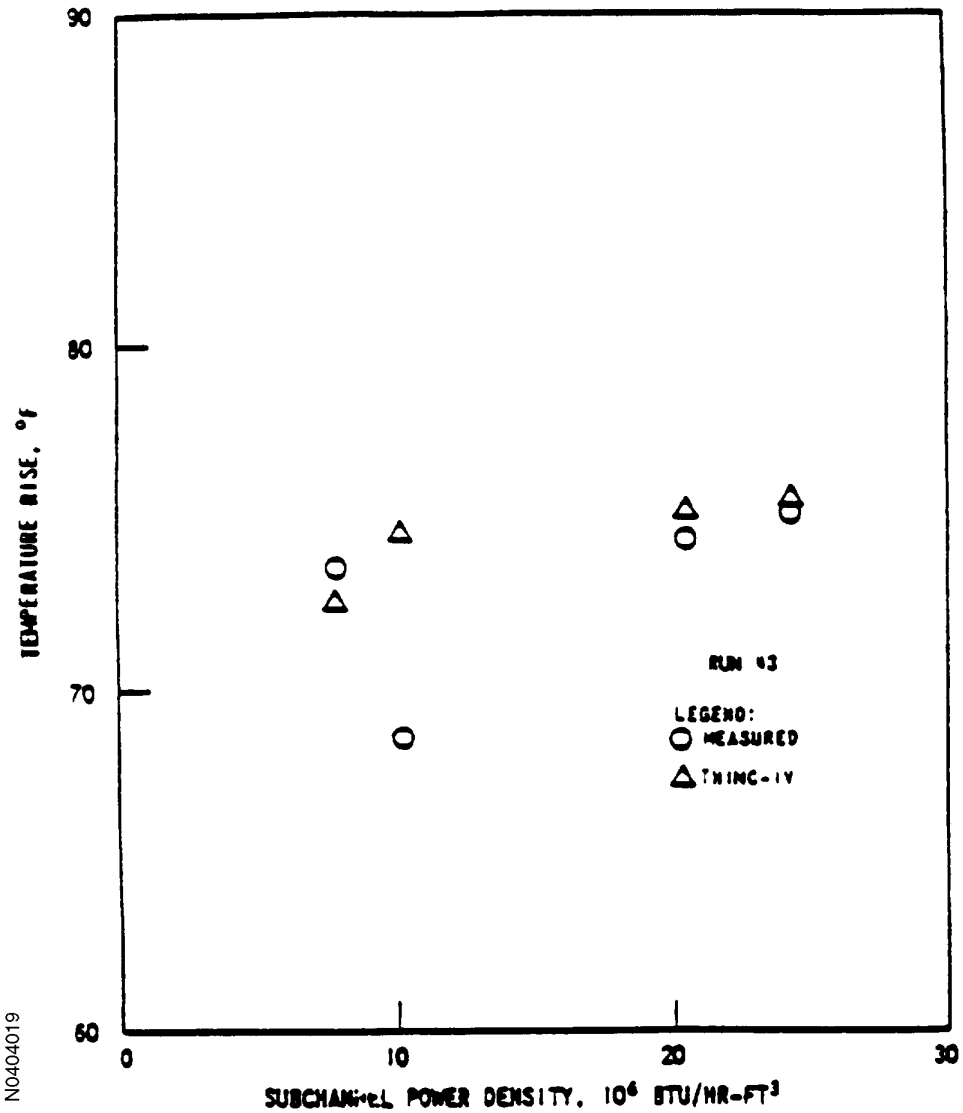

Figure 4.4-19
HANFORD SUBCRITICAL TEMPERATURE DATA COMPARISON WITH THINC-IV

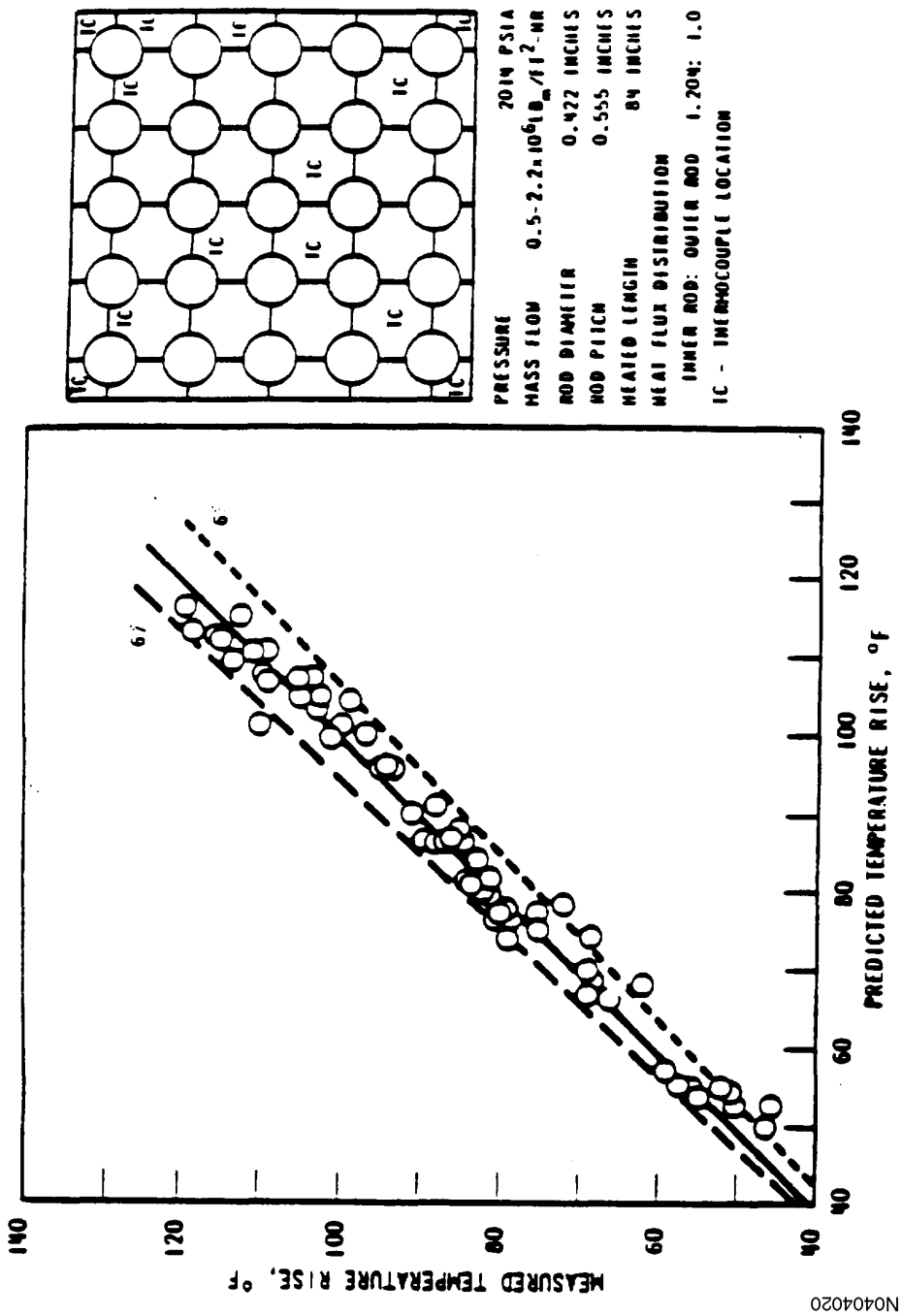

N040402O

Figure 4.4-20
DISTRIBUTION OF INCORE INSTRUMENTATION - UNIT 1

	R	P	N	M	L	K	J	H	G	F	E	D	C	B	A
1								D	T						
2							T		T	D					
3				TD		T	D	*TD		T		TD			
4			T		D			D		D	T				
5			D		D	T	D	T		T	D	TD		TD	
6			*T		TD			D	T	D					
7	T	T	D				D		D		T	D		D	
8	D	*T	TD		TD	T		T	T	D	*T		*TD	D	T
9				T	D			T	D	TD					D
10			TD				TD				T	D		TD	
11				T	D	T		TD		TD	D				
12			D		T		TD				T	D	TD		
13								TD		TD					
14					TD				D		*T				
15							D	T	T						

N0404026

T = Thermocouple (51)
D = Movable Incore Detector (50)

*Thermocouples TE-37 (H-03), TE-7 (E-14), TE-24 (N-06), TE-27 (C-08), TE-31 (E-08), and TE-25 (P-08) on Unit 1 are abandoned in place.

Figure 4.4-21
DISTRIBUTION OF INCORE INSTRUMENTATION - UNIT 2

	R	P	N	M	L	K	J	H	G	F	E	D	C	B	A
1								D	T						
2							T		T	D					
3				TD		T	D	TD		T		TD			
4			T		D			D		D	T				
5			D		D	T	D	T		*T	D	TD		TD	
6			*T		TD			D	T	D					
7	T	T	D				D		D		T	D		D	
8	D	T	TD		TD	T		T	T	D	T		TD	D	T
9				T	D			T	D	TD					D
10			TD				TD				*T	D		TD	
11				T	D	T		TD		*TD	D				
12			D		T		TD				T	D	TD		
13								TD		TD					
14					TD				D		T				
15							D	T	T						

N0404025

T = Thermocouple (51)
D = Movable Incore Detector (50)

* Thermocouples TE-11 (F-11), TE-24 (N-06), TE-9 (F-05), and TE-32 (E-10) on Unit 2 are abandoned in place.

4.5 ADVANCED MARK-BW FUEL

4.5.1 Summary Description

Cycle 17 of Unit 2 and Cycle 18 of Unit 1 mark the beginning of the North Anna Power Station transition to Advanced Mark-BW fuel supplied by Framatome ANP. Approximately two-thirds of these initial transition reload cores consist of Westinghouse fuel. This section provides the description of the Advanced Mark-BW fuel and the methods, models, and mechanical analysis that were used to design and qualify the fuel.

The basic design parameters of the Advanced Mark-BW are comparable to those of the Westinghouse resident fuel assemblies. The Advanced Mark-BW fuel assembly incorporates proven Framatome ANP design features while maintaining compatibility with the Westinghouse reactor internals and resident fuel assemblies. Compatibility of the Advanced Mark-BW fuel with the NAPS and its resident fuel is discussed in detail in Reference 1. The Advanced Mark-BW fuel has been evaluated for use at North Anna Units 1 and 2 to a lead rod burnup of 60,000 MWD/MTU (References 28 & 29).

4.5.2 Mechanical Design

4.5.2.1 Fuel

4.5.2.1.1 Design Basis

The fuel rod and fuel assembly design bases are established to satisfy the general performance and safety criteria presented in Section 4.2 and specific criteria noted below.

4.5.2.1.1.1 *Fuel Rods.* The integrity of the fuel rods is ensured by designing to prevent excessive fuel temperatures, excessive internal rod gas pressures due to fission gas releases, and excessive cladding stresses and strains. This is achieved by designing the fuel rods so that the following conservative design bases are satisfied during Condition I and Condition II events over the fuel lifetime:

4.5.2.1.1.1.1 *Fuel Pellet Temperatures.* During modes of operation associated with Condition I and Condition II events, the maximum fuel temperature for the UO_2 fuel rods shall be less than the melting temperature of UO2. Framatome uses a best-estimate melting point of 5173°F for unirradiated UO2 with the melting point decreasing by 65°F per 10,000 MWD/MTU.

4.5.2.1.1.1.2 *Internal Gas Pressure.* The internal pressure of the lead rod in the reactor is limited to a value below that which could cause the diametral gap to increase due to outward creep during steady-state operation and that could cause extensive departure from nucleate boiling (DNB) propagation to occur.

4.5.2.1.1.1.3 *Cladding Stress.* The cladding stress level is evaluated per the methodology given in Reference 2 based on the stress intensity levels defined by the ASME code (Reference 3). Conservative values are used for cladding thickness, oxide layer buildup, external pressure,

internal fuel rod pressure, differential temperature, and unirradiated cladding yield strength. The stress categories are divided into compressive stresses and tensile stresses according to the criteria of Reference 2. The stress levels during operation are required to remain below the stress limits based on the cladding yield strength defined in Reference 2.

4.5.2.1.1.1.4 *Cladding Strain.* The cladding strain is evaluated per the methodology given in Reference 2. The transient strain limit uses cladding circumferential changes before and after a linear heat rate (LHR) transient to determine the strain. The analysis is conducted using the TACO3 fuel rod thermal analysis code (Reference 4). The cladding strain during transient conditions remains below 1%.

4.5.2.1.1.1.5 *Cladding Strain Fatigue.* The cladding strain fatigue is evaluated per the methodology given in Reference 2. Conservative inputs are assumed for cladding thickness, oxide layer buildup, external pressure, internal fuel rod pressure, and differential temperature across the cladding. Testing has shown the fatigue endurance performance for the zirconium-based alloy M5 cladding is similar to Zircaloy-4 claddings, with the lower yield strength of the recrystallized annealed (RXA) claddings limiting the applied stresses. Therefore, the O'Donnell-Langer fatigue curve for irradiated Zircaloy of Reference 5 is used to determine the fatigue performance of the M5 cladding. The cladding fatigue usage factor is required to remain below 0.9 for a conservative fuel rod lifetime.

4.5.2.1.1.1.6 *Cladding Creep Collapse.* The cladding creep collapse lifetime is evaluated per the methodology given in References 2 and 6. The acceptance criterion is that the predicted creep collapse life of the fuel rod must exceed the maximum expected in-core life.

4.5.2.1.1.1.7 *Cladding Corrosion.* The cladding corrosion is evaluated per the methodology given in Reference 7. M5 fuel rod cladding exhibits a strong resistance to corrosion. The corrosion has been found to be less than one half the corrosion of low-tin Zircaloy claddings. The corrosion thickness is predicted based on the operating conditions and power histories of the high burnup fuel rods in the core. The maximum cladding corrosion level is required to remain below 100 microns during the lifetime of the fuel.

4.5.2.1.1.2 *Fuel Assembly Structure.* The fuel assemblies are designed to accommodate expected conditions for handling during assembly, inspection, and refueling operations, and shipping loads. The fuel assemblies are designed to accept control rod insertions in order to provide the required reactivity control for power operations and reactivity shutdown conditions. The reactor internals in conjunction with the fuel assemblies direct reactor coolant through the core to achieve acceptable flow distribution and to restrict bypass flow so that the heat transfer performance requirements can be met for all modes of operation.

Structural integrity of the Advanced Mark-BW fuel assemblies is ensured by setting limits for stresses and deformations due to various loads and by determining that the assemblies do not inhibit the functioning of other components. The following types of loads are considered:

1. Nonoperational loads such as those due to shipping and handling.
2. Normal and abnormal loads that are defined for Conditions I and II.
3. Abnormal loads that are defined for Conditions III and IV.

The fuel assembly acceptance criteria summarized below are consistent with the acceptance criteria of the Section 4.2 of Standard Review Plan, NUREG-0800 (Reference 8). Design analyses are performed using standard Framatome ANP codes and methods licensed for use with the NRC. Stress analyses follow the general format and procedures outlined in Section III, Subsection NG, of the ASME Boiler and Pressure Vessel Code (Reference 3). The stress intensity limits for the components fabricated from ASME Code recognized materials are per the ASME Boiler and Pressure Vessel Code, Section III. Stress intensity limits for components fabricated from non-ASME Code materials are developed based on the guidelines of the ASME Code. The Sm, the allowable membrane stress, and the other material properties for these materials are determined from sources other than the ASME Code. Allowable stress levels for the fuel rod are given in Reference 2. Allowable stress levels for the holddown springs are based on nuclear industry experience with the spring material. Bolts are analyzed following the ASME Code guidelines for threaded structural fasteners. Irradiation induced changes in the material properties are considered in determining the allowable stress levels for design verification. Worst case or 2s tolerance dimensions are used in all cases except where noted and justified.

4.5.2.1.1.2.1 *Spacer Grids.* The Advanced Mark-BW end and intermediate spacer grids position the fuel rods to be mutually parallel on the proper square pitch spacing, position the guide thimbles in the proper pattern, and provide lateral support to the fuel rods, guide thimbles, and instrument sheath. The grid component strength criterion is based on experimental tests. Per Reference 9, the grid component strength criterion is based on the lower 95% confidence level on the true mean from the distribution of grid strength data at operating temperature. The design bases for fuel assembly spacer grids require that no crushing deformations occur for normal operation and Operational Basis Earthquake (OBE) conditions. The grids must also maintain sufficient geometry to ensure control rod insertability for Safe Shutdown Earthquake (SSE) conditions. Grids must provide adequate support to maintain the fuel rods in a coolable configuration under all conditions, including Safe Shutdown Earthquake (SSE) and Loss of Coolant (LOCA) conditions.

4.5.2.1.1.2.2 *Vibration and Fatigue.* The spacer grids provide adequate support to maintain the fuel rods in a coolable geometry for all operating conditions. The grids also provide lateral and rotational restraint for the fuel rods. Contact surfaces for the fuel rods maintain acceptable cladding wear depths throughout the life of the fuel assembly. Fuel rod wear performance is established based on design verification testing and/or operating experience with similar designs.

4.5.2.1.1.2.3 *Guide Thimble Wear.* Guide thimble wear is considered in the structural analyses of the fuel assembly. Wear characteristics are based on operation experience (post irradiation examinations), design verification testing, and/or similarities with existing designs. The criterion for allowable guide thimble wear is determined based on structural analyses of the guide thimbles that account for tube wall thinning due to wear.

4.5.2.1.1.2.4 *Corrosion Allowance.* Material thinning due to corrosion is considered in the structural analyses as applicable. The corrosion allowance(s) are established based on operating experience.

4.5.2.1.1.2.5 *Fatigue Analyses.* The total fatigue usage factor for all Normal Condition events does not exceed 0.9 for the fuel rod assembly and 1.0 for all other fuel assembly components. Fatigue analyses are plant specific based on the transients given in Table 5.2-4.

4.5.2.1.1.2.6 *Normal Operation.* Structural integrity is verified for the fuel assembly and its components subjected to loading associated with normal operation and upset events (and emergency condition transients, if applicable).

4.5.2.1.1.2.7 *LOCA/Seismic.* Structural integrity is verified for the fuel assembly and its components subjected to loading associated with LOCA, Seismic (both Operating Basis Earthquake, or OBE, and Safe Shutdown Earthquake, or SSE), and combined LOCA and Seismic events. Rod Cluster Control Assembly insertion requirements are presented below. A coolable geometry is maintained at all times including Condition IV events:

1. During all normal operation (Condition I).
2. During all Condition II and III events.
3. During an OBE (Operating Base Earthquake)
4. Following a SSE (Safe Shutdown Earthquake)

4.5.2.1.1.2.8 *Fuel Handling Loads.* Handling equipment set points and accelerations limit the loads imposed on the fuel assembly. The structural integrity is verified for the fuel assembly and its components subjected to loading associated with handling operations.

4.5.2.1.1.2.9 *Shipping Loads.* The evaluation of the fuel assembly components for loads imposed on the fuel assembly during shipment addresses the following quasi-static loading:

Lateral: 6.0 Gs load factor
Axial: 4.0 Gs load factor

The structural integrity is verified for the fuel assembly and its components subjected to loading associated with shipping operations.

4.5.2.1.1.2.10 *Fuel Assembly Bow.* The fuel assembly is free standing as fabricated, and its as-built bow and tilt are sufficiently small to facilitate ease of handling and to minimize additional irradiation induced fuel assembly bow during operation.

4.5.2.1.1.2.11 *Fuel Assembly Growth Allowance.* The fuel assembly to reactor internals gap allowance for differential growth and thermal expansion is designed to ensure that a positive clearance is maintained during the assembly life.

4.5.2.1.1.2.12 *Fuel Rod Growth Allowance.* The fuel rod to fuel assembly top nozzle gap allowance for differential growth and thermal expansion is designed to ensure that a positive clearance is maintained during the assembly life.

4.5.2.1.2 Design Description

The Advanced Mark-BW fuel assembly is a 17 x 17, standard lattice, M5 intermediate spacer grid fuel assembly designed for use in Westinghouse-designed reactors. The fuel assembly incorporates many standard Framatome ANP design features while maintaining compatibility with the Westinghouse reactor internals and resident fuel assemblies. The nozzles and spacer grid designs are proven Framatome ANP designs that have operated in Westinghouse-designed reactor vessels. The guide thimble top section and dashpot diameters, the instrument sheath diameter, and the fuel rod outside diameter are compatible with the Westinghouse 17 x 17 standard and Vantage 5H designs. The fuel rod design has been developed based on standard Framatome ANP methods applied to a fuel rod with the same Westinghouse outside cladding outside diameter as standard 17 x 17 Westinghouse fuel rods. The features of the Advanced Mark-BW fuel assembly design include the M5 intermediate spacer grid, M5 Mid-Span Mixing Grids, the floating intermediate spacer grid restraint system, M5 cladding, M5 guide thimbles and instrument sheath, a reconstitutable top nozzle, and a debris filter bottom nozzle.

The Advanced Mark-BW fuel assembly consists of 264 fuel rods, 24 guide thimbles, and one instrument sheath in a 17 x 17 square array. The M5 guide thimbles provide guidance for control rod insertion and are attached to nozzles and Inconel end spacer grids at the top and bottom of the fuel assembly to form the structural skeleton. A reduced diameter section at the bottom of the guide thimbles acts as a dashpot and decelerates the control rod assembly during reactor trips. The M5 instrument sheath occupies the center lattice position and provides guidance and protection for the incore instrumentation assemblies. The fuel rod and guide thimble spacing is maintained along the length of the assembly by five vaned and one vaneless M5 intermediate spacer grids. Three mid-span mixing grids (MSMGs) provide additional flow mixing in the high heat flux region for improved DNB performance. Figure 4.2-1 shows a cross section of the fuel assembly array that is applicable for the Advanced Mark-BW fuel, except that the clad material is M5. Figure 4.5-1 shows a full-length view of the Advanced Mark-BW fuel assembly as well as cross section views of the assembly. Figure 4.5-2 shows a full-length view of the Advanced Mark-BW fuel rod assembly.

Reconstituted Advanced Mark-BW fuel assemblies, which contain a maximum of ten non-fueled solid rods of stainless steel in place of fuel rods, may also be used in North Anna reload cores. Assemblies which have low burnup and have been determined to contain failed rods may be reconstituted to allow for the continued utilization of the energy remaining in the fuel assembly. The non-fueled rods (also called dummy rods or filler rods) are manufactured from solid stainless steel. The dummy rods have the same nominal cold dimensions as fuel-bearing rods. Analyses supporting reconstitution were performed using the NRC-approved methodology of Reference 32. This methodology was evaluated and demonstrated to be applicable to North Anna.

4.5.2.1.2.1 *Fuel Rods.* The Advanced Mark-BW M5 fuel rod assembly design features M5 cladding, which significantly increases protection from corrosion associated with long cycles, high temperatures, and high burnup. At a burnup of 60,000 MWD/MTU, the oxide thickness of M5 is predicted to be less than one half that of low tin Zircaloy-4.

The Advanced Mark-BW M5 fuel rod design has been successfully irradiated for 3 cycles of operation at North Anna Unit 1 in four lead test assemblies. Post irradiation examinations performed after each cycle of operation have confirmed the acceptable performance of the fuel rod design.

The schematic diagram of Figure 4.5-2 shows an axial cross section of the Advanced Mark BW M5 fuel rod. The fuel rod design uses the advanced alloy M5 cladding. The fuel rod design consists of UO2 pellets contained in a seamless M5 tube with M5 end caps welded at each end. The design utilizes a 144-inch fuel stack length. The fuel rod cladding has a 0.374 outside diameter. This configuration leaves a small clearance between the inside diameter of the cladding and the outside diameter of the fuel pellets. The fuel rod utilizes one stainless steel spring in the upper plenum to prevent the formation of fuel stack gaps during shipping and handling, while also allowing for the expansion of the fuel stack during operation. The fuel stack rests on the lower end cap. The lower end cap is made from M5 and has a bullet nose shape to provide a smooth flow transition in addition to facilitating reinsertion of the rods into the assembly if any rods are removed after the assemblies have been irradiated (e.g., during fuel examination programs). The upper end cap is also made of M5 and has a grippable top hat shape that allows for the removal of the fuel rods from the fuel assembly if necessary. Each fuel rod is prepressurized with helium during fabrication.

The fuel pellets are a sintered ceramic of high density UO2. The fuel pellets are cylindrically shaped with a spherical dish at each end. The corners of the pellets have an outward land taper (chamfer) that eases the loading of the pellets into the cladding. The dish and taper geometry also reduces the tendency for the pellets to assume an hourglass shape during operation. The pellet enrichment is currently limited to 4.6 weight percent U-235 for the North Anna Units.

4.5.2.1.2.2 *Fuel Assembly Structure.* The fuel assembly structure consists of a bottom nozzle, top nozzle, guide and instrument thimbles, and grid assemblies. Each of these components is described in detail in the following paragraphs.

4.5.2.1.2.2.1 *TRAPPER™ Bottom Nozzle.* The stainless steel bottom nozzle consists of a frame of deep ribs connecting the guide thimble locations and conventional legs that interface with the reactor internals. The frame distributes the primary loads on the fuel assembly through the bottom nozzle. A high strength A-286 alloy filter plate is attached to the top of the frame. Upon skeleton assembly the guide thimble lower end plugs serve to clamp the filter plate to the structural frame at internal locations. The filter plate serves two functions. First, it provides the axial restraint for fuel rods, which are seated on the filter plate, by distributing these loads to the structural frame. Secondly, it provides a very effective barrier to debris while maintaining acceptable pressure drop.

4.5.2.1.2.2.2 *Top Nozzle.* The top nozzle assembly is a box-like structure of stainless steel. The grillage of the nozzle consists of a plate with a machined hole pattern for attaching the guide thimbles and providing flow area for the reactor coolant exiting the fuel assembly. The top surface of the grillage provides the interface for fixed core components such as thimble plug assemblies, burnable poison rod assemblies and rod cluster control assemblies.

The top plate of the top nozzle assembly provides the handling and reactor internals interface surfaces and supports four sets of three-leaf Inconel-718 holddown springs. Two guide pins on the upper core plate engage with two holes in diagonally opposing corners of the nozzle to position the assembly during operation. The holddown springs are attached to the nozzle by Inconel 718 clamp bolts. A tang extending from the main (top) leaf of the holddown springs is captured through a slot in the top plate to preload the spring and to capture the spring parts in the unlikely event of a spring fracture.

A mechanical joint provides the structural connection between the top nozzle and the guide thimbles. The top nozzle employs a quick disconnect (QD) feature that allows for rapid removal and reattachment of the top nozzle with no loose parts.

4.5.2.1.2.2.3 *Guide Thimble and Instrument Tubing.* The Advanced Mark-BW guide and instrument thimbles are fabricated from M5.

The Advanced Mark-BW guide thimble has two inner diameters. The larger diameter at the top provides a relatively large annular clearance that permits rapid insertion of the rod cluster control assembly (RCCA) during a reactor trip and accommodates coolant flow during normal operation. A reduced diameter section, at the lower end of the tube, provides a dashpot action that decelerates the control rods near the end of the control rod travel during a reactor trip. This deceleration limits the magnitude of the RCCA impact loads on the top nozzle. Four (4) small holes located just above the dashpot allow both outflow of the water during RCCA insertion and coolant flow to control components during operation.

The quick disconnect sleeve is attached to the upper end of the guide thimble tube for connection to the Top Nozzle. An M5 lower end plug is welded onto the end of the guide thimble dashpot section. The lower end plug is internally threaded for engagement with the guide thimble bolt which connects the guide thimble to the bottom nozzle. A small flow hole in the guide thimble bolt provides flow through the reduced diameter section.

4.5.2.1.2.2.4 *Grid Assemblies.*

1. End Spacer Grids

   The end spacer grids of the Advanced Mark-BW fuel assembly are fabricated from Inconel-718 straps slotted at the top or bottom for assembly in an "egg crate" fashion. The strips are welded at the top and bottom of the strip intersections to form an assembly. Punched projections on the strips form stops to support the fuel rods and saddles to support the guide thimbles and instrument tube. Each fuel rod cell contains two perpendicular sets of stops and each set consists of two hardstops near the edges of the strip opposed by one softstop at the center of the strip.

   The top and bottom end grid restraint systems employ short stainless steel sleeves attached to weld tabs at the guide thimble locations. On the upper end grid, these sleeves are attached to the top side of the grid and on the bottom end grids, the sleeves are attached to the lower side of the grid.

   The top end grid sleeves seat against the bottom surface of the quick disconnect (QD) sleeve. The QD sleeves restrain the grid as the fuel rods slip through due to irradiation growth.

   For the bottom end grid connection, mechanical crimping of the end grid sleeves into circular grooves in the guide thimble bottom end plugs attaches the grid to the guide thimble assembly.

2. Intermediate Spacer Grids

   The grids are fabricated from M5 strips slotted at the top or bottom for assembly in an "egg crate" fashion. The strips are welded at the top and bottom at the strip intersections to form a grid assembly. Fuel rod, guide thimble and instrument tube supports are of the standard Framatome ANP design previously described for the end spacer grids. Generous lead-in features and a robust corner facilitate ease of fuel assembly handling.

   The Advanced Mark-BW intermediate and end grids incorporate keying windows which allow 100% of the fuel rod cells to be opened, or "keyed," during fuel rod insertion. The keying process comprises thin keys, inserted through the keying windows, which are rotated to restrain the soft stop springs. This process is utilized to minimize fuel rod scratches, cell hardstop/softstop damage, and fuel assembly residual stresses. The keys are removed after fuel rod insertion to restore the grid's grip force on the fuel rods. The keying process is standard to Framatome ANP Mark-BW fuel.

The Advanced Mark-BW fuel assemblies utilize two types of intermediate spacer grid assemblies: vaned and vaneless. Five intermediate vaned (mixing) grids are used in the high heat flux region of the fuel assembly to promote mixing of the coolant while the intermediate grid towards the bottom of the assembly is vaneless (Figure 4.5-1). The vaned-grid incorporates mixing vanes in the strip, projecting from the trailing (upper) edges into the coolant stream.

The Advanced Mark-BW intermediate spacer grid restraint system allows for floating grid assemblies, which permits a limited amount of upward motion of the grids. The intermediate spacer grids are not rigidly attached to the guide thimbles, but are allowed to follow the fuel rods as they grow due to irradiation until burnup effects have significantly relaxed the M5 spacer grids. Gross axial spacer grid movement is limited by rigid stops incorporated on the instrument sheath and selected guide thimbles. The stops are short sleeves or ferrules attached to eight guide thimbles above each intermediate spacer grid. No flow mixing vanes are provided on the walls of the eight guide thimbles and instrument tube cells that interface with the ferrules. This spacer grid restraint system employs these eight guide thimbles as restraining members. The locations of the eight restraining guide thimbles are shown in Figure 4.5-1. There is also one ferrule attached to the instrument sheath below the top end spacer grid and below each intermediate spacer grid to prevent downward motion.

4.5.2.1.2.2.5 *Mid-span Mixing Grids.* Three (3) mid-span mixing grids (MSMGs) are incorporated onto each fuel assembly, one at each mid-span between the upper four (4) intermediate vaned grids. The MSMGs provide additional flow mixing in the high heat flux region for improved DNB performance.

Constructed from M5, the individual strips are slotted and assembled in an egg-crate fashion and welded at each of the grid strip intersections, the same as for the intermediate grid design. Hard stops formed in each wall of the fuel rod cells prevent the fuel rods from contacting the mixing vanes but impose no grip force (or slip load) onto the rods; thus, these are designated “non-contacting” grids. The guide thimbles and instrument tubes are supported by saddles formed into the walls of those cells. The outer strips incorporate a wrap-around corner design to improve the corner-handling interface.

The MSMG outer strip design precludes hang-up or damage during handling due to its large lead-in feature. The MSMGs have a reduced grid envelope that eliminates mechanical interaction with adjacent fuel assemblies during transition fuel cycles.

The MSMGs use the same mixing vane design and pattern as utilized on the Advanced Mark-BW intermediate vaned grid.

The MSMGs are attached to the guide thimbles at the sixteen (16) outside corner guide thimble locations, as shown in Figure 4.5-1. Different guide thimble locations are used to attach the MSMGs than are used to restrain the floating intermediate grids to help distribute the

hydraulic loads. The MSMGs are rigidly attached to the guide thimbles, as opposed to the floating grid concept, since they are non-contacting (i.e. no axial support from the fuel rods).

4.5.2.1.3 Design Evaluation

4.5.2.1.3.1 *Fuel Rods.*

4.5.2.1.3.1.1 *Cladding Material.* The Advanced Mark-BW M5 fuel rod assembly design features recrystallized M5 cladding, which significantly increases protection from corrosion associated with long cycles, high temperatures, and high burnup. At a burnup of 60,000 MWD/MTU, the oxide thickness of M5 is predicted to be less than one half that of low tin Zircaloy-4. Material strength properties are discussed in detail in Reference 2.

4.5.2.1.3.1.2 *Steady State Performance.* The steady state performance of the Advanced Mark-BW fuel rod is evaluated per the methodologies and design limits given in References 2, 4, 6, and 7. Evaluations are performed each cycle to verify acceptable fuel rod performance in the areas of cladding stress, cladding creep collapse, and fuel rod internal pressure.

4.5.2.1.3.1.3 *Transient Performance.* The transient performance of the Advanced Mark-BW fuel rod is evaluated per the methodologies and design limits given in References 2, 4, and 7. The fuel rod is shown to have acceptable performance in the areas of the cladding strain and strain fatigue.

Framatome performed sensitivity testing on the M5 cladding material, and determined that this zirconium-based alloy is less susceptible to stress corrosion cracking than standard Zircaloy-4 cladding.

4.5.2.1.3.2 *Fuel Assembly Structure.*

4.5.2.1.3.2.1 *Spacer Grids.* The top and bottom end grids are constructed of Inconel 718. Inconel 718 has high strength, exceptional corrosion resistance and low thermal stress relaxation at operating temperature. Analytical models based on test results determined that the end grids provide adequate stiffness and strength throughout the life of the fuel assembly (Reference 1).

The M5 intermediate and mid span mixing spacer grid elevations are designed to accommodate fuel rod irradiation growth but limit axial displacements that could result in grid mismatch. Tests and analytical models demonstrate that the intermediate spacer grids provide adequate structural stiffness and strength throughout the life of the fuel assembly. The fuel assembly analyses show that the spacer grids maintain an adequate guide thimble pattern and diameter to permit control rod insertion during normal operation and upset conditions (Conditions I, II, III, and following an OBE or SSE). The grid impact forces for the LOCA plus SSE loading condition exceeded the elastic limits and thus produced some permanent grid deformations.

The predicted deformations are evaluated in Section 15.4.1 to confirm that structural integrity and a coolable geometry are maintained. In addition control rod insertability is assured because there is no permanent grid deformation for fuel under control rod locations.

4.5.2.1.3.2.2 *Fuel Assembly Lift.* The Advanced Mark-BW fuel assembly lift evaluation compares the holddown force provided by the fuel assembly leaf springs with the hydraulic lift forces at various conditions, including the pump overspeed condition. The analysis indicates that the holddown springs provide enough holddown force to prevent fuel assembly liftoff under normal operating conditions. Under the 120% pump overspeed condition, the fuel assembly will experience liftoff but the liftoff will be small enough that holddown spring will not deflect to the solid state nor produce any permanent set (Reference 1).

4.5.2.1.3.2.3 *LOCA and/or Seismic Loadings.* Fuel assemblies are evaluated per Section 4.5.2.1.1.2 criteria. In the accident analyses, the lateral effect (LOCA and seismic) and the vertical effect (LOCA) are investigated separately. This leads to a development of a lateral model representing a row of assemblies located on a symmetry axis of the core and a vertical model of the fuel assembly. Only the LOCA effect is analyzed in the vertical direction, as the seismic excitation in this direction will not cause fuel assembly liftoff.

4.5.2.1.3.2.4 *Lateral Faulted Analysis.* The seismic and LOCA time history motions of the upper grid plate, lower grid plate and core barrel upper core plate elevation were applied to the reactor core model. The fuel assembly deflection and grid impact force responses were determined using the general procedure outlined in the NRC-approved topical report BAW-10133P, Addendum 1 (Reference 9).

The design basis LOCA time histories use “leak-before-break” methodology (Section 3.6.2.4). The displacements provided are those associated with a worst-case pipe break for branch lines attached to the main RCS piping. The cold leg and hot leg data correspond to the accumulator line and pressurizer surge line breaks, respectively. Separate case data was used for Unit 1 (upflow configuration) and Unit 2 (downflow configuration). These displacement data represent the worst-case branch line breaks as calculated by Westinghouse for the reactor vessel internals upflow modification.

Bounding analyses of a full core Mark-BW configuration and of a mixed core configuration (Advanced Mark-BW and resident fuel assemblies) representative of a transition cycle were performed. The requirements of coolable core geometry are met for these configurations.

4.5.2.1.3.2.5 *Vertical LOCA Analysis.* For the vertical LOCA analysis, a one-dimensional (axial) finite element model as described in BAW-10133P-A (Reference 9) was used to represent the fuel assembly structure and was analyzed using a general-purpose finite element code. The analysis determined the loads on an Advanced Mark-BW fuel assembly resulting from a postulated loss of coolant accident (LOCA). The vertical LOCA force time histories for the fuel assembly response analysis were calculated. The design basis LOCA for the fuel assembly

analysis was the "leak-before-break" LOCA event. The cold leg and hot leg force time histories were for an accumulator line break and a pressurizer surge line break, respectively.

Analyses were performed at both beginning and end of life to determine the worst case loading condition. The results of the LOCA analysis show that the fuel assembly does not contact the upper core plate due to sufficient holddown spring applied preload and stiffness. The resulting forces are well below conservatively calculated allowable loads for all components (Reference 1).

4.5.2.1.3.2.6 *Fuel Assembly Structural Analysis.* The evaluation of structural integrity under faulted conditions showed that the fuel assembly mechanical integrity is maintained with adequate structural margin during the SSE and the combined SSE plus LOCA event (Reference 1). The results of the SSE analysis meet the OBE design criterion for safe operation per Section 3 of Reference 9. Separate OBE stress results were not required. Also, the SSE requirement of control rod insertion was fulfilled. ASME Code subsection NG-3000 (Reference 3) stress criteria are used for the OBE (service Level B) and Appendix F (Reference 3) for the SSE plus LOCA (service Level D). In some cases, failure loads as established by component testing were incorporated per the ASME code.

The Advanced Mark-BW fuel assembly is structurally adequate for the faulted conditions presented for the North Anna Power Station Units 1 and 2 (Reference 1).

4.5.2.1.3.2.7 *Shipping Loads.* The analysis of the Advanced Mark-BW showed that the fuel assembly and its components will maintain structural integrity for the shipping loads specified in Section 4.5.2.1.1.2. Summaries of the results are provided below.

1. The fuel rod upper plenum spring maintains the fuel column position and prevents the formation of axial gaps in the fuel stack. A preload on the fuel stack equivalent to 4G is maintained to counter acceleration loads.
2. The fuel rod does not slip through the spacer grids under the maximum axial shipping loads.
3. The spacer grids maintain structural integrity under the maximum lateral shipping loads, and the maximum clamping loads as verified by testing.
4. Spacer grid soft stops maintain acceptable fuel rod grip forces under the '6G' lateral shipping loads.

4.5.2.1.3.2.8 *Handling Loads.* Sufficient margins of safety are shown for handling loads as established by equipment setpoints (Reference 1). In addition, the intermediate spacer grids of the Advanced Mark-BW fuel assembly include several design features, which resist hanging-up with other fuel assemblies or equipment during fuel handling. The Advanced Mark-BW design utilizes lead-in tabs between the fuel rods on the upper and lower edges of the outer strips of the spacer grid assemblies. The leading edges of the exterior strips of the spacer grid assemblies are inboard of the plane of the outer surface of the peripheral fuel rods, to provide better resistance to hang-up during fuel handling.

4.5.2.1.3.2.9 *Cycling and Fatigue.* The fuel assembly is subjected to cyclic fatigue loading due to transients, seismic events and flow induced vibration. The effects of this loading were assessed and, where appropriate, a fatigue analysis was performed. The results of these analyses show that the cumulative fatigue usage factor is less than 1.0. The allowable fatigue life is determined by using ASME fatigue curves or taking the mean fatigue life curve and applying a factor of 2 on stress or 20 on cycles, whichever is more conservative. The fatigue curve used for M5 material is the O'Donnell and Langer design curve (Reference 5).

The cyclic loads on the fuel assembly and its components have been divided into three categories: Conditions I, II and III transients; seismic and LOCA events; and flow induced vibration. Seismic and LOCA events are discussed earlier in this section. Transients and flow-induced vibration including tests performed are discussed below.

4.5.2.1.3.2.10 *Transients.* The reactor transients are mainly variations of temperature and pressure. Flow velocities do not increase significantly over the steady state value. The fuel assembly structural components are not pressure retaining boundaries and remain at bulk coolant temperature. Therefore, most transients do not cause significant loads on the fuel assembly or its components. In particular, pressure changes are insignificant loads. Compared to the design transients from Table 5.2-4, the allowable stress taken from the appropriate fatigue curve for the corresponding number of cycles for the normal operating life of a fuel assembly well exceeds the values determined in the static analysis. Since the static analysis accounts for the maximum loads caused by these transients the cumulative usage factor is less than one (Reference 1).

4.5.2.1.3.2.11 *Flow-Induced Vibration.* The fuel assembly is subjected to reactor coolant flow induced vibration. An Advanced Mark-BW prototype fuel assembly was tested to investigate this effect. The end of life condition was simulated with the Inconel end spacer grids relaxed approximately 60% and the intermediate spacer grids relaxed approximately 90%. End of life conditions are considered to be bounding for testing of fuel assembly vibration and wear characteristics. The hydraulic flow testing of the prototype fuel assembly was representative of reactor operating conditions, including flow rates, temperature, pressure, and water chemistry. Life and wear tests were conducted to verify the wear resistance due to vibrations. Thorough examinations, following 1000 hours of testing, revealed no abnormal wear (Reference 1).

In addition to the life and wear test, flow-induced vibration testing was performed on the Advanced Mark-BW prototype assembly in conjunction with the Mark-BW fuel assembly. The test determined the effects of crossflow attributed to different pressure drops of adjacent assemblies. The test was performed over a wide range of flow rates representative of reactor operation. Results showed negligible fuel assembly amplitudes and no flow or structure anomalies.

Flow-induced vibration analyses of the Advanced Mark-BW fuel assembly were also performed considering the effects of crossflow, fluid elastic instability, and vortex shedding. The analyses were benchmarked using fuel assembly free pluck and shaker test results in conjunction

with flow test results of similar fuel designs. Analysis results confirmed that no fluid/structure instabilities exist and vibration amplitudes are very small (Reference 1).

4.5.2.1.3.2.12 *Assembly Bow.* Four lead test assemblies (LTAs) similar in design to the Advanced Mark-BW assembly were inserted in the core of North Anna Unit 1 in 1997. The LTAs successfully completed three cycles of operation with a peak pin burnup of approximately 56,000 MWD/MTU. Fuel assembly bow measurements were taken on all four LTAs. Results were enveloped by bow data of other Framatome ANP fuel types. The bow results were also confirmed by the RCCA drag and trip time measurements (Reference 1). The North Anna LTA fuel assembly bow was typical for Mark-BW fuel assemblies and acceptable to ensure no handling or operational issues.

4.5.2.1.3.2.13 *Fretting Wear.* The Advanced Mark-BW fuel rod fretting wear performance has been verified based on the proven performance of the standard Mark-BW, the successful 3 cycle operation of the Advanced Mark-BW Lead Test Assemblies in North Unit 1, and out of core Life and Wear and Flow-Induced Vibration Testing, and analytical benchmarks and evaluations. The LTAs successfully completed three cycles of operation with leak-free performance. No abnormal wear was observed during the Life and Wear Testing. Low amplitudes of vibration were confirmed by the Flow-Induced Vibration Testing and the flow-induced vibration analyses (Reference 1).

4.5.2.1.3.3 *Operational Experience.* Framatome ANP has considerable experience with the Mark-BW and Advanced Mark-BW fuel assembly design starting with the lead test assemblies in Duke Power's McGuire Unit 1, Cycle 5. The design has since then been proven in both Duke Power's McGuire and Catawba Units, Portland General Electric's Trojan Unit, Sequoyah Units and North Anna Units 1 and 2. Operating experience has been verified by 2400 Mark-BW fuel assemblies in reactor operation to date.

4.5.2.1.4 Testing and Inspection Plan

4.5.2.1.4.1 *Quality Assurance Program.* Framatome ANP engineering specifications require that core components be fabricated under an approved quality control program. This includes shop quality control procedures, which are audited by Framatome ANP quality assurance personnel. In addition, special process procedures are approved by Framatome ANP design personnel as required by the procurement documents.

Framatome ANP manufactures core components under a controlled manufacturing system, which includes complementary written process procedures and inspection provisions. Extensive attention is given to processing details to ensure a reliable, reproducible, quality product.

4.5.2.1.4.2 *Quality Control.* The fabrication activities are supported and monitored by quality control. Additional inspections are performed routinely along with the required inspection program to further assure the quality of the final product.

4.5.2.1.4.3 *Onsite Inspection.* Framatome ANP provides documentation for the inspection of reload assemblies manufactured and delivered by Framatome ANP. The post-shipment inspections of new fuel assemblies and insert components performed by the station described in Section 4.2.1.4.3 are also applicable to Framatome ANP fuel.

4.5.3 Nuclear Design

4.5.3.1 Design Basis

This section describes the design bases and functional requirements used in the nuclear design of the fuel and reactivity control system and relates these design bases to the General Design Criteria (GDC) presented in 10 CFR 50, Appendix A. The following sections indicate how these design bases have been implemented in the licensing basis for use of the Advanced Mark-BW fuel at NAPS.

4.5.3.1.1 Fuel Burnup

No change to this entire section. See Section 4.3.1.1.

4.5.3.1.2 Negative Reactivity Feedbacks (Reactivity Coefficient)

No change to this entire section. See Section 4.3.1.2.

4.5.3.1.3 Control of Power Distribution

No change to this entire section. See Section 4.3.1.3.

4.5.3.1.4 Maximum Controlled Reactivity Insertion Rate

No change to this entire section. See Section 4.3.1.4.

4.5.3.1.5 Shutdown Margins

No change to this entire section. See Section 4.3.1.5.

4.5.3.1.6 Stability

No change to this entire section. See Section 4.3.1.6.

4.5.3.1.7 Anticipated Transients Without Trip

No change to this entire section. See Section 4.3.1.7.

4.5.3.2 Description

4.5.3.2.1 Nuclear Design Description

The implementation of the Advanced Mark-BW assembly does not change the basic conclusions drawn in Section 4.3.2.1; however, differences as a result of assembly design changes are noted in Table 4.5-2. The Advanced Mark-BW assemblies have similar characteristics as the Westinghouse fuel that has been used at North Anna. Core average and assembly-specific data

assuming a full core of Advanced Mark-BW assemblies are shown in Table 4.5-2. Reconstituted Advanced Mark-BW fuel assemblies (see Section 4.5.2.1.2) may be included among the fuel assemblies used for reloading the core.

4.5.3.2.2 Power Distributions

No change to this entire section. See Section 4.3.2.2.

4.5.3.2.2.1 *Definitions.* No change to this entire section. See Section 4.3.2.2.1.

4.5.3.2.2.2 *Radial Power Distributions.* No change to this entire section. See Section 4.3.2.2.2.

4.5.3.2.2.3 *Assembly Power Distributions.* No change to this entire section. See Section 4.3.2.2.3.

4.5.3.2.2.4 *Axial Power Distributions.* No change to this entire section. See Section 4.3.2.2.4.

4.5.3.2.2.5 *Local Power Peaking.* The spike densification peaking factor (Reference 12) is used to account for the increased peaking due to inter-pellet gap formation caused by fuel densification as described in Section 4.3.2.2.5. This factor currently is not applied in design analyses (e.g., LOCA linear heat rate limits and centerline fuel melt (CFM) limits) for Advanced Mark-BW fuel.

4.5.3.2.2.6 *Limiting Power Distribution.* The introduction of the Advanced Mark-BW in NAPS does not alter the conclusions reached in Section 4.3.2.2.6.

This section summarizes the considerations and calculational methods used to determine the core safety and operating limits that may be affected by the use of the Advanced Mark-BW fuel assembly. The uncertainty factors described in this section are applicable to the Advanced Mark-BW fuel assembly design. Appropriate uncertainty factors will be applied to other fuel assembly designs.

Section 4.5.3.2.2.5 indicates that no factor is required to augment the calculated power peaking due to densification for the Advanced Mark-BW fuel assembly design. The average power density at 2893 MWt is 5.665 kW/ft. The average power density at 2942.2 MWt is 5.762 kW/ft.

4.5.3.2.2.6.1 *Fuel Rod Bow.* Fuel rod bowing has the potential to affect both local power peaking and the margin to DNB. The Advanced Mark-BW fuel assembly design incorporates several features that make its fuel rod bow performance similar to that of other Framatome ANP fuel designs. As a result, the predicted rod bow for the Advanced Mark-BW fuel design can be taken from BAW-10147P-A, Rev. 1 (Reference 22).

4.5.3.2.2.6.2 *Linear Heat Rate to Fuel Melt.* For the Advanced Mark-BW fuel assembly design, the linear heat rate associated with fuel centerline melting is 21.9 kw/ft (Reference 1). This linear heat rate exceeds the 21.1 kw/ft value for Westinghouse fuel in Section 4.3.2.2.6.

4.5.3.2.2.6.3 *Fuel Densification.* The peaking increase due to the power spike that results from a gap between UO2 pellets has been analyzed and documented in topical report BAW-10054, Rev. 2 (Reference 12). These gaps may occur when pellet-cladding interaction causes a pellet to stick to the cladding. The underlying pellets densify and a gap beneath the stuck pellet is formed. Gap measurements have been performed on modern irradiated Framatome ANP fuel rods, and only very small gaps have been observed (< 0.1 inch) (Reference 13). The reported gap measurements were performed on fuel at cold temperature conditions. Since the fuel rod stack increases in length during heatup at a rate greater than the cladding (0.5 to 1 inch), the gaps are eliminated or reduced to less than 0.1 inch at power operation. Any remaining gaps during power operation will produce negligible power peaking effects. Therefore, no explicit penalty is included to account for densification spike effects as per BAW-10163P-A (Reference 10).

4.5.3.2.2.6.4 *Peaking Factor Uncertainty.* The Framatome methodology for determining the overall peaking factor uncertainty is described in Reference 1. The overall peaking factor uncertainty (F_{QU}) is a statistically combined factor that includes the effect of nuclear calculational uncertainty (F_{NU}), local engineering hot channel factor for fuel (F_{QE}), and allowance for lumped burnable poison, rod bow, and assembly bow. The overall uncertainty so obtained is less than the current maximum uncertainty factor of 1.0815 ($F_{NU} \times F_{QE}$) used in the methodology for evaluation of the total peaking factor, F_Q (Section 4.3.2.2.6). A conservative uncertainty factor value of 1.0815 (F_{QU}) is used in the calculation of the total peaking factor (F_Q) for centerline fuel melt, transient cladding strain, and LOCA.

4.5.3.2.2.7 *Experimental Verification of Power Distribution Analysis.* No change to this entire section. See Section 4.3.2.2.7.

4.5.3.2.2.8 *Testing.* No change to this entire section. See Section 4.3.2.2.8.

4.5.3.2.2.9 *Monitoring Instrumentation.* No change to this entire section. See Section 4.3.2.2.9.

4.5.3.2.3 Reactivity Coefficients

No change to this entire section. See Section 4.3.2.3.

4.5.3.2.3.1 *Fuel Temperature (Doppler) Coefficient.* No change to this entire section. See Section 4.3.2.3.1.

4.5.3.2.3.2 *Moderator Coefficients.* No change to this entire section. See Section 4.3.2.3.2.

4.5.3.2.3.3 *Power Coefficient.* No change to this entire section. See Section 4.3.2.3.3.

4.5.3.2.3.4 *Comparison of Calculated and Experimental Reactivity Coefficients.* No change to this entire section. See Section 4.3.2.3.4.

4.5.3.2.3.5 *Reactivity Coefficients Used in Transient Analysis.* No change to this entire section. See Section 4.3.2.3.5.

4.5.3.2.4 Control Requirements

No change to this entire section. See Section 4.3.2.4.

4.5.3.2.4.1 *Doppler Effect.* No change to this entire section. See Section 4.3.2.4.1.

4.5.3.2.4.2 *Variable Average Moderator Temperature.* No change to this entire section. See Section 4.3.2.4.2.

4.5.3.2.4.3 *Redistribution.* No change to this entire section. See Section 4.3.2.4.3.

4.5.3.2.4.4 *Void Content.* No change to this entire section. See Section 4.3.2.4.4.

4.5.3.2.4.5 *Rod Insertion Allowance.* No change to this entire section. See Section 4.3.2.4.5.

4.5.3.2.4.6 *Burnup.* No change to this entire section. See Section 4.3.2.4.6.

4.5.3.2.4.7 *Xenon and Samarium Poisoning.* No change to this entire section. See Section 4.3.2.4.7.

4.5.3.2.4.8 *pH Effects.* No change to this entire section. See Section 4.3.2.4.8.

4.5.3.2.4.9 *Experimental Confirmation.* No change to this entire section. See Section 4.3.2.4.9.

4.5.3.2.5 Control

No change to this entire section. See Section 4.3.2.5.

4.5.3.2.5.1 *Chemical Poison.* No change to this entire section. See Section 4.3.2.5.1.

4.5.3.2.5.2 *Rod Cluster Control Assemblies.* No change to this entire section. See Section 4.3.2.5.2.

4.5.3.2.5.3 *Thimble Plug Assemblies.* No change to this entire section. See Section 4.3.2.5.3.

4.5.3.2.5.4 *Burnable Poison Rods.* No change to this entire section. See Section 4.3.2.5.4.

4.5.3.2.5.5 *Peak Xenon Startup.* No change to this entire section. See Section 4.3.2.5.5.

4.5.3.2.5.6 *Load-Follow Control and Xenon Control.* No change to this entire section. See Section 4.3.2.5.6.

4.5.3.2.5.7 *Burnup.* No change to this entire section. See Section 4.3.2.5.7.

4.5.3.2.6 Control Rod Patterns and Reactivity Worth

No change to this entire section. See Section 4.3.2.6.

4.5.3.2.7 Criticality of Fuel Assemblies

Criticality analyses of the North Anna fresh fuel storage area (FFSA) and the Spent Fuel Pool (SFP) have been reviewed for applicability with Advanced Mark-BW fuel. The original analyses were performed using Westinghouse fuel design data (see Section 4.3.2.7). The NRC Safety Evaluation and approval of new Technical Specifications based on these calculations is contained in Reference 14. Differences in key analysis parameters between the Advanced Mark-BW fuel and the original analysis data were reviewed. The only differences of significance for the SFP and FFSA analyses are use of the M5 alloy (clad, grid, and guide thimbles), the increased nominal fuel density, and the tolerances on fuel density and pellet volume. Grid differences are not relevant since grids were intentionally ignored in the original calculations.

The calculation estimated the impact of the Advanced Mark-BW design differences using sensitivity, tolerance, uncertainty and margin data from the existing calculational documentation. Using the approved methodology upon which the Reference 14 amendment was based, the higher fuel density of the Advanced Mark-BW design was evaluated to quantify the increase in SFP and FFSA K-effective.

The calculations resulted, as expected, in slightly higher calculated K-effectives for the North Anna FFSA and the SFP. These calculations have demonstrated that there is sufficient margin to the K-effective limits to accommodate this increase. Therefore, the analysis approved in Reference 14 is bounding for the storage of Advanced Mark-BW with initial enrichments up to 4.6 weight percent U-235.

4.5.3.2.8 Stability

No change to this entire section. See Section 4.3.2.8 (including subsections).

4.5.3.2.9 Vessel Irradiation

No change to this entire section. See Section 4.3.2.9.

4.5.3.3 **Analytical Methods (PDQ Two-Zoned/NOMAD)**

No change to this entire section. See Section 4.3.3.

4.5.3.3.1 Fuel Temperature (Doppler) Calculations

No change to this entire section. See Section 4.3.3.1.

4.5.3.3.2 Macroscopic Group Constants

No change to this entire section. See Section 4.3.3.2.

4.5.3.3.2.1 *BP Cross Section Generation.* No change to this entire section. See Section 4.3.3.2.1.

4.5.3.3.2.2 *Cross Section Representation.* No change to this entire section. See Section 4.3.3.2.2.

4.5.3.3.2.3 *Normalization to KENO-V.a, Benchmark Cases.* No change to this entire section. See Section 4.3.3.2.3.

4.5.3.3.2.4 *KENO-V.a Control Rod Cross Section.* No change to this entire section. See Section 4.3.3.2.4.

4.5.3.3.2.5 *Reflector and Baffle Cross Sections.* No change to this entire section. See Section 4.3.3.2.5.

4.5.3.3.3 Spatial Few-Group Diffusion Calculations

No change to this entire section. See Section 4.3.3.3.

4.5.3.4 Analytical Methods (CMS)

No change to this entire section. See Section 4.3.4.

4.5.3.4.1 Fuel Temperature (Doppler) Calculations

No change to this entire section. See Section 4.3.4.1.

4.5.3.4.2 Macroscopic Group Constraints

No change to this entire section. See Section 4.3.4.2.

4.5.3.4.2.1 *Cross Section Representation.* No change to this entire section. See Section 4.3.4.2.1.

4.5.3.4.3 Spatial Few-Group Nodal Calculations

No change to this entire section. See Section 4.3.4.3.

4.5.4 Thermal and Hydraulic Design

4.5.4.1 Design Bases

Section 4.4.1 defines the performance and safety criteria that are the basis of thermal and hydraulic core design. Sections 4.4.1.1 through 4.4.1.5 establish a number of design bases that ensure that those criteria are met. The following section describes how Framatome ANP has addressed these design bases in licensing Advanced Mark-BW fuel for North Anna Units 1 & 2.

4.5.4.1.1 Departure from Nucleate Boiling (DNB) Design Basis

Basis:

The Framatome ANP Statistical Core Design (SCD) methodology has been implemented for DNB analyses for the NAPS licensing analyses with the Advanced Mark-BW fuel. SCD is an approved methodology that has been documented in Reference 15. The Dominion Statistical

DNBR Evaluation Methodology has also been implemented for DNB analyses of NAPS with the Advanced Mark-BW fuel. This Dominion specific methodology is an approved methodology that has been documented in Reference 30. Both methodologies ensure that there will be at least a 95-percent probability that DNB will not occur on the limiting fuel rods during normal operation and operational transients and any transient conditions arising from faults of moderate frequency (Condition I and II events) at a 95-percent confidence level. Historically, this criterion has been conservatively met by adhering to the following thermal design basis: there must be at least a 95-percent probability that the minimum departure from nucleate boiling ratio (DNBR) of the limiting power rod during Condition I and II events is greater than or equal to the DNBR limit of the DNB correlation being used. The DNBR limit for the correlation is established based on the variance of the correlation such that there is a 95-percent probability with 95-percent confidence that DNB will not occur when the calculated DNBR is at the DNBR limit.

Discussion:

For the NAPS licensing analyses, Framatome ANP has implemented a thermal-hydraulic analysis method referred to as the Statistical Core Design (SCD) method. SCD is an approved methodology that has been documented in Reference 15. In addition, Dominion has implemented the Statistical DNBR Evaluation Methodology, which is an in-house thermal-hydraulics methodology equivalent to the SCD methodology provided by Framatome ANP. The Dominion Statistical DNBR Evaluation Methodology is an approved methodology that has been documented in Reference 30. The CHF correlation that has been implemented is the BWU correlation documented in Reference 16. The BWU family of CHF correlations consists of three correlations that use the same basic equation form but are fit to different data bases; BWU-N is applicable to non-mixing vane grids, BWU-I is the basic mixing vane correlation, and BWU-Z is the enhanced mixing vane correlation approved for the Advanced Mark-BW fuel assembly design. The BWU-N and BWU-Z CHF correlations were used as the licensing basis for the Advanced Mark-BW fuel assembly.

BWU-N CHF Correlation

The applicable CHF correlation for DNB analysis of the Advanced Mark-BW fuel assembly in the non-mixing region of the fuel assembly is the BWU-N CHF correlation documented in Reference 16. The non-mixing region of the fuel assembly extends from the beginning of the heated length to the leading edge of the first mixing vane grid.

BWU-Z CHF Correlation

The applicable CHF correlation for analysis of the Advanced Mark-BW fuel assembly in the mixing region, but below the mid-span mixing grids, is BWU-Z documented in Reference 16. Improved CHF performance, relative to that of the Mark-BW mixing vane grid, is obtained by the addition of three Mid-Span-Mixing-Grids (MSMGs). This additional performance is incorporated into the BWU-Z CHF correlation by means of a direct CHF multiplication factor. An addendum (Reference 18) to the BWU-Z CHF topical report has been approved by the NRC for application

of the enhanced CHF performance of the MSMGs using the multiplicative enhancement factor applied to the BWU-Z CHF correlation. When using the BWU-Z correlation in this manner, documented specifically in Reference 18, it is referred to as BWU-ZM. The approved range of application has been reviewed and confirmed to create no impact on the limiting NAPS analyses.

For the evaluation of DNB effects for NAIF in the mixed-core, the BWU-N and BWU-I (N - non-mixing vane grid design, I - mixing vane grid design) CHF correlations (BAW-10199P-A, Reference 18) are used. Framatome justifies the application of these correlations to the NAIF on the fact that their databases include CHF data representative of the configuration for the Vantage 5H grids used on the Westinghouse NAIF fuel design (Reference 18). Therefore, these correlations apply without modification.

In their standard application with the Framatome ANP LYNXT computer code (Reference 23), a BWU-N design limit of 1.21 and BWU-Z/BWU-ZM DNBR design limit of 1.19 ensure that the 95/95 DNBR design basis is met. With the Dominion VIPRE-D computer code (Reference 31), a BWU-N design limit of 1.22 and BWU-Z/BWU-ZM DNBR design limit of 1.20 ensure that the 95/95 DNBR design basis is met. Under that application, all uncertainties in the thermal-hydraulic analysis input parameters are assumed to be at their worst case level. With the SCD method, uncertainties in the operating conditions, the peaking distribution and the fuel fabrication process are combined statistically and a statistical design limit (SDL) is determined. For the North Anna application, a value of 1.61 for BWU-N and 1.31 for BWU-Z/BWU-ZM have been established as the SDLs with the Framatome ANP LYNXT computer code (Reference 23). With the Dominion VIPRE-D computer code (Reference 31), the SDLs have been established as 1.38 for BWU-N and 1.34 for BWU-Z/BWU-ZM. To provide an extra measure of flexibility in the core design process a third design limit is also established. That design limit, the safety analysis limit (SAL), includes a provision for retained thermal margin. This retained thermal margin is included to offset conditions that are not included in the SDL development. Examples of offsets that might be assessed against the retained margin include transition core effects and penalties for input uncertainties greater than those considered in the SDL development. For the current application with the Framatome ANP LYNXT computer code (Reference 23), a common SAL of 1.70 is used for both correlations. With the Dominion VIPRE-D computer code (Reference 31), a SAL of 1.60 is used with both correlations.

4.5.4.1.2 Fuel Temperature Design Basis

Basis:

During modes of operation associated with Condition I and Condition II events, the maximum fuel temperature for the UO_2 fuel rods shall be less than the melting temperature of UO_2.

Discussion:

To determine the linear heat rates at which fuel melting occurs, Framatome ANP employs the fuel thermal analysis code; TACO3 for the UO2 rods. TACO3 is documented in Reference 4.

Since TACO3 is a best estimate thermal analysis code, an adjustment is made to conservatively reduce the respective fuel melt temperature, as described in Appendix I of Reference 4, to ensure that the melting temperature is not exceeded for at least 95-percent of the peak kW/ft fuel rods at the 95-percent confidence level. By precluding fuel melting, the fuel geometry is preserved and possible adverse effects of molten fuel on the cladding are eliminated. To preclude centerline melting and as a basis for overpower protection system setpoints, the UO_2 fuel melt temperature has been selected as the basis for setting the overpower limit.

4.5.4.1.3 Core Flow Design Basis

No change to this entire section. See Section 4.4.1.3.

4.5.4.1.4 Hydrodynamic Stability Design Basis

No change to this entire section. See Sections 4.4.1.4, 4.4.3.5, and 4.5.4.3.5.

4.5.4.1.5 Other Considerations

Discussion:

As discussed in Section 4.4.1.5, the design bases defined above, along with those defined in Sections 4.2.1 and 4.5.2.1, are sufficiently comprehensive so that additional limits are not required. However, there are additional conservatisms that are incorporated into the design methodologies that ensure plant safety. These include, but are not limited to, the treatment of the inlet flow distribution in the inputs to the core thermal-hydraulic (LYNXT or VIPRE-D) evaluation (Section 4.5.4.3.1.2) and the application of a clad temperature limit on those transients that experience a departure from nucleate boiling (i.e. the Loss-of-Coolant Accident (LOCA), the control rod ejection, and the locked rotor accident).

4.5.4.1.6 Use of Reconstituted Fuel

The design bases described herein are applicable for fuel rod reconstitution. The thermal-hydraulic evaluation of reconstituted fuel assemblies is performed in accordance with NRC approved codes and methodology.

Fuel rod reconstitution affects predictions of departure from nucleate boiling (DNB) in hot channels due to a local power reduction and the resultant effects of enthalpy and flow. Reference 32 documents the NRC-approved methodology for evaluating reconstituted fuel assemblies. This methodology has been demonstrated to be applicable to the methods and models applicable to the Advanced Mark-BW fuel assembly.

For reload cores using reconstituted fuel assemblies, a cycle-specific evaluation is performed to confirm that the exact configuration and associated core power distribution of the reconstituted assemblies do not introduce a change in radial gradients in the flow and enthalpy distribution that could invalidate the applicability of the CHF correlation.

4.5.4.2 **Description of Thermal and Hydraulic Design of the Reactor Core**

4.5.4.2.1 Summary

Table 4.5-3 provides a listing of reactor design parameters applicable with Framatome ANP's Advanced Mark-BW 17 x 17 fuel design and the Statistical Core Design (SCD) methodology. Table 4.5-3 also lists the reactor design parameters applicable to Framatome ANP's Advanced Mark-BW 17 x 17 fuel design and Dominion's Statistical DNBR Evaluation Methodology.

4.5.4.2.2 Fuel and Cladding Temperatures (Including Densification)

As specified in Section 4.5.4.1.2, during Condition I and Condition II events, the maximum fuel temperature is required to be less than the fuel melting temperature. To verify that this criterion is met, Framatome ANP uses the fuel thermal analysis code TACO3 for UO2 rods. TACO3 is documented in Reference 4. As discussed in this report, and summarized in Section 4.5.4.1.2, the TACO3 centerline melt methodology uses a statistically reduced fuel melt temperature to determine the linear heat rate at which fuel melt would occur. This reduced melt temperature accounts for uncertainties in fuel fabrication data and in the code predictions. TACO3 is also able to model time dependent densification effects by incorporating as-built densification data into the thermal analysis. The thermal analysis of the Advanced Mark-BW fuel rod has shown that the peak fuel temperature and the minimum heat rate to centerline melt occurs at the beginning of life for UO_2 rods.

Dimensional changes of the fuel and cladding are an integral part of the fuel rod temperature calculations. These dimensional changes affect the fuel-cladding gap and the contact pressure after gap closure affects the contact conductance. An important contributor to fuel diameter changes is the phenomenon of fuel densification, which has been observed to occur early in the life of the fuel and results in a shrinkage of the fuel pellet. The radial shrinkage of the pellet increases the thermal resistance of the fuel-cladding gap resulting in increased temperatures early in life. Pellet axial shrinkage, due to densification, results in an increased linear heat rate for a given core power level. Fuel rod thermal evaluations are performed throughout the fuel rod lifetime. Analyses have shown that maximum fuel temperatures typically occur at or near beginning of life.

The principal factors that are employed in TACO3 to calculate fuel temperatures are discussed below.

4.5.4.2.2.1 *Thermal Conductivity.* In TACO3, a quasi-cubic Hermite spline is used to model the temperature dependence of the thermal conductivity. The modified Loeb correlation has been selected to compensate for the unrestructured porosity effects. For the UO2 rods, expressions for both the thermal conductivity and the porosity factor are contained in Reference 4.

4.5.4.2.2.2 *Radial Power Distribution in Fuel Rods.* Fuel pin radial power profiles for UO_2 fuel pellets were calculated using the PEEL/NULIF neutronics codes (References 19 & 20).

To determine the pellet radial power at a specific point, TACO3 uses a table-look-up. A complete discussion of the methods used to determine the radial power profiles used in TACO3 is contained in Reference 4.

4.5.4.2.2.3 *Gap Conductance.* The gap conductance model used in TACO3 is made up of three components: open-gap conductance (gas conduction and transport), solid-solid (contact conductance), and radiation heat transfer. A complete discussion of the gap conductance models used in TACO3 is contained in Reference 4.

4.5.4.2.2.4 *Surface Heat Transfer Coefficients.* The fuel rod surface heat transfer coefficients used during subcooled forced convection and nucleate boiling are presented in Section 4.5.4.2.8.1.

4.5.4.2.2.5 *Fuel Clad Temperatures.* The outer surface of the fuel rod at the hot spot operates at a temperature of approximately 660°F for steady-state operation at rated power throughout core life due to the onset of nucleate boiling.

During operation over the life of the core, the buildup of oxides and crud on the fuel rod surface causes the temperature of the outer surface of the clad metal to increase. Allowance is made in the fuel center melt evaluation for this temperature rise. Since the thermal-hydraulic design basis limits DNB, adequate heat transfer was provided between the fuel clad and the reactor coolant so that the core thermal output was not limited by considerations of the clad temperature.

4.5.4.2.2.6 *Treatment of Peaking Factors.* The total heat flux hot-channel factor, F_Q, is defined by the ratio of the maximum to core average heat flux and is evaluated for its impact on thermal and hydraulic design criteria for each reload core. For the current value of F_Q, see the Core Operating Limits Report (COLR).

The Framatome ANP fuel melt limit methodology (outlined in Section 4.5.4.1.2) has shown that the peak linear power for prevention of centerline melt is 21.9 kW/ft.

4.5.4.2.3 Critical Heat Flux Ratio or DNBR and Mixing Technology

The minimum DNBR values for the nominal operating condition and for the design transient condition are given on Table 4.5-3. For this application, the DNBR values are calculated using the BWU CHF correlation. A complete discussion of the development of BWU is included in Reference 16 and Reference 18.

4.5.4.2.3.1 *Departure from Nucleate Boiling Technology.* Over the years experimental studies of DNB have progressed from crude single channel configurations to more realistic rod bundle arrays. As the technology developed, it was discovered that correlations based on local subchannel conditions were more accurate predictors of critical heat flux (CHF) than were correlations based on bundle average values. To predict local subchannel conditions, Framatome ANP developed the LYNXT thermal-hydraulic analysis code. LYNXT determines core conditions

by solving a set of conservation equations for mass, momentum, and energy. LYNXT provides a one-pass analysis by dividing the core into discrete subchannels and axial control volumes. The VIPRE-D code can also be used to predict local subchannel conditions. VIPRE-D, which also provides a one-pass analysis by dividing the core into subchannels and axial control volumes, and was originally developed for EPRI by Battelle Pacific Northwest Laboratories, was customized by Dominion in order to perform detailed thermal-hydraulic analyses to predict CHF and DNBR of reactor cores. The subchannel conditions generated by either of these codes provide the basis for the determination of CHF.

Framatome ANP has developed the approved BWU CHF correlations for the DNB analysis of the Advanced Mark-BW fuel assembly. The BWU family of CHF correlations consists of three correlations that use the same basic equation form but are fit to different data bases; BWU-N is applicable to non-mixing vane grids, BWU-I is the basic mixing vane correlation, and BWU-Z is the enhanced mixing vane correlation approved for the Advanced Mark-BW fuel assembly design. The BWU-N and BWU-Z CHF correlations were used as the licensing basis for the Advanced Mark-BW fuel assembly (Section 4.5.4.1.1).

The applicable range of variables for BWU-N is as follows:

Pressure (psia)	788 to 2616
Mass Velocity (10^6 lbm/hr-ft^2)	0.25 to 3.83
Thermodynamic Quality (%) at CHF	Less than 70
Spacer Grid	Non-Mixing Grid

The applicable range of variables for the application of BWU-Z to the Advanced Mark-BW spacer grid is as follows (Reference 16):

Pressure (psia)	400 to 2465
Mass Velocity (10^6 lbm/hr-ft^2)	0.36 to 3.55
Thermodynamic Quality (%)	Less than 74
Spacer Grid	Advanced Mark-BW

The applicable range of variables for the application of BWU-ZM to the Advanced Mark-BW spacer grid is as follows (Reference 18):

Pressure (psia)	400 to 2465
Mass Velocity (10^6 lbm/hr-ft^2)	0.47 to 3.55
Thermodynamic Quality (%)	Less than 68
Spacer Grid	Advanced Mark-BW

As stated in Section 4.5.4.1.1, a DNBR limit for each correlation is established such that there is a 95-percent probability with 95-percent confidence that DNB will not occur when the

calculated DNBR is a the DNBR limit. In order to meet this criterion, the DNBR limit value is determined using the one-sided tolerance theory of Owen. The DNBR limits so calculated are 1.21 for the BWU-N correlation and 1.19 for the BWU-Z/BWU-ZM correlation with the LYNXT code. The DNBR limits are 1.22 for the BWU-N correlation and 1.20 for the BWU-Z/BWU-ZM correlation when using the VIPRE-D code.

4.5.4.2.3.2 *Definition of Departure from Nucleate Boiling Ratio.* The BWU-Z and BWU-ZM CHF correlations are based on a form that uses local subchannel conditions with modifiers to account for nonuniform axial heat generation and bundle global conditions, and with a bundle-specific multiplier to account for the effects of grid spacing and heated length. Based on that form, DNBR is calculated with BWU-Z and BWU-ZM correlations as follows:

$$DNBR = q_{nu}''/q_{loc}''$$

where

$q_{nu}'' = FLS\ q_u''/F$

q_{loc}'' = local surface heat flux (BTU/hr-ft^2)

and

q_{nu}'' = Nonuniform CHF (BTU/hr-ft^2)

FLS = Bundle multiplier for length and grid spacing

q_u'' = Uniform CHF (BTU/hr-ft^2)

F = Nonuniform modifier on q_u''

This same form with different coefficients also applies to BWU-N.

4.5.4.2.3.3 *Mixing Technology.* Based on analysis of Laser Doppler Velocimeter testing, a turbulent mixing coefficient has been determined for the Mark-BW fuel design. Tests performed by Nuclear Fuel Industries (NFI) of Japan provided an indication of the turbulent intensity at various distances downstream of the spacer grids. Research has shown that the turbulent mixing coefficient is proportional to the turbulent intensity. A value of 0.038 is conservatively applied in core thermal-hydraulic analyses.

The turbulent mixing coefficient determined for the Mark-BW assembly is conservative for use with the Advanced Mark-BW. The coefficient is statistically derived from Laser Doppler Velocimeter (LDV) measurements of the three dimensional velocity profiles downstream of an intermediate spacer grid. The data measurements span over 22 inches of the assembly length representing the grid spacing within a Mark-BW assembly. The results showed a decrease in lateral or crossflow velocities as flow progressed downstream of the grid. The incorporation of

mid-span mixing grids in the Advanced Mark-BW design decreases the length between grids and results in an improvement in the span average value of the thermal diffusion coefficient.

4.5.4.2.3.4 *Hot Channel Factors.* Engineering hot channel factors (HCFs) are used to account for the effects of manufacturing variations on the maximum linear heat generation rate and enthalpy rise.

4.5.4.2.3.4.1 *Local Heat Flux Engineering Hot Channel Factor.* The local heat flux engineering hot channel factor, F_Q^E, is used in the evaluation of the maximum linear heat generation rate. This factor is determined by statistically combining manufacturing variances for pellet enrichment and weight and typically has a value of 1.03 or less at the 95% probability level with 95% confidence. It has been shown that relatively small heat flux spikes, such as those represented by F_Q^E, have no effect on DNB, therefore this factor is not used in DNBR calculations.

4.5.4.2.3.4.2 *Average Pin Power Engineering Hot Channel Factor.* The average pin power factor, $F_{\Delta H}^E$, accounts for the effects of variations in fuel stack weight, enrichment, fuel rod diameter, and pin pitch on hot pin average power. This factor, which typically has a value of 1.03 or less, is combined statistically with other uncertainties to establish the statistical design limit (SDL) DNBR used with the statistical core design method.

Since $F_{\Delta H}^E$ is incorporated into the statistical design limit (SDL), this factor is not included in the LYNXT or VIPRE-D models used for statistical analyses. For non-statistical analyses, $F_{\Delta H}^E$ is incorporated into the LYNXT and VIPRE-D models as a multiplier on the average power of the hot rod, and therefore, it affects the surface heat flux of the hot rod as well as the enthalpy rise in the adjacent subchannels.

4.5.4.2.3.4.3 *Local and Bundle Spacing Factor.* In addition to the Average Pin Power Engineering Hot Channel Factor, Framatome ANP has identified an uncertainty factor associated with the local and bundle spacing. This factor, which has a value of 1.015, is combined statistically with other uncertainties to establish the statistical design limit (SDL) DNBR used with the statistical evaluation methods.

Because the local and bundle spacing factor is incorporated into the statistical design limit (SDL), this factor is not included in the LYNXT or VIPRE-D models used for statistical analyses. For non-statistical analyses, the local and bundle spacing factor is incorporated into the LYNXT and VIPRE-D models as a multiplier on the average power of the hot rod, and therefore, it affects the surface heat flux of the hot rod as well as the enthalpy rise in the adjacent subchannels.

4.5.4.2.3.5 *Effects of Rod Bow on DNBR.* The bowing of fuel rods during reactor operation has the potential to affect both local power peaking and the margin to DNB. As discussed in Reference 21, the Mark-BW fuel design has several features that make its fuel rod bow performance similar to that of other Framatome ANP fuel designs. In Reference 7, Framatome ANP presented new data that extended the rod bow database for Framatome ANP fuel to

58,300 MWD/MTU. That topical concluded that the rod bow correlations from Reference 22 are applicable at extended burnups and apply to the Mark-BW.

The low growth characteristics of the M5 advanced material that is used on the Advanced Mark-BW indicate bow behavior no more severe than the Zircaloy clad fuel in the Mark-BW cage. The low growth of M5 has been demonstrated through the irradiation experience of the North Anna LTAs, in addition to Special Clad Assemblies in the McGuire plant and other Framatome fuel in Europe. Thus, the Advanced Mark-BW will have no greater penalty for rod bow than is assessed against the Mark-BW Zircaloy-4 design for burnups less than 24,000 MWD/MTU. For burnups greater than 24,000 MWD/MTU, the rod power is not expected to be limiting; however, this will be verified during cycle specific analyses.

4.5.4.2.4 Flux Tilt Considerations

No change to this entire section. See Section 4.4.2.4.

4.5.4.2.5 Void Fraction Distribution

The available void models that are in the Framatome ANP LYNXT thermal-hydraulic analysis code are described in LYNXT (Reference 23). Empirical correlations are available in LYNXT to calculate both subcooled and bulk boiling void fractions. Four models are available for calculating the subcooled void fractions: the standard B&W model, Levy's subcooled void model, the EPRI subcooled void model and the omission of subcooled voids. These are described in Reference 23. Seven models are available for calculating bulk void fractions: the standard B&W model, homogeneous model, slip model, modified Armand, polynomial function, EPRI model and omission of bulk voids. These are also described in Reference 23. The B&W void models are used in the Framatome ANP thermal hydraulic analyses using the LYNXT code. There are also several empirical correlations available in VIPRE-D to calculate both subcooled and bulk boiling void fractions. However, according to Reference 31, the EPRI models are used by Dominion in all the thermal-hydraulic analyses using the VIPRE-D code.

4.5.4.2.6 Core Coolant Flow Distribution

LYNXT and VIPRE-D are versatile thermal-hydraulics crossflow codes capable of predicting flow and temperature (enthalpy) distributions in confined geometries where wall shear forces are more dominant than intra-fluid shear forces. The primary domain of application of LYNXT and VIPRE-D is in rod bundle arrays. Typical rod bundle applications of LYNXT and VIPRE-D involve corewide flow/enthalpy predictions, subchannel DNBR calculations using one-pass models, and transient DNBR and fuel temperature calculations. LYNXT's and VIPRE-D's solution techniques have been verified for these types of applications using experimental, analytical and alternate code comparisons and are described in References 23 and 31, respectively.

4.5.4.2.7 Core Pressure Drops and Hydraulic Loads

4.5.4.2.7.1 *Core Pressure Drop.* The pressure drop presented on Table 4.5-3 for the Advanced Mark-BW fuel assembly is based on the minimum measured flow as described in Section 5.1. The pressure drop characteristics of the Advanced Mark-BW design were determined through a series of prototype flow tests. Results from those tests were used as the basis for the calculation of component formloss coefficients.

4.5.4.2.7.2 *Hydraulic Loads.* The triple-leaf holddown spring system is designed to maintain fuel assembly contact with the lower core plate during Condition I and II events with the exception of the pump overspeed transient associated with a loss of external load. Hydraulic loss characteristics of the Advanced Mark-BW design were determined as part of the prototype testing described in Section 4.5.4.2.7.1. An analysis of the predicted Advanced Mark-BW lift forces, which are based on the mechanical design flow and the minimum bypass, indicates that the assembly will not lift off under any Condition I or II event. The minimum margin to fuel assembly liftoff occurs at end of life (EOL) for cold startup conditions. At 120% pump overspeed condition, the fuel assembly will experience some liftoff. The liftoff will be minimal and the holddown spring deflection will be less than the worst-case normal operating cold shutdown condition. These margins are calculated assuming the full Advanced Mark-BW core, which bounds the mixed core configurations with resident Westinghouse fuel. The fuel assembly top and bottom nozzles were shown to maintain engagement with reactor internals for all Condition I through IV events using the triple-leaf holddown spring design.

4.5.4.2.8 Correlation and Physical Data

4.5.4.2.8.1 *Surface Heat Transfer Coefficients.* Forced convection heat transfer coefficients used by Framatome ANP's LYNXT code are based on an adaptation of the Colburn correlation (Reference 23), given below, with the properties evaluated at bulk fluid conditions.

$$\frac{hD_e}{K} = 0.03\frac{D_e G^{0.8}}{\mu}\frac{C_p \mu^{0.4}}{K}$$

where:

h heat transfer coefficient, Btu/s-ft^2-°F

D_e equivalent diameter, ft.

K thermal conductivity, Btu/s-ft-°F

G mass velocity, lb/s-ft^2

μ dynamic viscosity, Btu/lb-°F

Cp heat capacity, Btu/lb-°F

In the Framatome ANP LYNXT code the onset of nucleate boiling occurs when the cladding wall temperature reaches the amount of superheat predicted by the Jens and Lottes criteria (Reference 23). After this occurrence, the outer cladding wall temperature is determined by the Jens and Lottes correlation in the fuel rod thermal evaluations.

$$\Delta T_{sat} = \frac{60\left(\frac{q''}{10^6}\right)^{0.25}}{\exp^{\left(\frac{P}{900}\right)}}$$

where:

ΔT wall superheat, T_w-T_{sat}, °F

q'' wall heat flux, Btu/s-ft^2

P pressure, psia

T_w outer cladding wall temperature, °F

T_{sat} saturation temperature of coolant at P, °F

Dominion's VIPRE-D code (Reference 31) calculates forced convection heat transfer coefficients using the familiar Dittus-Boelter correlation (Section 4.4.2.8.1). VIPRE-D predicts the onset of nuclear boiling with the Thom correlation, and the outer clad wall temperature with the Thom correlation (Section 4.4.2.8.1).

4.5.4.2.8.2 *Total Core and Vessel Pressure Drop.* Section 4.4.2.8.2 provides a description of the models that are used to determine vessel and core pressure drop. To determine the mixed core pressure drop, these models are applied to each unique fuel design in the core. Assessments of core pressure drop are performed using the LYNXT thermal-hydraulics code. These assessments have shown that the small difference (increase) in total assembly pressure drop due to the introduction of the Advanced Mark-BW has a small but acceptable impact on the total vessel pressure drop.

4.5.4.2.8.3 *Void Fraction Coefficient.* Figure 4.4-14 illustrates the three separate void regions that are considered in flow boiling in a PWR. The Framatome ANP thermal-hydraulic analysis code, LYNXT, uses a number of different models and correlations to represent these three regions. A discussion of the various models and correlations is contained in Appendix B of the LYNXT topical report, BAW-10156-A (Reference 23). The Dominion thermal-hydraulic analysis code, VIPRE-D, also uses a number of different models and correlations to represent these regions (Reference 31).

4.5.4.2.9 Thermal Effects of Operational Transients

No change to this entire section. See Section 4.4.2.9.

4.5.4.2.10 Uncertainties in Estimates

4.5.4.2.10.1 *Uncertainties in Fuel and Clad Temperature.* As stated in Section 4.4.2.10.1, uncertainties in fuel temperature calculations can be defined in two categories: fabrication uncertainties and model uncertainties. The methodology established for use with the TACO3 thermal analysis code addressed both of these areas. For specific applications (e.g., fuel centerline melt analyses and internal pin pressure calculations), uncertainties in these parameters are factored into the calculation.

4.5.4.2.10.2 *Uncertainties in Pressure Drop.* The core pressure drop reported on Table 4.5-3 for the Advanced Mark-BW fuel design is based on the minimum measured flow. Uncertainties in the pressure drop analysis are treated as an analytical extension of manufacturing data from Advanced Mark-BW grids and are not included as an uncertainty on the final pressure drop value.

4.5.4.2.10.3 *Uncertainties Due to Inlet Flow Maldistribution.* No change to this entire section. See Section 4.4.2.10.3.

4.5.4.2.10.4 *Uncertainty in DNB Correlation.* The uncertainty in each of the BWU-Z/BWU-N CHF correlations has been treated in the determination of the correlation design limit for each correlation and as part of the Framatome ANP Statistical Core Design (SCD) Methodology (Reference 15) and as part of the Dominion Statistical DNBR Evaluation Methodology (Reference 30).

4.5.4.2.10.5 *Uncertainties in DNBR Calculations.* Code uncertainty is included in the Framatome ANP Statistical Core Design (SCD) Methodology (Reference 15) and in the Dominion Statistical DNBR Evaluation Methodology (Reference 30) to account for uncertainties in the DNBR calculations.

4.5.4.2.10.6 *Uncertainties in Flow Rates.* No change to this entire section. See Section 4.4.2.10.6.

4.5.4.2.10.7 *Uncertainties in Hydraulic Load.* As discussed in Section 4.5.4.2.7.2, hydraulic loads on the fuel assembly were evaluated for a pump overspeed transient that creates flow rates 20% greater than the mechanical design flow. In addition, the core bypass flow is assumed to be a minimum, thereby increasing the lift forces in the core.

4.5.4.2.10.8 *Uncertainty in Mixing Coefficient.* Based on an analysis of Laser Doppler Velocimeter testing of the Mark-BW Zircaloy-4 spacer grid, a turbulent mixing coefficient > 0.038 was determined to be applicable to the Mark-BW fuel design. However, the value of 0.038 is conservatively used in the thermal-hydraulic analyses.

4.5.4.2.11 Plant Configuration Data

No change to this entire section. See Section 4.4.2.11.

4.5.4.3 **Evaluation**

The thermal-hydraulic methods that Framatome ANP used to license Advanced Mark-BW fuel for operation in the North Anna Units 1 & 2 nuclear plants are outlined in Reference 1. The following sections briefly describe some of those methods.

4.5.4.3.1 Core Hydraulics

4.5.4.3.1.1 *Flow Paths Considered in Core Pressure Drop and Thermal Design.*

Section 4.4.3.1.1 provides a description of the flow paths considered when determining the nominal core bypass flow. That discussion remains applicable for the transition to the Advanced Mark-BW fuel design.

The change in core bypass flow due to the Advanced Mark-BW fuel assembly design was assessed. The assessment determined that the increase in bypass flow due to the incorporation of the Advanced Mark-BW fuel assembly was less than 0.2%. The nominal bypass flow was calculated to be less than 5.0% for a core loading pattern with no core inserts (e.g., discrete poison assemblies, secondary sources) located in the thimble guide tubes. The minimum bypass flow was calculated to be greater than 3.0% for a full core of Advanced Mark-BW fuel with a core loading pattern with 1500 core inserts (e.g., discrete poison assemblies, secondary sources) located in the thimble guide tubes.

A bypass flow of 5.5% is specified for use in the statistical DNB analysis for the Advanced Mark-BW. This value represents a bounding value for the nominal bypass flow for a core configuration with all Advanced Mark-BW fuel assemblies and no core inserts. A design core bypass flow of 6.5% is specified for non-statistical DNB applications and other deterministic NSSS evaluations. This is the current analytical value and includes an uncertainty of 1.0% on nominal bypass flow. A minimum bypass flow of 3.0% is specified for the lift force calculation. This is the current analytical value and includes uncertainties.

4.5.4.3.1.2 *Inlet Flow Distribution.* Thermal-hydraulic analyses impose a 5-percent reduction in inlet flow to the hot assembly.

4.5.4.3.1.3 *Empirical Friction Factor Correlations.* The Framatome ANP thermal-hydraulic analysis code, LYNXT, uses the Framatome ANP single-phase friction factor model with multipliers for the subcooled and two-phase flow regimes. A description of this model is contained in Reference 23. LYNXT also has a variable lateral resistance model in which the crossflow resistance coefficient varies with the pitch to diameter ratio and Reynolds number. Dominion's thermal-hydraulic analysis code VIPRE-D applies the EPRI two-phase friction multiplier to the single-phase friction factor. This model is described in Reference 31. VIPRE-D also has a variable lateral resistance model in which the crossflow resistance coefficient varies with the pitch to diameter ratio and the Reynolds number (Reference 31).

4.5.4.3.2 Influence of Power Distribution

No change to this entire section. See Section 4.4.3.2.

4.5.4.3.2.1 *Nuclear Enthalpy Rise Hot Channel Factor.* No change to this entire section. See Section 4.4.3.2.1.

4.5.4.3.2.2 *Axial Heat Flux Distribution.* No change to this entire section. See Section 4.4.3.2.2.

4.5.4.3.3 Core Thermal Response

A general summary of steady-state thermal-hydraulic design parameters applicable with Framatome ANP's Advanced Mark-BW fuel design and the Statistical Core Design (SCD) methodology is provided in Table 4.5-3 for all loops in operation.

4.5.4.3.4 Analytical Techniques

4.5.4.3.4.1 *Core Analysis.* To perform the various thermal-hydraulic analyses needed to license the Advanced Mark-BW design, Framatome ANP typically employs its LYNXT thermal-hydraulic analysis code. LYNXT, a single-pass code, evaluates subchannel thermal-hydraulic conditions for both steady-state and transient modes of operation using crossflow methodologies to determine core conditions. A more complete description of the code is provided in the following paragraph and in Reference 23, which includes comparisons of code predictions to experimental data. To perform the various thermal-hydraulic analyses needed to support the Framatome ANP Advanced Mark-BW fuel product, Dominion uses the VIPRE-D thermal-hydraulic analysis code. VIPRE-D, a single-pass code, evaluates subchannel thermal-hydraulic conditions for both steady-state and transient modes of operation using crossflow methodologies to determine core conditions (Reference 31). A more complete description is provided in Section 4.5.4.3.4.1.3.

4.5.4.3.4.1.1 *LYNXT.* LYNXT is approved by the NRC and provides the capability for single-pass core thermal-hydraulic analysis for both steady state and transient conditions. It also has the capability to analyze conditions with high lateral flow and/or recirculating flow, such as encountered in the analysis of a steamline break with reactor coolant pumps off. The single pass LYNXT model has been extensively benchmarked to multi-pass analyses and appropriate experimental data. LYNXT is used almost exclusively for determining core flow redistribution and for predicting the DNB performance of various fuel designs.

LYNXT has been qualified for the BWU-I, BWU-N, BWU-Z, BWU-ZM, BWC, BWCMV, BWCMV-A, B&W2 and W3 correlations by data base analysis. In every case where this evaluation has been performed LYNXT supported the licensed DNBR limit for the respective CHF correlation.

4.5.4.3.4.1.2 *Mixed-Core Methodology.* The process of evaluating the thermal-hydraulic performance in mixed-core configurations of the Framatome Advanced Mark-BW fuel and the resident Westinghouse fuel uses the Framatome mixed-core methodology outlined in Reference 1.

The specific analyses used to assess the compatibility of different fuel types are DNB, pressure drop, hydraulic loads, and crossflow velocity. LYNXT (Reference 23) is used for the thermal-hydraulic calculations to evaluate the compatibility of the resident and new fuel. The process uses a wide variety of LYNXT models selected to represent a range of mixed-core configurations. The Framatome mixed-core methodology as described in Reference 1 provides a systematic and conservative approach to these evaluations.

4.5.4.3.4.1.3 *VIPRE-D.* VIPRE-D is an NRC-approved subchannel analysis tool designed to help evaluate nuclear reactor core safety limits including departure from nucleate boiling ratio (DNBR), fuel and clad temperatures and coolant state in normal operation and analyzed accident conditions. VIPRE-01 was developed on the various COBRA codes for EPRI (Electric Power Research Institute) by Battelle Pacific Northwest Laboratories. The Dominion version of VIPRE-01, VIPRE-D, was customized by Dominion to fit the specific needs of North Anna and its fuel products by adding vendor specific CHF correlations and customizing its input and output. The NRC-approved constitutive models and algorithms in VIPRE-01 are unchanged in VIPRE-D (Reference 31).

4.5.4.3.4.2 *Fuel Temperatures.* As discussed in Section 4.5.4.2.2, Framatome ANP employs the fuel thermal performance code TACO3 to predict fuel rod temperature and internal pressure conditions during core operation. These analyses are used to determine the centerline melt limit and the maximum fuel rod burnup limit, which is based on the fuel rod internal pressure. In addition, the TACO3 analysis provides initial fuel temperature and pressure conditions for LOCA and non-LOCA safety analyses. A more complete discussion of the code and its associated analysis methods is contained in the paragraphs below and in Reference 4, which contains comparisons of the code predictions to measured data.

4.5.4.3.4.2.1 *TACO3.* The TACO3 code, with its Fuel Rod Gas Pressure Criterion discussed in Reference 24, is the methodology for fuel rod thermal performance analysis. Framatome ANP continually acquires data supporting the extension of burnup limits and evaluates the suitability of existing code models. The integration of French technology will aid this process by providing access to additional extended burnup data, models, codes, and methods.

TACO3 uses best-estimate models benchmarked to an extensive database of fuel performance data from numerous industry-sponsored experimental programs. TACO3 uses a complete set of thermal and mechanical models, as well as new fuel and cladding material relations. The TACO3 fuel temperature predictions have less uncertainty than other comparable codes. The NRC has reviewed and approved TACO3.

TACO3 uses best-estimate inputs to provide best-estimate predictions. Statistical evaluations are performed to estimate uncertainties and provide conservative results for use in licensing evaluations. Code and power prediction uncertainties and manufacturing variations are considered for internal gas pressure uncertainties. Statistical parameters obtained from the analysis of an extensive code benchmark database evaluate fuel temperature uncertainties.

Transient fission gas release and cladding oxide effects are also represented to provide appropriate conservatism.

4.5.4.3.4.3 *Hydrodynamic Instability.* No change to this entire section. See Section 4.4.3.4.3.

4.5.4.3.5 Hydrodynamic and Flow Power Coupled Instability

No change to this entire section. See Section 4.4.3.5.

4.5.4.3.6 Temperature Transient Effects Analysis

Water-logging damage of a previously defected fuel rod has occasionally been postulated as a mechanism for subsequent rupture of the cladding. Fuel rod failures of this type have never been observed in Framatome ANP fuel. Testing performed at INEL (Reference 25) has shown that energy depositions much greater than those experienced during normal operating transients are required for fuel failure. This is discussed further in Section 4.4.3.6. Additional testing (Reference 26) showed that if a failure did occur, the ruptured rod would not be expected to cause significant damage to the rest of the core. That test, which was performed under conditions that are much more severe than those seen under normal operation, showed that when a rupture did occur, there was no failure propagation and the most significant damage caused to the remainder of the core was the bowing of adjacent fuel rods.

4.5.4.3.7 Potentially Damaging Temperature Effects During Transients

The fuel rod experiences many operational transients during its residence in the core. A number of thermal effects must be considered when analyzing the fuel rod performance.

The clad can be in contact with the fuel pellet at some time in the fuel lifetime. Clad-pellet interaction contributes to clad stress and strain, particularly if the fuel pellet temperature increases after the clad is in contact with the pellet. Analysis of cladding stress and strain is discussed in Section 4.5.2.1.3.1.

Increasing the fuel temperature results in an increased fuel rod internal pressure. One of the fuel rod design bases requires that the fuel rod internal pressure of the peak fuel rod in the reactor be limited to a value below that which would cause the fuel-clad gap to increase due to cladding outward creep during steady-state operation, and extensive departure from nucleate boiling (DNB) propagation to occur. (See Sections 4.5.2.1.1.1 and 4.5.2.1.3.1).

The potential effects of operation with water-logged fuel are discussed in Section 4.5.4.3.6. As discussed in that section, water-logging is not a concern during operational transients.

If axial gaps in the fuel pellet column occur due to densification, the cladding has the potential of collapsing into a gap (i.e. flattening). As discussed in Sections 4.5.2.1.1.1 and 4.5.2.1.3.1, creep collapse is precluded by ensuring that the predicted creep collapse life of the fuel rod exceeds the maximum expected incore life.

There can be a differential thermal expansion between the fuel rods and the guide thimbles during a transient. Excessive bowing of the fuel rods could occur if the grid assemblies do not allow axial movement of the fuel rods relative to the grids. Thermal expansion of the fuel rods is considered in the grid design so that axial loads imposed on the fuel rods during a thermal transient will not result in excessively bowed fuel rods (see Sections 4.5.2.1.1.1, 4.5.2.1.2.1, and 4.5.2.1.2.2)

4.5.4.3.8 Energy Release During Fuel Element Burnout

As discussed in Section 4.4.1, the reactor core is designed to preclude any temperature effect that could cause damage to fuel rods during normal operation and Condition I and II transients. However, in the unlikely event that DNB occurs, the cladding temperature will increase, causing a potential increase in the chemical reaction rate between cladding and coolant. The Baker-Just equation was used to estimate the energy produced and the thickness of cladding reacted as a function of time with temperature as a parameter (Reference 22). It was concluded that the potential for chemical reaction between fuel rod cladding and coolant is small and no adverse effects will result during normal operation or the infrequent event type accidents considered in Chapter 15 of this document.

4.5.4.3.9 Energy Release or Rupture of Water-logged Fuel Elements

A full discussion of water-logging including energy release is contained in Section 4.5.4.3.6. It is noted that the resulting energy release is not expected to adversely affect neighboring fuel rods.

4.5.4.3.10 Fuel Rod Behavior Effects from Coolant Flow Blockage

Coolant flow blockages can occur within the coolant channels of a fuel assembly or external to the reactor core. In either case, the flow blockage will cause a local reduction in coolant flow. The effects of these flow reductions on core performance must be investigated.

A subchannel DNBR analysis determining the effect of a flow blockage in the hot subchannel showed that flow blockages up to 70% have only a minimal effect on the hot channel DNBR since flow recovery occurs rapidly above the blockage.

4.5.4.4 **Testing and Verification**

4.5.4.4.1 Tests Prior to Initial Criticality

No change to this entire section. See Section 4.4.4.1.

4.5.4.4.2 Initial Power and Plant Operation

Core power distribution measurements are made at regular intervals during core operation. These measurements ensure that conservative peaking factors are used in the core thermal and hydraulic analysis. Allowable peaking factors are specified in the Core Operating Limits Report (COLR).

4.5.4.4.3 Component and Fuel Inspections

Inspections performed on the manufactured fuel are delineated in Section 4.5.2.1.4. Fabrication measurements are taken to verify that the assumptions made in the fuel thermal analysis regarding fuel densification and manufacturing variations bound the actual fabrication data.

4.5.4.5 **Instrumentation Application**

No change to this entire section. See Section 4.4.5.

4.5 REFERENCES

1. Letter from Leslie N. Hartz (Virginia Electric and Power Company) to USNRC, *Virginia Electric and Power Company North Anna Power Station Units 1 and 2, Proposed Technical Specifications Changes and Exemption Request Use of Framatome ANP Advanced Mark-BW Fuel,* Serial Number 02-167, March 28, 2002.
2. BAW-10227P-A, *Evaluation of Advanced Cladding and Structural Material (M5) in PWR Reactor Fuel,* February 2000.
3. American Society of Mechanical Engineers, Boiler and Pressure Vessel Code, Section III, *Nuclear Power Plant Components*, 1992 Edition.
4. BAW-10162P-A, *TACO3 Fuel Pin Analysis Computer Code*, October 1989.
5. W.J. O'Donnell and B.F. Langer, *Fatigue Design Basis for Zircaloy Components*, Nuclear Science and Engineering, Volume 20, pp. 1-12.
6. BAW-10084P-A, *Program to Determine In-Reactor Performance of BWFC Fuel Cladding Creep Collapse*, July 1995.
7. BAW-10186P-A, *Extended Burnup Evaluation*, April 2000.
8. Standard Review Plan, Section 4.2, NUREG-0800, Rev. 2, U.S. Nuclear Regulatory Commission, July 1981.
9. BAW-10133P-A, *Mark C Fuel Assembly LOCA-Seismic Analyses*, Revision 1, May 1979; and Addendum 1, October 2000.
10. BAW-10163P-A, *Core Operating Limits Methodology for Westinghouse Designed PWRs,* Rev. 0, B&W Fuel Company, June 1989.
11. EPRI Report NP3966-CCM, *CEPAN Method of Analyzing Creep Collapse of Oval Cladding, Volume 5: Evaluation of Interpellet Gap Formation and Clad Collapse in Modern PWR Fuel Rods*, April 1985.
12. BAW-10054P, *Fuel Densification Report,* Rev. 2, May 1973.

13. Letter, D. M. Crutchfield (NRC) to J. H. Taylor (B&W), Subject: Acceptance for Referencing of a Special Licensing Report. December 5, 1986.

14. Letter from Stephen Monarque (NRC) to David A. Christian (Virginia Electric and Power Company), North Anna Power Station, *Units 1 and 2 - Issuance of Amendments Re: Technical Specifications Changes to Increase Fuel Enrichment and Spent Fuel Pool Soluble Boron and Fuel Burnup Credit (TAC Nos. MB0197 and MB0198)*, June 15, 2001.

15. BAW-10170P-A, *Statistical Core Design For Mixing Vane Cores*, December 1988.

16. BAW-10199P-A, *The BWU Critical Heat Flux Correlations*, December 1994.

17. BAW-10189P-A, *CHF Testing and Analysis of the Mark-BW Fuel Assembly Design,* January 1996.

18. BAW-10199P-A, Addendum 2, *Application of BWU-Z CHF Correlation to the Mark-BW17 Fuel Design with Mid-Span Mixing Grids*, June 2002.

19. BAW-1419, *PEEL - A Transport Code for Special Depletion,* May 1978.

20. BAW-10115A, *NULIF - Neutron Spectrum Generator, Few-Group Constant Calculator and Fuel Depletion Code*, February 1972.

21. BAW-10172P, *Mark-BW Mechanical Design Report,* July 1988.

22. BAW-10147PA-R1, *Fuel Rod Bowing in Babcock & Wilcox Fuel Designs - Revision 1,* May 1983.

23. BAW-10156-A, Revision 1, *LYNXT: Core Transient Thermal-Hydraulic Program,* August 1993.

24. BAW-10183P-A, *Fuel Rod Gas Pressure Criterion (FRGPC)*, July 1995.

25. Stephan, L.A., *The Effects of Cladding Material and Heat Treatment on the Response of Waterlogged UO2 Fuel Rods to Power Bursts,* IN-ITR-111, January 1970.

26. Grund, J.E., *Experimental Results of Potentially Destructive Reactivity Additions to an Oxide Core,* IDO-17028, December 1964.

27. Letter from USNRC to D. A. Christian, *North Anna Power Station, Units 1 and 2, Issuance of Exemption from the Requirements of 10 CFR 50.44, 10 CFR 50.46, and 10 CFR Part 50, Appendix K, to Allow the Use of the M5 Alloy for Fuel Cladding Material (TAC Nos. MB4700 and MB4701)*, September 23, 2003.

28. Letter from USNRC to D. A. Christian, *North Anna Power Station, Unit 2 - Issuance of Amendment Re: Use of Framatome ANP Advanced Mark-BW Fuel (TAC No. MB4715),* April 1, 2004.

29. Letter from USNRC to D. A. Christian, *North Anna Power Station, Unit 1 - Issuance of Amendments Re: Use of Framatome ANP Advanced Mark-BW Fuel (TAC No. MB4714,* August 20, 2004.

30. VEP-NE-2-A, *Statistical DNBR Evaluation Methodology,* R. C. Anderson, June 1987.

31. DOM-NAF-2-A, *Reactor Core Thermal-Hydraulics Using the VIPRE-D Computer Code,* including Appendix A, *Qualification of the F-ANP BWU CHF Correlations in the Dominion VIPRE-D Computer Code,* R. M. Bilbao y León, August 2006.

32. BAW-2149-A, *Evaluation of Replacement Rods in BWFC Fuel Assemblies*, September 1993.

Table 4.5-1
ADVANCED MARK-BW FUEL ASSEMBLY NOMINAL DESIGN PARAMETERS

Parameter	Advanced Mark-BW Design
Fuel Assembly Length	159.85 in.
Assembly Envelope	8.425 in.
Compatible with Core Internals	Yes
Fuel Rod Pitch	0.496 in.
Number of Fuel Rods/Assembly [a]	264
Number of Guide Thimbles/Assembly	24
Number of Instrumentation Tubes	1
Compatible w/Movable In-core Detector System	Yes
Fuel Tube Material	M5
Fuel Rod Clad O.D.	0.374 in.
Guide Thimble Material	M5
Structural Material - Six Intermediate Grids and MSMGs	M5
Structural Material - Two End Grids	Inconel 718
Grid Support for Fuel Rods	6 points (structural grids) 2 Springs 4 Dimples
Top Nozzle	Removable
Top Nozzle Holddown Springs	3-leaf
Bottom Nozzle	Coarse Mesh Debris Filter

a. Each reconstituted Advanced Mark-BW fuel assembly may contain up to 10 solid stainless steel filler rods in place of fuel rods.

Table 4.5-2
REACTOR CORE DESCRIPTION

This table supplements Table 4.3-1 to reflect the Advanced Mark-BW fuel assembly.

Fuel assemblies		
Number	157	
Rod Array	17 x 17	
Rods per assembly [a]	264	
Rod pitch, in.	0.496	
Overall transverse dimensions, in.	8.425 x 8.425	
Fuel weight (as UO_2), kg per assembly	466	
Number of grids per assembly	1 top	6 intermediate
	1 bottom	3 MSMG
Composition of grids	Inconel-718	M5
Number of Guide Thimbles per assembly	24	
Composition of guide thimbles	M5	
Fuel Rods		
Number [a]	264/assembly	
Outside diameter, in.	0.374	
Clad material	M5	
Fuel pellets		
Material	UO_2 sintered	
Density, %TD	96	

a. Each reconstituted Advanced Mark-BW fuel assembly may contain up to 10 solid stainless steel filler rods in place of fuel rods.

Table 4.5-3
THERMAL-HYDRAULIC ANALYSIS DESIGN PARAMETERS

Design Parameter	Value
Reactor Coolant System:	
Rated Thermal Power	2942.2 MWt [a]
Heat Generated In Fuel	97.4%
Nominal System Pressure	2250 psia
Minimum DNBR at nominal conditions	3.0922 [b] (LYNXT) 3.073 (VIPRE-D)
Minimum DNBR for design transients	1.60
DNB Correlation	BWU
Core Configuration:	
Number of Fuel Assemblies	157
Fuel Assembly Type	17 x 17
Number of Fuel Rods Per Assembly [c]	264
Number of Control Clusters	48
Number of Absorber Rods per Control Cluster	24
Stack Height	144 in
Fuel Rod Outer Diameter	0.374 in
Assembly Flow Area (hot)	38.7 in^2
Coolant Flow	
Minimum Measured Flow	295,000 gpm [d]
Flow Fraction Effective for Heat Transfer	0.945 [d]
Lower Bounding Design Flow	289,100 gpm [e]
Mechanical Design Flow	315,600 gpm
Hot Channel Core Inlet Flow Factor	0.95
Core Inlet Velocity	14.71 ft/sec
Inlet Mass Flux	2.47 Mlb/hr-ft^2
Vessel Mass Flow Rate	110.38 Mlb/hr
Core Pressure Drop (nozzle to nozzle)	27.7 psi

a. These parameters are for a core rated thermal power of 2942.2 MWt, which bounds the current licensed maximum core power of 2893 MWt.

b. DNB calculation based on full-power $F^N_{\Delta H}$ value of 1.49 (corresponds to 1.55 design value with 4% measurement uncertainty).

c. Each reconstituted Advanced Mark-BW fuel assembly may contain up to 10 solid stainless steel filler rods in place of fuel rods.

d. Value used in DNB analyses for statistical DNB events.

e. Value used in DNB analyses for non-statistical DNB events.

Table 4.5-3 (continued)
THERMAL-HYDRAULIC ANALYSIS DESIGN PARAMETERS

Design Parameter	Value
Coolant Temperatures (nominal at 100%RTP)	
Nominal inlet	553.7°F
Average rise in vessel	66.2°F
Average rise in core	65.9°F
Average in vessel	586.8°F
Average in core	588.5°F
Vessel outlet	619.9°F
Core outlet	623.3°F
Heat Transfer	
Average heat flux	206,200 Btu/hr-ft^2
Average thermal output	5.76 kW/ft
Maximum thermal output for normal operation	12.62 kW/ft [f]
Maximum thermal output at maximum overpower trip point (118% power)	21.9 kW/ft

f. This parameter value is associated with an F_Q value of 2.19.

Figure 4.5-1
ADVANCED MARK-BW FUEL ASSEMBLY OUTLINE

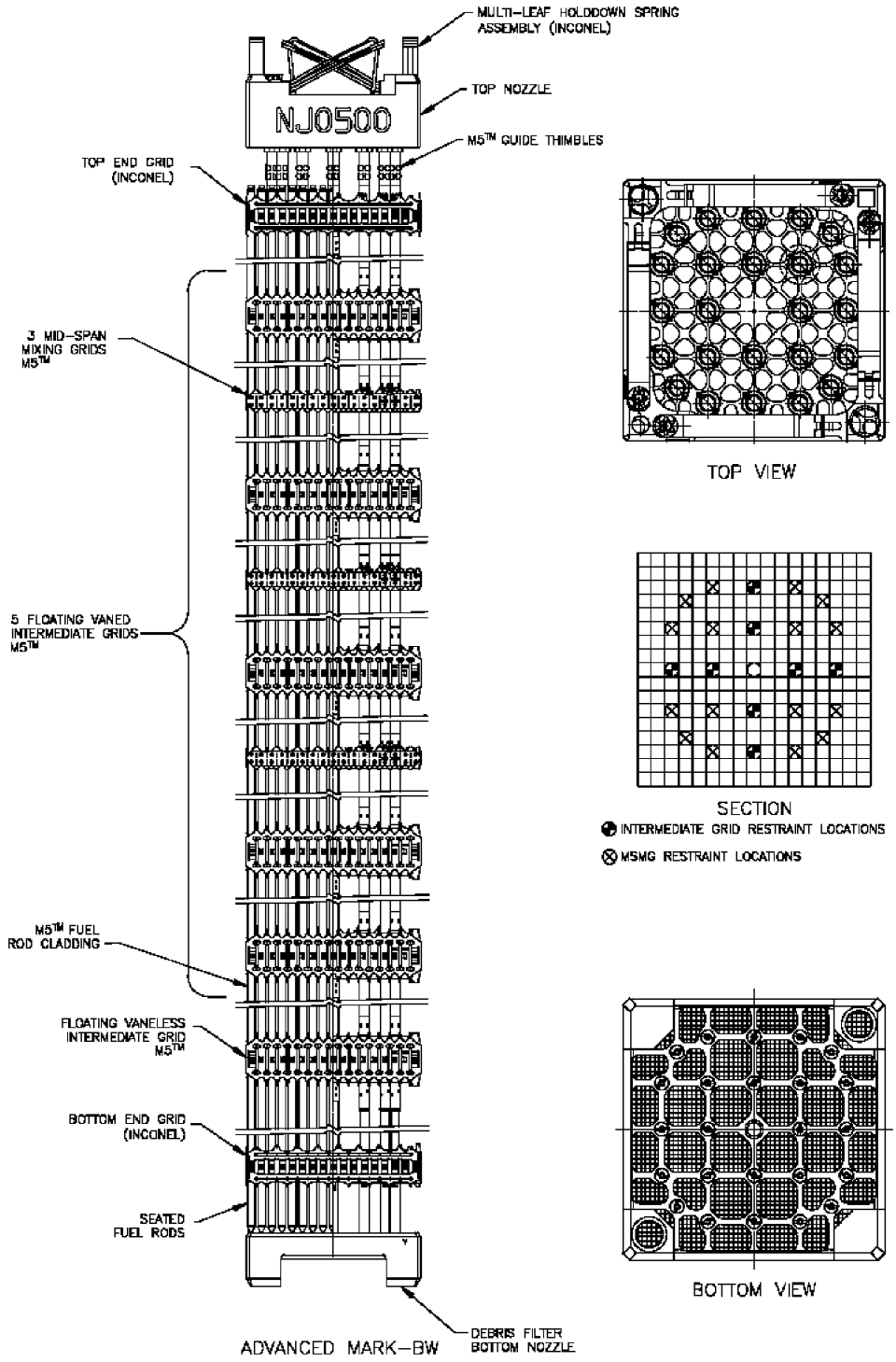
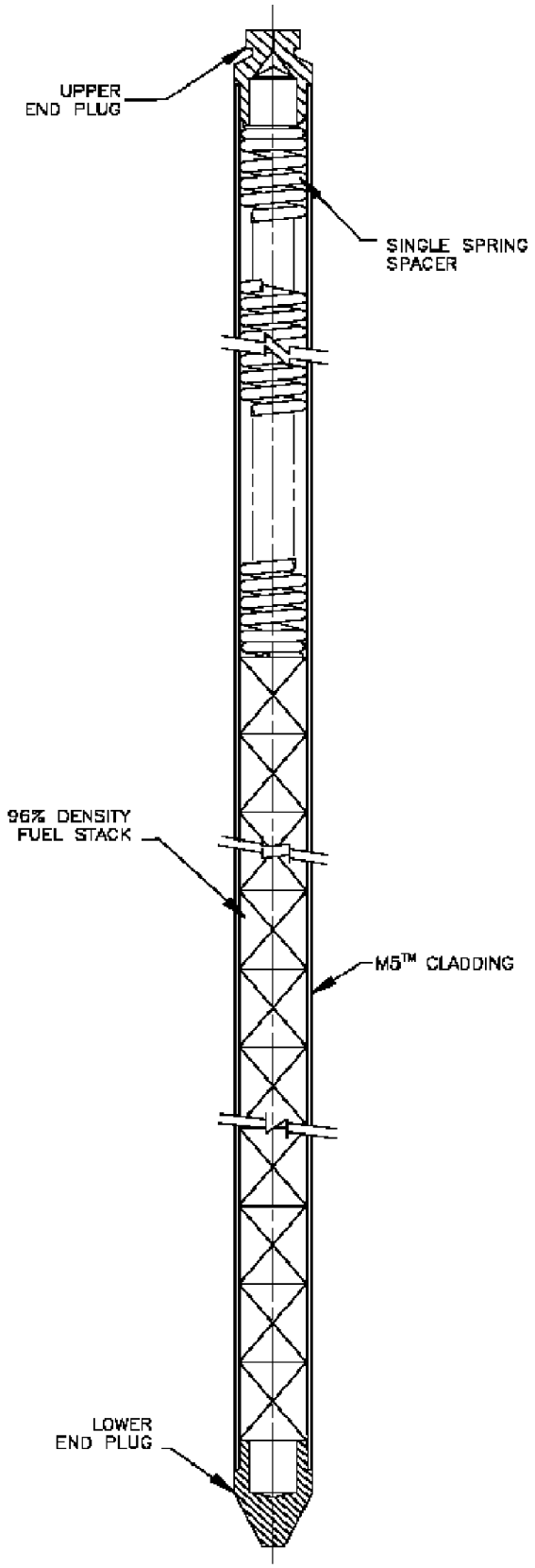
Figure 4.5-2
ADVANCED MARK-BW FUEL ROD ASSEMBLY